

The atmospheric reactivity of the NO_3 radical

Dissertation

zur Erlangung des Grades eines
'Doktor rerum naturalium (Dr. rer. nat.)' der Fachbereiche
08- Physik, Mathematik und Informatik
09 - Chemie, Pharmazie und Geowissenschaften
10 - Biologie,
Universitätsmedizin

verfasst und vorgelegt von
Jonathan Michael Liebmann

geboren am 22. März 1987
in Witzenhausen

Max Planck Graduate Center
mit der Johannes Gutenberg-Universität Mainz

angefertigt am Max-Planck-Institut für Chemie

Mainz, 2018

I hereby declare that I wrote the dissertation submitted without any unauthorized external assistance and used only sources acknowledged in the work. All textual passages which are appropriated verbatim or paraphrased from published and unpublished texts as well as all information obtained from oral sources are duly indicated and listed in accordance with bibliographical rules. In carrying out this research, I complied with the rules of standard scientific practice as formulated in the statutes of Johannes Gutenberg University Mainz to insure standard scientific practice.

Mainz, 4th June 2018, Jonathan Liebmann

Goats are like trees,
If you shoot a duck,
I'm scared of microwaves

Table of contents

Abstract	VIII
Zusammenfassung	X
1 Introduction	1
1.1 Global Emissions	1
1.2 Origin of NO _x	2
1.3 NO _x daytime chemistry	3
1.4 NO _x nighttime chemistry	6
1.5 Emission of Volatile Organic Compounds (VOCs)	8
2 Motivation and Targets	9
3 Discussion and results	12
3.1 Instrument development	12
3.2 Field campaigns	13
3.3 Measurements of NO ₃ -reactivity and derived stationary state mixing ratios	14
3.4 Vertical reactivity profiles	14
3.5 NO ₃ -reactivity calculated from measured VOCs	14
3.6 Contribution to NO _x losses	15
3.7 Comparison of NO ₃ - and OH-reactivity	15
4 Conclusion and outlook	17
Appendix A - Publications	27
A1: Liebmann et al. Atmos. Meas. Tech., 2017	29
A2: Liebmann et al. Atmos. Chem. Phys., 2018 A	53
A3: Liebmann et al. Atmos. Chem. Phys., 2018 B	83

Abstract

The nitrate radical (NO_3), formed from oxidation of NO_2 by O_3 , controls the oxidizing capacity of the Earth's atmosphere during nighttime. Reaction of NO_3 with (biogenic) volatile organic compounds (VOCs) and subsequent deposition into the particle phase represents an important loss process for nitrogen oxides ($\text{NO} + \text{NO}_2 = \text{NO}_x$) cleansing the Earth's atmosphere. The rate of loss of NO_x due to reaction of the NO_3 radical with VOCs can be accessed via the NO_3 -reactivity ($k_{\text{OTG}}^{\text{NO}_3}$, OTG = Organic Trace Gases) thus the inverse lifetime. This work focuses on i) the development of the first instrument for measuring $k_{\text{OTG}}^{\text{NO}_3}$ ii) the deployment of the instrument in field campaigns and interpretation of the data with special regard to boundary layer dynamics and VOCs iii) the assessment of the fractional contribution of $k_{\text{OTG}}^{\text{NO}_3}$ as NO_x loss process during day and night.

The instrument developed uses cavity ring down spectroscopy (CRDS) for the detection of synthetically generated NO_3 radicals after transmissions through a flow-tube reactor. The change in the NO_3 mixing ratio upon modulation of the bath gas between zero air and ambient air is used to derive $k_{\text{OTG}}^{\text{NO}_3}$. The instrument can measure NO_3 reactivities from 0.005 s^{-1} up to 45 s^{-1} using an automated dilution procedure. The uncertainty of the measurements is strongly dependent on the ambient NO and NO_2 mixing ratios and is $\approx 16\%$ at the center of its dynamic range ($0.01\text{-}0.4 \text{ s}^{-1}$).

During field campaigns in the boreal forest and at mountain tops, the variability in the reactivity was found to be driven mainly by the dynamics of the boundary layer. In the nocturnal boundary layer, very high reactivities were measured whereas in the residual layer very low reactivities partly below the detection limit of the instrument were measured. A strong vertical gradient in $k_{\text{OTG}}^{\text{NO}_3}$ was found in the nocturnal boundary layer which disappeared due to efficient mixing during daytime. NO_3 mixing ratios, calculated using $k_{\text{OTG}}^{\text{NO}_3}$, were in good agreement with the entire measured NO_3 mixing ratios. From organic trace gas measurements it was found that the reactivity was mainly determined by reaction with monoterpenes though their concentrations were insufficient to account for the measured $k_{\text{OTG}}^{\text{NO}_3}$. We suggest that sesquiterpenes, which were not covered by the trace gas analyzes, play an important role here. In forested regions, the high values of $k_{\text{OTG}}^{\text{NO}_3}$ imply that even during the day at least 20% of the formed NO_3 radicals react with organic trace substances and thus represent a NO_x loss that has been neglected in the literature so far. A comparison of NO_3 -reactivity with the OH-reactivity found only a minor correlation as already suggested by the different rate constants.

Zusammenfassung

Das Nitratradikal (NO_3), gebildet durch die Oxidation von NO_2 durch O_3 , kontrolliert die Oxidationskapazität der Atmosphäre bei Nacht. Die Reaktion von NO_3 mit (biogenen) volatilen organischen Verbindungen (VOCs) und darauffolgende Ablagerung in die Partikelphase stellen einen wichtigen Verlustprozess für Stickoxide ($\text{NO} + \text{NO}_2 = \text{NO}_x$) dar, der zur Reinigung der Atmosphäre beiträgt. Die NO_x Verlustrate durch Reaktion des NO_3 Radikals mit VOCs, kann über die NO_3 -Reaktivität ($k_{\text{OTG}}^{\text{NO}_3}$), daher die inverse Lebenszeit, erfasst werden. Der Schwerpunkt dieser Arbeit liegt in i) der Entwicklung des weltweit ersten Instruments zur Messung von $k_{\text{OTG}}^{\text{NO}_3}$ ii) dem Einsatz des Instrumentes in Feldmessungen und der Interpretation der Daten mit besonderem Augenmerk auf die Dynamik der nächtlichen Grenzschicht und auf VOCs iii) die Einschätzung der Reaktion von NO_3 und biogenen Emissionen als NO_x Verlustprozess bei Tag und bei Nacht.

Das neu entwickelte Instrument verwendet Cavity Ring Down Spektroskopie für die Detektion von synthetisch generierten NO_3 Radikalen nach dem passieren eines Durchflussrohr-Reaktors. Die Änderung in dem NO_3 Mischverhältnis bei Änderung des Badgases von Nullluft zu Umgebungsluft wird verwendet um $k_{\text{OTG}}^{\text{NO}_3}$ zu ermitteln. Das Instrument kann unter Verwendung eines automatischen Verdünnungsverfahrens NO_3 -Reaktivitäten von 0.005 s^{-1} bis zu 45 s^{-1} erfassen. Die Messunsicherheit hängt stark von den NO und NO_2 Mischverhältnissen in der Umgebungsluft ab und beträgt circa 16% im Zentrum des dynamischen Bereichs ($0.01\text{-}0.4 \text{ s}^{-1}$).

Während der Feldmessungen im borealen Wald aber auch in Höhenlagen wurde die Variabilität der Reaktivität hauptsächlich von der Dynamik der Grenzschicht bestimmt. In der nächtlichen Grenzschicht wurden sehr hohe Reaktivitäten und in der Restschicht über der Grenzschicht sehr niedrige Reaktivitäten unter dem Detektionslimit des Instruments gemessen. In der nächtlichen Grenzschicht bestand ein starker vertikaler Reaktivitätsgradient, der bei Tag durch effizientes Mischen verschwand. Unter Verwendung von $k_{\text{OTG}}^{\text{NO}_3}$ wurden für den stationären Zustand der NO_3 Radikale die Mischverhältnisse berechnet. Diese waren in guter Übereinstimmung mit den gemessenen NO_3 Mischverhältnissen. Aus organischen Spurengasmessungen lässt sich ableiten, dass die Reaktivität hauptsächlich durch Reaktion mit Monoterpenen und Isopren bestimmt wird, dennoch waren deren Konzentrationen nicht in der Lage die gesamte gemessenen Reaktivität zu erklären. Wir schlagen vor, dass Sesquiterpene, die über die Spurengasanalysen nicht erfasst wurden, hierbei eine wichtige Rolle spielen. In bewaldeten Regionen legen die hohen Werte für $k_{\text{OTG}}^{\text{NO}_3}$ nahe, dass auch bei Tag noch mindestens 20% der gebildeten NO_3 Radikale mit organischen Spurenstoffen reagieren

und somit einen NO_x Verlust darstellen, der bisher in der Literatur vernachlässigt wurde. Ein Vergleich der NO_3 -Reaktivität mit der OH-Reaktivität zeigte, dass nur eine geringe Korrelation besteht, wie es bereits die unterschiedlichen Ratenkonstanten suggerieren.

1 Introduction

1.1 Global Emissions

With the dawn of the industrial revolution, life on Earth has changed faster than ever before in the history of humankind. The global population proliferated, great advances in technology, communication and transport were achieved and with substantial improvements in medicine and hygienic standards many once life threatening diseases have become nugatory. This progress, however, is accompanied by problems such as, for example, global warming, loss of biodiversity and pollution of land, air and sea [Butchart et al., 2010]. Within this framework, Nobel laureate Paul Crutzen proposed to refer to our current epoch as “Anthropocene”, a concept subsuming the fact that humans and our societies have become a global geophysical force [Steffen et al., 2007].

The planetary boundary layer is most severely affected by this “Global Change” given that it is in direct contact with the planetary surface where a plethora of anthropogenic and biogenic trace gases are directly released into the atmosphere. In the last 200 years, the emissions of especially nitrogen-monoxide (NO), nitrogendioxide (NO₂), sulphur compounds, carbondioxide and volatile organic compounds (VOCs) have increased, changing the trace gas signature of the Earth’s atmosphere [Hartmann et al., 2013]. This has a direct effect on both the climate on Earth as well as human health. In many industrial areas, high levels of NO_x (NO and NO₂) and ozone (O₃) cause photochemical smog leading to respiratory and cardiovascular problems for millions of people worldwide every year [Lelieveld et al., 2002, Kampa and Castanas, 2008]. A strong interaction of NO_x and VOCs in the presence of sunlight leads to a further increase of O₃ and consequent transport can affect even remote clean air regions such as farm lands, resulting in damaged plants and the severe reduction of crop yields [Avnery et al., 2011]. With NO_x mainly generated via combustion processes, current efforts to improve air quality try to diminish atmospheric pollution by reducing the use of fossil energy towards more sustainable and regenerative energies [Skalska et al., 2010]. Especially in rapidly developing countries with economies based on fossil fuels (e.g. India, China), the mitigation of anthropogenic emissions poses a challenge [Hilboll et al., 2013].

The Earth’s atmosphere comprises a complex system of self-cleansing mechanisms that involve, among others, reactive oxygen and nitrogen species in a cascade of reactions. Radicals reacting with VOCs play an important role in particular. The products of these reactions can form or deposit on particles, actively removing NO_x and VOCs from the atmosphere. In order

to reduce and control our emissions, a fundamental knowledge of these atmospheric processes is crucial. In the following sections, a basic overview on the NO_x chemistry will be given.

1.2 Origin of NO_x

NO_x is usually emitted in the form of NO and originates primarily from combustion processes. A mechanism for the production of NO at high temperatures was described by Zel'dovich and Raizer [1966] (R1-R3).



This process accounts for NO produced anthropogenically from fossil fuels in combustion engines and power plants as well as for NO produced naturally by lightning and biomass burning events. Another significant fraction of NO originates from microbial activity in soils [Conrad, 1996]. Here, nitrates in the ground undergo denitrification, a microbially facilitated process whereby nitrate is reduced and ultimately produces N_2 via various i. a. gaseous intermediates (e.g. NO, N_2O). This process is enhanced by the use of nitrogen rich fertilizer in agriculture to increase crop production [Li, 2013].

The global burden of NO_x emissions was estimated to be as high as 48.4 Tg of nitrogen per year ($\text{Tg}(\text{N})\text{yr}^{-1}$) from 2000 to 2010. During this time period, combustion of fossil fuels and industrial processes can account for 77% whereas naturally emitted NO_x from soils and lightning represents 23% of the globally emitted NO_x .

Source	Emissionrate ($\text{Tg}(\text{N}) \text{ yr}^{-1}$)
Fossil fuel combustion and industrial processes	28.3
Biomass and biofuel burning	5.5
Agriculture	3.7
Soils under natural vegetation	7.3
Lightning	4
Total	48.4

Table 1: Emission rates of NO_x from 2000-2010 as recommended from the IPCC report [Ciais et al., 2013].

Preindustrial estimations for NO_x emissions of 13 Tg (N)yr^{-1} show impressively how industrial development has effected the Earth's nitrogen chemistry [Galloway et al., 2004]. Nowadays, NO_x emissions in Europe but also in North America have started to decrease, whereas emissions in India, China and the Middle East are steadily increasing [Hilboll et al., 2013]. The future of NO_x emission is difficult to predict as they are strongly dependent on the global climate policy as well as to technical innovations. For the year 2100, modeling studies predict a wide range of emission scenarios so that a global mitigation of NO_x emissions down to 20 Tg(N)yr^{-1} as well as an increase up to 150 Tg(N)yr^{-1} seem possible [Nakicenovic and Swart, 2000]. NO_x chemistry changes fundamentally during day and nighttime. In the following sections an overview on the related chemical processes will be given.

1.3 NO_x daytime chemistry

During daytime NO_x chemistry is driven by photolysis. NO is rapidly converted to NO_2 in the presence of O_3 while NO_2 is photolysed at light $\lambda < 420 \text{ nm}$ to reform NO and O_3 (Fig. 1A). The corresponding photostationary state is also known as Leighton relationship [Leighton, 1961]. The Leighton relationship does however not lead to a production of O_3 as NO formed at the same time serves as sink for O_3 . In the presence of OH radicals and VOCs this cycle changes.

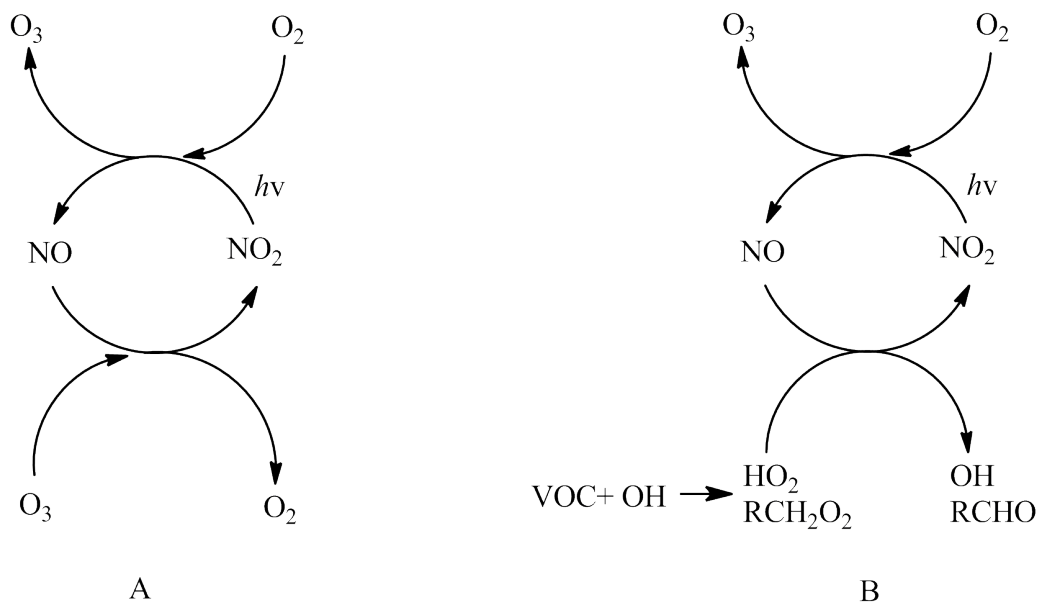


Figure 1: Leighton cycle and influence of VOCs on the Leighton cycle

OH-radicals control the oxidation capacity of the atmosphere during daytime. Primary OH-radicals are formed mainly from photolysis of ozone and consequent reaction with water vapor and react efficiently with VOCs either by abstraction of an H-atom or via addition to a double bond [Gligorovski et al., 2015]. The mechanism and reaction pathways of the OH radical after H-abstraction are exemplarily displayed in Fig. 2. After H-abstraction and subsequent reaction with O₂ a peroxy radical (**1**) is formed. The peroxy radical (**1**) reacts with NO forming an alkoxy radical (**2**) which reacts, in the presence of oxygen, to a (multi-functionalized) carbonyl compound (**3**) and HO₂. The OH radical is recycled by reaction of HO₂ and NO that yields OH and NO₂. The OH radical is recycled by reaction of HO₂ and NO that yields OH and NO₂.

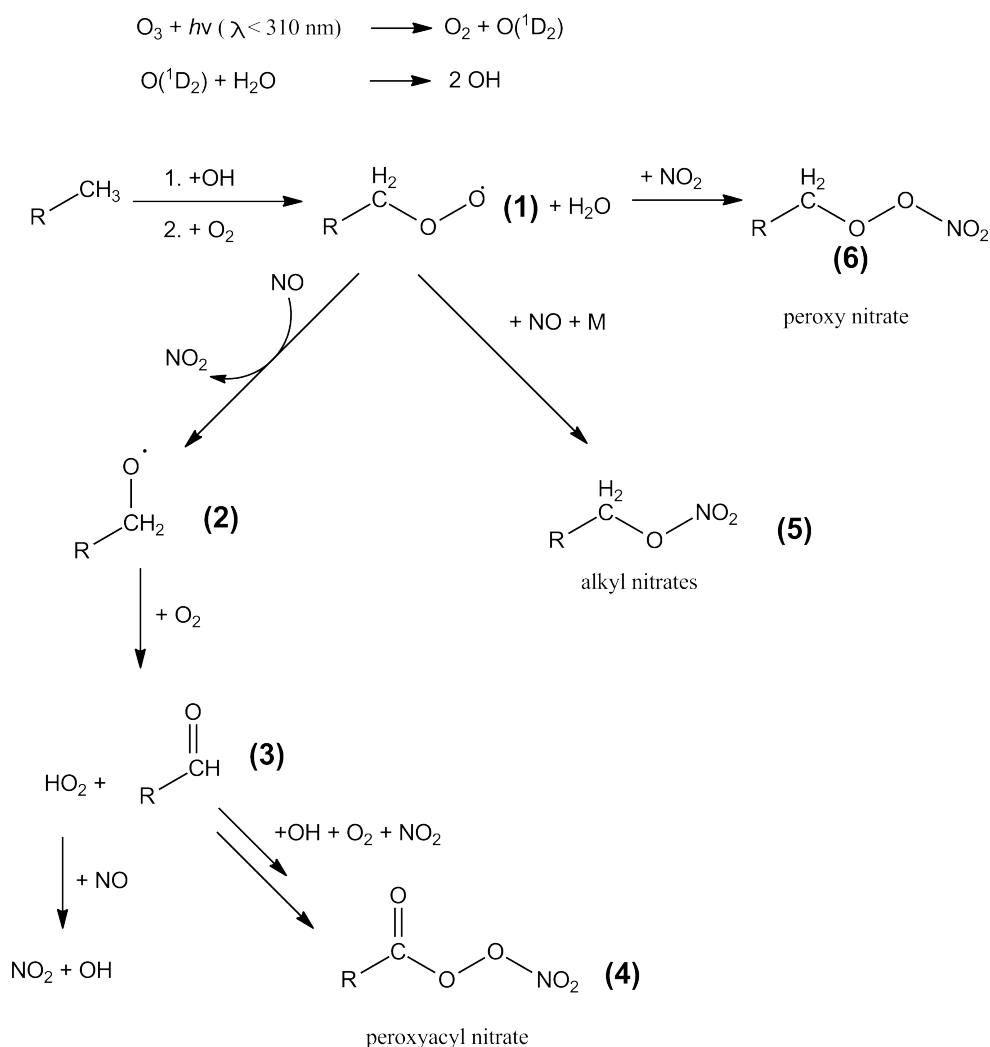


Figure 2: Daytime chemistry of the OH radical with VOCs

It is obvious that this mechanism converts NO to NO₂ without consuming O₃. This implies that VOCs from anthropogenic and biogenic sources cause a deviation from the Leighton photo stationary state according to Fig. 1B and therefore an increase of O₃ that has been observed globally [Lelieveld and Dentener, 2000, Haagen-Smit et al., 1953].

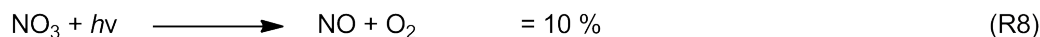
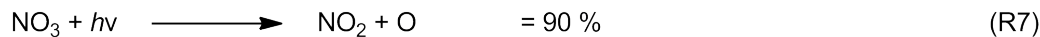
The formation of stable organic nitrates is another possible fate of VOCs and NO_x. Peroxy acyl nitrates (PANs) (**4**) can be formed via degradation of aldehydes. OH radicals react via abstraction of hydrogen forming acyl peroxy radicals which can react then with oxygen and NO₂ to yield into the formation of PANs in an mechanism analogue to the formation of (**3**) [Singh and Hanst, 1981, Roberts, 1990]. PANs are a major species responsible for the formation of photochemical (toxic) smog. Alkyl nitrates (ANs, (**5**)) are produced by the reaction of the peroxide (**1**) with NO via an intermediate peroxy nitrite [Darnall et al., 1976, Arenas et al., 2008]. Direct reaction of NO₂ with a non-acyl peroxy radical leads to the formation of a peroxy nitrate (**6**) which is short lived and can only persist in very cold regions of the troposphere [Nault et al., 2015]. Both PANs and ANs can serve as a NO_x reservoir species as well as represent a NO_x loss process by deposition on particles.

OH radicals can also serve as an important direct sink for NO_x via formation of HNO₃ (R5) [Gligorovski et al., 2015].



HNO₃ is washed out or lost to surfaces in the atmosphere. At high NO₂ and comparably low VOC mixing ratios, the production of organic radicals and O₃ is suppressed by radical termination via reaction R5.

NO₂ reacts with O₃ to form NO₃ radicals (R6) [Atkinson, 2000].



NO₃ radicals are short lived during daytime as they undergo rapid photolysis (R7, R8) and fast reaction with NO (R9). The corresponding daytime mixing ratios are usually below the detection limit of most instruments [Brown et al., 2003, Crowley et al., 2010]. This changes fundamentally at night.

1.4 NO_x nighttime chemistry

At night, the formation of OH is mostly suppressed due to the lack of photolysis. NO reacts with O₃ but is not reformed by photolysis of NO₂ (Fig. 1A). Hence, far away from direct sources, NO mixing ratios usually approach zero within a couple of minutes after sunset. The NO₃ radical, formed by reaction of NO₂ and O₃ and lacking its main daytime losses (R7, R8, R9) can now persist in mixing ratios of up to several (hundred) pptv. In pristine conditions, the lifetime of the radical, restricted to a few seconds during daytime, can reach minutes up to hours at night [Sobanski et al., 2016].

The nitrate radical is a strong oxidant reacting with a wide variety of VOCs including alkenes, oxygenates and reduced sulfur compounds [Ng et al., 2017]. Reactions with isoprene and monoterpenes are particularly rapid and proceed via an addition mechanism leading to the formation of nitroperoxy radicals [Wayne et al., 1991], though hydrogen abstraction may occur, most favorably for aldehydic species [Zhang and Morris, 2015].

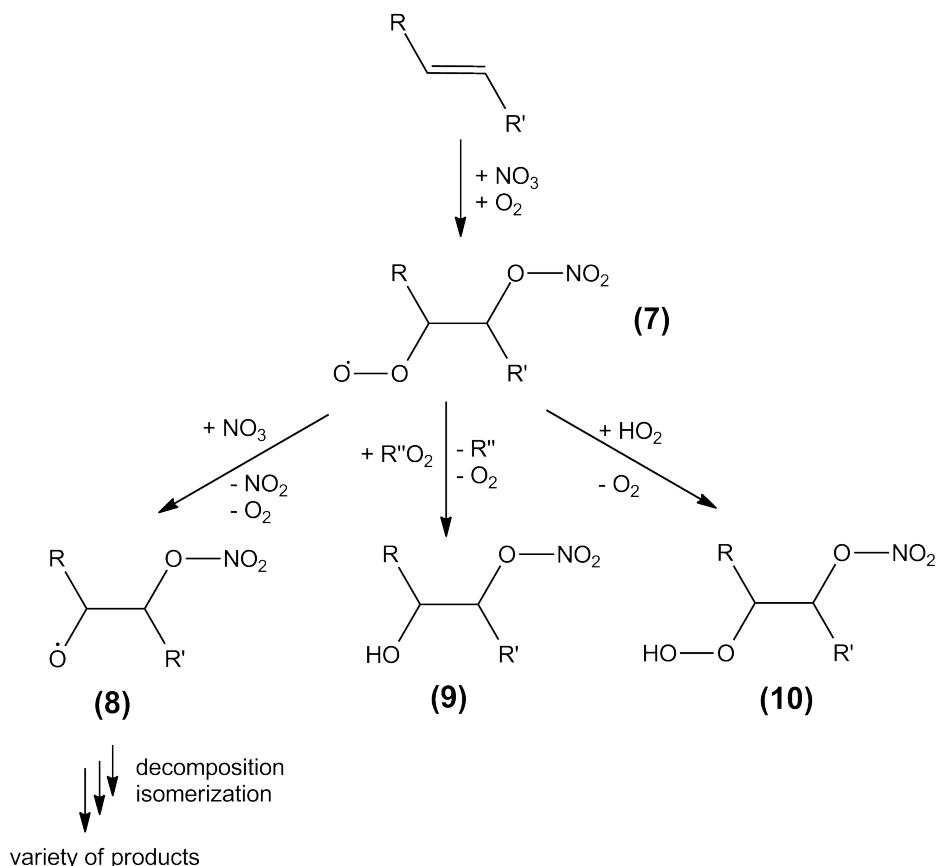


Figure 3: Nighttime reactions of the NO₃ radical

Figure 3 summarizes the most important reaction products of NO_3 . A peroxy nitrate (**7**) is formed by electrophilic addition of the nitrate radical to unsaturated compounds. The peroxy nitrate will isomerize with other reactive atmospheric trace gases such as HO_2 , NO_3 and RO_2 to form e.g. alkoxy nitrates (**8**), hydroxy nitrates (**9**) and nitrooxy hydroperoxides (**10**) [Atkinson, 2000, Ng et al., 2017]. The extremely low volatility of heavy (multi-substituted) alkyl nitrates suggests that they play an important role in nucleation and nanoparticle growth [Ehn et al., 2014, Tröstl et al., 2016]. The secondary organic aerosol yield depends strongly on the specific VOC and on the reaction path of the peroxy nitrate (**7**) [Ng et al., 2008].

One way to access the role of NO_3 as an oxidizing agent is via the reactivity or inverse stationary-state lifetime. It can be calculated according to Eq. (1) using the NO_3 production rate (with k_6 being the rate coefficient for Reaction (R6)) and the measured radical mixing ratio $[\text{NO}_3]$.

$$k_{ss} = \frac{1}{\tau} = \frac{\text{production rate}}{\text{loss rate}} = \frac{[\text{NO}_2][\text{O}_3]k_6}{[\text{NO}_3]} \quad (1)$$

This method is applicable when the chemical lifetime of NO_3 is sufficiently short so that stationary state can be achieved within transport time from emission to measurement location [Brown et al., 2003].

Apart from direct loss processes, there are indirect loss processes for NO_3 that also imply a reduction of NO_x and thus a reduction in the rate of photochemical O_3 formation [Dentener and Crutzen, 1993]. NO_3 can react with NO_2 , forming dinitrogen pentoxide (N_2O_5 , (R10)), which thermally decomposes to set up a thermal equilibrium, with N_2O_5 formation favored at lower temperatures (R11) [Platt et al., 1980, Wayne et al., 1991]. N_2O_5 is lost via hydrolysis in both the gas phase and, after uptake, in the particle phase forming HNO_3 (R12). This indirect loss process becomes dominating at low BVOC mixing ratios that can be found for example in the upper troposphere.



In particles containing chlorine, N_2O_5 can also form ClNO_2 that will decompose to NO_2 and Cl radicals by photolysis after escaping the particle [Behnke et al., 1992, 1997, Phillips et al., 2016].

1.5 Emission of Volatile Organic Compounds (VOCs)

Volatile Organic Compounds (VOCs) emitted from anthropogenic and biogenic sources influence the atmospheric composition and climate. Hence, quantitative and qualitative estimates of their emissions into the atmosphere are necessary for numerical assessments of past, present and future air quality and climate [Derwent et al., 2007, Guenther et al., 2012]. Methane, a potent greenhouse gas (550 Tg yr^{-1}), is the most abundant VOC in the Earth's atmosphere with a global annual mean mixing ratio of 1.8 ppm and tropospheric lifetimes up to ≈ 9 years [Wuebbles and Hayhoe, 2002, Hartmann et al., 2013]. In addition to methane, large amounts of organic carbon are emitted into the atmosphere. Anthropogenic non-methane VOC emissions were estimated to 142 Tg y^{-1} and are mainly represented by alkanes, alkenes and polycyclic aromatic hydrocarbons from fuel and biomass burning [Goldstein and Galbally, 2007, Hartmann et al., 2013]. A much larger fraction of different VOCs is emitted globally by vegetation. This mixture of biogenic VOCs consists mainly of terpenoids (isoprene, monoterpenes, sesquiterpenes) and oxygenated hydrocarbons (e.g. alcohols, aldehydes, ketones, esters) [Kesselmeier and Staudt, 1999, Duhl et al., 2008]. Günther et al. [2012] estimated a global total non-methane BVOC flux of about 1000 Tg consisting of 50% isoprene and 15% monoterpenes. These estimations are however connected with large uncertainties due to inter annual variations or compounds that were neither measured nor considered in the models [Goldstein and Galbally, 2007].

Terpenoids are compounds composed of characteristic C₅ units containing one or more unsaturated bonds. They are usually strong smelling, hardly water-soluble compounds and can be found in plants, animals and microorganisms. The atmospheric lifetime of terpenoids is typically restricted from several minutes to hours due to reaction with e.g. O₃, OH and NO₃ radicals [Yu et al., 1999]. BVOCs can undergo a number of atmospheric degradation processes to produce a range of oxidized products, which in turn may or may not contribute to Secondary Organic Aerosol (SOA) formation and growth [Hoffmann et al., 1997, Tsigaridis and Kanakidou, 2007, Hallquist et al., 2009].

2 Motivation and Targets

As discussed above, NO_x and VOCs play an important role in relation to phenomena such as the formation of O_3 in urban and rural areas and the production of SOA leading to photochemically produced smog directly affecting human health. A deep understanding of both production and loss processes is therefore crucial. New, more sensitive sampling and measurement techniques have revealed a plethora of different VOCs (e.g. many sesquiterpenes) in the atmosphere that could not be detected a few years ago. Nevertheless, a large fraction of VOCs can, even today, not be measured or lack identification [Goldstein and Galbally, 2007]. Therefore, in order to access the overall influence of VOCs on the radical chemistry, apart from concentration measurements and stationary state considerations, reactivity measurements constitute an essential tool. Those measurements directly quantify the atmospheric loss rate constant for a specific compound taking into account all atmospheric trace gases. While this has been done for the OH radical in many different locations [Sinha et al., 2008, Nölscher et al., 2012, Lelieveld et al., 2016, Ferracci et al., 2018], no such measurement has been made for the nitrate radical.

Within the scope of this work an instrument for the measurement of the NO_3 -reactivity ($k_{\text{OTG}}^{\text{NO}_3}$, OTG = Organic Trace Gases) was developed. Data from several field campaigns is interpreted and further implications for VOC and NO_x removal are discussed. The simplified NO_3 formation and loss processes are displayed in Fig. 4.

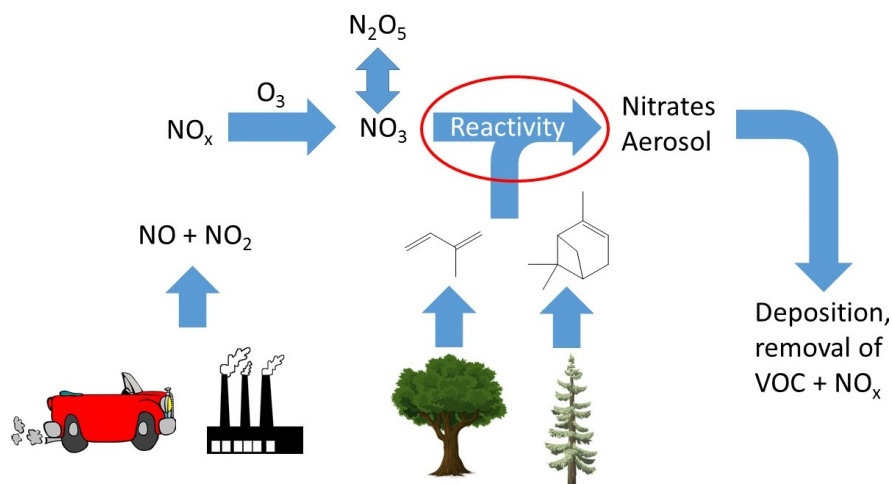


Figure 4: Basic scheme of NO_3 chemistry. The goal of this work i.e. measurement and interpretation of the NO_3 -reactivity - is highlighted by the red circle

Ambient NO_3 radical measurements were conducted in the past using, for example, cavity ring down spectroscopy (CRDS), cavity enhanced absorption spectroscopy (CEAS), chemical ionization mass spectrometry (CIMS) and differential optical absorption spectroscopy (DOAS). These techniques usually have a detection limit between 1 – 10 pptv [Ng et al., 2017], which may not be sufficient to detect NO_3 in locations with very high biogenic emissions or low NO_3 . By using NO_3 -reactivity measurements, this work aimed to calculate NO_3 mixing ratios in multiple locations where NO_3 measurements were not available or the radical concentration was under the detection limit of the specific instruments.

During the day, heating of the ground leads to a vertically very well mixed boundary layer that does not show strong gradients in NO_x and VOC mixing ratios. At night, mixing is vastly reduced and a very shallow boundary layer develops that can accumulate VOCs and NO_x . The residual layer above the nighttime boundary layer is however characterized by relatively clean air masses. This can make heterogeneous uptake of N_2O_5 in the residual layer the main loss process for NO_x , whereas NO_x loss in the nighttime boundary layer is dominated by reaction of NO_3 with VOCs. One aim of this work is to investigate the NO_3 -reactivity in the nighttime boundary layer as well as in the transition zone in between the boundary layer and the residual layer in different locations in Europe. Vertical gradients over 25 m were measured and possible sources and explanations for the obtained profiles are discussed.

To some extent, the NO_3 -reactivity can be calculated using measured VOCs and the corresponding rate constants. Yet, as indicated above, not all VOCs may be measured and the loss rate constant for reaction with NO_3 is not known for all compounds. In the scope of this work, the measured NO_3 -reactivity is compared to loss rate constants derived from measured VOCs and the missing reactivity in between both is discussed.

In recent literature, the role of NO_3 as a daytime oxidant is generally considered negligible due to rapid photolysis and fast reaction with NO [Brown et al., 2003, Crowley et al., 2010, Ng et al., 2017]. This work examined the role of NO_3 as a daytime oxidant and raises the question as to whether or not these assumptions can be maintained.

Ambient OH-reactivity measurements have also shown large amounts of reactivity that could not be accounted for by VOC measurements, especially in conditions of high temperatures and stressed vegetation [Nölscher et al., 2012, Ferracci et al., 2018]. With OH and NO_3 having different reaction mechanisms and rate constants, the question arises, whether a correlation in between both radical reactivities exists and whether or not missing reactivities may originate from the same VOCs. During an intensive measurement period, simultaneous NO_3 - and OH-reactivity measurements were conducted

at the Hohenpeissenberg whose results are presented and compared.

3 Discussion and results

3.1 Instrument development

The instrument used for the NO_3 -reactivity measurements is a technical evolution of an instrument formerly used for the detection of NO_3 and N_2O_5 [Schuster et al., 2009, Crowley et al., 2010]. For the reactivity measurements NO_3 and N_2O_5 are produced in situ using NO_2 and O_3 in a PTFE coated, darkened reactor (reaction time ≈ 5 min). After thermal decomposition of N_2O_5 at 140°C , NO_3 radicals (30-50 pptv) are mixed alternating with zero air/ambient air and passed through a flowtube (reaction time variable, usually 10.5 s). Cavity ring down spectroscopy is used to detect NO_3 at its absorption maximum at 662 nm. The change in concentration of NO_3 upon modulation of the bath gas between zero air and ambient air is used to derive its loss rate constant, which is then corrected for the contribution of NO (reaction R9), the formation of NO_3 from ambient NO_2 and O_3 (reaction R6) and for the formation and decomposition of N_2O_5 (reactions R10/R11) via numerical simulation. The derived loss rate constant $k_{\text{OTG}}^{\text{NO}_3}$ incorporates only the loss of NO_3 due to a reaction with VOCs. A detailed working scheme of the NO_3 -reactivity measurement is depicted in Fig. 5.

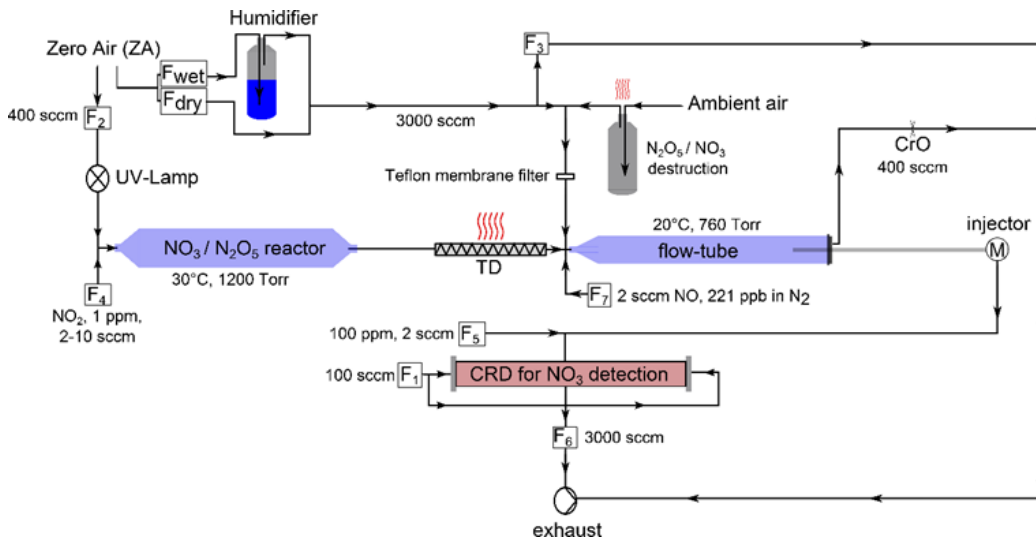


Figure 5: Schematic of the NO_3 -reactivity instrument

The instrument performs best in low NO_x and high VOC environments due to large uncertainties at high NO_x mixing ratios. A cavity for measurement of NO_2 was implemented in the setup as NO_2 mixing ratios are required for the derivation of $k_{\text{OTG}}^{\text{NO}_3}$. A detailed description of the instrument

as well as its characterization can be found in Appendix A1, the NO₂ cavity is described in Appendix A3.

3.2 Field campaigns

After the successful characterization of the instrument, it was deployed in Finland and Germany in the course of three different field campaigns. These campaigns represent two different topographical and meteorological scenarios. The NOTOMO campaign (NOcturnal chemistry at the Taunus Observatorium: Insights into Mechanisms of Oxidation) took place at the top of the Kleiner Feldberg mountain at the Taunus Observatory 20 km northwest of Frankfurt in summer 2015. The site is impacted by anthropogenic emission of NO_x and VOCs from urban areas (Frankfurt, Mainz, Wiesbaden) and local biogenic emissions from forested areas in the Taunus mountains. Previous studies encountered air masses from the nocturnal boundary layer as well as from the residual layer at this site [Sobanski et al., 2016]. NO₃ and N₂O₅ measurements were conducted simultaneously. NO and VOC measurements were not available, hence the obtained k_{RTG} (RTG = Reactive Trace Gases) includes the contribution of NO and cannot directly be compared to $k_{\text{OTG}}^{\text{NO}_3}$ obtained during the other campaigns. The NOTOMO campaign will therefore not be discussed in detail here.

The transition from summer to autumn was monitored in a Finnish boreal forest during the IB AIRN campaign (Influence of Biosphere-Atmosphere Interactions on the Reactive Nitrogen budget) in September 2016. The site, located in Hyytiälä, \approx 200 km north of Helsinki, is characterized by an extensive homogenous fetch with mostly biogenic origin. Previous campaigns reported NO₃ as well as N₂O₅ to be under the detection limit during a campaign in summer 2010 [Mogensen et al., 2015]. With two measurement towers (128 m and 35 m), the site offers good opportunities to investigate boundary layer dynamics and reactivity profiles. During IB AIRN, a large suite of other trace gas measurements such as NO, NO₂, NO₃, N₂O₅ and O₃ took place. The biogenic emissions were monitored by three independent mass spectrometers located at and around the NO₃-reactivity measurement site.

In summer 2017, the NO₃-reactivity was measured on a rural mountain site (Hoheneissenberg) in southern Germany. During nighttime, the air masses encountered often originated from the residual layer and hence represent a good opportunity to monitor the transition from the nocturnal boundary layer to the residual layer. The Meteorological Observatory Hoheneissenberg operates different atmospheric trace gas measurements (i.a. O₃, NO, NO₂, VOCs) and permanent OH-reactivity measurements.

The results from the IBAIRN campaign and the Hohenpeissenberg intensive measurement period are presented in the following sections.

3.3 Measurements of NO₃-reactivity and derived stationary state mixing ratios

In the Finnish boreal forest, nights were characterized by a strong temperature inversion and a very stable nocturnal boundary layer. The reactivity was generally high (maximum observed reactivity of 0.94 s⁻¹) and showed a strong diel variation pattern. On average, daytime reactivity was 0.04 s⁻¹ compared to 0.11 s⁻¹ at nighttime. This results in lifetimes of less than 10 s during nighttime. Stationary state NO₃ mixing ratios using $k_{\text{OTG}}^{\text{NO}_3}$ were constantly below < 1pptv. In good accordance to this, parallel NO₃ measurements could not find NO₃ mixing ratios exceeding the detection limit of the instrument (1.3 pptv) at the measurement site.

At the mountain site of the Hohenpeissenberg, measured NO₃ reactivities reached maximum values during daytime (max $k_{\text{OTG}}^{\text{NO}_3} = 0.31 \text{ s}^{-1}$) and were close or below the detection limit of the instrument ($k_{\text{OTG}}^{\text{NO}_3} \leq 0.005 \text{ s}^{-1}$, $\tau \geq 200 \text{ s}$) during nighttime. Evidence for air masses originating from the residual layer was found in O₃ and meteorological measurements. Stationary state NO₃ mixing ratios were in between 4-15 pptv which is in good agreement with one night of ambient NO₃ measurements that found 2-13 pptv of NO₃. Heterogeneous uptake of N₂O₅ as indirect NO₃ loss process played only a minor role at both measurement sites.

3.4 Vertical reactivity profiles

During IBAIRN, vertical reactivity gradients found the highest values near ground decreasing rapidly above canopy height. During day, no gradient could be found due to efficient mixing within the boundary layer. We conclude, that on the one hand, reactive emissions near ground from microbial activity as well as decomposing litter, and on the other hand, the strong temperature inversion with reduced mixing below the canopy induced this gradient.

3.5 NO₃-reactivity calculated from measured VOCs

According to Eq. 2, VOC measurements were used to calculate a NO₃ loss rate, $k_{\text{VOC}}^{\text{NO}_3}$, from the corresponding measured terpenoids ($[C_i]$) and their individual rate coefficients ($k_i^{\text{NO}_3}$).

$$k_{\text{VOC}}^{\text{NO}_3} = \sum k_i^{\text{NO}_3} [C_i] \quad (2)$$

Subtraction of $k_{\text{VOC}}^{\text{NO}_3}$ from $k_{\text{OTG}}^{\text{NO}_3}$ results in a missing reactivity that VOC measurements can not account for (Eq. 3).

$$\text{missing reactivity} = k_{\text{OTG}}^{\text{NO}_3} - k_{\text{VOC}}^{\text{NO}_3} \quad (3)$$

Monoterpenes determined the NO_3 -reactivity at both measurement sites with minor contributions from isoprene. Other measured VOCs were found to be insignificant for the NO_3 -reactivity due to low mixing ratios or low rate coefficients (e.g. alkenes, aldehydes, alkanes and aromatic compounds). Measurements of sesquiterpenes were not available at both locations. During IBAIRN, measured VOCs accounted for 70% of the measured reactivity at nighttime and 40% at daytime, indicating a significant fraction of missing reactivity. This missing reactivity is possibly a result of reactive compounds (e.g. sesquiterpenes) that were not covered by the VOC measurements, but have a sufficiently fast rate coefficient to react with NO_3 [Duhl et al., 2008, IUPAC, 2018]. We did not find a clear seasonal reduction in the VOC mixing ratios during the ongoing transition from summer to autumn in the course of the campaign. During the intensive period at the Hohenpeissenberg, the calculated loss rate $k_{\text{VOC}}^{\text{NO}_3}$ could account for 65% of the measured $k_{\text{OTG}}^{\text{NO}_3}$. Considering the uncertainties of both measurements, the missing reactivity was not significant.

3.6 Contribution to NO_x losses

The high reactivities observed in both campaigns raise the question whether $k_{\text{OTG}}^{\text{NO}_3}$ can compete with photolysis and reaction with NO during daytime. We found that on average in both, the boreal forest as well as on the Hohenpeissenberg, no less than 20% of the formed NO_3 reacts with BVOCs at the peak of the actinic flux. The contribution grows in the late afternoon up to 60% and approaches 100% at nighttime. These results imply that NO_3 radicals are an important daytime oxidant for biogenic VOCs in forested areas, affecting the diel cycle of organic nitrates and SOA formation.

3.7 Comparison of NO_3 - and OH-reactivity

During the intensive period at the Hohenpeissenberg, we conducted the first simultaneous measurements of NO_3 - and OH-reactivity. For a better comparison, we subtracted the contributions of organic and inorganic trace gases (NO , NO_2 , CH_4 , CO , SO_2) from the total measured OH-reactivity that are

not considered in $k_{\text{OTG}}^{\text{NO}_3}$ or do not react to a significant extent with NO_3 to derive $k_{\text{OTG}}^{\text{OH}}$. The OH radical showed a diel profile with high daytime and low nighttime reactivities similar to the diel profile of $k_{\text{OTG}}^{\text{NO}_3}$. In general, the correlation between OH- and NO_3 -reactivity was weak as their divergent trends in rate constants with many organic trace gases already suggest. During nighttime, a tighter correlation dominated by a less variable, isoprene like reactivity was observed. During daytime, more complex and variable air masses led to a weaker correlation.

4 Conclusion and outlook

Within the scope of this work a new instrument for the measurement of NO_3 -reactivity was developed and successfully deployed in three different field campaigns. Observations showed a highly variable NO_3 -reactivity that is driven by boundary layer dynamics coupled with biogenic emissions. Simultaneously made VOC measurements indicated that biogenic monoterpene emissions are the dominating loss process for NO_3 . Yet, measured VOCs could not account for the entire measured reactivity indicating the presence of not detected organic trace gases. Stationary state radical mixing ratios using $k_{\text{OTG}}^{\text{NO}_3}$ were found to be in good agreement with the measured NO_3 mixing ratios. Vertical reactivity profiles in the boreal forest revealed the highest values near ground probably originating from microbial activity, decomposition of needle litter and a strong temperature inversion. Furthermore, it was found that a significant fraction of NO_3 reacts with VOCs during daytime representing a NO_x loss and a possible source of SOA. The comparison of direct NO_3 and OH-reactivity measurements showed only a very weak correlation as it was already implied by the different rate coefficients and reaction mechanisms of both radicals.

For future projects, a closer analysis of the daytime chemistry of NO_3 is certainly rewarding. During IBAIRN, PANs and ANs were measured and can be used to investigate whether daytime NO_x loss by reaction of NO_3 and VOCs can compete with OH induced NO_x loss. Modeling studies would be a worthy tool to explore the influence of daytime NO_3 chemistry globally.

Another interesting aspect is the measurement of reactivity- and VOC profiles simultaneously in order to investigate the strong vertical gradients in reactivities near ground, observed in the boreal forest. Chamber experiments of ground emissions could help to clarify if the reactivity is primarily a result of ground emissions or rather an effect of strong gradients in the nocturnal boundary layer. More over, reactivity measurements in combination with the measurement of sesquiterpenes are recommended to investigate in how far these compounds can account for missing reactivities observed during IBAIRN.

References

- J. F. Arenas, F. J. Avila, J. C. Otero, D. Peláez, and J. Soto. Approach to the atmospheric chemistry of methyl nitrate and methylperoxy nitrite. chemical mechanisms of their formation and decomposition reactions in the gas phase. *J. Phys. Chem. A*, 112(2):249–255, 2008. doi: 10.1021/jp075546n.
- R. Atkinson. Atmospheric chemistry of VOCs and NO_x. *Atmos. Environ.*, 34(12):2063–2101, 2000. doi: 10.1016/S1352-2310(99)00460-4.
- S. Avnery, D. L. Mauzerall, J. Liu, and L. W. Horowitz. Global crop yield reductions due to surface ozone exposure: 2. year 2030 potential crop production losses and economic damage under two scenarios of O₃ pollution. *Atmos. Environ.*, 45(13):2297–2309, 2011. doi: 10.1016/j.atmosenv.2011.01.002.
- W. Behnke, H.-U. Krüger, V. Scheer, and C. Zetzsch. Formation of ClNO₂ and HONO in the presence of NO₂, O₃ and wet NaCl aerosol. *J. Aerosol. Sci.*, 23:933–936, 1992.
- W. Behnke, C. George, V. Scheer, and C. Zetzsch. Production and decay of ClNO₂ from the reaction of gaseous N₂O₅ with NaCl solution: Bulk and aerosol experiments. *J. Geophys. Res.-Atmos.*, 102:3795–3804, 1997. doi: 10.1029/96JD03057.
- S. S. Brown, H. Stark, and A. R. Ravishankara. Applicability of the steady state approximation to the interpretation of atmospheric observations of NO₃ and N₂O₅. *J. Geophys. Res.-Atmos.*, 108(D17), 2003. doi: 10.1029/2003JD003407.
- S. H. M. Butchart, M. Walpole, B. Collen, A. van Strien, J. P. W. Scharlemann, R. E. A. Almond, J. E. M. Baillie, B. Bomhard, C. Brown, J. Bruno, K. E. Carpenter, G. M. Carr, J. Chanson, A. M. Chenery, J. Csirke, N. C. Davidson, F. Dentener, M. Foster, A. Galli, J. N. Galloway, P. Genovesi, R. D. Gregory, M. Hockings, V. Kapos, J. F. Lamarque, F. Leverington, J. Loh, M. A. McGeoch, L. McRae, A. Minasyan, M. H. Morcillo, T. E. E. Oldfield, D. Pauly, S. Quader, C. Revenga, J. R. Sauer, B. Skolnik, D. Spear, D. Stanwell-Smith, S. N. Stuart, A. Symes, M. Tierney, T. D. Tyrrell, J. C. Vie, and R. Watson. Global biodiversity: Indicators of recent declines. *Science*, 328(5982):1164–1168, 2010. doi: 10.1126/science.1187512.
- P. Ciais, C. Sabine, G. Bala, L. Bopp, V. Brovkin, J. Canadell, A. Chhabra, R. DeFries, J. Galloway, M. Heimann, C. Jones, C. Le Quéré, R. Myneni,

- S. Piao, and P. Thornton. *Carbon and Other Biogeochemical Cycles*, book section 6, pages 465–570. Cambridge University Press, Cambridge, United Kingdom and New York, NY, USA, 2013. ISBN 978-1-107-66182-0. doi: 10.1017/CBO9781107415324.015.
- R. Conrad. Soil microorganisms as controllers of atmospheric trace gases (H_2 , CO , CH_4 , OCS , N_2O , and NO). *Microbiol. Rev.*, 60(4):609–640, 1996.
- J. Crowley, G. Schuster, N. Pouvesle, U. Parchatka, H. Fischer, B. Bonn, H. Bingemer, and J. Lelieveld. Nocturnal nitrogen oxides at a rural mountain site in south-western Germany. *Atmos. Chem. Phys.*, 10:2795–2812, 2010. doi: 10.5194/acp-10-2795-2010.
- K. R. Darnall, W. P. L. Carter, A. M. Winer, A. C. Lloyd, and J. N. Pitts. Importance of RO_2 + nitric oxide in alkyl nitrate formation from C4-C6 alkane photooxidations under simulated atmospheric conditions. *J. Phys. Chem.*, 80(17):1948–1950, 1976. doi: 10.1021/j100558a029.
- F. J. Dentener and P. J. Crutzen. Reaction of N_2O_5 on tropospheric aerosols: Impact on the global distributions of NO_x , O_3 , and OH . *J. Geophys. Res.-Atmos.*, 98(D4):7149–7163, 1993. doi: 10.1029/92JD02979.
- R. G. Derwent, M. E. Jenkin, N. R. Passant, and M. J. Pilling. Photochemical ozone creation potentials (POCPs) for different emission sources of organic compounds under European conditions estimated with a master chemical mechanism. *Atmos. Environ.*, 41(12):2570–2579, 2007. doi: 10.1016/j.atmosenv.2006.11.019.
- T. R. Duhl, D. Helmig, and A. Guenther. Sesquiterpene emissions from vegetation: A review. *Biogeosciences*, 5(3):761–777, 2008. doi: 10.5194/bg-5-761-2008.
- M. Ehn, J. A. Thornton, E. Kleist, M. Sipila, H. Junninen, I. Pullinen, M. Springer, F. Rubach, R. Tillmann, B. Lee, F. Lopez-Hilfiker, S. Andres, I. H. Acir, M. Rissanen, T. Jokinen, S. Schobesberger, J. Kangasluoma, J. Kontkanen, T. Nieminen, T. Kurten, L. B. Nielsen, S. Jorgensen, H. G. Kjaergaard, M. Canagaratna, M. Dal Maso, T. Berndt, T. Petaja, A. Wahner, V. M. Kerminen, M. Kulmala, D. R. Worsnop, J. Wildt, and T. F. Mentel. A large source of low-volatility secondary organic aerosol. *Nature*, 506(7489):476–479, 2014. doi: 10.1038/nature13032.
- V. Ferracci, I. Heimann, N. L. Abraham, J. A. Pyle, and A. T. Archibald. Global modelling of the total OH reactivity: Investigations on the "miss-

- ing” OH sink and its atmospheric implications. *Atmos. Chem. Phys. Discuss.*, 2018:1–33, 2018. doi: 10.5194/acp-2018-12.
- J. N. Galloway, F. J. Dentener, D. G. Capone, E. W. Boyer, R. W. Howarth, S. P. Seitzinger, G. P. Asner, C. C. Cleveland, P. A. Green, E. A. Holland, D. M. Karl, A. F. Michaels, J. H. Porter, A. R. Townsend, and C. J. Vorosmarty. Nitrogen cycles: Past, present, and future. *Biogeochemistry*, 70(2):153–226, 2004. doi: 10.1007/s10533-004-0370-0.
- S. Gligorovski, R. Strekowski, S. Barbati, and D. Vione. Environmental implications of hydroxyl radicals ($\cdot\text{OH}$). *Chem. Rev.*, 115(24):13051–13092, 2015. doi: 10.1021/cr500310b.
- A. H. Goldstein and I. E. Galbally. Known and unexplored organic constituents in the Earth’s atmosphere. *Envir. Sci. Tech.*, 41(5):1514–1521, 2007. doi: 10.1021/es072476p.
- A. B. Guenther, X. Jiang, C. L. Heald, T. Sakulyanontvittaya, T. Duhl, L. K. Emmons, and X. Wang. The model of emissions of gases and aerosols from nature version 2.1 (MEGAN2.1): an extended and updated framework for modeling biogenic emissions. *Geosci. Model Dev.*, 5(6):1471–1492, 2012. doi: 10.5194/gmd-5-1471-2012.
- A. J. Haagen-Smit, C. E. Bradley, and M. M. Fox. Ozone formation in photochemical oxidation of organic substances. *Ind. Eng. Chem.*, 45(9):2086–2089, 1953. doi: 10.1021/ie51400a033.
- M. Hallquist, J. C. Wenger, U. Baltensperger, Y. Rudich, D. Simpson, M. Claeys, J. Dommen, N. M. Donahue, C. George, A. H. Goldstein, J. F. Hamilton, H. Herrmann, T. Hoffmann, Y. Iinuma, M. Jang, M. E. Jenkin, J. L. Jimenez, A. Kiendler-Scharr, W. Maenhaut, G. McFiggans, T. F. Mentel, A. Monod, A. S. H. Prevot, J. H. Seinfeld, J. D. Surratt, R. Szmigielski, and J. Wildt. The formation, properties and impact of secondary organic aerosol: Current and emerging issues. *Atmos. Chem. Phys.*, 9(14):5155–5236, 2009. doi: 10.5194/acp-9-5155-2009.
- D. Hartmann, A. Klein Tank, M. Rusticucci, L. Alexander, S. Brönnimann, Y. Charabi, F. Dentener, E. Dlugokencky, D. Easterling, A. Kaplan, B. Soden, P. Thorne, M. Wild, and P. Zhai. *Observations: Atmosphere and Surface*, book section 2, pages 159–254. Cambridge University Press, Cambridge, United Kingdom and New York, NY, USA, 2013. ISBN 978-1-107-66182-0. doi: 10.1017/CBO9781107415324.008.

- A. Hilboll, A. Richter, and J. P. Burrows. Long-term changes of tropospheric NO₂ over megacities derived from multiple satellite instruments. *Atmos. Chem. Phys.*, 13(8):4145–4169, 2013. doi: 10.5194/acp-13-4145-2013.
- T. Hoffmann, J. R. Odum, F. Bowman, D. Collins, D. Klockow, R. C. Flagan, and J. H. Seinfeld. Formation of organic aerosols from the oxidation of biogenic hydrocarbons. *J. Atmos. Chem.*, 26(2):189–222, 1997. doi: 10.1023/A:1005734301837.
- IUPAC. Task group on atmospheric chemical kinetic data evaluation (Ammann, M., Cox, R.A., Crowley, J.N., Herrmann, H., Jenkin, M.E., McNeill, V.F., Mellouki, A., Rossi, M. J., Troe, J. and Wallington, T. J.). <http://iupac.pole-ether.fr/index.html>, 2018.
- M. Kampa and E. Castanas. Human health effects of air pollution. *Environ. Pollut.*, 151(2):362–367, 2008. doi: 10.1016/j.envpol.2007.06.012.
- J. Kesselmeier and M. Staudt. Biogenic volatile organic compounds (VOC): An overview on emission, physiology and ecology. *Atmos. Chem. Phys.*, 33(1):23–88, 1999. doi: 10.1023/a:1006127516791.
- P. A. Leighton. *Photochemistry of Air Pollution*. Academic Press, 1961.
- J. Lelieveld and F. J. Dentener. What controls tropospheric ozone? *J. Geophys. Res-Atmos.*, 105(D3):3531–3551, 2000. doi: 10.1029/1999JD901011.
- J. Lelieveld, H. Berresheim, S. Borrmann, P. J. Crutzen, F. J. Dentener, H. Fischer, J. Feichter, P. J. Flatau, J. Heland, R. Holzinger, R. Korrman, M. G. Lawrence, Z. Levin, K. M. Markowicz, N. Mihalopoulos, A. Minikin, V. Ramanathan, M. de Reus, G. J. Roelofs, H. A. Scheeren, J. Sciare, H. Schlager, M. Schultz, P. Siegmund, B. Steil, E. G. Stephanou, P. Stier, M. Traub, C. Warneke, J. Williams, and H. Ziereis. Global air pollution crossroads over the mediterranean. *Science*, 298(5594):794–799, 2002.
- J. Lelieveld, S. Gromov, A. Pozzer, and D. Taraborrelli. Global tropospheric hydroxyl distribution, budget and reactivity. *Atmos. Chem. Phys.*, 16(19):12477–12493, 2016. doi: 10.5194/acp-16-12477-2016.
- D. J. Li. Emissions of NO and NH₃ from a typical vegetable-land soil after the application of chemical N fertilizers in the pearl river delta. *Plos One*, 8(3):1–8, 2013. doi: 10.1371/journal.pone.0059360.

- D. Mogensen, R. Gierens, J. N. Crowley, P. Keronen, S. Smolander, A. Sogachev, A. C. Nölscher, L. Zhou, M. Kulmala, M. J. Tang, J. Williams, and M. Boy. Simulations of atmospheric OH, O₃ and NO₃ reactivities within and above the boreal forest. *Atmos. Chem. Phys.*, 15(7):3909–3932, 2015. doi: 10.5194/acp-15-3909-2015.
- N. Nakicenovic and R. Swart. *IPCC Emissions Scenarios*. Cambridge University Press, 2000.
- B. A. Nault, C. Garland, S. E. Pusede, P. J. Wooldridge, K. Ullmann, S. R. Hall, and R. C. Cohen. Measurements of CH₃O₂NO₂ in the upper troposphere. *Atmos. Meas. Tech.*, 8(2):987–997, 2015. doi: doi:10.5194/amt-8-987-2015.
- N. L. Ng, A. J. Kwan, J. D. Surratt, A. W. H. Chan, P. S. Chhabra, A. So-rooshian, H. O. T. Pye, J. D. Crouse, P. O. Wennberg, R. C. Flagan, and J. H. Seinfeld. Secondary organic aerosol (SOA) formation from reaction of isoprene with nitrate radicals (NO₃). *Atmos. Chem. Phys.*, 8(14): 4117–4140, 2008. doi: 10.5194/acp-8-4117-2008.
- N. L. Ng, S. S. Brown, A. T. Archibald, E. Atlas, R. C. Cohen, J. N. Crowley, D. A. Day, N. M. Donahue, J. L. Fry, H. Fuchs, R. J. Griffin, M. I. Guzman, H. Herrmann, A. Hodzic, Y. Iinuma, J. L. Jimenez, A. Kiendler-Scharr, B. H. Lee, D. J. Luecken, J. Mao, R. McLaren, A. Mutzel, H. D. Osthoff, B. Ouyang, B. Picquet-Varrault, U. Platt, H. O. T. Pye, Y. Rudich, R. H. Schwantes, M. Shiraiwa, J. Stutz, J. A. Thornton, A. Tilgner, B. J. Williams, and R. A. Zaveri. Nitrate radicals and biogenic volatile organic compounds: oxidation, mechanisms, and organic aerosol. *Atmos. Chem. Phys.*, 17(3):2103–2162, 2017. doi: 10.5194/acp-17-2103-2017.
- A. C. Nölscher, J. Williams, V. Sinha, T. Custer, W. Song, A. M. Johnson, R. Axinte, H. Bozem, H. Fischer, N. Pouvesle, G. Phillips, J. N. Crowley, P. Rantala, J. Rinne, M. Kulmala, D. Gonzales, J. Valverde-Canossa, A. Vogel, T. Hoffmann, H. G. Ouwersloot, J. Vil  -Guerau de Arellano, and J. Lelieveld. Summertime total OH reactivity measurements from boreal forest during HUMPPA-COPEC 2010. *Atmos. Chem. Phys.*, 12(17):8257–8270, 2012. doi: 10.5194/acp-12-8257-2012.
- G. J. Phillips, J. Thieser, M. J. Tang, N. Sobanski, G. Schuster, J. Fachinger, F. Drewnick, S. Borrmann, H. Bingemer, J. Lelieveld, and J. N. Crowley. Estimating N₂O₅ uptake coefficients using ambient measurements of NO₃, N₂O₅, ClNO₂ and particle-phase nitrate. *Atmos. Chem. Phys.*, 16(20): 13231–13249, 2016. doi: 10.5194/acp-16-13231-2016.

- U. Platt, D. Perner, A. Winer, G. Harris, and J. J. Pitts. Detection of NO_3 in the polluted troposphere by differential optical absorption. *Geophys. Res. Lett.*, 7:89–92, 1980. doi: 10.1029/GL007i001p00089.
- J. M. Roberts. The atmospheric chemistry of organic nitrates. *Atmos. Environ. A*, 24(2):243–287, 1990. doi: 10.1016/0960-1686(90)90108-Y.
- G. Schuster, I. Labazan, and J. Crowley. A cavity ring down / cavity enhanced absorption device for measurement of ambient NO_3 and N_2O_5 . *Atmo. Meas. Tech.*, 2:1–13, 2009. doi: 10.5194/amt-2-1-2009.
- H. B. Singh and P. L. Hanst. Peroxyacetyl nitrate (PAN) in the unpolluted atmosphere - An important reservoir for nitrogen-oxides. *Geophys. Res. Lett.*, 8(8):941–944, 1981. doi: 10.1029/GL008i008p00941.
- V. Sinha, J. Williams, J. N. Crowley, and J. Lelieveld. The comparative reactivity method - a new tool to measure total OH reactivity in ambient air. *Atmos. Chem. Phys.*, 8(8):2213–2227, 2008.
- K. Skalska, J. S. Miller, and S. Ledakowicz. Trends in NO_x abatement: A review. *Sci. Total Environ.*, 408(19):3976–3989, 2010. doi: 10.1016/j.scitotenv.2010.06.001.
- N. Sobanski, M. J. Tang, J. Thieser, G. Schuster, D. Pöhler, H. Fischer, W. Song, C. Sauvage, J. Williams, J. Fachinger, F. Berkes, P. Hoor, U. Platt, J. Lelieveld, and J. N. Crowley. Chemical and meteorological influences on the lifetime of NO_3 at a semi-rural mountain site during parade. *Atmos. Chem. Phys.*, 16(8):4867–4883, 2016. doi: 10.5194/acp-16-4867-2016.
- W. Steffen, P. J. Crutzen, and J. R. McNeill. The anthropocene: Are humans now overwhelming the great forces of nature. *Ambio*, 36(8):614–621, 2007. doi: 10.1579/0044-7447(2007)36[614:taahno]2.0.co;2.
- J. Tröstl, W. K. Chuang, H. Gordon, M. Heinritzi, C. Yan, U. Molteni, L. Ahlm, C. Frege, F. Bianchi, R. Wagner, M. Simon, K. Lehtipalo, C. Williamson, J. S. Craven, J. Duplissy, A. Adamov, J. Almeida, A.-K. Bernhammer, M. Breitenlechner, and U. Baltensperger. The role of low-volatility organic compounds in initial particle growth in the atmosphere. *Nature*, 533:527–531, 2016. doi: 10.1038/nature18271.
- K. Tsigaridis and M. Kanakidou. Secondary organic aerosol importance in the future atmosphere. *Atmos. Environ.*, 41(22):4682–4692, 2007. doi: 10.1016/j.atmosenv.2007.03.045.

- R. P. Wayne, I. Barnes, P. Biggs, J. P. Burrows, C. E. Canosamas, J. Hjorth, G. Lebras, G. K. Moortgat, D. Perner, G. Poulet, G. Restelli, and H. Sidebottom. The nitrate radical - Physics, chemistry, and the atmosphere. *Atmos. Environ.*, 25(1):1–203, 1991. doi: [https://doi.org/10.1016/0960-1686\(91\)90192-A](https://doi.org/10.1016/0960-1686(91)90192-A).
- D. J. Wuebbles and K. Hayhoe. Atmospheric methane and global change. *Earth-Sci. Rev.*, 57(3):177–210, 2002. doi: 10.1016/S0012-8252(01)00062-9.
- J. Z. Yu, D. R. Cocker, R. J. Griffin, R. C. Flagan, and J. H. Seinfeld. Gas-phase ozone oxidation of monoterpenes: Gaseous and particulate products. *J. Atmos. Chem.*, 34(2):207–258, 1999. doi: 10.1023/a:1006254930583.
- Y. B. Zel'dovich and Y. P. Raizer. *Physics Of Shock Waves and High-temperature Hydrodynamic Phenomena*. Academic Press, 1966.
- Y. Zhang and J. R. Morris. Hydrogen abstraction probability in reactions of gas-phase NO₃ with an OH-functionalized organic surface. *J. Phys. Chem. C*, 119(26):14742–14747, 2015. doi: 10.1021/acs.jpcc.5b00562.

Appendix - Publications

A1: Measurement of ambient NO₃ reactivity: Design, characterization and first deployment of a new instrument

Liebmann, J. M., Schuster, G., Schuladen, J. B., Sobanski, N., Lelieveld, J., and Crowley, J. N.: *Measurement of ambient NO₃ reactivity: design, characterization and first deployment of a new instrument*, Atmos. Meas. Tech., 10, 1241-1258, <https://doi.org/10.5194/amt-10-1241-2017>, **2017**.

A2: Direct measurement of NO₃ reactivity in a boreal forest

Liebmann, J., Karu, E., Sobanski, N., Schuladen, J., Ehn, M., Schallhart, S., Quéléver, L., Hellen, H., Hakola, H., Hoffmann, T., Williams, J., Fischer, H., Lelieveld, J., and Crowley, J. N.: *Direct measurement of NO₃ reactivity in a boreal forest*, Atmos. Chem. Phys., 18, 3799-3815, <https://doi.org/10.5194/acp-18-3799-2018>, **2018**.

A3: Direct measurements of NO₃-reactivity in and above the boundary layer of a mountain-top site: Identification of reactive trace gases and comparison with OH-reactivity.

Liebmann, J., Muller, J. B. A., T., Kubistin, D., Claude, A., Holla, R., Plaß-Dülmer, C., Lelieveld, J., and Crowley, J. N.: *Direct measurements of NO₃ reactivity in and above the boundary layer of a mountain-top site: Identification of reactive trace gases and comparison with OH-reactivity.*, submitted to: Atmos. Chem. Phys., 26.03.2018.

A1: Liebmann et al., Atmos. Meas. Tech., 2017

**Measurement of ambient NO₃ reactivity: Design, characterization
and first deployment of a new instrument**

**Jonathan M. Liebmann¹, Gerhard Schuster¹, Jan B. Schuladen¹, Nicolas
Sobanski¹, Jos Lelieveld¹, and John N. Crowley¹**

¹ *Atmospheric Chemistry Department, Max-Planck-Institut für Chemie,
55128 Mainz, Germany*

Atmospheric Measurement Techniques, 10, 1241-1258, 2017



Measurement of ambient NO₃ reactivity: design, characterization and first deployment of a new instrument

Jonathan M. Liebmann, Gerhard Schuster, Jan B. Schuladen, Nicolas Sobanski, Jos Lelieveld, and John N. Crowley

Atmospheric Chemistry Department, Max-Planck-Institut für Chemie, 55128 Mainz, Germany

Correspondence to: John N. Crowley (john.crowley@mpic.de)

Received: 23 November 2016 – Discussion started: 29 November 2016

Revised: 1 March 2017 – Accepted: 3 March 2017 – Published: 30 March 2017

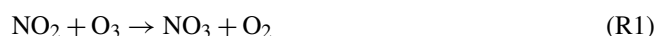
Abstract. We describe the first instrument for measurement of the rate constant (s^{-1}) for reactive loss (i.e., the total reactivity) of NO₃ in ambient air. Cavity-ring-down spectroscopy is used to monitor the mixing ratio of synthetically generated NO₃ (≈ 30 – 50 pptv) after passing through a flow-tube reactor with variable residence time (generally 10.5 s). The change in concentration of NO₃ upon modulation of the bath gas between zero air and ambient air is used to derive its loss rate constant, which is then corrected for formation and decomposition of N₂O₅ via numerical simulation. The instrument is calibrated and characterized using known amounts of NO and NO₂ and tested in the laboratory with an isoprene standard. The lowest reactivity that can be detected (defined by the stability of the NO₃ source, instrumental parameters and NO₂ mixing ratios) is $0.005 s^{-1}$. An automated dilution procedure enables measurement of NO₃ reactivities up to $45 s^{-1}$, this upper limit being defined mainly by the dilution accuracy. The typical total uncertainty associated with the reactivity measurement at the center of its dynamic range is 16 %, though this is dependent on ambient NO₂ levels. Results from the first successful deployment of the instrument at a forested mountain site with urban influence are shown and future developments outlined.

1 Introduction

Large amounts of biogenic and anthropogenic trace gases are emitted annually into the atmosphere. Recent estimates (Guenther et al., 2012) suggest that about 1000 Tg of biogenic volatile organic compounds (VOCs), especially isoprene (contributing 50 %) and monoterpenes (15 %), are emitted annually by vegetation. The global burden of anthro-

pogenic emission is dominated by CO₂, CO, N₂O, CH₄, SO₂, NO₂ and organic carbon, the latter contributing about 11 Tg (Huang et al., 2015). In particular, nitrogen oxides from combustion and microbial activity in soils have a major impact on the chemistry of the natural atmosphere (Crutzen, 1973). Most VOCs are oxidized efficiently in the Earth's boundary layer, the oxidizing capacity of which represents 15 % of that of the entire atmosphere (Lelieveld et al., 2016). Biogenic and anthropogenic VOCs have a significant impact on air quality and human health and knowing and understanding their lifetimes, which are determined by the oxidizing capacity of the atmosphere, is a prerequisite to predicting future atmospheric composition and related climate phenomena (Lelieveld et al., 2008).

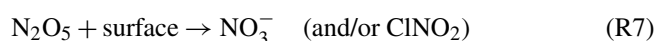
During daytime, photochemically formed OH radicals represent the dominant contribution to the oxidative capacity of the atmosphere. As OH levels are vastly reduced in the absence of sunlight, the NO₃ radical (formed by reaction of NO₂ with O₃; Reaction R1) is the major oxidizing agent at elevated NO_x for many biogenic terpenoids and other unsaturated compounds at nighttime (Wayne et al., 1991; Atkinson, 2000; Atkinson and Arey, 2003a, b; Brown and Stutz, 2012; Ng et al., 2017).



NO₃ reacts rapidly with NO (Reaction R2, rate constant $2.6 \times 10^{-11} \text{ cm}^3 \text{ molecule}^{-1} \text{ s}^{-2}$ at 298 K; Atkinson et al., 2004) and undergoes rapid photolysis (Reactions R5, R6) so that its lifetime is usually of the order of seconds during the day and its concentration too low for it to be considered an important daytime oxidant.

At night, NO₃ can react with NO₂, forming N₂O₅, which thermally decomposes to set up a thermal equilibrium between NO₂, NO₃ and N₂O₅ (Reactions R3, R4) with N₂O₅

formation favored by lower temperatures. As both NO₃ and N₂O₅ are formed from NO_x (NO_x = NO + NO₂) the loss of either NO₃ via gas-phase reactions or N₂O₅ via heterogeneous uptake to particles or deposition implies a reduction in NO_x, and thus a reduction in the rate of photochemical O₃ formation (Dentener and Crutzen, 1993). In addition, heterogeneous loss of N₂O₅ can also result in release of ClNO₂ from chloride-containing particles (Reaction R7) (Osthoff et al., 2008; Thornton et al., 2010; Mielke et al., 2011; Phillips et al., 2012; Riedel et al., 2012). The main loss processes of NO₃ are summarized in Fig. 1.



In rural and forested areas, reaction with biogenic VOCs can dominate the loss of NO₃ (Mogensen et al., 2015). Especially terpenoids like limonene ($k = 1.2 \times 10^{-11} \text{ cm}^3 \text{ molecule}^{-1} \text{ s}^{-1}$), α -pinene ($k = 6.2 \times 10^{-12} \text{ cm}^3 \text{ molecule}^{-1} \text{ s}^{-1}$) and isoprene ($k = 6.5 \times 10^{-13} \text{ cm}^3 \text{ molecule}^{-1} \text{ s}^{-1}$) have high rate constants for reaction with NO₃ (IUPAC, 2016; Ng et al., 2017). In such environments, when NO_x levels are low, NO₃ mixing ratios may be sub-pptv and below the detection limit for most instruments (Rinne et al., 2012).

The reaction of NO₃ with trace gases containing unsaturated C=C bonds proceeds via addition to form nitrooxyalkyl radicals that undergo rapid reaction with O₂ to form nitrooxyalkyl peroxy radicals. The peroxy radicals react further (with HO₂, NO, NO₂ or NO₃), to form multifunctional organic nitrates, which can contribute to generation and growth of secondary organic aerosols (Fry et al., 2014; Ng et al., 2017) or be lost by deposition.

The role of NO₃ as an oxidizing agent may be assessed via its total reactivity (or inverse lifetime). Whereas for OH, experimental methods for measuring total reactivity in ambient air exist (Kovacs and Brune, 2001; Sinha et al., 2008), NO₃ reactivity has not yet been directly measured. Stationary-state approximations have often been used to calculate NO₃ lifetimes from its mixing ratio and production rate, the latter being given by $k_1[\text{NO}_2][\text{O}_3]$ (Heintz et al., 1996; Geyer and Platt, 2002; Brown et al., 2007a, b, 2009; Sobanski et al., 2016b). Thus the stationary-state turnover lifetime, τ_{ss} , can be calculated according to Eq. (1), where k_1 is the rate constant for Reaction (R1).

$$k_{\text{ss}} = \frac{1}{\tau_{\text{ss}}} = \frac{k_1 [\text{O}_3][\text{NO}_2]}{[\text{NO}_3]} \quad (1)$$

This method is applicable when the chemical lifetime of NO₃ is sufficiently short so that stationary state can be achieved

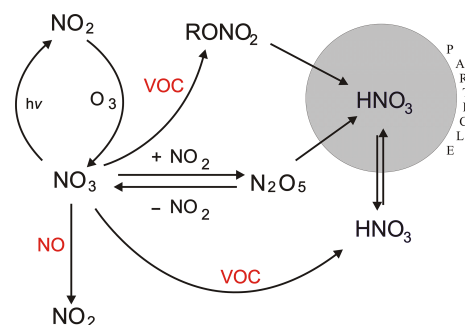


Figure 1. Gas-phase formation and loss of tropospheric NO₃, indicating processes which transfer reactive nitrogen to the particle phase. RONO₂ are alkyl nitrates. VOC is volatile organic compound.

within transport time from emission to measurement location (Brown et al., 2003). Formally it is achieved when the production and loss of NO₃ and N₂O₅ are balanced (Brown et al., 2003; Crowley et al., 2011). The time to acquire stationary state depends on production and loss rates for NO₃ and N₂O₅ and can take several hours. This approach can break down under conditions of moderate to high NO₂ levels, strong sinks, low temperatures or very clean air masses in which the sinks for NO₃ and N₂O₅ become small (Brown et al., 2003). Indeed, Sobanski et al. (2016b) observed much lower stationary-state loss rates compared to those calculated from measured VOC mixing ratios during the PARADE 2011 campaign and concluded that this was mainly the result of sampling from a low-lying residual layer with VOC emissions that were too close for NO₃ concentrations to achieve stationary state. They also considered the possibility that NO₃ may be formed by the oxidation of NO₂ by Criegee intermediates, which would bias calculations of its reactivity.

Summarizing, NO₃ reactivity with respect to gas-phase losses is an indication of nighttime oxidation rates of VOCs, with direct impacts on NO_x levels by forming long-lived reservoir species (alkyl nitrates), some of which will partition to the particle phase. Via modification of N₂O₅ concentrations (formed in an association reaction of NO₃ with NO₂, Reaction R3), the NO₃ reactivity indirectly controls heterogeneous NO_x losses and ClNO₂ formation rates.

In this paper we describe a newly developed instrument that enables point measurements of NO₃ reactivity in ambient air. After introducing the methodology in Sect. 2, we show the results of extensive laboratory characterization of the instrument along with discussion of the uncertainties associated with those measurements in Sects. 3 to 5. In Sect. 6 we present a data set of ambient NO₃ reactivity obtained at a forested/urban location in southwestern Germany.

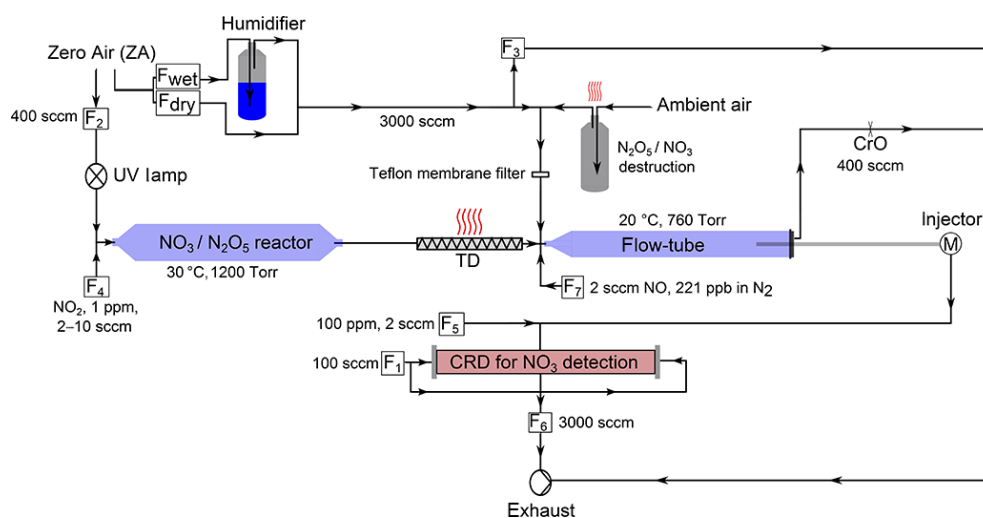


Figure 2. Schematic diagram of the NO₃-reactivity measurement. F₁–F₇ are mass flow controllers: F₁ is mirror purge flow, F₂ is zero air for O₃ generation, F₃ is dilution/inlet overflow (switching between zero air and ambient), F₄ is NO₂ for NO₃/N₂O₅ generation, F₅ is NO titration of NO₃, F₆ is cavity flow to pump and F₇ is NO flow for online reactivity calibration. CrO is critical orifice. TD is heated tubing for thermal decomposition of N₂O₅ to NO₃ at 140 °C.

2 Methodology

Our experiments to measure NO₃ reactivity involve comparison of loss rates of synthetically generated NO₃ in zero air and in ambient air introduced into a flow-tube reactor. In zero air, the loss of NO₃ is due to its reaction with NO₂ (present as a necessary component in the generation of NO₃, see below) and losses on surfaces of the flow tube. When zero air is replaced by ambient air, NO₃ is additionally removed by reaction with reactive gases present and its mixing ratio reduced accordingly. An analysis of the change in signal for a fixed reaction time enables the NO₃ reactivity to be derived once certain corrections have been applied (see below).

Figure 2 displays a schematic diagram of the experimental setup. The three central components are a dark reactor for generation of NO₃, the flow tube in which NO₃ reacts with trace gases in ambient air samples and the detection system for NO₃.

2.1 Generation of NO₃

Many laboratory studies of NO₃ kinetics have used the thermal decomposition of N₂O₅ as NO₃ source (Reaction R4) (Wayne et al., 1991). The generation of NO₃ from gas-phase N₂O₅ eluted from samples of crystalline N₂O₅ (at –80 °C) was found to be insufficiently stable for the present application and is also difficult (though not impossible; see, e.g., Fuchs et al., 2008; Wagner et al., 2011) to use during field campaigns where adequate laboratory facilities for the safe generation and purification of N₂O₅ are frequently not available. In addition, generation of NO₃ from N₂O₅ was also accompanied by an NO₂ impurity of several parts per billion (ppbv).

We therefore generate NO₃ and N₂O₅ in situ, via the oxidation of NO₂ by O₃ (Reactions R1, R3). For this purpose, 400 standard cm³ min^{–1} (sccm) of synthetic air from a zero-air generator (Fuhr Cap 180) is passed over a Hg lamp (low-pressure, Penray type) at a pressure of 1200 Torr. The photo-dissociation of O₂ at 184.95 nm results in formation of oxygen atoms that recombine with O₂ to form ≈ 400 ppbv O₃. The O₃/air flow is then mixed with NO₂ in synthetic air (0.93 ppmv, 1–10 sccm) and directed into a temperature-stabilized (30 °C), darkened, FEP-coated reactor (length 70 cm, diameter 6 cm) also at a pressure of 1200 Torr. The reactor is darkened to prevent the photolysis of NO₃ by room lights. Operation at above-ambient pressure extends the reaction time for a given flow rate, thus optimizing the conversion of NO₂ to NO₃ via the reaction between NO₂ and O₃, which has a low rate constant of $4.05 \times 10^{-17} \text{ cm}^3 \text{ molecule}^{-1} \text{ s}^{-1}$ at 30 °C. The use of high pressures also optimizes the formation of N₂O₅ in the termolecular Reaction R3 and reduces the rate of diffusion and loss of NO₃ to the walls of the reactor. A high pressure in the darkened reactor also has the advantage of partially decoupling it from fluctuations in ambient pressure which influence the formation of N₂O₅. Heating the reactor to above room temperature is carried out to stabilize the formation of N₂O₅, which otherwise shows strong fluctuations owing to variations in laboratory temperature, typically about 3–5° within the course of a day or night. The approximate reaction time for the stepwise conversion of NO₂ to N₂O₅ in the darkened reactor is ≈ 5 min. Based on the O₃ concentration and the rate constant for Reaction (R1), the initial conversion of NO₂ to NO₃ is about 15 %.

The gas exiting the darkened reactor passes through a pin-hole ($\varnothing \approx 250 \mu\text{m}$) to reduce the pressure to roughly ambient level and then enters a $\approx 30 \text{ cm}$ long piece of 1/4 in. ($\approx 6.4 \text{ mm}$) PFA tubing (residence time $\approx 0.5 \text{ s}$), which is heated to 140°C in order to thermally decompose N_2O_5 to NO_3 . Calculations using the thermal decomposition rate constant for N_2O_5 (lifetime of 0.001 s at 140°C) indicate that after $\approx 0.1 \text{ s}$ the N_2O_5 is stoichiometrically converted to NO_3 . The temperature is measured on the outside of the PFA tubing and does not necessarily reflect the temperature of the gas flowing through it. The value of 140°C is chosen based on a series of experiments in which the tubing temperature was varied and the yield of NO_3 monitored. A PFA T-piece located immediately behind the heated tubing is used to add a 2900 sccm flow of either zero or ambient air to the synthetic NO_3 sample. After this dilution step the air contains $\approx 30\text{--}50 \text{ pptv}$ NO_3 , $\approx 1 \text{ ppbv}$ NO_2 and $\approx 50 \text{ ppbv}$ O_3 . As described later, keeping NO_2 and O_3 levels as low as possible has important consequences for the data analysis. Low levels of NO_3 also help to ensure that the addition of NO_3 does not significantly change the reactivity of the air, i.e., by removing a large fraction of the reactive trace gases (RTG). We later assess the potential change in air-mass reactivity (i.e., by depletion of RTG or formation of reactive radicals) following addition of NO_3 at these levels to ambient air.

As described below, the present instrument is a modification of one designed to measure ambient mixing ratios of NO_3 and N_2O_5 and is equipped with a second cavity connected to a heated inlet that measures the sum of NO_3 and N_2O_5 . Experiments in which both cavities were used to analyze the flow out of the heated piping indicated that there was no residual N_2O_5 .

2.2 Detection of NO₃ using cavity-ring-down spectroscopy (CRDS)

For detection of the NO_3 radical we used CRDS, a sensitive technique for measurements of atmospheric trace gases and often used for measurement of ambient NO_3 (Brown et al., 2002). In essence, CRDS is an extinction measurement in a closed optical resonator (cavity) where light is trapped between mirrors with high reflectivity to generate a very long absorption path. Ring-down refers to the decay of light intensity (monitored behind the cavity exit mirror) and the general expression to derive the concentration of an absorbing or scattering gas is given by (Berden et al., 2000)

$$[X] = \frac{1}{c\sigma_{(X,\lambda)}} \left(\frac{1}{\tau_X} - \frac{1}{\tau_0} \right), \quad (2)$$

where τ_0 and τ_X correspond to inverse-decay constants in the absence and presence of an absorbing or scattering trace gas X , respectively, and $\sigma_{(X,\lambda)}$ is the absorption cross section/scattering coefficient of X at wavelength λ .

The instrument used is a two-channel CRDS that was previously used to measure ambient levels of N_2O_5 and NO_3

(Schuster et al., 2009; Crowley et al., 2010). Important modifications to the previous setup include use of FEP-coated glass cavities of equivalent size and fibre optics for the coupling of the laser to the cavity. The thermal dissociation cavity previously used for detection of atmospheric N_2O_5 is not necessary for the measurement of NO_3 lifetimes but was used for calibration and characterization experiments. Only the central features and important modifications compared to the prototype described in Schuster et al. (2009) are described in detail here.

The light source is a 625 Hz, square-wave modulated, 100 mW laser diode located in a Thorlabs TCLDM9 housing and thermally stabilized at 36°C using a Thorlabs ITC502 laser diode combi controller to produce light at 661.95 nm (0.5 nm full width at half maximum) and therefore close to the NO_3 absorption maximum. The effective cross section of NO_3 was calculated as $2.09 \times 10^{-17} \text{ cm}^2 \text{ molecule}^{-1}$ by convoluting the temperature-dependent NO_3 absorption spectrum (Orphal et al., 2003; Osthoff et al., 2007) with the laser diode emission spectrum. Coupling between the laser diode and the cavities is achieved by using either optical fibres (0.22 NA , $50 \mu\text{m}$ core, $400\text{--}2400 \text{ nm}$) for measuring NO_3 reactivity or using fibre optics with a beam splitter (Thorlabs FCMM50-50A-FC, 50:50 ratio) in order to operate both cavities. The beam was collimated (Thorlabs FiberPort Collimator PAF-X-18-PC-A) and directed through an optical isolator (Thorlabs IO-3D-660-VLP), focused by a lens (Thorlabs A230TM-A) into the optical fibre and then collimated again to a beam diameter of about 6 mm before entering the cavity.

The NO_3 cavity (Teflon-coated glass (DuPont, FEP, TE 9568), length 70 cm , volume 79 cm^3) was operated at room temperature, while the N_2O_5 cavity was operated at 80°C with a pre-cavity section heated to 85°C in order to convert N_2O_5 to NO_3 . The NO_3 cavity was connected to the flow tube using $1/8''$ ($\approx 3.2 \text{ mm}$) PFA tubing that lined the $1/4''$ ($\approx 6.4 \text{ mm}$) injector. The use of small-diameter tubing results in short transport times between the flow tube and CRDS and also induces a pressure drop of 133 mbar , so that the pressure in the cavity was 880 mbar . Gases entered the middle of the cavity via a T-piece and were pumped from the ends via a flow controller into the exhaust. The flow rates in both cavities were 3000 cm^3 (STP) min^{-1} (sccm), resulting in a residence time of approximately 1.6 s as calculated from the volume flow rate. Gas entering the CRDS detector always passed through a $2 \mu\text{m}$ membrane filter (Pall Teflo) to remove particles. Light exiting the cavities through the rear mirror was detected by a photomultiplier (Hamamatsu E717-500) which was screened by a 662 nm interference filter. The pre-amplified PMT signal was digitized and averaged with a 10 MHz , 12 bit USB scope (Picoscope 3424) which was triggered at the laser modulation frequency of 625 Hz .

The ring-down constant in the absence of NO_3 was obtained by adding NO ($1\text{--}3 \text{ sccm}$ of a 100 ppmv mixture NO in N_2) every 40 points of measurement for approximately

15 s. Titration with NO took place at the inlet of the T-shaped glass cavity, giving the gas mixture sufficient time to react with NO₃. The L/d ratio (the ratio of the distance between the cavity mirrors, L , and the length of the cavity that is filled by absorber, d) was determined as described previously (Schuster et al., 2009; Crowley et al., 2010) and was 1.01 ± 0.03 . Values of τ_0 in dry zero air at 760 Torr were usually between 140 and 160 μ s, indicating optical path lengths of ≈ 42 –48 km. When operated at a flow of 3000 sccm, the noise levels on the NO₃ signal are such that the precision (3 s integration interval) is better than 1 pptv. As we describe later, the NO₃ reactivity is derived from measurements of the relative change in the NO₃ mixing ratio, so that the precision rather than total uncertainty in the NO₃ mixing ratio defines the accuracy of the reactivity measurement.

2.3 Flow tube for NO₃ reactivity measurement

The flow tube, thermostated to 20 °C by flowing water through an outer jacket, is an FEP-coated glass tube of length 50 cm and internal diameter 4 cm. Gas enters the flow tube at one end via a conical section with a 3/8 in. (≈ 9.5 mm) glass fitting through which 1/4 in. (≈ 6.4 mm) PFA tubing could be inserted. The total flow through the flow tube was 3300 sccm, consisting of 400 sccm from the darkened reactor and 2900 sccm zero air/ambient air. The flow and pressures indicated above result in a Reynolds number of ≈ 123 (i.e., laminar flow) in the cylindrical part of the flow tube, but with an entrance length (L_e) to acquire laminar flow of 27 cm, indicating that the flow tube operates in a mixed turbulent/laminar flow regime.

$$L_e = 0.112rRe \quad (3)$$

Gases exit the flow tube via a length of 1/8 in. PFA tubing supported in an axially centered stainless steel tube (length 50 cm, diameter 1/4 in.) which could be translated along the major flow-tube axis, thus changing the contact (reaction) time between NO₃ and any reactive species or the flow-tube wall. In principal, this enables the dynamic range of the measurement to be adjusted (i.e., long contact times for low reactivity, short contact times for high reactivity) though we found that reactivity-dependent dilution of the ambient air was a better method to extend the dynamic range to high reactivities as very short reaction times were not possible due to a finite residence time in the CRDS detection system and to mixing effects in the flow tube. In order to prevent formation of a “dead volume” at the back of the flow tube beyond the tip of the outlet, 400 sccm was removed via a critical orifice to the exhaust pump. During measurement of NO₃ reactivity the extraction point was usually set for a reaction time of about 10.5 s, which was determined as described below.

As described later, to derive the NO₃ reactivity we compare its concentration in zero air to that in ambient air samples. We found that when switching between sampling ambient air and dry zero air, the resulting change in relative hu-

midity caused an abrupt change in NO₃, which then slowly recovered towards its original value. Measurement of the wall loss rate of NO₃ in dry and humidified zero air by moving the injector (see below) revealed no substantial difference and we conclude that the change in NO₃ is due to wall loss at the point of mixing of NO₃ flows and the zero-air flow, which is very turbulent. In order to eliminate data loss while waiting for signals to stabilize following zeroing, we humidify the zero air to the same absolute humidity ($\pm 2\%$) as ambient. To do this, the ambient relative humidity was monitored by passing 100 sccm air over a sensor that recorded both temperature and relative humidity. The zero air was humidified by directing a variable fraction of the (constant) total flow through a 2 L gas wash bottle filled with HPLC-grade water. The relative humidity of the resulting mixture was matched to ambient levels by dynamic adjustment of the fractional flow passing through the wash bottle. The zero air used for purging the mirrors as well that used for NO₃ generation was not humidified.

In order to ensure that air from the zero-air generator was free of reactive gases that survived the catalytic purification process, we compared it to hydrocarbon-free, bottled synthetic air (Westfalen). No change in the concentration of [NO₃] could be observed when switching between zero air and bottled air, indicating that the zero-air generator was suitable. However, poisoning of the catalyst of the zero-air generator by amines, sulfides or thiols or contamination of the filters could potentially become problematic when using compressed, highly polluted ambient air.

Derivation of the effective reaction time and wall loss rate constant for NO₃

In flow tubes where radial, diffusive mixing of gases is rapid (i.e., at low pressures of He and “plug-flow” conditions), the effective reaction time can be close to that calculated from the volumetric flow rate once axial diffusion is accounted for (Howard, 1979). At higher pressures and laminar flow, reaction times are defined by the parabolic velocity distribution and extent of radial mixing whereas high-pressure flow tubes operated under turbulent conditions (Reynolds numbers > 3000) plug flow can be achieved (Seeley et al., 1993; Donahue et al., 1996). According to the calculations of Reynolds numbers outlined above, our flow tube is not operated in either a pure laminar or turbulent regime, which can make accurate calculation of the reaction time difficult. Using the volumetric flow rate and flow-tube diameter, we calculate an average, linear velocity of the gas of 4.78 cm s^{-1} at 760 Torr and 298 K in the cylindrical section of the flow tube. This enables us to calculate the injector-position-dependent reaction time in the flow tube, which for 45 cm is 9.5 s. This should be regarded as an initial estimate of the true reaction time as it does not consider the non-cylindrical section of the flow tube (2.5 % of total volume), the radial distribution of velocities in the flow tube or mixing effects. A further additional

1.6 s must be added to this to take the average reaction time in the cavity into account (calculated from the cavity volume and the flow rate), resulting in an approximate, total reaction time of 11.1 s.

A further method to derive an “effective” or averaged reaction time is to add a short pulse of gas to the flow tube and monitor its arrival time at the detector. However, as NO₃ cannot be easily stored, we instead add a pulse of a reactant that removes NO₃. A syringe was therefore used to add a short pulse (0.1 cm³ in <0.5 s) of NO diluted in N₂ (0.22 ppbv) to the flow tube at the T-piece where the NO₃ source and zero air are mixed.

The resultant depletion in the NO₃ signal (measured at a time resolution of 0.35 s) displayed an inverted Gaussian form with an elongated flank after the minimum (Fig. 3) which can be attributed to non-isothermal effects, secondary flows and recirculation processes in the flow tube (Huang et al., 2017), which require fluid dynamics simulations to be fully characterized. The average reaction time, t , can however be derived from

$$t = \frac{\sum I_j t_j}{\sum I_j}, \quad (4)$$

where I_j is the signal recorded at each time step t_j .

In total, 25 experiments were conducted, resulting in an effective reaction time of 11.4 ± 0.5 s determined via Eq. (4). The two methods outlined above thus provide approximate values for the reaction time which are in good agreement (< 3 % deviation).

As the reaction time is a central parameter for calculating the NO₃ reactivity, a third method was employed, in which a known amount of NO was added at the usual mixing point and the depletion in NO₃ observed. As the rate constant for reaction of NO with NO₃ is known with an uncertainty (at room temperature) of 13 %, this should enable derivation of an effective reaction time that also takes all mixing effects (both in the flow tube and cavity) into account. In a series of experiments, known amounts NO were added to the 2900 sccm flow of zero air (via a calibrated mass flow controller) at the usual mixing point. In the absence of other processes which remove or form NO₃, its change in concentration upon adding NO is described by

$$[\text{NO}_3]_t = [\text{NO}_3]_0 \exp^{-(k_2[\text{NO}] + k_w + k_3[\text{NO}_2])t}, \quad (5)$$

where $[\text{NO}_3]_0$ and $[\text{NO}_3]_t$ are the concentrations of NO₃ before and after addition of NO, respectively. k_2 and k_3 are the rate constants for reaction of NO₃ with NO and NO₂, respectively, at the flow-tube/cavity temperature, k_w is the rate constant (s⁻¹) for loss of NO₃ at the flow-tube walls and t is the desired parameter. Rearranging, we get the simple Eq. (6), which shows that a plot of $\ln([\text{NO}_3]_t)$ versus $[\text{NO}]$ should yield a slope of $k_2 t$, from which t can be derived using an evaluated and recommended value of k_2 (Atkinson et

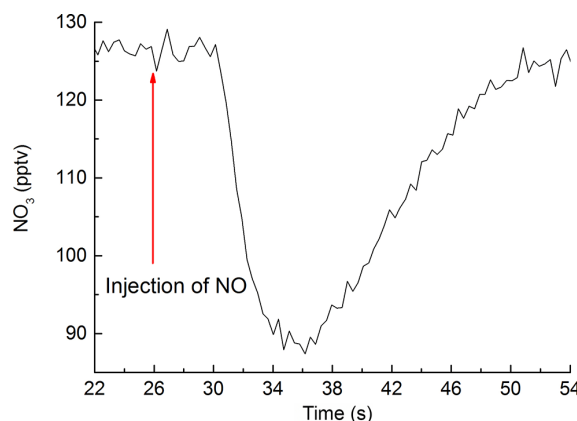


Figure 3. Derivation of effective reaction time by addition of a pulse (at $t = 26$ s) of NO using a syringe. The subsequent depletion in the NO₃ signal was analyzed using Eq. (4).

al., 2004). Once corrected for the contribution from $k_3[\text{NO}_2]$, the intercept should, in principal, give a value of k_w .

$$\ln \frac{[\text{NO}_3]_0}{[\text{NO}_3]_t} = (k_2[\text{NO}] + k_w + k_3[\text{NO}_2])t \quad (6)$$

A plot of $[\text{NO}_3]_t$ versus $[\text{NO}]$ is displayed in Fig. 4a for three different amounts of added NO₂. Although the curves follow roughly exponential behavior as expected, the slopes and thus the value of t obtained were found to depend on the initial NO₂ concentration, with values of 5.7, 5.1 and 4.5 s obtained for NO₂ mixing ratios of 2.94, 5.88 and 8.82 ppbv, respectively. This indicates that the kinetics of NO₃ formation and loss are more complex than defined by Eq. (6) and the relative rates of reaction of NO₃ with NO (Reaction R2) and NO₂ (Reaction R3) and its formation via N₂O₅ decomposition (Reaction R4) and reaction of O₃ with NO₂ (Reaction R1) in the flow tube all impact the NO₃ mixing ratio. In Fig. 4b we display the results of a similar experiment in which NO₂ as added. In this case, there is obvious curvature in the plot of $[\text{NO}_3]_t$ versus $[\text{NO}_2]$, which is not predicted by Eq. (5). The decomposition of N₂O₅ formed by Reaction (R3) as well as oxidation of NO₂ by O₃ (Reaction R1, see Sect. 3) both lead to the formation of NO₃ and are the causes of this behavior, especially at high $[\text{NO}_2]$ and low $[\text{NO}]$. At the flow-tube and cavity temperature (circa 298 K), the rate constant for decomposition of N₂O₅ (k_4) is $4.4 \times 10^{-2} \text{ s}^{-1}$ (Atkinson et al., 2004).

Extraction of the reaction time thus required numerical simulation of the data obtained by adding various amounts of NO to the flow tube in the presence of different NO₃ and NO₂ concentrations. The impact of Reactions (R2), (R3) and (R4) was assessed by numerical simulations using FACSIMILE (Curtis and Sweetenham, 1987) and considering the reactions listed in Table 1. The input parameters for the simulations were the concentrations of NO, NO₂ and O₃ and the rate constants, which were taken from IUPAC recommenda-

Table 1. FACSIMILE* simulations.

$\text{NO}_2 + \text{O}_3 \rightarrow \text{NO}_3 + \text{O}_2$	$k_1 = 3.52 \times 10^{-17} \text{ cm}^3 \text{ molecule}^{-1} \text{ s}^{-1}$	k_1
$\text{NO}_3 + \text{NO} \rightarrow 2\text{NO}_2$	$k_2 = 2.60 \times 10^{-11} \text{ cm}^3 \text{ molecule}^{-1} \text{ s}^{-1}$	k_2
$\text{NO}_3 + \text{NO}_2 + \text{M} \rightarrow \text{N}_2\text{O}_5 + \text{M}$	$k_3 = 1.24 \times 10^{-12} \text{ cm}^3 \text{ molecule}^{-1} \text{ s}^{-1}$	k_3
$\text{N}_2\text{O}_5 + \text{M} \rightarrow \text{NO}_2 + \text{NO}_3 + \text{M}$	$k_4 = 4.44 \times 10^{-2} \text{ cm}^3 \text{ molecule}^{-1} \text{ s}^{-1}$	k_4
$\text{NO} + \text{O}_3 \rightarrow \text{NO}_2 + \text{O}_2$	$k_5 = 1.89 \times 10^{-14} \text{ cm}^3 \text{ molecule}^{-1} \text{ s}^{-1}$	k_5
$\text{NO}_3 + \text{wall} \rightarrow \text{NO}_2$	$k_w = 4 \times 10^{-3} \text{ s}^{-1}$	k_w
k_{RTG}	variable/fitted	k_{RTG}

* For all simulations FACSIMILE/CHEKMAT (release H010 date 28 April 1987 version 1) was used. The rate constants (k_i) listed were taken from the IUPAC recommendations (Atkinson et al., 2004; IUPAC, 2016) at 298 K and 1 bar.

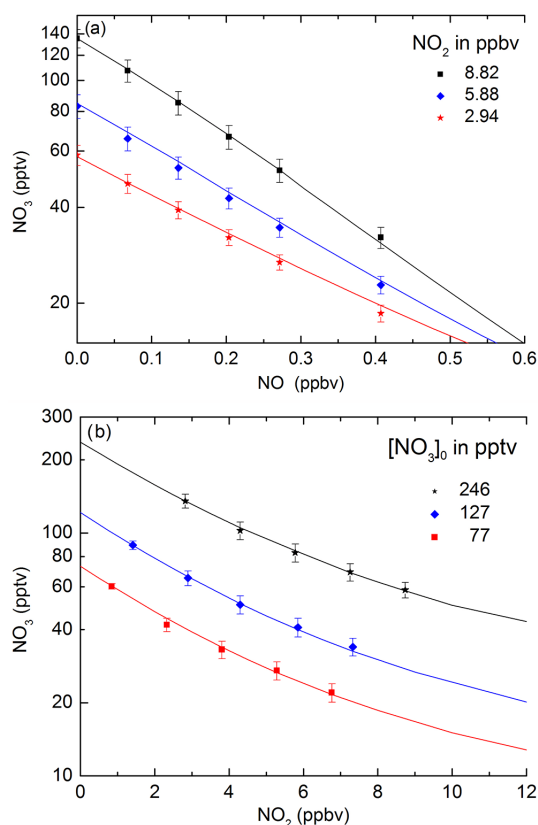


Figure 4. Characterization of the flow tube by numerical simulation of the NO₃ change following addition of NO and NO₂ at different mixing ratios. The symbols are measured NO₃ mixing ratios; the lines are the results of numerical simulations.

tions (Atkinson et al., 2004). The total reaction time (t) and the wall loss constant for NO₃ (k_w) were adjusted until each of the six data sets could be reproduced with a single value for each parameter. The initial concentration of [NO₃]₀ was allowed to float until best agreement was achieved. This way, the reaction time was determined to be 10.5 s, which is in good agreement with that derived by pulsed addition of NO. As our reactivity derivation relies on the change in NO₃ signal upon adding a reactant to the flow tube, we consider

the value of 10.5 s, which takes mixing, diffusion, etc. into account, to be the most appropriate value but assign an uncertainty (± 1 s) that overlaps with the other methods. The wall loss rate of NO₃ (which is independent of the NO and NO₂ concentrations) was found to be $4 \times 10^{-3} \text{ s}^{-1}$.

For analysis of ambient reactivity we use a reaction time of 10.5 s as derived from the addition of NO. This means that our ambient reactivities are directly tied to the rate constant for reaction between NO₃ and NO. As described later, during ambient measurements we periodically add a known amount of NO to the zero air to monitor a known reactivity under real operating conditions.

Figure 5a and b show the correlation between simulated and measured NO₃ concentrations in these experiments. In both cases the slope is close to unity (0.97–1.02) with an intercept close to zero. A set of similar experiments performed at 30 and 80 % humidity also showed excellent agreement using the same values of t and k_w . We conclude that the behavior of NO₃ in this system can be very accurately predicted by numerical simulations using a simple reaction scheme under a variety of conditions (initial NO₃, NO and NO₂ varied), giving us confidence in our ability to extract loss rates for NO₃ in ambient air.

When gas-phase reactivity is low, a substantial fraction of NO₃ may be lost via collisions with the walls rather than due to reactive gases. For this reason, we remeasured the value of k_w obtained above in a further set of experiments in which the NO₃ concentration was measured as a function of injector position (contact time in the flow tube) at a constant initial mixing ratio of NO₃ and NO₂ and in the absence of NO. For this we calculate the reaction time for each of the three injector positions from pulsed addition of NO as described above, but normalized to the reaction time derived from addition of NO with numerical simulation. The results of such an experiment are displayed in Fig. 6 and we draw attention to the fact that, even at maximum reaction time (10.5 s), the change in the NO₃ concentration is only about 10 %. This reflects the low efficiency of reaction of NO₃ with the FEP-coated glass walls. Similar experiments performed before and after the NOTOMO campaign (NOcturnal chemistry at the Taunus Observatorium: insights into Mechanisms of Oxidation) (see

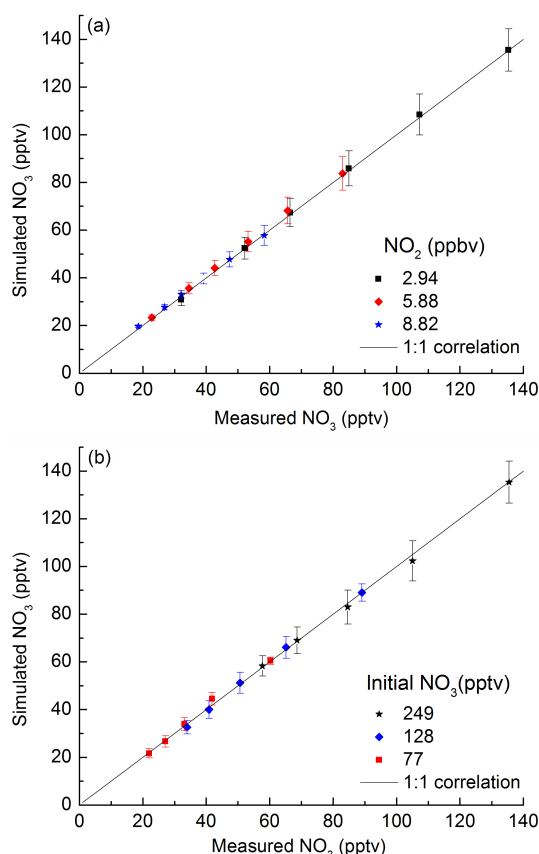


Figure 5. (a) Measured versus simulated NO₃ for different amounts of added NO (67, 134, 201, 268, 402 pptv) and at three different mixing ratios of NO₂. (b) Measured versus simulated NO₃ (initially 77, 128 or 249 pptv) at different amounts (1.5, 3, 4.5, 6 ppbv) of added [NO₂]. The solid lines represent 1 : 1 correlation.

below) indicated that the FEP coating did not degrade significantly following sampling of filtered, ambient air. The numerical simulation was initialized with the same set of rate parameters described above, a fixed NO₂ concentration and only k_w and the initial NO₃ concentration were varied. The best fit was obtained when k_w was $4 \times 10^{-3} \text{ s}^{-1}$, in agreement with the simulations at fixed time and variable NO and NO₂. Using Eq. (7) where r is the flow-tube radius, \bar{c} the mean molecular speed and which assumes laminar flow and no diffusive limitation to uptake, this value of k_w can be converted to an approximate uptake coefficient for NO₃ to the FEP-coated tube of $\approx 5 \times 10^{-7}$.

$$\gamma = \frac{2rk_w}{\bar{c}} \quad (7)$$

3 Data analysis and derivation of NO₃ reactivity

We first consider the passage of NO₃ through the flow tube in a flow of zero air. If NO₃ is lost in one or more pseudo-

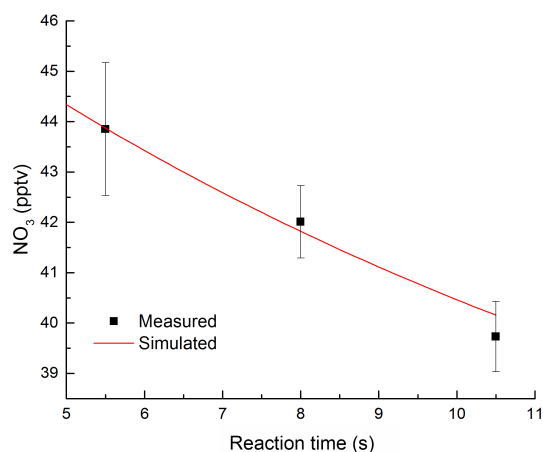


Figure 6. Determination of the NO₃ wall loss constant by variation of the reaction time (injector position). The simulation indicates a wall loss constant of $k_w = 0.004 \text{ s}^{-1}$.

first-order processes, its decay should be exponential and its concentration, $[\text{NO}_3]_t^{\text{ZA}}$ after a reaction time t , is given by Eq. (8).

$$[\text{NO}_3]_t^{\text{ZA}} = [\text{NO}_3]_0^{\text{ZA}} \exp(-k_{\text{ZA}}t), \quad (8)$$

where ZA refers to use of zero air. As NO₃ is lost only via reaction with NO₂ and to the wall, $k_{\text{ZA}} = k_{\text{wall}} + k_{\text{NO}_2}$, where k_w is the first-order loss rate constant for wall loss and k_{NO_2} is the first-order loss rate constant for reaction with NO₂ and is equal to $k_3[\text{NO}_2]$. When zero air is switched for ambient air containing reactive trace gases, we have

$$[\text{NO}_3]_t^{\text{Amb}} = [\text{NO}_3]_0^{\text{Amb}} \exp(-k_{\text{Amb}}t), \quad (9)$$

where $k_{\text{Amb}} = k_w + k_{\text{NO}_2} + k_{\text{RTG}}$ and k_{RTG} is the first-order loss rate constant for reaction of NO₃ with trace gases present in ambient air other than NO₂.

If $[\text{NO}_3]_0^{\text{ZA}}$ and $[\text{NO}_3]_0^{\text{Amb}}$ are equivalent, Eq. 10 is obtained.

$$\frac{[\text{NO}_3]_t^{\text{ZA}}}{\exp(-k_{\text{ZA}}t)} = \frac{[\text{NO}_3]_t^{\text{Amb}}}{\exp(-k_{\text{Amb}}t)} \quad (10)$$

Rearranging and substituting for k_{ZA} and k_{Amb} leads to

$$k_{\text{RTG}} = \frac{\ln\left(\frac{[\text{NO}_3]_t^{\text{ZA}}}{[\text{NO}_3]_t^{\text{Amb}}}\right)}{t} = \frac{1}{\tau}, \quad (11)$$

where τ is the NO₃ lifetime. In principal, it should thus be possible to calculate the reactivity of NO₃ in ambient air by measuring $[\text{NO}_3]_t^{\text{ZA}}$ and $[\text{NO}_3]_t^{\text{Amb}}$ and knowing the reaction time t . Later we discuss the applicability of this expression and show that corrections are necessary to take the reformation of NO₃ into account, especially when dealing with air masses with high NO₂ content. This is similar to the laboratory experiments described above and required numerical simulation, which we present below.

The concentration of NO₃ in zero air measured when the injector is positioned for maximum reaction time, $[\text{NO}_3]_t^{\text{ZA}}$, was measured by flushing the inlet with 3000 sccm zero air creating an overflow of ≈ 100 sccm. When switching to ambient measurements, the zero-air overflow was redirected via a flow controller (F₃ in Fig. 2) that connected the zero-air overflow line to the exhaust and which was set to 3500 sccm. This setup has the advantage of enabling dynamic dilution of ambient air. If the reactivity is so high that the NO₃ levels approached the detection limit, F₃ does not withdraw the entire 3500 sccm overflow but allows, e.g., 2000 sccm to be added to the inlet, resulting in sampling 900 sccm of ambient air plus 2000 sccm of zero air, a dilution factor of 2900/900 which is slightly increased by the 400 sccm flow from the darkened reactor. A five-point dynamic dilution with zero air is implemented in the software, which changes the set point for F₃ and dilutes the ambient air with zero air if $[\text{NO}_3]_t^{\text{Amb}}$ decreases below 10 pptv for a time period of 30 s. Conversely, the dilution can be decreased again if $[\text{NO}_3]_t^{\text{Amb}}$ becomes $\geq [\text{NO}_3]_t^{\text{ZA}} - 10$ ppt. Dilution factors (D_i) were determined using a Gilibrator flow meter (Gilian Gilibrator-2) and were $D_1 = 1.14$ for the measurement of pure ambient air (here the small dilution effect is caused by the 400 sccm zero air used in the production of NO₃), $D_2 = 1.74$, $D_3 = 3.71$, $D_4 = 8.98$ and $D_5 = 14.07$ when diluting ambient air. With increasing dilution, errors in the measurement will increase as well (see Sect. 5).

The analytical expression given above to derive the NO₃ reactivity is an ideal case in which NO₃ is lost by a number of first-order processes and is not formed in the flow tube to a significant extent. However, as we already demonstrated in the laboratory experiments to examine the effects of varying NO, NO₂ and NO₃ concentrations, the formation of N₂O₅ in the reaction of NO₃ with NO₂ (Reaction R3) and its thermal decomposition back to NO₃ can impact the NO₃ concentration as NO₂ is present both in the mixture used to generate N₂O₅ and NO₃ and in ambient air. While the formation of N₂O₅ from NO₂ and NO₃ (Reaction R2) is, to a good approximation, independent of temperature between about 280 and 305 K, the rate constant for thermal decomposition of N₂O₅ (Reaction R3) varies by a factor of 26 over the same temperature range. The simple, analytical approach outlined above thus fails at temperatures where the decomposition of N₂O₅ is important and when sufficient NO₂ is present to account for a significant fraction of the loss of NO₃. This is illustrated in Fig. 7a, in which simulations of the NO₃ concentration at a reaction time of 10.5 s and at different temperatures and amounts of NO₂ (as reactant) are displayed and compared with the simple exponential behavior (black data points) calculated from Eq. (11). The simulations show that the dependence of the NO₃ concentration on NO₂ is non-exponential, indicating that regeneration of NO₃ from the N₂O₅ formed is significant, especially at higher temperatures. Figure 7b plots the ratio of the true reactivity (i.e., that used as input into the numerical simulation) versus that obtained by ana-

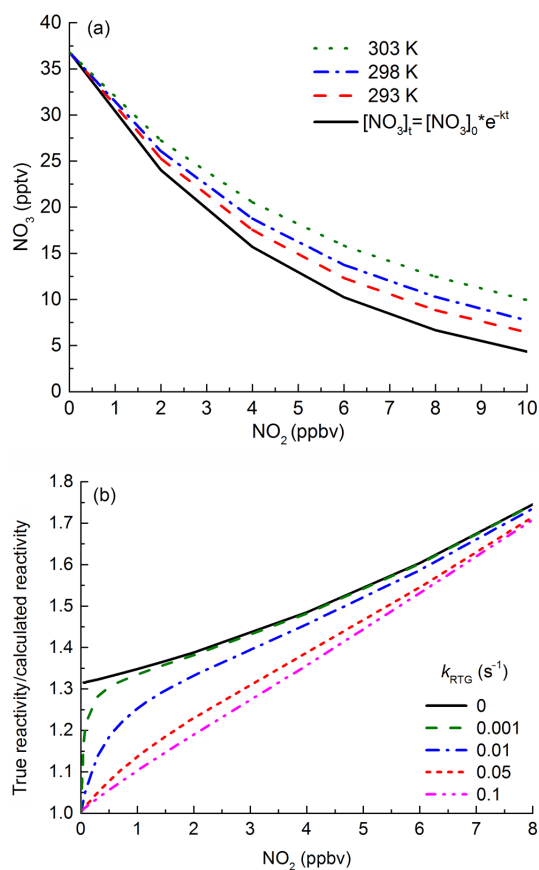


Figure 7. Influence of N₂O₅ formation and decomposition in the flow tube. **(a)** Simulated (red, blue and green) mixing ratio of NO₃ versus added NO₂ at a reaction time of 10.5 s at various temperatures and thus thermal decomposition rates of N₂O₅. The simple exponential decay of NO₃ (Eq. 9) is given by the black line. **(b)** Effect of NO₂ level on the ratio of true reactivity/reactivity calculated from Eq. (8) for different loss rate constants for NO₃ reacting with reactive traces gases.

lyzing the simultaneous change in NO₃ concentration using Eq. (11). It is evident that the use of this expression generally results in underestimation of the true reactivity due to the formation and decomposition of N₂O₅. The bias will be largest when sampling polluted air where the reactivity has a large component due to NO₂ and small under conditions of low NO₂ and high k_{RTG} typical for remote, forested areas. However, as previously mentioned, the decomposition of N₂O₅ is strongly temperature dependent so that the bias will increase with rising temperature and decrease with sinking flow-tube temperature.

Apart from the formation and thermal dissociation of N₂O₅, the reaction of NO₂ with O₃ may, under some conditions, represent a further potential source of NO₃ in the flow tube despite the low rate constant for Reaction (R1). Due to the in situ method of production of N₂O₅ and NO₃ in the dark reactor, NO₂ (0.6–3 ppbv) and O₃ (40–50 ppbv) are al-

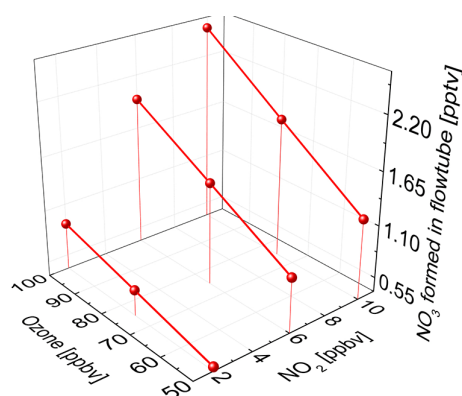


Figure 8. Simulated NO₃ production in the flow tube at different O₃ and NO₂ mixing ratios at a fixed reaction time of 10.5 s.

ways present in the flow tube. NO₃ generated in the flow tube was therefore simulated for different amounts of O₃ and NO₂ corresponding to the minimum and maximum mixing ratios used in our experiments. Figure 8 indicates that with 50 ppbv of O₃ and 2 ppbv NO₂, <0.5 pptv of NO₃ is formed in the 10.5 s available for reaction in the flow tube, which would not strongly impact the results if the analytical expressions above were used to derive the NO₃ reactivity. Under highly polluted conditions (e.g., 100 ppbv O₃ and 20 ppbv NO₂) the effect is, however, measurable (> 2 pptv).

The discussion above indicates that the use of Eq. (11) can, under certain circumstances (e.g., low NO_x, high NO₃ reactivity to VOCs), give a reasonable representation of the NO₃ reactivity. However, in order to be able to derive NO₃ reactivities from any air mass we use numerical simulation take NO₃ reformation into account and enable extraction of accurate values in any conditions.

Numerical simulations for extraction of ambient reactivity

In this section we outline the experimental procedure and the associated data analysis for extracting the NO₃ reactivity from an ambient data set as exemplified by the data shown in Fig. 9. These data cover a 1 h period in which several phases of inlet overfilling with humidified zero air and titration with NO are apparent as are periods of mixing NO₃ with ambient air. The data set has already been corrected for baseline drift in the NO₃ zero during titration, and hence each titration-zero is scattered around 0 pptv NO₃.

The periods marked “ZA” (zero air) were used to extract the NO₃ concentration after a residence time of 10.5 s in flow tube in the absence of ambient reactive trace gases. The data show that a plateau in the NO₃ signal with zero air is observed after about two–three titration cycles are complete, which is the result of slow flushing through the inlet of reactive gases, which have extended surface residence times on the inlet material and fittings. Once a stable signal is ac-

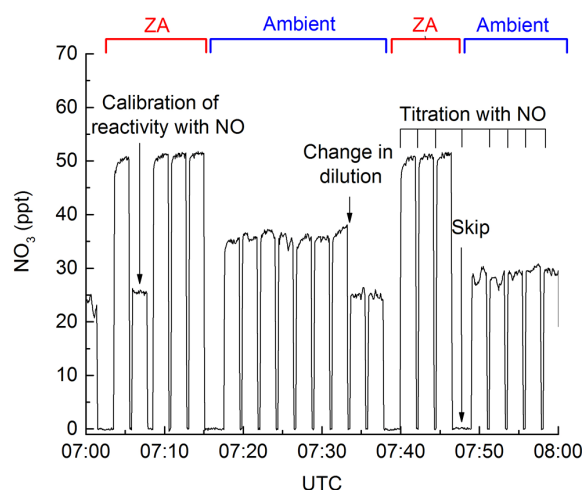


Figure 9. Raw data showing the change in NO₃ (10.5 s reaction time) between zero air (ZA, periods marked with red brackets) and ambient air (Ambient, blue brackets). The figure also shows periods of titration of NO₃ with NO (≈ 2 min intervals), a change in the dilution factor from 4 to 3 (at ≈ 07:33 UTC) and an in situ reactivity calibration (at ≈ 07:07). The “skip” periods are those in which data are not analyzed due to switching from ambient air to zero air and vice versa.

quired, $[\text{NO}_3]_{t=10.5}^{\text{ZA}}$ can be taken as an average value for each 300 s zero-air phase. These values are then used to calculate the initial NO₃ concentration $[\text{NO}_3]_0^{\text{ZA}}$, i.e., before NO₃ enters the flow tube. This was done in an iterative procedure using numerical simulation with FACSIMILE embedded in a separate program. Input values are the O₃ and NO₂ concentration (from the darkened reactor), a first estimate for $[\text{NO}_3]_{t=0}^{\text{ZA}}$ and the rate coefficients for the NO₃ reactions listed in Table 1. At the end of the simulation (a few seconds of computing time) the simulated and measured values of $[\text{NO}_3]_{t=10.5}^{\text{ZA}}$ are compared and the ratio used to adjust the next input value for $[\text{NO}_3]_{t=0}^{\text{ZA}}$. The iteration continued until convergence was reached. Convergence was considered satisfactory when the deviation between measured and simulated values of $[\text{NO}_3]_{t=10.5}^{\text{ZA}}$ was less ≤ 1 %. This usually took only 5 simulations per data point as the initial value for each new time point was chosen to be the final value for the preceding time point. Ideally, $[\text{NO}_3]_{t=0}^{\text{ZA}}$ should be constant over long periods of time. In fact, deviations of several pptv, especially during field measurements, were observed over periods of hours and so values of $[\text{NO}_3]_{t=0}^{\text{ZA}}$ were linearly interpolated to each time point in which ambient reactivity was recorded.

Once initial NO₃ concentrations had thus been obtained a new set of simulations was started to simulate the measured values of $[\text{NO}_3]_{t=10.5}^{\text{Amb}}$. In this case, the simulation was initialized with the values of $[\text{NO}_3]_{t=0}^{\text{ZA}}$ obtained as described above and the total NO₂ concentration and O₃ concentrations, which contained a constant contribution from the dark reactor and a variable concentration from ambient NO₂ and

O₃ once corrected by the dilution factor (see above). An initial estimate of the total NO₃ reactivity, k_{RTG} , was made and the simulated value of $[\text{NO}_3]_t^{\text{Amb}}$ compared to that measured. The simulation was iterated, with incremental adjustment of k_{RTG} until agreement between simulation and observation was $\leq 1\%$. For ambient data sets, in which the reactivity can be highly variable, this sometimes took several iterations, though as each simulation took less than a second this is not a particularly time-consuming procedure.

4 Reactivity of an isoprene standard

To validate our experimental and analytical procedure, we performed reactivity measurements on a bottled isoprene standard (0.933 ± 0.09 ppmv, Westfalen), diluted in zero air. Isoprene was chosen as it is an important biogenic reactant for NO₃ in the troposphere and also because the rate coefficient, k_{isoprene} , for its reaction with NO₃ has been studied on many occasions (Atkinson et al., 2006; IUPAC, 2016) and therefore has a low associated uncertainty ($k_{\text{isoprene}} = 6.5 \pm 0.15 \times 10^{-13}$ cm³ molecule⁻¹ s⁻¹ at 298 K).

Experiments were carried out at various isoprene and NO₂ mixing ratios and the results are summarized in Fig. 10, which indicates excellent agreement between the measured reactivity and that calculated from the isoprene mixing ratio and rate coefficient, the slope of an unweighted fit being 1.00 ± 0.03 . The error bars on the calculated reactivity represent total uncertainty in the isoprene and NO₂ mixing ratio, the reaction time and the rate coefficient. These results confirm that the instrument and data analysis procedure measure accurate values of NO₃ reactivity in the presence of NO₂ and organic reactants.

5 Detection limit, dynamic range and overall uncertainty

While the overall uncertainty associated with absolute NO₃ concentration measurement are influenced by factors such as uncertainty in the cross section as well as in the measurement of the laser emission spectrum, the fractional change in concentration used to derive the NO₃ reactivity is not impacted. The detection limit for measuring NO₃ reactivity is defined by the minimal detectable change (MDC_{NO_3}) in the NO₃ mixing ratio. This depends on noise levels and drift in ring-down time, i.e., on the precision of the NO₃ signal and also on the stability of the synthetically generated NO₃. The instrumental noise on the NO₃ signal was reduced by averaging over ≈ 3 s per data point (≈ 1800 ring-down events) to give a noise-limited detection limit (1σ) of ≈ 0.2 pptv. Precision is limited by the stability of the CRDS setup where changes in the mirror reflectivity induced by thermal or mechanical stress can lead to a drift in the ring-down time. The precision can be estimated from the standard deviation of the

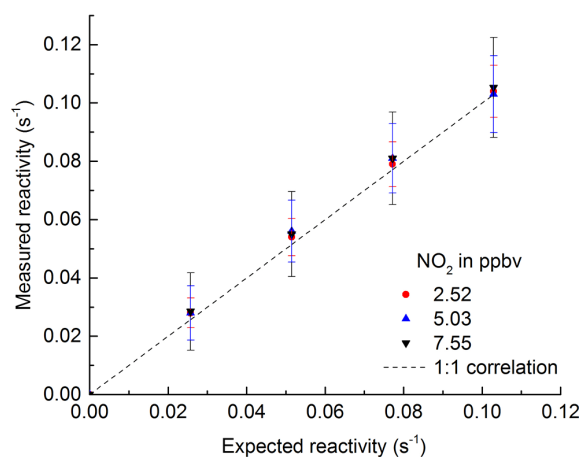


Figure 10. Verification of the experimental procedure by addition of isoprene at different NO₂ mixing ratios. The known reactivity was calculated from the isoprene mixing ratio (1.5–6 ppbv) and the rate coefficient for reaction of isoprene with NO₃. Experiments were performed in dry zero air. The error bars in the simulation are due to uncertainties in [isoprene] and [NO₂] (both 5 %) and the reaction time (10 %).

signal from one zeroing period to the next over the measurement period. Under typical laboratory conditions this was normally ≈ 0.7 pptv.

Since $[\text{NO}_3]_0^{\text{ZA}}$ is interpolated onto the measured $[\text{NO}_3]_t^{\text{Amb}}$ time series to calculate the reactivity, the stability of the NO₃ source is of great importance. Changes in the amount of synthetically generated NO₃ are caused by fluctuations in the temperature or pressure of the dark reactor, the flow of NO₂ and changes in the intensity of light from the O₃ generator. In general, the poorer the stability of the NO₃ source chemistry, the more frequently the NO₃ mixing ratio in zero air has to be measured. In laboratory conditions, changes of ± 1 pptv within 1 h were typical, making $[\text{NO}_3]_t^{\text{ZA}}$ measurements every 1200 s more than sufficient. In field conditions, where the instrument housing may be subject to larger temperature fluctuations, more frequent determination of $[\text{NO}_3]_t^{\text{ZA}}$ may be necessary. The NO₃ source stability was obtained from the standard deviation of the averaged $[\text{NO}_3]_t^{\text{ZA}}$ concentrations and propagating this with the standard deviation of two consecutive $[\text{NO}_3]_t^{\text{ZA}}$ measurements, for which typical values in laboratory conditions were ≈ 1 ppt. To define an overall, minimal detectable change in NO₃ (MDC_{NO_3}), the noise- and drift-limited precision was combined with the NO₃ source stability to result in $\text{MDC}_{\text{NO}_3} = 2.5$ pptv.

An MDC_{NO_3} of 2.5 pptv results in a lower limit for the measurement of NO₃ reactivity of 0.005 s⁻¹ (obtained from Eq. 11 with $[\text{NO}_3]_t^{\text{ZA}} = 50$ pptv and $[\text{NO}_3]_t^{\text{Amb}} = [\text{NO}_3]_t^{\text{ZA}} - \text{MDC}_{\text{NO}_3} = 47.5$ pptv, at the lowest dilution factor of 1.14). An upper limit for the measurable reactivity is 45 s⁻¹, largely defined by the uncertainty of the dilution factor. Dilution fac-

tors were obtained by measurements of the actual flows going into the flow tube using a Gilibrator flow meter (Gilian Gilibrator-2, stated accuracy $\pm 1\%$). The total uncertainty in the dilution factor is defined by the accuracy of the measurement of the dilution flows as well as by the accuracy of the flow controllers used for flow regulation ($\pm 2\%$) and was calculated to be 2.5%. The error in the calculated reactivity is lowest for the lowest dilution but if the $[\text{NO}_3]_t^{\text{Amb}}$ gets close to the detection limit this will also have a strong influence on the calculated reactivities making a higher dilution factor favorable. Dilution factors were chosen to keep the instrument operating in a region ($10 \text{ pptv} < \text{NO}_3 < 40 \text{ pptv}$) where both effects are minimized.

A minimum detectable change in NO₃ of 2.5 pptv leads to an uncertainty of $\approx 15\%$, when NO₃ varies between ≈ 10 and 30 pptv (starting from 50 pptv in zero air). The uncertainty increases dramatically when NO₃ levels are close to 50 pptv (i.e., very low reactivity) or less than 5 pptv (very high reactivity without dilution). This is illustrated in Fig. S1 of the Supplement. As mentioned in Sect. 2.3 the uncertainty in the reaction time (10%) also contributes to the overall uncertainty.

To assess the uncertainty associated with derivation of the NO₃ reactivity from numerical simulation, uncertainties associated with the input parameters have to be considered. As previously demonstrated (Groß et al., 2014) this is best assessed in a Monte Carlo approach in which the key parameters are varied within a range reflecting their uncertainty limits. The parameters that most sensitively influence the derived value of NO₃ reactivity are the NO₂ mixing ratio and the rate coefficients for N₂O₅ formation ($k_3 = 1.2 \pm 0.1 \times 10^{-12} \text{ cm}^3 \text{ molecule}^{-1} \text{ s}^{-1}$) and decomposition ($k_4 = 4.4 \pm 0.4 \times 10^{-2} \text{ cm}^3 \text{ molecule}^{-1} \text{ s}^{-1}$). The rate coefficients listed are for 1 bar and room temperature as appropriate for the experimental conditions, the uncertainties quoted ($\approx 10\%$) are based on assessment of kinetic data (Burkholder et al., 2016). The Monte Carlo simulations were initiated with a NO₃ mixing ratio (in zero air) of 50 pptv, decreasing to 20 pptv upon reaction with air. In total, six sets of ≈ 1200 simulations were carried with variation of the initial NO₂ mixing ratio between 1 and 5 ppbv and the associated error in NO₂ mixing ratio was taken as 8%. For any given simulation, the output value of the NO₃ reactivity (k_{RTG}) was stored. The 2σ uncertainty was derived from the Gaussian fits to histograms of k_{RTG} (insets at NO₂ = 1.0, 3.0 and 5.0 ppbv) and is plotted (as a percent of k_{RTG}) versus $k_{\text{RTG}}/\text{NO}_2$. The latter may be considered a measure of whether NO₃ reacts predominantly with NO₂ to form N₂O₅ (k_3) or with reactive trace gases. Figure 11 shows that the uncertainty associated with the simulations is very sensitive to ambient NO₂ levels, varying between $> 100\%$ (at 5 ppbv NO₂ and a reactivity of 0.017 s^{-1}) and 3.1% (at 1 ppbv NO₂ and a reactivity of 0.092 s^{-1}) of the extracted k_{RTG} . Clearly, the extraction of k_{RTG} is most accurate in conditions of low NO_x and when

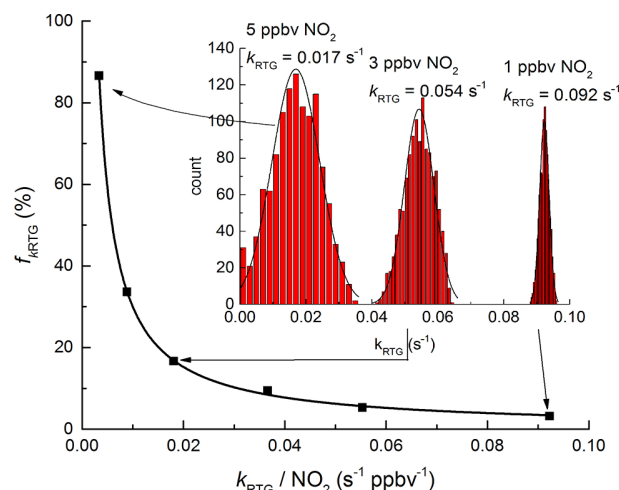


Figure 11. Uncertainty factor ($f k_{\text{RTG}}$) as a function of the ratio $k_{\text{RTG}}/[\text{NO}_2]$ as derived from Monte Carlo simulations. The relationship (black line) is described by $f(k_{\text{RTG}}) = 0.33 \times (k_{\text{RTG}}/[\text{NO}_2])^{-0.977}$. The results of three individual sets of 1200 simulations are shown as histograms.

NO₃ lifetimes are short (e.g., forested regions far from anthropogenic activity).

Another potential bias in the measurement is the temperature dependence of the rate constant of the reactions of trace gases with NO₃. Measurements were normally conducted at 20 °C in the flow tube whilst outside temperature can differ from this. However, (unlike OH) the NO₃ reactions which dominate its reactivity involve addition to double bonds (e.g., of terpenes) and are only weakly temperature dependent. Therefore, to a good approximation, this error can generally be neglected. To illustrate this, we consider the reaction between NO₃ and the usually most abundant monoterpene, α -pinene. The rate constant at the flow-tube temperature (20 °C) is 6.4×10^{-12} , increasing to $7.0 \times 10^{-12} \text{ cm}^3 \text{ molecule}^{-1} \text{ s}^{-1}$ at 5 °C and decreasing to $5.9 \times 10^{-12} \text{ cm}^3 \text{ molecule}^{-1} \text{ s}^{-1}$ at 35 °C, which are changes of $< 10\%$. Note also that for many monoterpenes, the temperature dependence of the rate constant is not known but expected to be weak (IUPAC, 2016).

Under circumstances where the reactivity is known to be driven by reaction with reactive trace gases for which NO₃ has large temperature dependence this error has to be taken into consideration.

We now examine the potential bias caused by use of NO₃ concentrations as large as 50 pptv, which may change the reactivity of the air either by removing a significant fraction of gas-phase reactants or via formation of peroxy radicals (RO₂), which may also react with NO₃. In a first scenario, we assume that the reactivity is caused by a single species, namely the generally dominant terpene, α -pinene and consider both low ($k_{\text{RTG}} = 0.005 \text{ s}^{-1}$) and high reactivity regimes ($k_{\text{RTG}} = 0.1 \text{ s}^{-1}$). A value of $k_{\text{RTG}} = 0.005 \text{ s}^{-1}$

would result if 34 pptv of α -pinene were available for reaction. In a first approximation, assuming first-order kinetics, we calculate that 2.5 pptv of the initially available 50 pptv of NO₃ is lost in the 10.5 s reaction time, and consequently a change in α -pinene of 2.5 pptv would also occur. This is only 7 % of the initial concentration, indicating an upper limit to a negative bias of 7 %. This is an upper limit, as the assumption of first-order kinetics is not entirely appropriate. As NO₃ reacts with α -pinene in air to form a nitrooxyperoxy radical (RO₂) we also consider a positive bias due to reaction of NO₃ with this RO₂. To do this we assume a rate constant of $1.2 \times 10^{-12} \text{ cm}^3 \text{ molecule}^{-1} \text{ s}^{-1}$ for the reaction as observed for NO₃+CH₃O₂ (Atkinson et al., 2006) and assume that this rate constant is approximately independent of the nature of the organic fragment (*R*) as is the case for reactions of RO₂ with NO. The 2.5 pptv RO₂ thus generated results in an incremental NO₃ reactivity of $7 \times 10^{-5} \text{ s}^{-1}$, a positive bias of 1.5 %. Again, this is an upper limit, as the calculation assumes that this concentration of RO₂ is constant and available for the whole 10.5 s of reaction time. For higher reactivity (0.1 s^{-1}) a similar calculation shows that the 670 pptv required would reduce the NO₃ concentration to 17.5 pptv, itself being diminished to ~ 640 pptv, a change of just 5 %. The 32.5 pptv RO₂ generated would result in a loss rate constant for NO₃ of $\sim 9 \times 10^{-4} \text{ s}^{-1}$, a positive bias of $\sim 1\%$. In conclusion, for reactive systems in which a large concentration of reactive trace gases with moderate reactivity towards NO₃ are encountered, we expect no significant bias. The only scenario in which a large bias can ensue is when a low reactivity is caused by a very low concentration of an extremely reactive trace gas. Taking the example of 1 pptv of a highly reactive terpenoid ($k = 2 \times 10^{-10} \text{ cm}^3 \text{ molecule}^{-1} \text{ s}^{-1}$) it is easy to show that it would be reduced to just a few percent of its initial concentration when mixed with 50 pptv of NO₃ for 10.5 s. In this case a large negative bias would result. In the real atmosphere, this situation is however unlikely to occur as such reactive species are usually substantially reduced in concentration compared to the generally dominant biogenics such as α -pinene.

The overall uncertainty thus derives from a combination of measurement errors (cavity instability, drift in NO₃ source, etc.) and the need to correct for NO₃ reactions with NO₂. Under ideal conditions (e.g., as described above for laboratory operation) the former can be reduced to $\approx 16\%$. For a scenario in which biogenic VOCs dominate NO₃ reactivity in a low NO_x (< 1 ppbv) environment an additional uncertainty of $\approx 6\text{--}10\%$ from the numerical simulations results in a total uncertainty of $\approx 17\text{--}20\%$. In a high-NO_x environment, the total uncertainty will be dominated by that associated with the simulations. For example, at 5 ppbv NO₂ and a reactivity of 0.03 s^{-1} the total error would be close to 45–50 %.

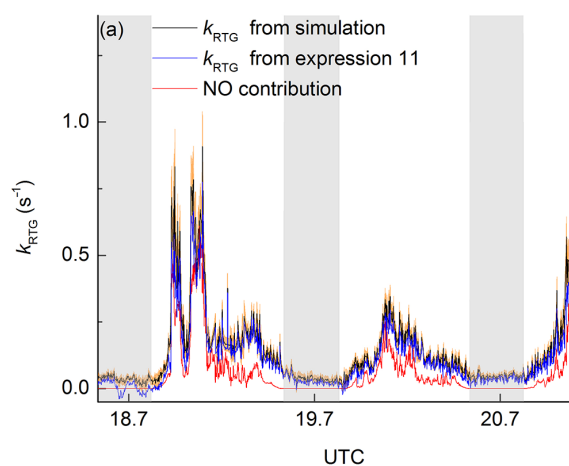


Figure 12. Measured values of k_{RTG} over a 3-day period. The overall uncertainty is represented by the amber, shaded area. The black lines are k_{RTG} obtained by full simulations; the blue lines are calculated using Eq. (11) (without correction for N₂O₅ formation and decomposition). The contribution of NO to the NO₃ reactivity is displayed as the red line. Grey shaded regions correspond to nighttime; ticks are at midnight.

6 Deployment in the NOTOMO campaign, 2015

The NO₃ reactivity setup described above was deployed for the first time in the field during the NOTOMO campaign in the Taunus mountains (southwestern Germany) in 2016. The site, previously described in detail (Crowley et al., 2010; Sobanski et al., 2016b), is situated on top of the “Kleiner Feldberg” mountain (850 m above sea level) in a forested area with urban influence. The site is impacted by biogenic emissions from forested regions (mainly in the northwest) and by anthropogenic emissions from the local urban centers of Frankfurt, Mainz and Wiesbaden in the southeast to southwest.

Reactivity measurements during NOTOMO

The NO₃ reactivity instrument was located in a research container and sampled from a common high-flow inlet together with other instruments. The high-flow inlet was driven by an industrial fan drawing $10 \text{ m}^3 \text{ min}^{-1}$ through a 15 cm diameter stainless steel pipe with its opening about 8 m above the ground. This flow was sub-sampled with a 4 m length of 1/4 in. PFA tubing that extracted the required 3300 sccm air from the center of the stainless steel pipe and directed it through a 2 μm PFA filter to the NO₃-reactivity instrument. Due to thermostat breakdown during NOTOMO, the NO₃-reactivity measurements were performed with the flow tube at container temperature, which was variable (14–31 °C).

Previous campaigns at the Taunus Observatory have revealed occasionally high nighttime mixing ratios of NO₃ and N₂O₅ (Sobanski et al., 2016b). As sampling NO₃ and N₂O₅ from ambient air would bias the NO₃-reactivity measure-

ments to low values, a 2 L glass flask heated to $\approx 40\text{--}50\text{ }^\circ\text{C}$ was placed at night in the ambient air stream to decompose N₂O₅ to NO₃ and NO₂. Based on its thermal dissociation rate coefficient (0.75 s^{-1} at $50\text{ }^\circ\text{C}$), N₂O₅ completely decomposes within the $\approx 40\text{ s}$ residence time in this glass vessel, and the NO₃ formed is expected to be lost on the uncoated glass walls, thus preventing reformation of N₂O₅. Measurements with $\approx 200\text{ pptv}$ of N₂O₅ added directly to the heated vessel and measured by the ambient and heated channels of the two-cavity CRDS (see Sect. 2.2) confirmed that neither NO₃ nor N₂O₅ survived. As the N₂O₅ mixing ratio was measured during NOTOMO it is in principle possible to correct the data for the additional NO₂ thus generated. However, on most nights N₂O₅ levels were too low for this to have a significant effect. Further experiments with isoprene and α -pinene indicated that there was no significant change in NO₃ reactivity when the glass vessel was used or not, indicating no significant losses of these VOCs in the glass flask. We cannot exclude that other, less volatile organic trace gases including, e.g., acids or peroxides may be lost in the glass vessel, but these are not expected to contribute significantly to NO₃ losses as their rate coefficients for reaction with NO₃ are generally too low. A further potential bias related to the use of the glass trap is the thermal decomposition of PAN and related peroxy nitrates, which can acquire concentrations of up to a few ppb at this site (Sobanski et al., 2016c; Thieser et al., 2016). If PAN decomposes in the glass vessel NO₂ will form, thus contributing to the measured reactivity. Simulations indicate that during the 40 s residence time in the heated flask (at $50\text{ }^\circ\text{C}$) only a small fraction ($\approx 2.6\%$) of the PAN decomposes to form NO₂. For future experiments in environments of high NO_x with N₂O₅ and NO₃ present, the glass trap will be operated at a lower temperature (e.g., $35\text{ }^\circ\text{C}$, $\tau_{\text{PAN}} \approx 500\text{ s}$, $\tau_{\text{N}_2\text{O}_5} \approx 6\text{ s}$) to make sure all of the N₂O₅/NO₃ is removed but PAN is preserved. We note that when measuring NO₃ reactivity in regions with large biogenic emissions, the use of the glass vessel to remove NO₃ and N₂O₅ is generally not necessary as high levels of biogenic VOCs and the low levels of NO_x often found in forested/rural environments remote from anthropogenic influence will result in very low levels of NO₃ or N₂O₅.

During NOTOMO, ambient levels of NO₂, NO₃, N₂O₅ and organic nitrates were measured with the CRDS instruments previously described by Sobanski et al. (2016a; Thieser et al., 2016). The uncertainty in the measurements was 8 % for NO₂ and 20 % for NO₃, whereas the uncertainty for PAN was highly variable for each data point (Sobanski et al., 2016c). The O₃ mixing ratios were measured using a dual beam ozone monitor (2B Technology model 205) with an uncertainty of 2 %. [NO] was not directly measured but its daytime concentration was calculated assuming photo-stationary state via Eq. (12):

$$[\text{NO}]_{\text{calc}} = \frac{J(\text{NO}_2)[\text{NO}_2]}{k_{(\text{NO}+\text{O}_3)}[\text{O}_3]} \quad (12)$$

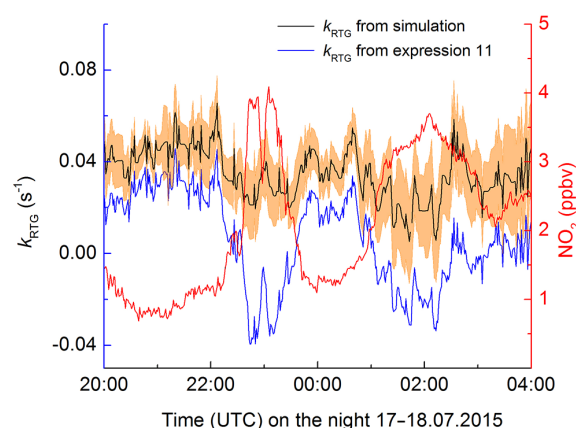


Figure 13. Zoom in on a nighttime period with low reactivity emphasizing the effect of NO₂-induced formation and decomposition of N₂O₅.

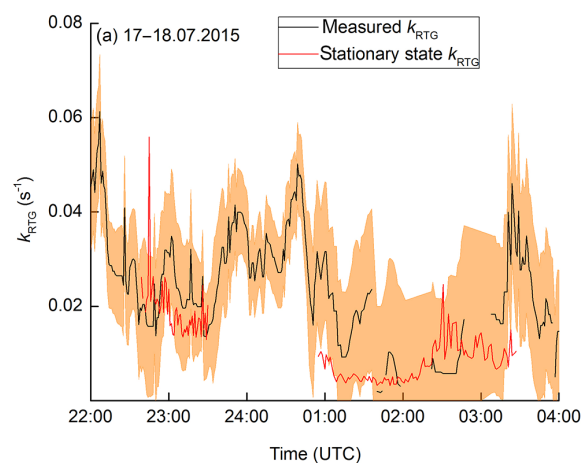


Figure 14. Comparison of stationary-state and measured NO₃ loss rates on two nights (17–18 July and 18–19 July 2015). Uncertainty in k_{RTG} (see text) is displayed as the amber shaded area.

where $J(\text{NO}_2)$ is the photolysis frequency of NO₂ and $k_{(\text{NO}+\text{O}_3)}$ is the rate constant for reaction of NO with O₃. This expression ignores the oxidation of NO to NO₂ via, e.g., reactions of peroxy radicals and thus overestimates NO. $J(\text{NO}_2)$ was measured using a spectral radiometer located close to the inlet (MetCon).

In this paper we focus on a 3-day period, during which NO₃ reactivity was measured (Fig. 12). The NO₃ reactivity, k_{RTG} , varied from 0.005 to 0.1 s^{-1} during nighttime but reached values as high as 1.4 s^{-1} during daytime. The total uncertainty of the measurement is depicted by the amber, shaded area. The red line indicates that daytime losses are dominated by reaction with NO (up to 1.3 s^{-1}). Nighttime values of k_{RTG} were between 0.005 and 0.1 s^{-1} . Assuming that NO levels are close to zero as measured previously at this site during nighttime (Crowley et al., 2010), k_{RTG} is then expected to be dominated by VOCs.

In Fig. 13, we compare values of k_{RTG} obtained by rigorous data correction (black curve) to those calculated directly from Eq. (11) (blue curve). The simple analytical expression (blue line) results in an underestimation of the reactivity, especially during night, when the overall reactivity is low, and in periods of high [NO₂]. Owing to lack of temperature stabilization of the darkened reactor (at this time not yet incorporated) and breakdown of the flow-tube thermostat during the campaign, temperature fluctuations in the container resulted in $\text{MDC}_{\text{NO}_3} = 5.6$ pptv and hence an average, lowest measurable reactivity of $\approx 0.01 \text{ s}^{-1}$ during the campaign. As described in Sect. 5 the minimum detectable change in NO₃ was combined with the uncertainty associated with the dilution factor, reaction time, [NO₂], [PAN] and rate constants used to calculate the overall uncertainty for the reactivity at every data point. The overall uncertainty for the measurement period illustrated in Fig. 13 was $\approx 25 \%$.

In Fig. 14, we compare the measured nighttime NO₃ reactivity with that obtained from the stationary-state analysis using Eq. (1). For the two nights in the period analyzed, NO₃ mixing ratios were between 5 and 37 pptv and the calculated stationary-state loss rate coefficients varied between 0.03 and 0.003 s^{-1} compared to the measured reactivity which was between 0.05 and 0.006 s^{-1} with a short time period in which k_{RTG} fell below the detection limit of the instrument. Within the total uncertainty, the measured and stationary-state reactivities are in reasonable agreement for most of the night from the 17 to the 18 July. From the night 18 to the 19 July the stationary-state reactivity is much lower (up to a factor of 8) than that measured. This difference and also the higher variability can be attributed to rapid variations in concentrations of VOCs at the inlet (due, e.g., to emissions from nearby trees) that are not considered in the stationary-state approach; i.e., very local emissions of reactive gases will result in breakdown of the stationary-state assumption, leading to the underestimation of the reactivity of the local mixture of VOCs and NO_x. As the direct measurement of the NO₃ reactivity with this device sums over all VOCs present in the air mass sampled, it should give the same result as summing each VOC concentration multiplied by the individual rate coefficients for reaction with NO₃, i.e. NO₃ reactivity = $\sum[\text{VOC}]_i k_i$. As demonstrated previously for this mountain site (Sobanski et al., 2016b), summed losses based on measurement of VOCs can significantly exceed the reactivity based on a stationary-state analysis especially under some meteorological situations in which a low-lying residual layer (with high NO₃ concentrations) influences the measurement.

7 Conclusion and outlook

We present the first instrument for measurement of NO₃ reactivity in ambient air. The flow-tube-based instrument utilizes the depletion of synthetically generated NO₃ when mixed with ambient air and has a dynamic range of 0.005 to 45 s^{-1} .

Following intensive laboratory characterization to determine the effective reaction time, the wall loss constant of NO₃ and the effect of NO₃ formation and reformation in the flow tube, it was successfully tested against an isoprene standard. The overall uncertainty depends on the relative rate of reaction of NO₃ with NO₂ or with other traces gases (e.g., VOCs or NO) that do not generate N₂O₅ and which, under ideal conditions, is close to 15 %. The instrument is thus best suited for measurement of NO₃ reactivity in regions with high biogenic activity and relatively low direct anthropogenic emissions of NO_x, i.e., regions where the measurement of NO₃ concentrations is difficult owing to low production rates and a high loss term.

First deployment of the instrument was during the NOTOMO observational experiment in summer 2015 at a forested, mountain site with urban influence. The measured NO₃ reactivity ranged from 0.006 to 0.1 s^{-1} at nighttime and reached values as high as 1.4 s^{-1} during daytime. As expected, daytime reactivity was dominated by reaction with NO while nighttime reactivity involved other (presumably organic) trace gases. A comparison with stationary-state calculations of the NO₃ reactivity revealed occasional poor agreement, presumably related to very local emissions causing a breakdown of the stationary-state assumption.

Improvements to the dynamic range of the instrument require further stabilization of the NO₃ source and cavity optics to reduce the minimal detectable change in NO₃ (presently $\text{MDC}_{\text{NO}_3} = 2.5$ pptv). This could also be achieved by the use of larger volume flow tubes. Reduction in the initial NO₃ concentration used would also reduce any potential bias caused by depletion of reactants or secondary chemistry. Future deployment with simultaneous measurements of NO₃, NO₂, O₃ and VOCs will be conducted to compare direct measurements of NO₃ reactivity with those obtained from the stationary-state approach and also those calculated from summing losses due to individual VOCs.

Data availability. The NOTOMO data will be released at the end of 2017 when they can be obtained on request (via John Crowley) from the owners.

The Supplement related to this article is available online at doi:10.5194/amt-10-1241-2017-supplement.

Competing interests. The authors declare that they have no conflict of interest.

Acknowledgements. We would like to thank Heinz Bingemer and the staff and department of the Johann Wolfgang Goethe-University, Frankfurt am Main, for logistical support and access to the Taunus Observatory during NOTOMO. We also would like to thank Eva Pfannerstil for providing the isoprene standard. We

thank DuPont for the sample of FEP used to coat the walls of the flow tube and darkened reactor. This work was carried out in partial fulfilment of the PhD (Johannes Gutenberg University, Mainz, Germany) of Jonathan Liebmann.

The article processing charges for this open-access publication were covered by the Max Planck Society.

Edited by: A. Hofzumahaus

Reviewed by: S. Brown and one anonymous referee

References

- Atkinson, R.: Atmospheric chemistry of VOCs and NO_x, *Atmos. Environ.*, 34, 2063–2101, 2000.
- Atkinson, R. and Arey, J.: Gas-phase tropospheric chemistry of biogenic volatile organic compounds: a review, *Atmos. Environ.*, 37, S197–S219, 2003a.
- Atkinson, R. and Arey, J.: Atmospheric degradation of volatile organic compounds, *Chem. Rev.*, 103, 4605–4638, doi:10.1021/cr0206420, 2003b.
- Atkinson, R., Baulch, D. L., Cox, R. A., Crowley, J. N., Hampson, R. F., Hynes, R. G., Jenkin, M. E., Rossi, M. J., and Troe, J.: Evaluated kinetic and photochemical data for atmospheric chemistry: Volume I – gas phase reactions of O_x, HO_x, NO_x and SO_x species, *Atmos. Chem. Phys.*, 4, 1461–1738, doi:10.5194/acp-4-1461-2004, 2004.
- Atkinson, R., Baulch, D. L., Cox, R. A., Crowley, J. N., Hampson, R. F., Hynes, R. G., Jenkin, M. E., Rossi, M. J., Troe, J., and IUPAC Subcommittee: Evaluated kinetic and photochemical data for atmospheric chemistry: Volume II – gas phase reactions of organic species, *Atmos. Chem. Phys.*, 6, 3625–4055, doi:10.5194/acp-6-3625-2006, 2006.
- Berden, G., Peeters, R., and Meijer, G.: Cavity ring-down spectroscopy: Experimental schemes and applications, *Int. Rev. Phys. Chem.*, 19, 565–607, 2000.
- Brown, S. S. and Stutz, J.: radical observations and chemistry, *Chem. Soc. Rev.*, 41, 6405–6447, 2012.
- Brown, S. S., Stark, H., and Ravishankara, A. R.: Cavity ring-down spectroscopy for atmospheric trace gas detection: application to the nitrate radical (NO₃), *Appl. Phys. B-Lasers O.*, 75, 173–182, 2002.
- Brown, S. S., Stark, H., and Ravishankara, A. R.: Applicability of the steady state approximation to the interpretation of atmospheric observations of NO₃ and N₂O₅, *J. Geophys. Res.-Atmos.*, 108, 4539, doi:10.1029/2003JD003407, 2003.
- Brown, S. S., Dube, W. P., Osthoff, H. D., Stutz, J., Ryerson, T. B., Wollny, A. G., Brock, C. A., Warneke, C., De Gouw, J. A., Atlas, E., Neuman, J. A., Holloway, J. S., Lerner, B. M., Williams, E. J., Kuster, W. C., Goldan, P. D., Angevine, W. M., Trainer, M., Fehsenfeld, F. C., and Ravishankara, A. R.: Vertical profiles in NO₃ and N₂O₅ measured from an aircraft: Results from the NOAA P-3 and surface platforms during the New England Air Quality Study 2004, *J. Geophys. Res.-Atmos.*, 112, D22304, doi:10.1029/2007jd008893, 2007a.
- Brown, S. S., Dubé, W. P., Osthoff, H. D., Wolfe, D. E., Angevine, W. M., and Ravishankara, A. R.: High resolution vertical distributions of NO₃ and N₂O₅ through the nocturnal boundary layer, *Atmos. Chem. Phys.*, 7, 139–149, doi:10.5194/acp-7-139-2007, 2007b.
- Brown, S. S., Dube, W. P., Fuchs, H., Ryerson, T. B., Wollny, A. G., Brock, C. A., Bahreini, R., Middlebrook, A. M., Neuman, J. A., Atlas, E., Roberts, J. M., Osthoff, H. D., Trainer, M., Fehsenfeld, F. C., and Ravishankara, A. R.: Reactive uptake coefficients for N₂O₅ determined from aircraft measurements during the Second Texas Air Quality Study: Comparison to current model parameterizations, *J. Geophys. Res.-Atmos.*, 114, D00F10, doi:10.1029/2008JD011679, 2009.
- Burkholder, J. B., Sander, S. P., Abbatt, J., Barker, J. R., Huie, R. E., Kolb, C. E., Kurylo, M. J., Orkin, V. L., Wilmouth, D. M., and Wine, P. H.: Chemical Kinetics and Photochemical Data for Use in Atmospheric Studies, Evaluation No. 18, JPL Publication 15-10, Jet Propulsion Laboratory, Pasadena, USA, available at: <http://jpldataeval.jpl.nasa.gov>, 2016.
- Crowley, J. N., Schuster, G., Pouvesle, N., Parchatka, U., Fischer, H., Bonn, B., Bingemer, H., and Lelieveld, J.: Nocturnal nitrogen oxides at a rural mountain-site in south-western Germany, *Atmos. Chem. Phys.*, 10, 2795–2812, doi:10.5194/acp-10-2795-2010, 2010.
- Crowley, J. N., Thieser, J., Tang, M. J., Schuster, G., Bozem, H., Beygi, Z. H., Fischer, H., Diesch, J.-M., Drewnick, F., Borrmann, S., Song, W., Yassaa, N., Williams, J., Pöhler, D., Platt, U., and Lelieveld, J.: Variable lifetimes and loss mechanisms for NO₃ and N₂O₅ during the DOMINO campaign: contrasts between marine, urban and continental air, *Atmos. Chem. Phys.*, 11, 10853–10870, doi:10.5194/acp-11-10853-2011, 2011.
- Crutzen, P.: A discussion of the chemistry of some minor constituents in the stratosphere and troposphere, *Pure Appl. Geophys.*, 106–108, 1385–1399, 1973.
- Curtis, A. R. and Sweetenham, W. P.: Facsimile, AERE, Report R-12805, Harwell Laboratory, Oxfordshire, UK, 1987.
- Dentener, F. J. and Crutzen, P. J.: Reaction of N₂O₅ on tropospheric aerosols – Impact on the global distributions of NO_x, O₃, and OH, *J. Geophys. Res.-Atmos.*, 98, 7149–7163, 1993.
- Donahue, N. M., Clarke, J. S., Demerjian, K. L., and Anderson, J. G.: Free-radical kinetics at high pressure: A mathematical analysis of the flow reactor, *J. Phys. Chem.*, 100, 5821–5838, 1996.
- Fry, J. L., Draper, D. C., Barsanti, K. C., Smith, J. N., Ortega, J., Winkle, P. M., Lawler, M. J., Brown, S. S., Edwards, P. M., Cohen, R. C., and Lee, L.: Secondary Organic Aerosol Formation and Organic Nitrate Yield from NO₃ Oxidation of Biogenic Hydrocarbons, *Environ. Sci. Technol.*, 48, 11944–11953, doi:10.1021/es502204x, 2014.
- Fuchs, H., Dube, W. P., Cicciola, S. J., and Brown, S. S.: Determination of inlet transmission and conversion efficiencies for in situ measurements of the nocturnal nitrogen oxides, NO₃, N₂O₅ and NO₂, via pulsed cavity ring-down spectroscopy, *Anal. Chem.*, 80, 6010–6017, 2008.
- Geyer, A. and Platt, U.: Temperature dependence of the NO₃ loss frequency: A new indicator for the contribution of NO₃ to the oxidation of monoterpenes and NO_x removal in the atmosphere, *J. Geophys. Res.-Atmos.*, 107, 4431, doi:10.1029/2001JD001215, 2002.
- Groß, C. B. M., Dillon, T. J., Schuster, G., Lelieveld, J., and Crowley, J. N.: Direct kinetic study of OH and O₃ formation in the reaction of CH₃C(O)O₂ with HO₂, *J. Phys. Chem. A*, 118, 974–985, doi:10.1021/jp412380z, 2014.

- Guenther, A. B., Jiang, X., Heald, C. L., Sakulyanontvittaya, T., Duhl, T., Emmons, L. K., and Wang, X.: The Model of Emissions of Gases and Aerosols from Nature version 2.1 (MEGAN2.1): an extended and updated framework for modeling biogenic emissions, *Geosci. Model Dev.*, 5, 1471–1492, doi:10.5194/gmd-5-1471-2012, 2012.
- Heintz, F., Platt, U., Flentje, H., and Dubois, R.: Long-term observation of nitrate radicals at the tor station, Kap Arkona (Rügen), *J. Geophys. Res.-Atmos.*, 101, 22891–22910, 1996.
- Howard, C. J.: Kinetic measurements using flow tubes, *J. Phys. Chem.*, 83, 3–9, 1979.
- Huang, Y., Shen, H. Z., Chen, Y. L., Zhong, Q. R., Chen, H., Wang, R., Shen, G. F., Liu, J. F., Li, B. G., and Tao, S.: Global organic carbon emissions from primary sources from 1960 to 2009, *Atmos. Environ.*, 122, 505–512, doi:10.1016/j.atmosenv.2015.10.017, 2015.
- Huang, Y., Coggon, M. M., Zhao, R., Lignell, H., Bauer, M. U., Flagan, R. C., and Seinfeld, J. H.: The Caltech Photooxidation Flow Tube reactor: design, fluid dynamics and characterization, *Atmos. Meas. Tech.*, 10, 839–867, doi:10.5194/amt-10-839-2017, 2017.
- IUPAC: Task Group on Atmospheric Chemical Kinetic Data Evaluation, Ammann, M., Cox, R. A., Crowley, J. N., Herrmann, H., Jenkin, M. E., McNeill, V. F., Mellouki, A., Rossi, M. J., Troe, J. and Wallington, T. J., available at: <http://iupac.pole-ether.fr/index.html>, last access: November 2016.
- Kovacs, T. A. and Brune, W. H.: Total OH loss rate measurement, *J. Atmos. Chem.*, 39, 105–122, doi:10.1023/a:1010614113786, 2001.
- Lelieveld, J., Butler, T. M., Crowley, J. N., Dillon, T. J., Fischer, H., Ganzeveld, L., Harder, H., Lawrence, M. G., Martinez, M., Taraborrelli, D., and Williams, J.: Atmospheric oxidation capacity sustained by a tropical forest, *Nature*, 452, 737–740, 2008.
- Lelieveld, J., Gromov, S., Pozzer, A., and Taraborrelli, D.: Global tropospheric hydroxyl distribution, budget and reactivity, *Atmos. Chem. Phys.*, 16, 12477–12493, doi:10.5194/acp-16-12477-2016, 2016.
- Mielke, L. H., Furgeson, A., and Osthoff, H. D.: Observation of CINO₂ in a mid-continental urban environment, *Environ. Sci. Technol.*, 45, 8889–8896, doi:10.1021/es201955u, 2011.
- Mogensen, D., Gierens, R., Crowley, J. N., Keronen, P., Smolander, S., Sogachev, A., Nölscher, A. C., Zhou, L., Kulmala, M., Tang, M. J., Williams, J., and Boy, M.: Simulations of atmospheric OH, O₃ and NO₃ reactivities within and above the boreal forest, *Atmos. Chem. Phys.*, 15, 3909–3932, doi:10.5194/acp-15-3909-2015, 2015.
- Ng, N. L., Brown, S. S., Archibald, A. T., Atlas, E., Cohen, R. C., Crowley, J. N., Day, D. A., Donahue, N. M., Fry, J. L., Fuchs, H., Griffin, R. J., Guzman, M. I., Herrmann, H., Hodzic, A., Iinuma, Y., Jimenez, J. L., Kiendler-Scharr, A., Lee, B. H., Luecken, D. J., Mao, J., McLaren, R., Mutzel, A., Osthoff, H. D., Ouyang, B., Picquet-Varrault, B., Platt, U., Pye, H. O. T., Rudich, Y., Schwantes, R. H., Shiraiwa, M., Stutz, J., Thornton, J. A., Tilgner, A., Williams, B. J., and Zaveri, R. A.: Nitrate radicals and biogenic volatile organic compounds: oxidation, mechanisms, and organic aerosol, *Atmos. Chem. Phys.*, 17, 2103–2162, doi:10.5194/acp-17-2103-2017, 2017.
- Orphal, J., Fellows, C. E., and Flaud, P. M.: The visible absorption spectrum of NO₃ measured by high-resolution Fourier transform spectroscopy, *J. Geophys. Res.-Atmos.*, 108, 4077, doi:10.1029/2002JD002489, 2003.
- Osthoff, H. D., Pilling, M. J., Ravishankara, A. R., and Brown, S. S.: Temperature dependence of the NO₃ absorption cross-section above 298 K and determination of the equilibrium constant for NO₃+NO₂ <-> N₂O₅ at atmospherically relevant conditions, *Phys. Chem. Chem. Phys.*, 9, 5785–5793, 2007.
- Osthoff, H. D., Roberts, J. M., Ravishankara, A. R., Williams, E. J., Lerner, B. M., Sommariva, R., Bates, T. S., Coffman, D., Quinn, P. K., Dibb, J. E., Stark, H., Burkholder, J. B., Talukdar, R. K., Meagher, J., Fehsenfeld, F. C., and Brown, S. S.: High levels of nitryl chloride in the polluted subtropical marine boundary layer, *Nat. Geosci.*, 1, 324–328, 2008.
- Phillips, G. J., Tang, M. J., Thieser, J., Brickwedde, B., Schuster, G., Bohn, B., Lelieveld, J., and Crowley, J. N.: Significant concentrations of nitryl chloride observed in rural continental Europe associated with the influence of sea salt chloride and anthropogenic emissions, *Geophys. Res. Lett.*, 39, L10811, doi:10.1029/2012GL051912, 2012.
- Riedel, T. P., Bertram, T. H., Crisp, T. A., Williams, E. J., Lerner, B. M., Vlasenko, A., Li, S. M., Gilman, J., de Gouw, J., Bon, D. M., Wagner, N. L., Brown, S. S., and Thornton, J. A.: Nitryl Chloride and Molecular Chlorine in the Coastal Marine Boundary Layer, *Environ. Sci. Technol.*, 46, 10463–10470, doi:10.1021/es204632r, 2012.
- Rinne, J., Markkanen, T., Ruuskanen, T. M., Petäjä, T., Keronen, P., Tang, M. J., Crowley, J. N., Rannik, Ü., and Vesala, T.: Effect of chemical degradation on fluxes of reactive compounds – a study with a stochastic Lagrangian transport model, *Atmos. Chem. Phys.*, 12, 4843–4854, doi:10.5194/acp-12-4843-2012, 2012.
- Schuster, G., Labazan, I., and Crowley, J. N.: A cavity ring down/cavity enhanced absorption device for measurement of ambient NO₃ and N₂O₅, *Atmos. Meas. Tech.*, 2, 1–13, doi:10.5194/amt-2-1-2009, 2009.
- Seeley, J. V., Jayne, J. T., and Molina, M. J.: High-Pressure Fast-Flow Technique for Gas-Phase Kinetics Studies, *Int. J. Chem. Kinet.*, 25, 571–594, 1993.
- Sinha, V., Williams, J., Crowley, J. N., and Lelieveld, J.: The Comparative Reactivity Method – a new tool to measure total OH Reactivity in ambient air, *Atmos. Chem. Phys.*, 8, 2213–2227, doi:10.5194/acp-8-2213-2008, 2008.
- Sobanski, N., Schuladen, J., Schuster, G., Lelieveld, J., and Crowley, J. N.: A five-channel cavity ring-down spectrometer for the detection of NO₂, NO₃, N₂O₅, total peroxy nitrates and total alkyl nitrates, *Atmos. Meas. Tech.*, 9, 5103–5118, doi:10.5194/amt-9-5103-2016, 2016a.
- Sobanski, N., Tang, M. J., Thieser, J., Schuster, G., Pöhler, D., Fischer, H., Song, W., Sauvage, C., Williams, J., Fachinger, J., Berkes, F., Hoor, P., Platt, U., Lelieveld, J., and Crowley, J. N.: Chemical and meteorological influences on the lifetime of NO₃ at a semi-rural mountain site during PARADE, *Atmos. Chem. Phys.*, 16, 4867–4883, doi:10.5194/acp-16-4867-2016, 2016b.
- Sobanski, N., Thieser, J., Schuladen, J., Sauvage, C., Song, W., Williams, J., Lelieveld, J., and Crowley, J. N.: Day- and Night-time Formation of Organic Nitrates at a Forested Mountain-site in South West Germany, *Atmos. Chem. Phys. Discuss.*, accepted, 2016c.
- Thieser, J., Schuster, G., Schuladen, J., Phillips, G. J., Reiffs, A., Parchatka, U., Pöhler, D., Lelieveld, J., and Crowley, J. N.: A

- two-channel thermal dissociation cavity ring-down spectrometer for the detection of ambient NO₂, RO₂NO₂ and RONO₂, *Atmos. Meas. Tech.*, 9, 553–576, doi:10.5194/amt-9-553-2016, 2016.
- Thornton, J. A., Kercher, J. P., Riedel, T. P., Wagner, N. L., Cozic, J., Holloway, J. S., Dube, W. P., Wolfe, G. M., Quinn, P. K., Middlebrook, A. M., Alexander, B., and Brown, S. S.: A large atomic chlorine source inferred from mid-continental reactive nitrogen chemistry, *Nature*, 464, 271–274, doi:10.1038/nature08905, 2010.
- Wagner, N. L., Dubé, W. P., Washenfelder, R. A., Young, C. J., Pollack, I. B., Ryerson, T. B., and Brown, S. S.: Diode laser-based cavity ring-down instrument for NO₃, N₂O₅, NO, NO₂ and O₃ from aircraft, *Atmos. Meas. Tech.*, 4, 1227–1240, doi:10.5194/amt-4-1227-2011, 2011.
- Wayne, R. P., Barnes, I., Biggs, P., Burrows, J. P., Canosa-Mas, C. E., Hjorth, J., Le Bras, G., Moortgat, G. K., Perner, D., Poulet, G., Restelli, G., and Sidebottom, H.: The nitrate radical: Physics, chemistry, and the atmosphere, *Atmos. Environ. A*, 25A, 1–206, 1991.



Corrigendum to “Measurement of ambient NO₃ reactivity: design, characterization and first deployment of a new instrument” published in Atmos. Meas. Tech., 10, 1241–1258, 2017

Jonathan M. Liebmann, Gerhard Schuster, Jan B. Schuladen, Nicolas Sobanski, Jos Lelieveld, and John N. Crowley
Atmospheric Chemistry Department, Max-Planck-Institut für Chemie, 55128 Mainz, Germany

Correspondence: John N. Crowley (john.crowley@mpic.de)

Published: 1 March 2018

Panel b of Fig. 14 was missing in the published paper.

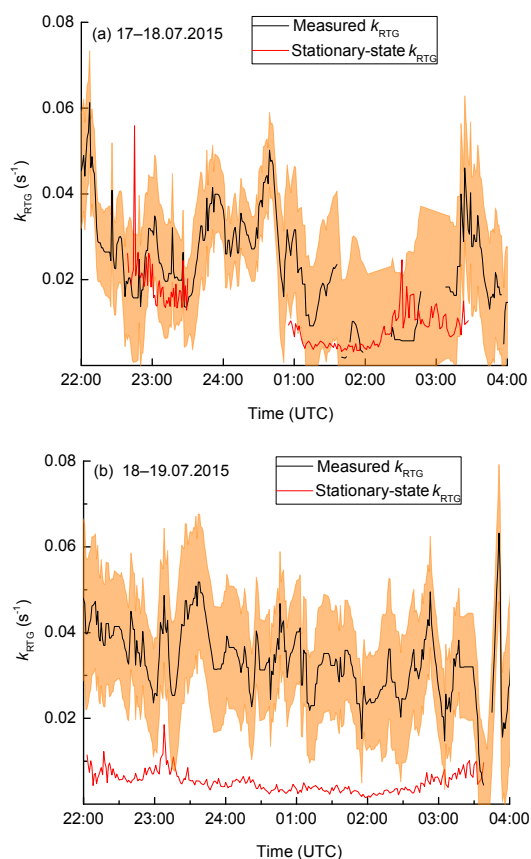


Figure 14. Comparison of stationary-state and measured NO₃ loss rates on two nights (17–18 July and 18–19 July 2015). Uncertainty in k_{RTG} (see text) is displayed as the amber shaded area.

Supplement of Atmos. Meas. Tech., 10, 1241–1258, 2017
<http://www.atmos-meas-tech.net/10/1241/2017/>
doi:10.5194/amt-10-1241-2017-supplement
© Author(s) 2017. CC Attribution 3.0 License.



Atmospheric
Measurement
Techniques



Supplement of

Measurement of ambient NO₃ reactivity: design, characterization and first deployment of a new instrument

Jonathan M. Liebmann et al.

Correspondence to: John N. Crowley (john.crowley@mpic.de)

The copyright of individual parts of the supplement might differ from the CC-BY 3.0 licence.

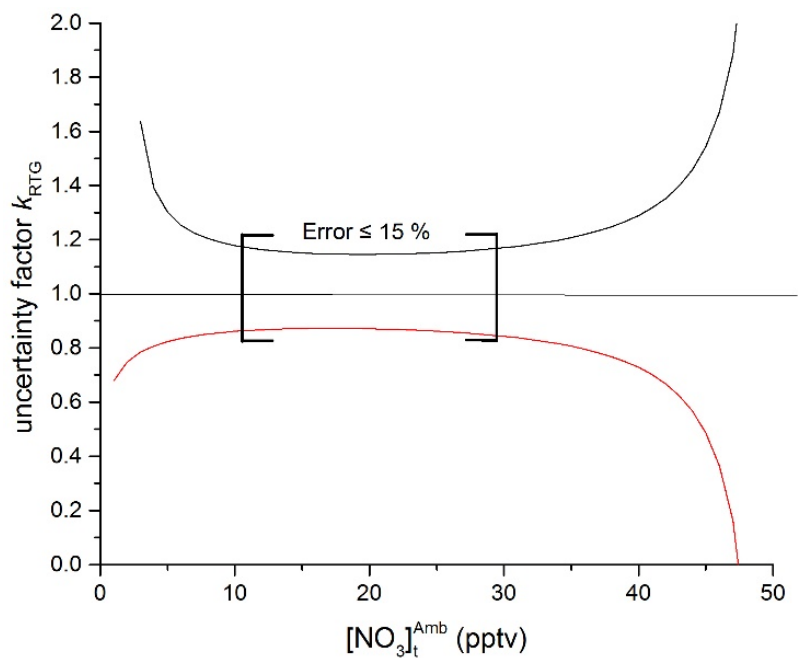


Fig S1: Upper and lower bounds to the uncertainty in the reactivity measurement calculated for a fixed minimal detectable change ($MDC_{NO_3} = 2.5$ pptv) in NO_3 (initially $[NO_3]_t^{ZA} = 50$ pptv) for different reactivities resulting in various measured NO_3 mixing ratios at 10.5 s ($[NO_3]_t^{Amb}$). The straight line ($y=1$) is the ideal case where the MDC_{NO_3} tends to zero. The square brackets indicate the dynamic range in which the uncertainty associated with signal stability is $< \approx 15\%$. When $[NO_3]_t^{Amb}$ and $[NO_3]_t^{ZA}$ are very similar (reactivity tends to zero) or when NO_3 is entirely depleted (very high reactivity) the uncertainty increases rapidly.

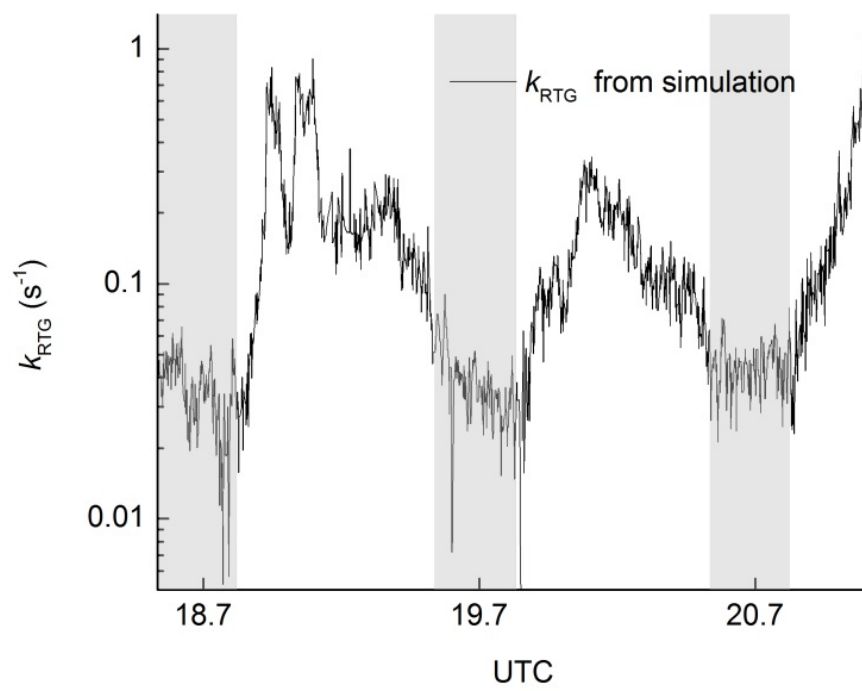


Fig S2: As Figure 12 in the manuscript but showing only k_{RTG} derived from simulation and with the y-axis in log scale.

A2: Liebmann et al., Atmos. Chem. Phys., 2018 A

Direct measurement of NO₃ reactivity in a boreal forest

Jonathan Liebmann¹, Einar Karu¹, Nicolas Sobanski¹, Jan Schuladen¹,
Mikael Ehn³, Simon Schallhart³, Lauriane Quéléver³, Heidi Hellen²,
Hannele Hakola², Thorsten Hoffmann⁴, Jonathan Williams¹, Horst
Fischer¹, Jos Lelieveld¹ and John N. Crowley¹

¹ *Atmospheric Chemistry Department, Max-Planck-Institut für Chemie,
55128 Mainz, Germany*

² *Finnish Meteorological Institute, 00560, Helsinki, Finland*

³ *Department of Physics, University of Helsinki, 00140, Helsinki, Finland*

⁴ *Johannes Gutenberg University, 55128, Mainz, Germany*

Atmospheric Chemistry and Physics, 18, 3799–3815, 2018



Direct measurement of NO₃ radical reactivity in a boreal forest

Jonathan Liebmann¹, Einar Karu¹, Nicolas Sobanski¹, Jan Schuladen¹, Mikael Ehn³, Simon Schallhart³, Lauriane Quéléver³, Heidi Hellen², Hannele Hakola², Thorsten Hoffmann⁴, Jonathan Williams¹, Horst Fischer¹, Jos Lelieveld¹, and John N. Crowley¹

¹Division of Atmospheric Chemistry, Max Planck Institut für Chemie, 55128, Mainz, Germany

²Finnish Meteorological Institute, 00560, Helsinki, Finland

³Department of Physics, University of Helsinki, 00140, Helsinki, Finland

⁴Johannes Gutenberg University, 55128, Mainz, Germany

Correspondence: John N. Crowley (john.crowley@mpic.de)

Received: 19 October 2017 – Discussion started: 16 November 2017

Revised: 1 February 2018 – Accepted: 12 February 2018 – Published: 15 March 2018

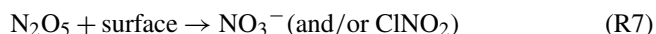
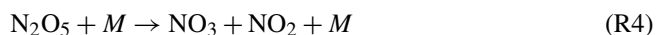
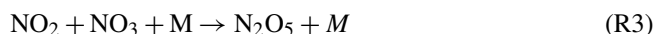
Abstract. We present the first direct measurements of NO₃ reactivity (or inverse lifetime, s⁻¹) in the Finnish boreal forest. The data were obtained during the IBairn campaign (Influence of Biosphere-Atmosphere Interactions on the Reactive Nitrogen budget) which took place in Hyytiälä, Finland during the summer/autumn transition in September 2016. The NO₃ reactivity was generally very high with a maximum value of 0.94 s⁻¹ and displayed a strong diel variation with a campaign-averaged nighttime mean value of 0.11 s⁻¹ compared to a daytime value of 0.04 s⁻¹. The highest nighttime NO₃ reactivity was accompanied by major depletion of canopy level ozone and was associated with strong temperature inversions and high levels of monoterpenes. The daytime reactivity was sufficiently large that reactions of NO₃ with organic trace gases could compete with photolysis and reaction with NO. There was no significant reduction in the measured NO₃ reactivity between the beginning and end of the campaign, indicating that any seasonal reduction in canopy emissions of reactive biogenic trace gases was offset by emissions from the forest floor. Observations of biogenic hydrocarbons (BVOCs) suggested a dominant role for monoterpenes in determining the NO₃ reactivity. Reactivity not accounted for by in situ measurement of NO and BVOCs was variable across the diel cycle with, on average, ≈ 30 % “missing” during nighttime and ≈ 60 % missing during the day. Measurement of the NO₃ reactivity at various heights (8.5 to 25 m) both above and below the canopy, revealed a strong nighttime, vertical gradient with maximum values closest to the ground. The gradient disappeared during the daytime due to efficient vertical mixing.

1 Introduction

Biogenic and anthropogenic volatile organic compounds (VOCs) have a significant impact on air quality and human health and knowledge of their tropospheric lifetimes, determined by the oxidizing capacity of the lowermost atmosphere, is a prerequisite to predicting future atmospheric composition and climate change (Lelieveld et al., 2008). Recent estimates (Guenther et al., 2012) suggest that about 1000 Tg of biogenic volatile organic compounds (BVOCs), are emitted annually by vegetation. The boreal forest covers an area of ≈ 15 million km² worldwide, which is comparable to that covered by tropical rainforest (Eerdeken et al., 2009). Forests emit large amounts of unsaturated hydrocarbons in the form of the terpenoids such as, isoprene (2-methylbuta-1,3-diene, C₅H₈), monoterpenes (C₁₀H₁₆), and sesquiterpenes (C₁₅H₂₄) that have a significant impact on HO_x (HO + HO₂) and NO_x (NO + NO₂) budgets (Hakola et al., 2003; Tarvainen et al., 2005; Holzke et al., 2006; Lapalainen et al., 2009) and the formation of secondary organic particle (Hallquist et al., 2009).

Along with the reaction with O₃, BVOCs are oxidized in the troposphere by reactions with OH and NO₃ radicals. OH radical-induced oxidation mainly takes place during daytime with the NO₃ radical (formed by reaction of O₃ with NO₂, Reaction R1) accounting for the major fraction of radical-induced loss of BVOC at nighttime (Wayne et al., 1991; Atkinson, 2000; Atkinson and Arey, 2003a, b; Brown and Stutz, 2012; Mogensen et al., 2015; Ng et al., 2017; Liebmann et al., 2017). The rapid photolysis of NO₃ by sunlight

(Reactions R5, R6) and reaction with NO (Reaction R2) typically reduces its lifetime to a few seconds during daytime. At nighttime, reaction of NO₃ with NO₂ results in thermal equilibrium between NO₃ and N₂O₅ (Reactions R3, R4).



Reactions (R1) to (R6) do not represent a reduction of NO_x as no reactive nitrogen species are removed from the gas phase. However, heterogeneous uptake of N₂O₅ to particles (R7) and the reaction of NO₃ with BVOCs (forming either HNO₃ or organic nitrates, see below) both result in the transfer of gas-phase NO_x to particulate forms, thus reducing the rate of photochemical O₃ formation from NO₂ photolysis (Dentener and Crutzen, 1993).

In forested environments at low NO_x the lifetime of NO₃ with respect to chemical losses during the temperate months will generally be driven by the terpenoids (isoprene, monoterpenes, and sesquiterpenes), the reaction proceeding via addition to the carbon–carbon double bond to form nitrooxyalkyl peroxy radicals. The peroxy radicals react further (with HO₂, NO, NO₂, or NO₃) to form multi-functional peroxides and organic nitrates, which can contribute to the generation and growth of secondary organic aerosols (Ehn et al., 2014; Fry et al., 2014; Ng et al., 2017; Liebmann et al., 2017) or be lost by deposition. The main processes outlining the role of NO₃ in removing NO_x from the atmosphere are summarized in Fig. 1. Clearly, the lifetime of NO₃ with respect to reaction with BVOCs (the subject of this article) determines the relative rate of formation of inorganic nitrate via heterogeneous processes (HNO₃) and organic nitrates, which have different lifetimes with respect to chemical and depositional loss and thus different efficiencies of NO_x removal. It also indirectly determines the rate of generation of reactive chlorine (in the form of ClNO₂) resulting from the heterogeneous reactions of N₂O₅ with chloride containing particles (Osthoff et al., 2008; Thornton et al., 2010; Phillips et al., 2012, 2016; Ammann et al., 2013).

Reactivity measurements have previously been applied to assess the overall loss rates of the OH radical in the boreal forest and to test for closure in its budget (Hens et al., 2014). In forested environments, the measured reactivity has generally been found to be significantly higher than that calculated from summing up reactivity due to individual reactive trace gases, (Sinha et al., 2010; Nölscher et al., 2012, 2016) resulting in an apparent “missing reactivity”. In a similar vein, O₃ flux measurements in Californian pine forests required monoterpene emissions that were 10 times higher

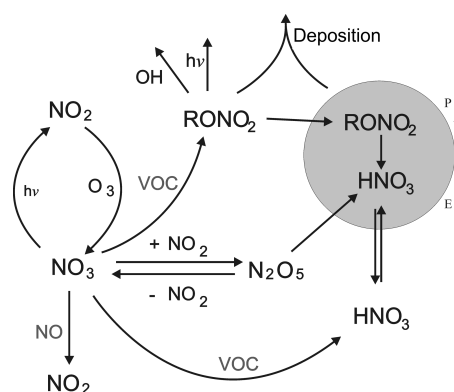


Figure 1. Gas-phase formation and loss of tropospheric NO₃ indicating processes which transfer reactive nitrogen to the particulate phase. RONO₂ are alkyl nitrates. VOC is volatile organic compound.

than measured in order to explain the O₃ losses (Goldstein et al., 2004). These studies argue for the presence of monoterpenes/sesquiterpenes that are not detected by standard instruments used to measure BVOCs. Direct measurements of NO₃ reactivity were not available until very recently (Liebmann et al., 2017); hence the reactivity of NO₃ has traditionally been calculated from concentration measurements by assuming balanced production and loss terms (stationary state, see Sect. 3.4), or from measurements of the VOCs that contribute to its loss and the known rate constant for reaction of each VOC with NO₃. The first method may break down when stationary state is not achieved (Brown et al., 2003). For example, Sobanski et al. (2016b) observed much lower stationary-state loss rates of NO₃ compared to those calculated from measured VOC mixing ratios in a forested/urban location. It was therefore concluded that this was mainly the result of sampling from a low-lying residual layer with VOC emissions that were too close to the sampling point for NO₃ concentrations to achieve stationary state. The second method relies on comprehensive measurement and accurate quantification of all VOCs that react with NO₃, which, in a chemically complex environment such as a forest, may not always be possible.

In this paper we describe direct, point measurements of NO₃ reactivity in ambient air in the boreal forest of southern Finland and analyse the results using ancillary measurements of NO_x, NO₃, O₃, and biogenic hydrocarbons as well as meteorological parameters.

2 Measurement site and instrumentation

The IBairn campaign took place in September 2016 in the boreal forest at Hyytiälä, Finland. September marks the transition from late summer to autumn at Hyytiälä, with the number of daylight hours at the site changing from ≈ 14 to 11.5 from the beginning to the end of September, with the

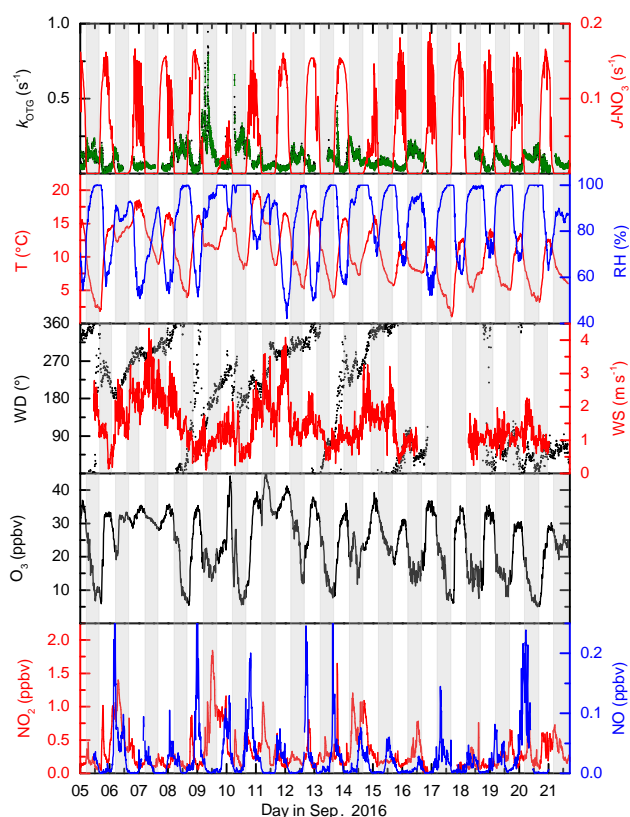


Figure 2. Overview of measurements during IBairn. The grey shaded regions represent nighttime. The uncertainty in k_{OTG} is given by the green shaded region. Measurements were obtained from the common inlet at a height of 8.5 m apart from the NO₃ photolysis rate (taken from a height of 35 m on an adjacent tower), wind direction (WD) and wind speed (WS) (both at 16.5 m on the 128 m tower). A time series of k_{OTG} is given in log scale in the Supplement (Fig. S1).

first widespread ground frost occurring close to the end of the campaign. The relative humidity within the canopy frequently reached 100 % at nighttime, though there was little rainfall during the study period. By the end of the campaign, the initially green leaves of deciduous trees had turned brown and fresh needle/leaf litter was accumulating on the forest floor. The daily profiles of temperature, relative humidity and the NO₃ photolysis rate constant (J_{NO_3}) are displayed in Fig. 2.

2.1 SMEAR II site

The measurements presented here were conducted at the “Station for Measuring Forest Ecosystem-Atmosphere Relations II” (SMEAR II) in Hyytiälä (61°51′ N, 24°17′ E) in southern Finland at 180 m above sea level (Hari and Kulmala, 2005). This site has been the focus of intensive research investigating BVOCs (Rinne et al., 2005; Holzke et al., 2006; Hakola et al., 2009; Lappalainen et al., 2009;

Aaltonen et al., 2011) and their influence on O₃ reactivity (Mogensen et al., 2015; Zhou et al., 2017), OH reactivity (Sinha et al., 2010; Nölscher et al., 2012) and simulations on NO₃ lifetimes (Hakola et al., 2003; Peräkylä et al., 2014). SMEAR II is located 49 km north-east of Tampere (pop. ≈ 226 000; 430 inh. km⁻²) and 88 km south-west of Jyväskylä (pop. ≈ 137 000; 120 inh. km⁻²). Anthropogenic influence at the site is generally low, especially when the wind comes from the sparsely populated northern sector. Operations of a sawmill, a wood mill, and a pellet factory in Korkeakoski, 5 km southeast of Hyytiälä, can result in elevated levels of monoterpenes at SMEAR II (Eerdeken et al., 2009; Liao et al., 2011; Williams et al., 2011; Hakola et al., 2012). Furthermore, pollution from forest management as well as minor influences from nearby settlements with low population densities are possible.

Figure 2 shows the local wind speed and wind direction at a height of 16 m (close to the top of the canopy) during the campaign. The wind rose in Fig. 3a indicates that the prevailing wind was from the north-west and north-east sectors (≈ 60 % of the time) compared to 28 % from the southern sector, of which only ≈ 8 % came from the south-east. Nonetheless, two isolated plumes from Korkeakoski were evident as greatly increased values of the NO₃ reactivity and BVOC levels, as discussed later. In general wind speeds at a height of 16 m were low, favouring a stable boundary layer during nighttime. Wind speed, wind direction, temperature, precipitation, and relative humidity were monitored at various heights on the 128 m SMEAR II tower. Details regarding these and other supporting measurements made at this site can be found elsewhere (Hari and Kulmala, 2005; Hari et al., 2013). The vegetation at the site consists mostly of Scots pine (*Pinus sylvestris*, > 60 %) with occasional Norway spruce (*Picea abies*), aspen (*Populus sp.*) and birch (*Betula sp.*). The most common vascular plants are lingonberry (*Vaccinium vitis-idea* L.), bilberry (*Vaccinium myrtillus* L.), wavy hair grass (*Deschampsia flexuosa* (L.) Trin.) and heather (*Calluna vulgaris* (L.) Hull.). The ground is covered with common mosses as such as Schreber’s big red stem moss (*Pleurozium schreberi* (Brid.) Mitt.) and a dicranum moss (*Dicranum Hedw. sp.*). The canopy height is ≈ 20 m with an average tree density of 1370 stems (diameter at breast height > 5 cm) per hectare (Ilvesniemi et al., 2009).

2.2 NO₃ reactivity measurement

NO₃ reactivity was measured using an instrument that was recently described in detail by Liebmann et al. (2017). Initially, 40 to 60 pptv of synthetically generated NO₃ radicals (Reaction R1) were mixed with either zero air (ZA) or ambient air in a cylindrical flow-tube thermostatted to 21 °C. After a reaction time of 10.5 s, the remaining NO₃ was detected by cavity-ring-down spectroscopy (CRDS) at 662 nm. The measurement cycle was typically 400 s for synthetic air

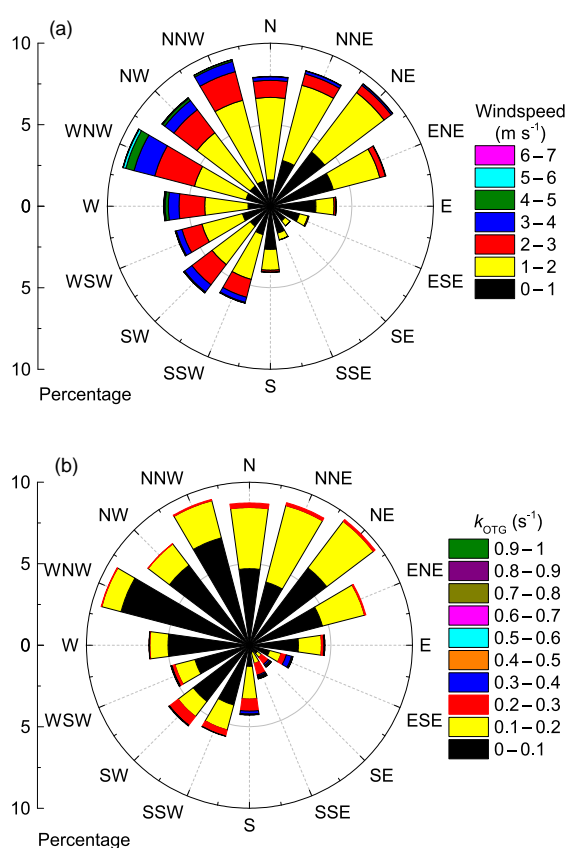


Figure 3. (a) Wind rose coloured according to wind speed. (b) Wind rose coloured according to k_{OTG} .

and 1200 s for ambient air, with intermittent signal zeroing (every ≈ 100 s) by addition of NO.

The observed loss of NO₃ in ambient air compared to ZA was converted to a reactivity via numerical simulation of a simple reaction scheme (Liebmann et al., 2017) using measured amounts of NO, NO₂, and O₃. The parameter obtained, k_{OTG} , is a loss rate constant for NO₃ from which contributions from NO and NO₂ have been removed, and thus refers to reactive loss to organic trace gases (OTGs) only. Throughout the article, NO₃ reactivity and k_{OTG} are equivalent terms, with units of s⁻¹. The dynamic range of the instrument was increased to 0.005–45 s⁻¹ by automated, dynamic dilution of the air sample, the limit of detection being defined by the stability of the NO₃ source. Online calibration of the reactivity using an NO standard was performed every 2 h for 10 min. The uncertainty of the measurement was between 0.005 and 0.158 s⁻¹, depending mainly on dilution accuracy, NO levels, and the stability of the NO₃ source (Liebmann et al., 2017).

The instrument was operated in a laboratory container located in a gravel-bedded clearing in the forest. Air samples were drawn at a flow rate of 2900 standard cubic centimetres per minute (sccm) through a 2 μm membrane filter (Pall Teflo) and 4 m of PFA tubing (6.35 mm OD) from the centre

of a high-flow inlet ($\varnothing = 15$ cm, flow = 10 m³ min⁻¹) which sampled at a height of 8 m, 3 m above the roof of the container and circa 8 m away from the forest edge. Several instruments sampled from the high-flow and we refer to this as the “common inlet”. Relative humidity and temperature were monitored in the common inlet using standard sensors (1st Innovative Sensor Technology, HYT939, $\pm 1.8\%$ RH). Vertical profiles of NO₃ reactivity (8.5 to 25 m) were measured by attaching 30 m of PFA tubing directly to the flow tube and raising/lowering the open end (with membrane filter) using a rope hoist attached to a 30 m tower about 5 m from the container.

2.3 NO, NO₂, O₃, and NO₃ measurements

NO was sampled from the common inlet using a modified commercial chemiluminescence detector (CLD 790 SR) based on the reaction between NO and O₃ (ECO Physics, Dürnten, Switzerland). The detection limit for NO was 5 pptv for an integration period of 5 s, the total uncertainty (2σ) was 20 % (Li et al., 2015). Ozone was measured by two instruments based on optical absorption, both sampling from the common inlet. These were a 2B-Technology, Model 202 and a Thermo Environmental Instruments Inc., Model 49 both with detection limits of ≈ 1 ppb. The two instruments had uncertainties (provided by manufacturer) of 5 and 2 % respectively. Agreement between the two O₃ measurements was excellent (slope = 1.000 ± 0.001 , offset of -0.21 ppbv, $R^2 = 0.98$). Vertical profiles in O₃ (up to 125 m) were made using a TEI 49 C analyser sampling from inlets at various heights on a tower located 130 m north–north-west of the measurement container. NO₂ and NO₃ were measured from the common inlet using a multi-channel, thermal dissociation-cavity ring down spectrometer (TD-CRDS) recently described in detail by (Sobanski et al., 2016a). NO₃ radicals were detected at 662 nm with a detection limit of 1.3 pptv (1 min averaging) and an uncertainty of 25 %. NO₂ was detected at 405 nm with an uncertainty of 6 % and a detection limit of 60 pptv (1 min averaging).

2.4 VOC measurements

Three different instruments were used to monitor VOCs, including (1) a gas chromatograph equipped with an atomic emission detector (GC-AED) which sampled from the common inlet; (2) a thermal desorption gas chromatograph with mass spectrometric detection (GC-MS) sampling about 1.5 m above the ground and ≈ 10 m away from the reactivity measurements; and (3) and a proton transfer reaction time of flight mass spectrometer (PTR-TOF-MS) located about 170 m away in dense forest and sampling at a height of ≈ 2.5 m above the ground.

2.4.1 GC-AED

The GC-AED consisted of a cryogenic pre-concentrator coupled to an Agilent 7890B GC and an atomic emission detector (JAS AEDIII, Moers, Germany). The GC-AED sampled air through a 15 m long, 1/2" (1.27 cm) outer diameter PFA Teflon tube (flow rate = 20 L min⁻¹, transmission time 3.3 s) which was heated to ≈ 10 °C above ambient. The instrument was calibrated in situ with an 84-component gravimetrically prepared gas-phase calibration reference standard with a stated accuracy of better than ±5 % (Apel-Riemer Environmental, Inc., Florida, USA). The average total uncertainty of the species measured from repeated calibration standard measurements combined with the flow measurements and calibration standard uncertainty was calculated to be 14 %. α -pinene, Δ -3-carene, β -pinene, camphene, and *d*-limonene were all calibrated individually. Detection limits for the monoterpene species were 1.0, 0.9, 0.4, 0.5, and 0.3 pptv respectively. As this is the first deployment of this instrument, more details are provided in the Supplement: a full description will be the subject of an upcoming publication.

2.4.2 GC-MS

The GC-MS was located in a container in a gravel-bedded clearing about 4 m from the edge of the forest and ≈ 30 m away from the common inlet. Air samples were taken every other hour (30 min sampling time) at a height of 1.5 m by drawing air at 1 L min⁻¹ through a 1 m long fluorinated ethylene propylene (FEP) inlet (inner diameter 1/8 inch). Ozone was removed via a heated (120 °C) stainless steel tube (Hellén et al., 2012). VOCs were collected from a 40 mL min⁻¹ subsample flow into the cold trap (Tenax TA/Carbopack B) of the thermal desorption unit (TurboMatrix, 650, Perkin-Elmer) connected to a gas chromatograph (Clarus 680, Perkin-Elmer) with HP-5 column (60 m, inner diameter 0.25 mm, film thickness 1 μ m) coupled to a mass spectrometer (Clarus SQ 8 T, Perkin-Elmer). The instrument was used for measurements of isoprene, monoterpenes, and aromatic hydrocarbons and was calibrated for all individual compounds using liquid standards in methanol solutions, which were injected into the Tenax TA/Carbopack B adsorbent tubes and analysed with the same method as the air samples. Detection limits for monoterpenes (α -pinene, camphene, β -pinene, 3 Δ -carene, myrcene, *p*-cymene, limonene, 1,8-cineol, and terpinolene) were 0.2–1.2 pptv and for β -caryophyllene 0.8 pptv. The average total uncertainty (10 % for all monoterpenes and β -caryophyllene) was calculated from the reproducibility of the calibrations, uncertainty of the standard preparation and the uncertainty in the sampling flow.

2.4.3 PTR-TOF-MS

The PTR-TOF-MS (PTR-TOF 8000, Ionicon Analytic GmbH) measures whole VOC spectra in real time (Jordan et al., 2009; Graus et al., 2010) with mass resolution of 4500 (full width at half maximum). The instrument was located in the main cottage, approximately 170 m away from the common inlet. Ambient air was sampled from 2.5 m above the ground, using a 3.5 m long (4 mm inner diameter) PTFE sampling air at 20 L min⁻¹. A subsample flow of 1 L min⁻¹ was passed via 10 cm of PTFE tubing (1.6 mm inner diameter), by way of a three-way valve and 15 cm of PEEK tubing (1 mm inner diameter) to the PTR-TOF-MS. The raw data was collected with 10 s resolution. The instrument measured total monoterpenes at $m/z = 137$ and isoprene at $m/z = 69$, which were calibrated with a gas standard (Apel Riemer Environmental Inc., USA) containing isoprene and α -pinene. The calibration set up and routine are described in detail in Schallhart et al. (2016). The campaign average limit of detection (LOD, 3 σ , 10 min time resolution) was 5.5 and 3.2 pptv for isoprene and monoterpenes respectively.

3 Results and discussion

NO_x mixing ratios were generally low during the campaign with NO₂ between 0.1 to 1.84 ppbv with a campaign average of 0.32 ppbv showing little variation across the diel cycle. The mean daytime NO mixing ratio was 43 pptv while nighttime NO was close to or below the limit of detection (≈ 5 pptv) and its contribution to the loss of NO₃ was generally insignificant (see below). Ozone mixing ratios showed large day/night differences with daily maxima between 30 and 40 ppbv, whilst nighttime values were as low as 5–10 ppbv. Possible reasons for the large changes in O₃ across the diel cycle are addressed in Sect. 3.1.

3.1 NO₃ reactivity and nighttime loss of O₃

NO₃ reactivity was measured from 5 September 12:00 UTC to 22 September 05:30 UTC; the 1 min averaged time series of k_{OTG} is displayed in Fig. 2. The overall uncertainty in k_{OTG} is given by the green, shaded region. NO₃ photolysis and reaction with NO result in concentrations that are generally below the detection limit of modern instruments during daytime and steady-state calculations of NO₃ reactivity are lower limit estimates. In contrast, our direct approach allows us to derive and analyse daytime values of k_{OTG} as long as NO_x measurements are available (see above). Figure 2 indicates that, in general, the NO₃ reactivity was highest at nighttime; the maximum observed values in k_{OTG} was 0.94 s⁻¹, (at 21:00 UTC on 9 September) implying a lifetime of just 1 s and a very reactive air mass at this time. The mean nighttime value of k_{OTG} was ≈ a factor ten lower at 0.11 s⁻¹, the daytime mean even lower at 0.04 s⁻¹. Broadly speaking, the nighttime NO₃ lifetimes during IBAIRN were very short

(≈ 10 s on average) compared to previous indirect, ground level measurements in other locations where several groups have reported lifetimes of hundreds to thousands of seconds (Heintz et al., 1996; Allan et al., 1999; Geyer et al., 2001; Aldener et al., 2006; Ambrose et al., 2007; Brown et al., 2009; Crowley et al., 2010, 2011; Sobanski et al., 2016b). Our short NO₃ lifetimes are, however, compatible with the very low NO₃ mixing ratios observed in forested regions with high rates of emission of biogenic trace gases (Gölz et al., 2001; Rinne et al., 2012; Ayres et al., 2015).

Figure 3b illustrates the dependence of k_{OTG} on wind direction. Air masses from the northern sector were generally associated with lower reactivity ($< 0.2 \text{ s}^{-1}$) whereas all incidents of reactivity larger than 0.3 s^{-1} were associated with air masses from the SE sector. Enhanced reactivity from the south-east may be caused by emissions from the sawmill at Korkeakoski (Eerdekens et al., 2009), or a local woodshed storing freshly cut timber about 100 m away from the containers. This may have been compounded by the lower than average wind speeds associated with air masses from the south-east, which reduced the rate of exchange between the nocturnal boundary layer and above canopy air, effectively trapping ground-level emissions into a shallow boundary layer. Emissions from the sawmill reaching the site on the night of the 9–10 September provided a useful test of our method at high reactivity.

In order to examine the difference in daytime and nighttime NO₃ reactivity and also explain the large nighttime variability in k_{OTG} we categorize the nights into three broad types: (1) nights with strong temperature inversion where the NO₃ reactivity was greatly increased compared to the previous or following day, (2) nights without temperature inversion with comparable (usually low) daytime and nighttime NO₃ reactivity, and (3) events with unusually high NO₃ reactivity. Figure 4 shows an expanded view of k_{OTG} over a five day/night period (5–10 September) in which all three types are represented. It also plots the temperature at different heights as well as the RH and O₃ measured in the common inlet at 8.5 m height.

3.1.1 Type 1 and type 2 nights

Within this 5-day period, the nights on which the reactivity was high relative to the day (type 1) are the 5–6 and 8–9. These nights are characterized by large depletion in O₃, a significant temperature inversion of 5–7 °C between heights of 8 and 128 m, and a relative humidity of 100 % directly after sunset. In contrast, two interspersed nights with comparable reactivity to daytime values (6–7, 7–8, type 2) display much weaker (if any) nighttime loss of O₃ compared to levels during the previous day, no significant temperature inversion and a relative humidity less than 100 %. The observations within this period can be extended to all campaign days. Figure 5 presents the diel cycle of k_{OTG} and O₃ mixing ratios separated into nights of type 1 (with temper-

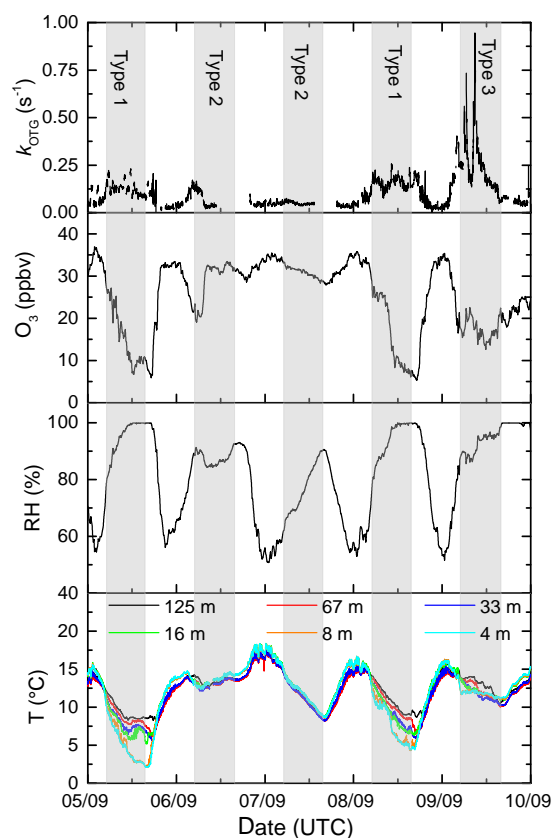


Figure 4. Expanded view of five campaign days illustrating the three types (1–3) of night encountered. Type 1 has a strong vertical gradient in temperature (T) and significant O₃ loss with relative humidity (RH) at 100 %. Type 2 (no temperature inversion), has little or no O₃ loss. Type 3 is influenced by emissions from the Korkeakoski sawmill.

ature inversion) and type 2 (no temperature inversion). The shaded regions represent the variability of the measured values. During 24 h periods in which the night was characterized by strong temperature inversion (panel (a) in Fig. 5), the O₃ mixing ratios display a large diel variation, with a maximum of 35 ppbv at about 13:00 UTC dropping rapidly to a minimum of ≈ 13 ppb between midnight and sunrise at around 05:00 UTC. O₃ depletion due to its slow reaction with NO₂ (present at maximum 2 ppbv at night) does not contribute significantly to its loss even if all resultant NO₃ reacts to form organic nitrates rather than to form N₂O₅ and re-release NO_x.

The O₃ mixing ratio shows an inverse diel profile to the NO₃ reactivity raising the possibility that the rapid loss of ozone is linked to high NO₃ reactivity; the large values of k_{OTG} and rapid O₃ depletion observed on nights with a significant temperature inversion are clear indicators that nighttime boundary layer dynamics plays a key role in controlling both the NO₃ reactivity and O₃ loss. A strong nocturnal temperature inversion will weaken the mixing within or ventila-

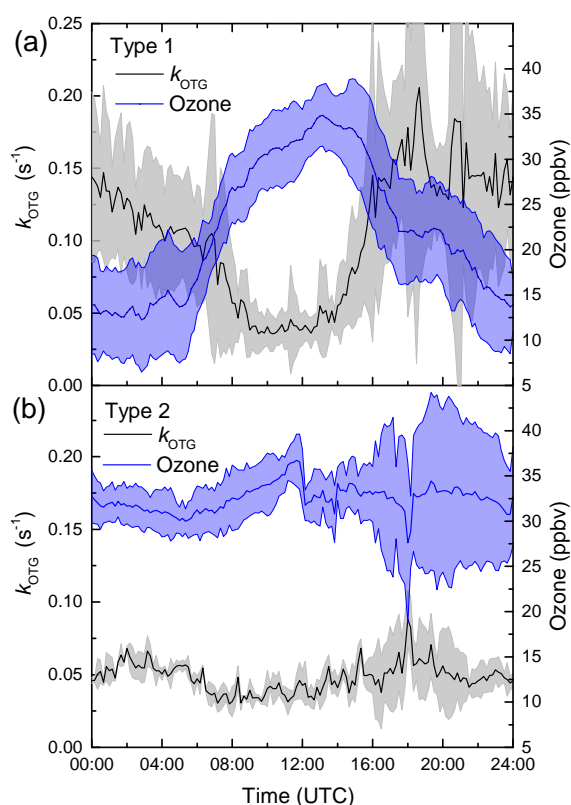


Figure 5. Diel profiles of k_{OTG} (black line) and O₃ (blue line) on two different types of days/nights. (a) Type 1 (strong nighttime temperature inversion). (b) Type 2, (no temperature inversion). The shaded areas represent 2 σ uncertainty and indicate variability over the diel cycle.

tion of the lowermost boundary layer causing a build-up of reactive, biogenic emissions in the lower layer, and also prevent down-mixing of drier, O₃-rich air leading to the apparent higher loss rate of O₃ and higher relative humidity. The strong anti-correlation between k_{OTG} and O₃ may also provide a clue to the origin of the O₃ loss. Whilst the generally high NO₃ reactivity can, to a large extent, be explained by the presence of reactive trace gases (see Sect. 3.2), the precipitous loss of O₃ on several nights when k_{OTG} was high (see Figs. 2 and 4) may have components of both dry deposition and gas-phase reactions.

The campaign averaged, diel variation of ozone at different heights (4 to 125 m) as measured at the SMEAR II tower (Fig. S2 of the Supplement) indicate that the most rapid losses of ozone are at the lowest heights, around and below the canopy. Ozone is generally removed from the lower troposphere by both stomatal and non-stomatal deposition, the latter involving loss to surfaces and soil. The reactive, gas-phase loss mechanisms of O₃ and NO₃ are in some ways similar, as both react with NO to form NO₂, or with unsaturated VOCs by addition to the double bond. We estimated the loss rate constant for O₃ due to its reaction

with terpenes using approximate ambient mixing ratios from 20:00 to 00:00 UTC on the 20 September for *d*-limonene (20 pptv), α -pinene (400 pptv), Δ -carene (100 pptv), and β -pinene (100 pptv) and using literature rate constants for the O₃ + terpene reactions. The calculated O₃ loss (only 2% from 20:00 to 00:00 UTC) is clearly insufficient to explain the IBAIRN observations. We also note that the presence of high concentrations of terpenes when the site was impacted by the Korkeakoski sawmill resulted in the largest NO₃ reactivity observed, but did not lead to large O₃ losses (Fig. 4). As leaf stomata are closed during nighttime, the decrease in O₃ can be attributed either to non-stomatal deposition or chemical sinks due to reaction with reactive biogenic trace gases (not the measured monoterpenes) and NO. Previous studies of O₃ loss in forests have highlighted the potential role of unidentified, reactive organic compounds (Kurpius and Goldstein, 2003; Goldstein et al., 2004; Holzinger et al., 2006; Rannik et al., 2012). In contrast to monoterpenes, which react only slowly with O₃ (rate constants are $\approx 10^{-16}$ – 10^{-17} cm³ molecule⁻¹ s⁻¹), sesquiterpenes can react rapidly; for example, for β -caryophyllene the rate coefficient is $k_{O_3} = 1.2 \times 10^{-14}$ cm³ molecule⁻¹ s⁻¹ (IUPAC, 2017). The presence of sesquiterpenes would therefore provide an explanation for the observations of high NO₃ reactivity and rapid O₃ loss. We examine the potential role of sesquiterpenes in more detail in Sect. 3.2 where the contribution of measured terpenoids to NO₃ reactivity is discussed. We also note that recent modelling studies using Hyytiälä data (Chen et al., 2018; Zhou et al., 2017) conform that O₃ depletion events are associated with the formation of a shallow boundary layer and high relative humidity. Zhou et al. (2017) conclude that chemical reaction plays only a minor role in ozone loss processes during the night, which was suggested to be dominated by deposition to wet surfaces at relative humidity > 70%, which is in accord with laboratory investigations (Sun et al., 2016).

3.1.2 Type 3 nights

The period between the evening and midnight on the 9 September is an example of a type 3 night, with extremely high NO₃ reactivity, which was not accompanied by significant O₃ depletion, temperature inversion or a RH of 100%. The apparently anomalously high reactivity on this night can be traced back to a change in wind direction, which swept from easterly to southerly during this period, bringing air that was impacted by monoterpene emissions from the sawmill in Korkeakoski. High mixing ratios of terpenoids in air masses that have passed over the sawmill have been documented frequently (Eerdeken et al., 2009; Sinha et al., 2010; Liao et al., 2011; Hakola et al., 2012; Nölscher et al., 2012). Other occurrences of sawmill contaminated air during IBAIRN were on the 10 September from 18:40 to 19:00 UTC and on the 14 September from 06:30 to 08:00 UTC, HYSPLIT back-trajectories (GDAS global, 0.5°), indicating that

the air mass passed over Korkeakoski ≈ 0.5 h prior to reaching the SMEAR II site.

3.2 Comparison of k_{OTG} with NO₃ reactivity derived from VOC measurements

In this section we compare k_{OTG} with NO₃ reactivity calculated from ambient VOC mixing ratios. During IBAIRN, three instruments (GC-MS, GC-AED, and PTR-TOF) measuring VOCs were deployed (see Sect. 2.5 for details). As the PTR-TOF reports only a summed mixing ratio of all monoterpenes, $\Sigma\text{MT}(\text{PTR-TOF})$, we first generated an equivalent parameter for the two GCs, $\Sigma\text{MT}(\text{GC-MS})$ and $\Sigma\text{MT}(\text{GC-AED})$. For the GC-MS, α -pinene, β -pinene, Δ -carene, d -limonene, camphene, myrcene, and terpinolene were considered whereas for the GC-AED, α -pinene, β -pinene, Δ -carene, camphene, and d -limonene were taken into account. The ΣMT data are displayed as a time series in Fig. 6, which indicates large differences between the three measurements as highlighted in Fig. S3 of the Supplement). While the $\Sigma\text{MT}(\text{GC-AED})$ and $\Sigma\text{MT}(\text{PTR-TOF})$ data are in reasonable agreement, especially when mixing ratios were large, the values reported by the GC-MS are consistently and significantly lower (factor 2 to > 10) than those of the others instruments. The time dependent variability in the differences in ΣMT reported by the GC-MS, GC-AED, and PTR-TOF is a strong indication that the cause is most likely related to instrument location and inhomogeneity in terpene emissions within the forest. Whilst the GC-AED sampled from the common inlet at a height of 8.5 m, which was also used for the NO₃ reactivity measurements, the inlet of the GC-MS was ≈ 10 m away and sampled 1.5 m above the gravel covered clearing, very close to the side of the container which housed the instrument. The PTR-TOF-MS was located roughly 170 m away in a wooden cottage directly surrounded by dense forest and sampled close to the forest floor at a height of ≈ 1.5 m. With very low within-canopy wind speeds, especially during nighttime, both horizontal as well as vertical mixing in the forest and in the clearing are weak so that each VOC measurement may, to some extent, reflect the mixture and total amount of BVOCs that are very locally emitted. This aspect was examined by comparing individual monoterpenes measured by the GC-MS and the GC-AED. The results, presented as correlation plots for 4 monoterpenes in Fig. S4 of the Supplement, show that the monoterpene ratios measured by the two instruments (GC-AED/GC-MS), were variable with values of 1.69 ± 0.06 for α -pinene, 2.51 ± 0.09 for β -pinene, 4.29 ± 0.21 for Δ -carene, and 0.45 ± 0.03 for d -limonene. A similar picture emerges for isoprene, for which the GC-AED measured mixing ratios that were a factor 2–5 larger than measured by the GC-MS. The variable relative concentrations of monoterpenes reported by each instrument is further evidence of the inhomogeneity of emissions within the forest and also the influence of different tree chemotypes within single tree-

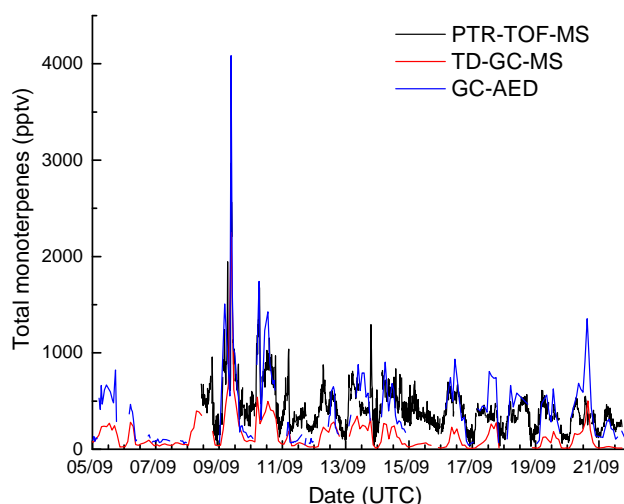


Figure 6. Time series of total monoterpenes from GC-AED (black), GC-MS (red), and PTR-TOF-MS (blue). The data are reproduced as histograms in Fig. S3 of the Supplement.

families in Hyytiälä, which can exhibit vastly different emission rates of various monoterpenes (Bäck et al., 2012; Yassaa et al., 2012).

For the purpose of comparing our point measurements of k_{OTG} with NO₃ reactivity calculated from BVOC measurements, we restricted our analysis to the data set obtained by the GC-AED, which sampled from the same inlet. Nonetheless, when comparing measured NO₃ mixing ratios with those calculated from NO₃ reactivity and its production term (see Sect. 3.4) we use both GC-based datasets.

The loss rate constant, k_{OTG} , represents chemical reactions of [NO₃] with all organic trace gases present, and can be compared to the loss rate constant ($k_{\text{GC-AED}}$) obtained from the concentrations of VOCs in the same air mass as measured by the GC-AED, and the rate coefficient for reaction with NO₃:

$$k_{\text{GC-AED}} = \sum k_i [C_i], \quad (1)$$

A difference in the values of k_{OTG} and $k_{\text{GC-AED}}$ is defined as missing reactivity (s^{-1}):

$$\text{missing reactivity} = k_{\text{OTG}} - k_{\text{GC-AED}}; \quad (2)$$

where $[C_i]$ is the measured VOC concentration and k_i the corresponding rate constant. The rate constants used in these calculations of $k_{\text{GC-AED}}$ were taken from the IUPAC evaluation (IUPAC, 2017). Figure 7 (lower panel) shows the concentrations of the monoterpenes as measured by the GC-AED. The dominant monoterpene was α -pinene followed by Δ -carene, β -pinene, d -limonene, and camphene. The GC-AED also detected myrcene and linalool and some other terpenes but the very low mixing ratios meant that none of them contributed significantly to NO₃ loss.

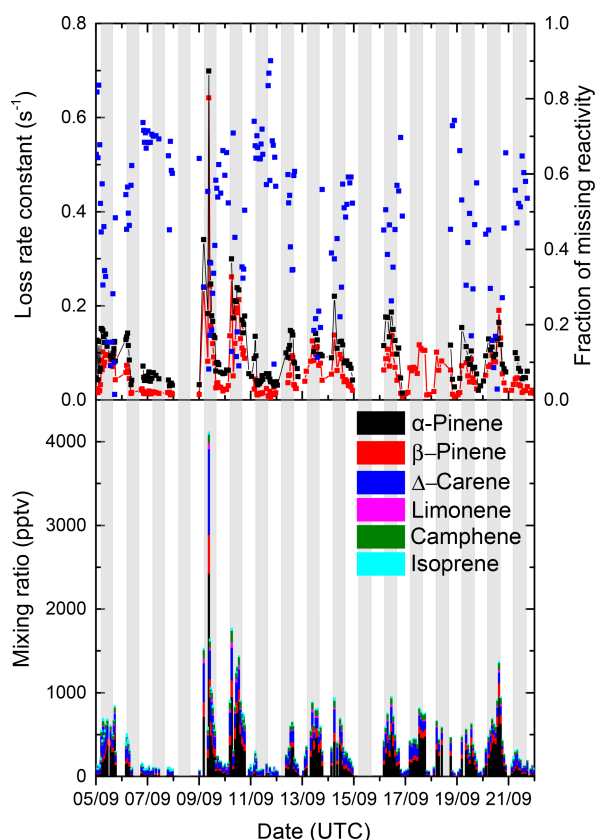


Figure 7. Upper plot: comparison of k_{GC-AED} (red data points) and measured NO₃ reactivity (k_{OTG} , black data points). The fractional missing reactivity (blue data points) was calculated as $(k_{OTG} - k_{GC-AED})/k_{OTG}$. Lower plot: mixing ratios of individual monoterpenes as measured by the GC-AED and their contribution to the NO₃ reactivity. The grey shaded areas represent nighttime.

In Fig. 7 (upper panel) we overlay the time series of k_{OTG} and k_{GC-AED} . For clarity of presentation we have omitted to plot the overall uncertainty of each measurement, which was calculated as described previously (Liebmann et al., 2017) and is plotted in Fig. S6 of the Supplement. The correlation between k_{OTG} and k_{GC-AED} is displayed as Fig. S7 of the Supplement and indicates, on average, that measured organics accounted for $\approx 70\%$ of the total NO₃ reactivity.

The uncertainty associated with k_{GC-AED} was calculated by propagating uncertainty in the mixing ratios of the individual terpenes (14%, mainly resulting from uncertainty in the calibration standard and the calibration reproducibility) and assuming 15% uncertainty in the rate coefficients for reactions of NO₃ with each terpene. The values of k_{OTG} and k_{GC-AED} do not agree within their combined uncertainties, indicating that the missing reactivity calculated in Eq. (3) is statistically significant. Figure 8 plots the time series of the fractional contribution to k_{GC-AED} made by monoterpenes detected by the GC-AED. The GC-AED derived NO₃ reactivity is dominated by α -pinene and Δ -carene and to a lesser

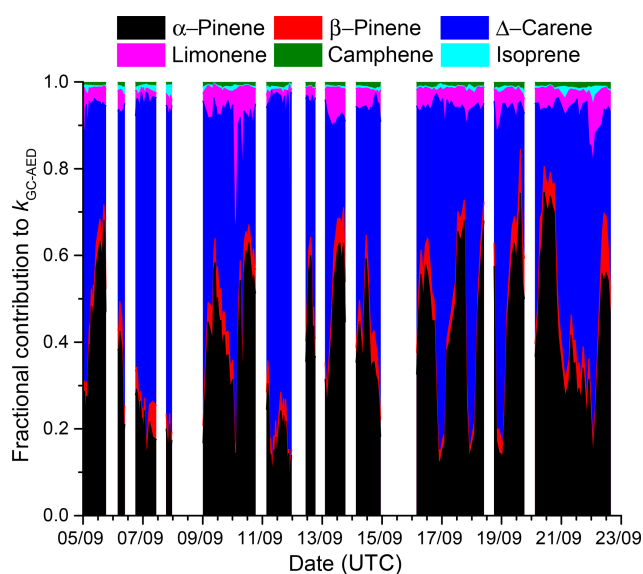


Figure 8. Fractional contribution of individual monoterpenes (measured by the GC-AED) to k_{GC-AED} indicating the dominant role of α -pinene and Δ -carene.

extent *d*-limonene, with minor contributions from β -pinene, camphene, and isoprene.

In Fig. 9 we plot the diel profiles of k_{OTG} and k_{GC-AED} (s⁻¹) averaged for the whole campaign. To do this, we interpolated the values of k_{OTG} , obtained with 60 s time resolution averaged to 900 s data onto the low-time resolution (≈ 60 min) GC-AED dataset. In the lower panels of Fig. 9 we plot two separate diel profiles, separating the data into nights with (middle panel) and without (lower panel) strong temperature inversion. The missing reactivity (in s⁻¹) across the entire diel profile is between ≈ 0.02 and 0.07 , the larger value encountered during nighttime. In contrast, the fraction of missing reactivity within the campaign averaged diel cycle was observed during daytime ($\approx 60\%$), with only 30% missing at nighttime. The lowermost panel of Fig. 9 highlights the fact that k_{OTG} was lower during campaign day/night periods with no temperature inversion and shows that it is roughly constant across the diel cycle. Likewise, the diel cycle in the reactivity attributed to the monoterpenes is also constant, with a missing reactivity of between 0.02 and 0.04 s⁻¹. A different picture emerges for the diel cycle considering only the days/nights with strong temperature inversion. On average, we see a much higher nighttime reactivity, which is tracked in its diel profile by that calculated from the measured monoterpenes. In this case, the missing reactivity is generally higher and more variable, with values between 0 and 0.1 s⁻¹.

Although statistically significant, the fraction of reactivity missing is much smaller than that reported for OH at this site (Nölscher et al., 2012) whereby up to 90% of the observed reactivity was unaccounted for when the forest was under stress due to high temperatures. For OH, the fractional

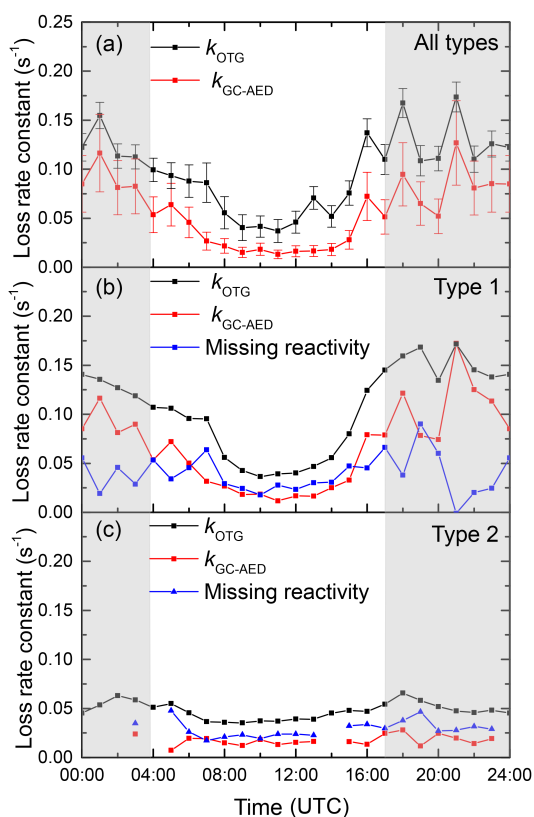


Figure 9. (a) Campaign averaged diel cycle of NO₃ reactivity (k_{OTG}) and the reactivity calculated from the monoterpenes reported by the GC-AED. The error bars represent the overall uncertainty in each parameter and not variability. Panels (b) and (c) show data from type 1 nights (significant nocturnal temperature inversion) and type 2 nights (weak or no nocturnal temperature inversion) respectively.

missing reactivity was also greatest when the overall reactivity was high, which is in contrast with the situation for NO₃ where missing reactivity was highest when the overall reactivity was low (i.e. during daytime). The OH radical reacts with most hydrocarbons and many inorganic trace gases and may be considered unselective in its reactivity, whereas NO₃ is a more specific oxidant of VOCs, its reactions in the forest dominated by addition to unsaturated VOCs or reaction with NO.

As the nighttime mixing ratios of NO were low (< 5 pptv apart from the night 20–21 September when a mixing ratio of ≈ 25 pptv was measured), its contribution to the overall nighttime loss of NO₃ was insignificant. Figure S8 of the Supplement indicates that, averaged over the entire campaign, NO accounted for less than 2% of the reactive loss of NO₃ at night. A different picture emerges for daytime, for which the campaign averaged contribution of NO to the overall chemical reactivity of NO₃ peaked at 40% at about 10:00 UTC. However, even during daytime, the average missing reactivity of 0.025 s^{-1} (Fig. 9) would require an

extra 40 pptv of NO to account for it, which is clearly not within the total uncertainty of the NO measurement.

A more plausible explanation for the missing NO₃ reactivity is incomplete detection of all reactive BVOCs by the GC-AED, which does not report mixing ratios of some hydrocarbons such as 2-methyl-3-buten-2-ol, *p*-cymene, and 1,8 cineol, which the GC-MS showed to be present. The GC-MS mixing ratios of these species (which react slowly with NO₃) were however too low for them to contribute significantly, even taking into account the potentially larger concentrations at the common inlet.

We also consider the potential role of sesquiterpenes. Mixing ratios of β -caryophyllene reported by the GC-MS were generally low, with a maximum value of 25 pptv. However, the rate coefficient reported (Shu and Atkinson, 1995) for the reaction of NO₃ with β -caryophyllene is large ($1.9 \times 10^{-11} \text{ cm}^3 \text{ molecule}^{-1} \text{ s}^{-1}$) and sesquiterpenes at levels of 10s of pptv can contribute significantly to NO₃ loss rates. Like monoterpenes, the emissions of sesquiterpenes are driven by temperature, with tree emissions most important during the hottest months (Duhl et al., 2008). Whilst previous studies at this site (Hakola et al., 2006) found no correlation between the β -caryophyllene and monoterpene emissions of an enclosed Scots pine branch, we find that β -caryophyllene mixing ratios (reported by the GC-MS) are correlated with those of several monoterpenes measured by the same instrument. This is illustrated in Fig. S5 of the Supplement which indicates β -caryophyllene/monoterpene ratios (α -pinene β -pinene and Δ -carene) of 0.061 ± 0.002 (R^2 0.86), 0.294 ± 0.011 (R^2 0.86), and 0.181 ± 0.007 (R^2 0.84), respectively. As the monoterpenes and sesquiterpenes have very different lifetimes with respect to chemical loss, we have excluded the sawmill impacted data (red data point) as sesquiterpenes are unlikely to survive the ≈ 0.5 h. transport time from Korkeakoski due to their rapid reaction with O₃. The high levels of β -caryophyllene measured may indicate that the source during IBAIRN is unlikely to be Scots pine, the emissions from which are strongly temperature dependent during the summer months but low and independent of temperature in September (Hakola et al., 2006).

A rough estimate of the β -caryophyllene mixing ratio at the common inlet may be obtained from the GC-AED measurement of α -pinene and the α -pinene/ β -caryophyllene ratios measured by the GC-MS (see above). The resulting β -caryophyllene mixing ratios lie between 10 and 60 pptv, which, based on a rate constant of $1.9 \times 10^{-11} \text{ cm}^3 \text{ molecule}^{-1} \text{ s}^{-1}$, results in a contribution to NO₃ reactivity of up to 0.03 s^{-1} . As β -caryophyllene emissions from pine tree needles reveals a strong temperature dependence (Hakola et al., 2006) it seems unlikely that this is an important source of β -caryophyllene during the relatively cold September nights of the IBAIRN campaign and its emissions from other sources, especially those at ground level including soil may be more important (Insam and Seewald, 2010; Penuelas et al., 2014).

In summary, the BVOC measurements indicate that NO₃ reactivity in this boreal environment is dominated by reaction with monoterpenes with, on average, 70 % of the reactivity during nighttime and 40 % of the reactivity during daytime explained by α - and β -pinene, Δ -carene, limonene, and camphene. Unidentified monoterpenes/sesquiterpenes are likely to account for a significant fraction of the VOC-derived missing reactivity.

3.3 NO₃ levels: measurements versus calculations using production and loss terms

Previous estimates of NO₃ reactivity (often reported as its inverse lifetime) have relied on NO₃ concentration measurements and the assumption that the production and loss of NO₃ are in stationary state. By combining k_{OTG} and other loss processes such as photolysis and reaction with NO with the NO₃ production term, we can also calculate the NO₃ concentration:

$$[\text{NO}_3]_{\text{ss}} = \frac{\text{NO}_3 \text{ production rate}}{\text{NO}_3 \text{ loss rate}} = \frac{[\text{O}_3][\text{NO}_2]k_1}{([k_{OTG}] + [J_{\text{NO}_3}] + [\text{NO}]k_2)}, \quad (3)$$

where k_1 is the rate constant ($\text{cm}^3 \text{ molecule}^{-1} \text{ s}^{-1}$) for reaction of NO₂ with O₃ and k_2 is the rate constant ($\text{cm}^3 \text{ molecule}^{-1} \text{ s}^{-1}$) for the reaction of NO₃ with NO and J_{NO_3} is its photolysis rate constant (s^{-1}). J_{NO_3} was calculated from actinic flux measurements (spectral radiometer, Metcon GmbH; Meusel et al., 2016) and NO₃ cross sections/quantum yields from an evaluation (Burkholder et al., 2016). This expression does not consider indirect loss of NO₃ via heterogeneous loss processes of N₂O₅, which, given the high levels of BVOC (short NO₃ lifetimes) and low aerosol surface area, cannot contribute significantly.

Figure 10 plots the time series of measured NO₃ mixing ratios (1 min averages, blue lines) for the entire campaign, which indicates that NO₃ was always below the detection limit of 1.3 pptv, which is defined by variation in the zero-signal rather than random noise (Sobanski et al., 2016a). The fact that the measured NO₃ mixing ratios are slightly negative (by ≈ 0.2 pptv) is due to a few percent NO₂ contamination of the NO sample used to zero the NO₃ signal. We also plot the time series (black line) of the stationary state NO₃ mixing ratios, $[\text{NO}_3]_{\text{ss}}$, calculated according to (Eq. 3). The low NO_x levels and moderate O₃ levels combine to result in a weak production rate for NO₃ of less than 0.03 pptv s^{-1} for the entire campaign resulting in predicted levels of $[\text{NO}_3]_{\text{ss}}$ of less than 0.2 pptv. On two nights, higher mixing ratios close to 1 pptv (nights of 6–7 and 10–11) are predicted, a result of elevated production rates due to higher NO₂ levels.

The advantages of directly measured k_{OTG} rather than reactivity calculations based on measurements of reactive trace gases is illustrated by plotting the predicted NO₃ levels based on the reactive hydrocarbons reported by the GC-AED and

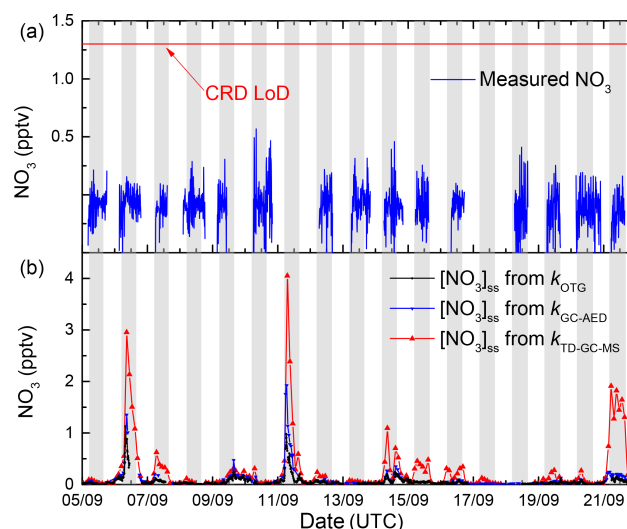


Figure 10. Stationary state NO₃ mixing ratios calculated from the production term ($k_1[\text{NO}_2][\text{O}_3]$) and using either $k_{OTG} + k_2[\text{NO}] + J_{\text{NO}_3}$ (b, black line), $k_{GC-MS} + k_2[\text{NO}] + J_{\text{NO}_3}$ (b, red line), or $k_{GC-MS} + k_2[\text{NO}] + J_{\text{NO}_3}$ (b, blue line) as loss terms. For comparison, the measured NO₃ mixing ratios are also plotted (a, blue line) as well as the 1.3 pptv limit of detection (horizontal red line).

GC-MS, i.e. use of k_{GC-MS} and k_{GC-AED} rather than k_{OTG} . Use of the GC-MS data, which reported the lowest levels of biogenic hydrocarbons, would lead to the prediction of measurable amounts (up to 4 pptv) of NO₃ on several nights, contradicting our NO₃ measurements and previous reports (Rinne et al., 2012) of very low NO₃ levels at this site.

3.4 Vertical gradient in NO₃ reactivity

Both column and point measurements of tropospheric NO₃ indicate a strong vertical gradient in its mixing ratio with significantly elevated levels aloft (Aliwell and Jones, 1998; Allan et al., 2002; von Friedeburg et al., 2002; Stutz et al., 2004; Brown et al., 2007a, b; Brown and Stutz, 2012). The NO₃ gradient is the result of lower production rates close to the ground, where O₃ levels are depleted due to deposition and also lower loss rates aloft as the concentration of reactive trace gases from ground level emissions decreases with altitude. High resolution data (Brown et al., 2007b) indicate that the largest gradient in NO₃ concentration is often found in the lowermost 50 m. Nighttime monoterpene mixing ratios in forested, boreal regions have been found to display a vertical gradient, with highest mixing ratios at lower levels (Holzinger et al., 2005; Rinne et al., 2005; Eerdekens et al., 2009). This is a result of direct emissions, such as monoterpenes from the trees at canopy level; and emissions of monoterpenes and sesquiterpenes from rotting leaf litter into a shallow, stratified boundary layer, suggesting that reactive species close to the ground will dominate in con-

trolling the NO₃ lifetime and thus mixing ratio (Aaltonen et al., 2011). We explored this by measuring k_{OTG} at various heights above ground, including measurements from a few metres below the canopy, to a few metres above the tree tops. Altogether we recorded 14 vertical profiles on the 18 September 2016, five obtained during the daytime (10:15–05:15 UTC) and nine obtained at nighttime (16:00–24:00 UTC).

Figure 11 displays the averaged nighttime and daytime values of k_{OTG} recorded at 8.5, 12.0, 17.0, 22.0, and 27.0 m. The total time to take a single profile was < 15 mins. During the day (black data points), we find no significant vertical gradient in NO₃ reactivity, which was roughly constant at $\approx 0.03 \text{ s}^{-1}$. In contrast, the average nighttime vertical profile (red data points) reveals a strong gradient in k_{OTG} with the highest values slightly below canopy height (8.5 to 12.5 m) with a rapid decrease above. At 20 m and above, daytime and nighttime values of k_{OTG} were comparable. These observations are qualitatively consistent with gradients in monoterpene mixing ratios in this forest (Rinne et al., 2005) and with the conclusion of Mogensen et al. (2015), who considered NO₃ reactions with monoterpenes and sesquiterpenes emitted from Scots pines at canopy height for the exceptionally warm summer of 2010. The modelled, nighttime vertical gradient in NO₃ described by Mogensen et al. (2015) displays a maximum at 12 m but differs from the measured gradient from IBAIRN in that lower reactivity was modelled at the lowest heights, which may be expected as the model considered only emissions of reactive BVOCs from trees and not from ground sources. In contrast to the vertical gradient measured during IBAIRN, the modelled NO₃ reactivity showed highest values during daytime, coincident with the maximum NO mixing ratio (Mogensen et al., 2015) but was generally lower than our measured values. Mogensen et al. (2015) indicate that the model is likely to underestimate the NO₃ reactivity due to compounds that cannot be measured by GC-MS as well as by the unknown products of their oxidation.

The increase in k_{OTG} below the canopy may be caused by ground level emissions of reactive trace gases from tree and plant debris or other flora (mosses, lichens) at forest-floor level. α -pinene and Δ^3 -carene, emissions from ground level may vary with litter quality and quantity, soil microbial activity and the physiological stages of plants (Warneke et al., 1999; Insam and Seewald, 2010; Aaltonen et al., 2011; Penuelas et al., 2014). Previous work in the tropical forest has indicated that sesquiterpenes concentrations can peak at ground level rather than within the canopy (Jardine et al., 2011), although the applicability of this result to the boreal forest is unclear.

We conclude that high rates of emission of reactive gases into the stratified nocturnal boundary layer along with ventilation and dilution above canopy height result in strong nocturnal gradients in NO₃ reactivity. During the daytime, efficient turbulent mixing removes the gradient. We did not obtain a vertical profile of k_{OTG} on a night when the tempera-

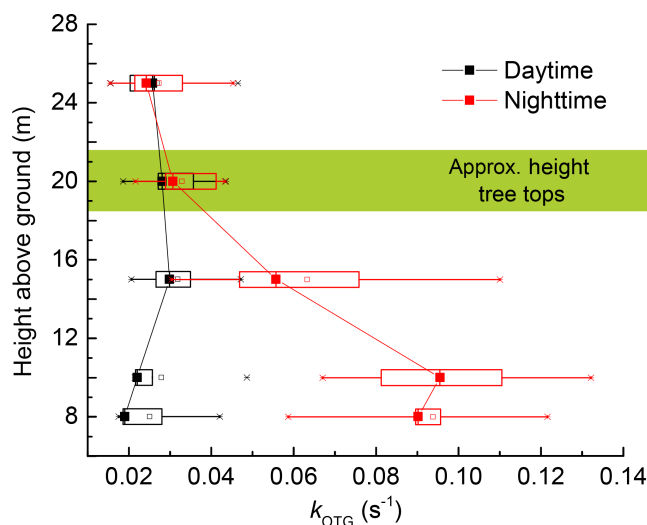


Figure 11. Vertical profiles of NO₃ reactivity (k_{OTG}) on 17–18 September 2016. The data represent the average of five profiles during the day and nine profiles during the night.

ture inversion was absent, but expect it would be significantly weaker, as is the gradient in O₃ on such nights.

3.5 High NO₃ reactivity and its contribution to NO_x loss

The high reactivity of NO₃ towards organic trace gases in the boreal environment means that other loss processes, including formation of N₂O₅ or reaction with NO are suppressed. To a first approximation we can assume that, at nighttime, in the absence of NO and sunlight, each NO₃ radical formed in the reaction of NO₂ with O₃ will react with a biogenic hydrocarbon, resulting in formation of an organic nitrate at a yield of between 20 and 100 %, depending on the identity of the organic reactant (Ng et al., 2017). The large values for k_{OTG} obtained during the day mean that a significant fraction of the NO₃ formed can be converted to organic nitrates rather than result in re-formation of NO₂ via reaction with NO or photolysis. The fraction, f , of NO₃ that will react with organic trace gases is given by

$$f = \frac{k_{\text{OTG}}}{([k_{\text{OTG}}] + [J_{\text{NO}_3}] + [\text{NO}]k_2)}. \quad (4)$$

Figure 12 illustrates the time series (upper plot) and the campaign averaged diel cycle (lower plot) for f which varies between ≈ 0.1 and 0.4 at the peak of the actinic flux, the variation is largely caused by day-to-day variability in insolation. As the spectral radiometer was located at a height of 35 m, J_{NO_3} will be slightly overestimated around midday as light levels within the canopy are lower. The overestimation will be magnified during the early morning and late afternoon when the forest is in shade at lower levels but the spectral radiometer is not. The daytime values for f are thus

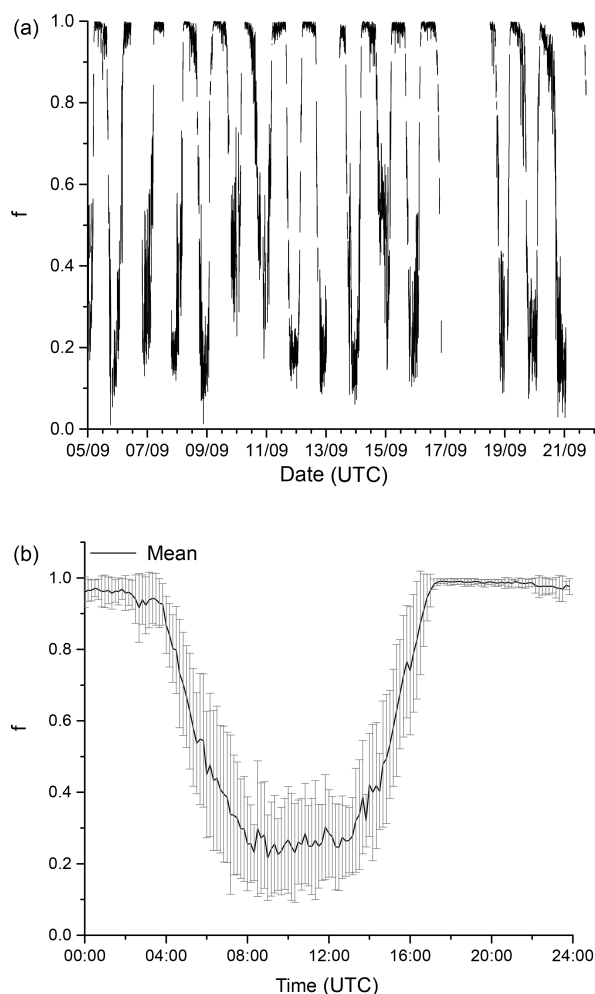


Figure 12. The fraction, f , of the total NO₃ loss with organic trace gases as a time series (a) and as a campaign averaged, diel cycle (b) where $f = k_{\text{OTG}} / (k_{\text{OTG}} + J_{\text{NO}_3} + k_{\text{NO}})$.

lower limits. With typical daytime NO levels of 50–100 pptv, the term $[\text{NO}]k_2$ contributes $\approx 0.03\text{--}0.06\text{ s}^{-1}$ to NO₃ loss, whereas J_{NO_3} has maxima of close to 0.1 s^{-1} each day. For comparison daytime values of k_{OTG} of $\approx 0.05\text{ s}^{-1}$ were often observed (Fig. 2).

The diel cycle for f shows that even at the peak of the actinic flux, on average circa 20 % of the NO₃ formed will react with an organic trace gas rather than be photolysed or react with NO in this environment. This implies that, in the summer–autumn boreal forest, NO₃ reactions may represent a significant loss of NO_x not only during the nighttime but over the full diel cycle, with a significant enhancement in the daytime production of alkyl nitrates, generally assumed to proceed only via reactions of organic peroxy radicals with NO.

4 Conclusions

The first direct measurements of NO₃ reactivity to organic trace gases (k_{OTG}) in the boreal forest indicate that NO₃ is very short lived in this environment with lifetimes generally less than 10 s, mainly due to reaction with monoterpenes. The highest NO₃ reactivities were encountered during nights with strong temperature inversions and a relative humidity of 100 %, and were accompanied by rapid O₃ depletion, together highlighting the important role of nocturnal boundary layer dynamics in controlling canopy-level NO₃ reactivity. The daytime reactivity was sufficiently large that reactions of NO₃ with organic trace gases could compete with photolysis and the reaction with NO, so that NO₃-induced losses of NO_x and the formation of organic nitrates was significant. Measurements of the vertical profile in NO₃ reactivity indicate a strong gradient during nighttime, with the highest reactivity observed below canopy height, highlighting a potential role for emissions of reactive trace gases from the forest floor. The hydrocarbons measured did not fully account for the observed NO₃ reactivity, indicating the presence of unsaturated organic trace gases that were not identified, sesquiterpenes being potential candidates.

Data availability. The IBairn data will be released at the end of 2018 when they can be obtained on request (via John Crowley) from the owners.

The Supplement related to this article is available online at <https://doi.org/10.5194/acp-18-3799-2018-supplement>.

Competing interests. The authors declare that they have no conflict of interest.

Acknowledgements. We are grateful to ENVRIplus for partial financial support of the IBairn campaign. We also thank Uwe Parchatka for provision of the NO dataset.

The article processing charges for this open-access publication were covered by the Max Planck Society.

Edited by: Dwayne Heard

Reviewed by: two anonymous referees

References

- Aaltonen, H., Pumpanen, J., Pihlatie, M., Hakola, H., Hellén, H., Kulmala, L., Vesala, T., and Bäck, J.: Boreal pine forest floor biogenic volatile organic compound emissions peak in early summer and autumn, *Agr. Forest Meteorol.*, 151, 682–691, doi:<https://doi.org/10.1016/j.agrformet.2010.12.010>, 2011.

- Aldener, M., Brown, S. S., Stark, H., Williams, E. J., Lerner, B. M., Kuster, W. C., Goldan, P. D., Quinn, P. K., Bates, T. S., Fehsenfeld, F. C., and Ravishankara, A. R.: Reactivity and loss mechanisms of NO₃ and N₂O₅ in a polluted marine environment: Results from in situ measurements during New England Air Quality Study 2002, *J. Geophys. Res.-Atmos.*, 111, D23S73, <https://doi.org/10.1029/2006JD007252>, 2006.
- Aliwell, S. R. and Jones, R. L.: Measurements of tropospheric NO₃ at midlatitude, *J. Geophys. Res.-Atmos.*, 103, 5719–5727, 1998.
- Allan, B. J., Carslaw, N., Coe, H., Burgess, R. A., and Plane, J. M. C.: Observations of the nitrate radical in the marine boundary layer, *J. Atmos. Chem.*, 33, 129–154, 1999.
- Allan, B. J., Plane, J. M. C., Coe, H., and Shillito, J.: Observations of NO₃ concentration profiles in the troposphere, *J. Geophys. Res.-Atmos.*, 107, 4588, <https://doi.org/10.1029/2002jd002112>, 2002.
- Ambrose, J. L., Mao, H., Mayne, H. R., Stutz, J., Talbot, R., and Sive, B. C.: Nighttime nitrate radical chemistry at Appledore island, Maine during the 2004 international consortium for atmospheric research on transport and transformation, *J. Geophys. Res.-Atmos.*, 112, D21302, doi:10.1029/2007JD008756, 2007.
- Ammann, M., Cox, R. A., Crowley, J. N., Jenkin, M. E., Mellouki, A., Rossi, M. J., Troe, J., and Wallington, T. J.: Evaluated kinetic and photochemical data for atmospheric chemistry: Volume VI – heterogeneous reactions with liquid substrates, *Atmos. Chem. Phys.*, 13, 8045–8228, <https://doi.org/10.5194/acp-13-8045-2013>, 2013.
- Atkinson, R.: Atmospheric chemistry of VOCs and NO_x, *Atmos. Environ.*, 34, 2063–2101, 2000.
- Atkinson, R. and Arey, J.: Gas-phase tropospheric chemistry of biogenic volatile organic compounds: a review, *Atmos. Environ.*, 37, 197–219, 2003a.
- Atkinson, R. and Arey, J.: Atmospheric degradation of volatile organic compounds, *Chem. Rev.*, 103, 4605–4638, <https://doi.org/10.1021/cr0206420>, 2003b.
- Ayres, B. R., Allen, H. M., Draper, D. C., Brown, S. S., Wild, R. J., Jimenez, J. L., Day, D. A., Campuzano-Jost, P., Hu, W., de Gouw, J., Koss, A., Cohen, R. C., Duffey, K. C., Romer, P., Baumann, K., Edgerton, E., Takahama, S., Thornton, J. A., Lee, B. H., Lopez-Hilfiker, F. D., Mohr, C., Wennberg, P. O., Nguyen, T. B., Teng, A., Goldstein, A. H., Olson, K., and Fry, J. L.: Organic nitrate aerosol formation via NO₃ + biogenic volatile organic compounds in the southeastern United States, *Atmos. Chem. Phys.*, 15, 13377–13392, <https://doi.org/10.5194/acp-15-13377-2015>, 2015.
- Bäck, J., Aalto, J., Henriksson, M., Hakola, H., He, Q., and Boy, M.: Chemodiversity of a Scots pine stand and implications for terpene air concentrations, *Biogeosciences*, 9, 689–702, <https://doi.org/10.5194/bg-9-689-2012>, 2012.
- Brown, S. S. and Stutz, J.: Nighttime radical observations and chemistry, *Chem. Soc. Rev.*, 41, 6405–6447, 2012.
- Brown, S. S., Stark, H., and Ravishankara, A. R.: Applicability of the steady state approximation to the interpretation of atmospheric observations of NO₃ and N₂O₅, *J. Geophys. Res.-Atmos.*, 108, 4539, <https://doi.org/10.1029/2003JD003407>, 2003.
- Brown, S. S., Dube, W. P., Osthoff, H. D., Stutz, J., Ryerson, T. B., Wollny, A. G., Brock, C. A., Warneke, C., De Gouw, J. A., Atlas, E., Neuman, J. A., Holloway, J. S., Lerner, B. M., Williams, E. J., Kuster, W. C., Goldan, P. D., Angevine, W. M., Trainer, M., Fehsenfeld, F. C., and Ravishankara, A. R.: Vertical profiles in NO₃ and N₂O₅ measured from an aircraft: Results from the NOAA P-3 and surface platforms during the New England Air Quality Study 2004, *J. Geophys. Res.-Atmos.*, 112, D22304, <https://doi.org/10.1029/2007jd008893>, 2007a.
- Brown, S. S., Dubé, W. P., Osthoff, H. D., Wolfe, D. E., Angevine, W. M., and Ravishankara, A. R.: High resolution vertical distributions of NO₃ and N₂O₅ through the nocturnal boundary layer, *Atmos. Chem. Phys.*, 7, 139–149, <https://doi.org/10.5194/acp-7-139-2007>, 2007b.
- Brown, S. S., deGouw, J. A., Warneke, C., Ryerson, T. B., Dubé, W. P., Atlas, E., Weber, R. J., Peltier, R. E., Neuman, J. A., Roberts, J. M., Swanson, A., Flocke, F., McKeen, S. A., Brioude, J., Sommariva, R., Trainer, M., Fehsenfeld, F. C., and Ravishankara, A. R.: Nocturnal isoprene oxidation over the Northeast United States in summer and its impact on reactive nitrogen partitioning and secondary organic aerosol, *Atmos. Chem. Phys.*, 9, 3027–3042, <https://doi.org/10.5194/acp-9-3027-2009>, 2009.
- Burkholder, J. B., Sander, S. P., Abbatt, J., Barker, J. R., Huie, R. E., Kolb, C. E., Kurylo, M. J., Orkin, V. L., Wilmouth, D. M., and Wine, P. H.: Chemical Kinetics and Photochemical Data for Use in Atmospheric Studies, Evaluation No. 18, JPL Publication 15–10, Jet Propulsion Laboratory, Pasadena, available at: <http://jpldataeval.jpl.nasa.gov>, 2016.
- Chen, X., Quéléver, L. L. J., Fung, P. L., Kesti, J., Rissanen, M. P., Bäck, J., Keronen, P., Junninen, H., Petäjä, T., Kerminen, V.-M., and Kulmala, M.: Observations of ozone depletion events in a Finnish boreal forest, *Atmos. Chem. Phys.*, 18, 49–63, <https://doi.org/10.5194/acp-18-49-2018>, 2018.
- Crowley, J. N., Schuster, G., Pouvesle, N., Parchatka, U., Fischer, H., Bonn, B., Bingemer, H., and Lelieveld, J.: Nocturnal nitrogen oxides at a rural mountain-site in south-western Germany, *Atmos. Chem. Phys.*, 10, 2795–2812, <https://doi.org/10.5194/acp-10-2795-2010>, 2010.
- Crowley, J. N., Thieser, J., Tang, M. J., Schuster, G., Bozem, H., Beygi, Z. H., Fischer, H., Diesch, J.-M., Drewnick, F., Borrmann, S., Song, W., Yassaa, N., Williams, J., Pöhler, D., Platt, U., and Lelieveld, J.: Variable lifetimes and loss mechanisms for NO₃ and N₂O₅ during the DOMINO campaign: contrasts between marine, urban and continental air, *Atmos. Chem. Phys.*, 11, 10853–10870, <https://doi.org/10.5194/acp-11-10853-2011>, 2011.
- Dentener, F. J. and Crutzen, P. J.: Reaction of N₂O₅ on tropospheric aerosols – Impact on the global distributions of NO_x, O₃, and OH, *J. Geophys. Res.-Atmos.*, 98, 7149–7163, 1993.
- Duhl, T. R., Helmig, D., and Guenther, A.: Sesquiterpene emissions from vegetation: a review, *Biogeosciences*, 5, 761–777, <https://doi.org/10.5194/bg-5-761-2008>, 2008.
- Eerdekens, G., Yassaa, N., Sinha, V., Aalto, P. P., Aufmhoff, H., Arnold, F., Fiedler, V., Kulmala, M., and Williams, J.: VOC measurements within a boreal forest during spring 2005: on the occurrence of elevated monoterpene concentrations during night time intense particle concentration events, *Atmos. Chem. Phys.*, 9, 8331–8350, <https://doi.org/10.5194/acp-9-8331-2009>, 2009.
- Ehn, M., Thornton, J. A., Kleist, E., Sipila, M., Junninen, H., Pullinen, I., Springer, M., Rubach, F., Tillmann, R., Lee, B., Lopez-Hilfiker, F., Andres, S., Acir, I. H., Rissanen, M., Jokinen, T., Schobesberger, S., Kangasluoma, J., Kontkanen, J.,

- Nieminen, T., Kurten, T., Nielsen, L. B., Jorgensen, S., Kjaergaard, H. G., Canagaratna, M., Dal Maso, M., Berndt, T., Petaja, T., Wahner, A., Kerminen, V. M., Kulmala, M., Worsnop, D. R., Wildt, J., and Mentel, T. F.: A large source of low-volatility secondary organic aerosol, *Nature*, 506, 476–479, <https://doi.org/10.1038/nature13032>, 2014.
- Fry, J. L., Draper, D. C., Barsanti, K. C., Smith, J. N., Ortega, J., Winkle, P. M., Lawler, M. J., Brown, S. S., Edwards, P. M., Cohen, R. C., and Lee, L.: Secondary Organic Aerosol Formation and Organic Nitrate Yield from NO₃ Oxidation of Biogenic Hydrocarbons, *Environ. Sci. Technol.*, 48, 11944–11953, <https://doi.org/10.1021/es502204x>, 2014.
- Geyer, A., Alicke, B., Konrad, S., Schmitz, T., Stutz, J., and Platt, U.: Chemistry and oxidation capacity of the nitrate radical in the continental boundary layer near Berlin, *J. Geophys. Res.-Atmos.*, 106, 8013–8025, 2001.
- Goldstein, A. H., McKay, M., Kurpius, M. R., Schade, G. W., Lee, A., Holzinger, R., and Rasmussen, R. A.: Forest thinning experiment confirms ozone deposition to forest canopy is dominated by reaction with biogenic VOCs, *Geophys. Res. Lett.*, 31, L22106, <https://doi.org/10.1029/2004gl021259>, 2004.
- Gözl, C., Senzig, J., and Platt, U.: NO₃-initiated oxidation of biogenic hydrocarbons, *Chemosphere – Global Change Science*, 3, 339–352, [https://doi.org/10.1016/S1465-9972\(01\)00015-0](https://doi.org/10.1016/S1465-9972(01)00015-0), 2001.
- Graus, M., Müller, M., and Hansel, A.: High Resolution PTR-TOF: Quantification and Formula Confirmation of VOC in Real Time, *J. Am. Soc. Mass Spectrom.*, 21, 1037–1044, 2010.
- Guenther, A. B., Jiang, X., Heald, C. L., Sakulyanontvittaya, T., Duhl, T., Emmons, L. K., and Wang, X.: The Model of Emissions of Gases and Aerosols from Nature version 2.1 (MEGAN2.1): an extended and updated framework for modeling biogenic emissions, *Geosci. Model Dev.*, 5, 1471–1492, <https://doi.org/10.5194/gmd-5-1471-2012>, 2012.
- Hakola, H., Tarvainen, V., Laurila, T., Hiltunen, V., Hellén, H., and Keronen, P.: Seasonal variation of VOC concentrations above a boreal coniferous forest, *Atmos. Environ.*, 37, 1623–1634, [doi:https://doi.org/10.1016/S1352-2310\(03\)00014-1](https://doi.org/10.1016/S1352-2310(03)00014-1), 2003.
- Hakola, H., Tarvainen, V., Bäck, J., Ranta, H., Bonn, B., Rinne, J., and Kulmala, M.: Seasonal variation of mono- and sesquiterpene emission rates of Scots pine, *Biogeosciences*, 3, 93–101, <https://doi.org/10.5194/bg-3-93-2006>, 2006.
- Hakola, H., Hellén, H., Tarvainen, V., Bäck, J., Patokoski, J., and Rinne, J.: Annual variations of atmospheric VOC concentrations in a boreal forest, *Boreal Environ. Res.*, 14, 722–730, 2009.
- Hakola, H., Hellén, H., Hemmilä, M., Rinne, J., and Kulmala, M.: In situ measurements of volatile organic compounds in a boreal forest, *Atmos. Chem. Phys.*, 12, 11665–11678, <https://doi.org/10.5194/acp-12-11665-2012>, 2012.
- Hallquist, M., Wenger, J. C., Baltensperger, U., Rudich, Y., Simpson, D., Claeys, M., Dommen, J., Donahue, N. M., George, C., Goldstein, A. H., Hamilton, J. F., Herrmann, H., Hoffmann, T., Iinuma, Y., Jang, M., Jenkin, M. E., Jimenez, J. L., Kiendler-Scharr, A., Maenhaut, W., McFiggans, G., Mentel, Th. F., Monod, A., Prévôt, A. S. H., Seinfeld, J. H., Surratt, J. D., Szmigielski, R., and Wildt, J.: The formation, properties and impact of secondary organic aerosol: current and emerging issues, *Atmos. Chem. Phys.*, 9, 5155–5236, <https://doi.org/10.5194/acp-9-5155-2009>, 2009.
- Hari, P. and Kulmala, M.: Station for Measuring Ecosystem–Atmosphere Relations (SMEAR II), *Boreal Environ. Res.*, 10, 315–322, 2005.
- Hari, P., Heliövaara, K., and Kulmala, L.: Physical and Physiological Forest Ecology: Physical and Physiological Forest Ecology, edited by: Hari, P., Heliövaara, K., and Kulmala, L., Springer, 2013.
- Heintz, F., Platt, U., Flentje, H., and Dubois, R.: Long-term observation of nitrate radicals at the tor station, Kap Arkona (Rügen), *J. Geophys. Res.-Atmos.*, 101, 22891–22910, 1996.
- Hellén, H., Kuronen, P., and Hakola, H.: Heated stainless steel tube for ozone removal in the ambient air measurements of mono- and sesquiterpenes, *Atmos. Environ.*, 57, 35–40, [doi:https://doi.org/10.1016/j.atmosenv.2012.04.019](https://doi.org/10.1016/j.atmosenv.2012.04.019), 2012.
- Hens, K., Novelli, A., Martinez, M., Auld, J., Axinte, R., Bohn, B., Fischer, H., Keronen, P., Kubistin, D., Nölscher, A. C., Oswald, R., Paasonen, P., Petäjä, T., Regelin, E., Sander, R., Sinha, V., Sipilä, M., Taraborrelli, D., Tatum Ernest, C., Williams, J., Lelieveld, J., and Harder, H.: Observation and modelling of HO_x radicals in a boreal forest, *Atmos. Chem. Phys.*, 14, 8723–8747, <https://doi.org/10.5194/acp-14-8723-2014>, 2014.
- Holzinger, R., Lee, A., Paw, K. T., and Goldstein, U. A. H.: Observations of oxidation products above a forest imply biogenic emissions of very reactive compounds, *Atmos. Chem. Phys.*, 5, 67–75, <https://doi.org/10.5194/acp-5-67-2005>, 2005.
- Holzinger, R., Lee, A., McKay, M., and Goldstein, A. H.: Seasonal variability of monoterpene emission factors for a ponderosa pine plantation in California, *Atmos. Chem. Phys.*, 6, 1267–1274, <https://doi.org/10.5194/acp-6-1267-2006>, 2006.
- Holzke, C., Hoffmann, T., Jaeger, L., Koppmann, R., and Zimmer, W.: Diurnal and seasonal variation of monoterpene and sesquiterpene emissions from Scots pine (*Pinus sylvestris* L.), *Atmos. Environ.*, 40, 3174–3185, <https://doi.org/10.1016/j.atmosenv.2006.01.039>, 2006.
- Iivesniemi, H., Levula, J., Ojansuu, R., Kolari, P., Kulmala, L., Pumpanen, J., Launiainen, S., Vesala, T., and Nikinmaa, E.: Long-term measurements of the carbon balance of a boreal Scots pine dominated forest ecosystem, *Boreal Environ. Res.*, 14, 731–753, 2009.
- Insam, H. and Seewald, M. S. A.: Volatile organic compounds (VOCs) in soils, *Biol. Fertil. Soils*, 46, 199–213, <https://doi.org/10.1007/s00374-010-0442-3>, 2010.
- IUPAC (Ammann, M., Cox, R. A., Crowley, J. N., Herrmann, H., Jenkin, M. E., McNeill, V. F., Mellouki, A., Rossi, M. J., Troe, J., and Wallington, T. J.): Task Group on Atmospheric Chemical Kinetic Data Evaluation, available at: <http://iupac.pole-ether.fr/index.html> (last access: October 2017), 2017.
- Jardine, K., Serrano, A. Y., Arneft, A., Abrell, L., Jardine, A., van Haren, J., Artaxo, P., Rizzo, L. V., Ishida, F. Y., Karl, T., Kesselmeier, J., Saleska, S., and Huxman, T.: Within-canopy sesquiterpene ozonolysis in Amazonia, *J. Geophys. Res.-Atmos.*, 116, D19301, <https://doi.org/10.1029/2011jd016243>, 2011.
- Jordan, A., Haidacher, S., Hanel, G., Hartungen, E., Mark, L., Sehauser, H., Schottkowsky, R., Sulzer, P., and Mark, T. D.: A high resolution and high sensitivity proton-transfer-reaction time-of-flight mass spectrometer (PTR-TOF-MS), *Int. J. Mass Spectrom.*, 286, 122–128, 2009.
- Kurpius, M. R. and Goldstein, A. H.: Gas-phase chemistry dominates O₃ loss to a forest, implying a source of aerosols and hy-

- droxyl radicals to the atmosphere, *Geophys. Res. Lett.*, 30, 1371, <https://doi.org/10.1029/2002gl016785>, 2003.
- Lappalainen, H. K., Sevanto, S., Bäck, J., Ruuskanen, T. M., Kollari, P., Taipale, R., Rinne, J., Kulmala, M., and Hari, P.: Daytime concentrations of biogenic volatile organic compounds in a boreal forest canopy and their relation to environmental and biological factors, *Atmos. Chem. Phys.*, 9, 5447–5459, <https://doi.org/10.5194/acp-9-5447-2009>, 2009.
- Lelieveld, J., Butler, T. M., Crowley, J. N., Dillon, T. J., Fischer, H., Ganzeveld, L., Harder, H., Lawrence, M. G., Martinez, M., Taraborrelli, D., and Williams, J.: Atmospheric oxidation capacity sustained by a tropical forest, *Nature*, 452, 737–740, 2008.
- Li, J., Reiffs, A., Parchatka, U., and Fischer, H.: In situ measurements of atmospheric CO and its correlation with NO_x and O₃ at a rural mountain site, *Metrol. Meas. Sys.*, XXII, 25–38, 2015.
- Liao, L., Dal Maso, M., Taipale, R., Rinne, J., Ehn, M., Junninen, H., Aijala, M., Nieminen, T., Alekseychik, P., Hulkkonen, M., Worsnop, D. R., Kerminen, V. M., and Kulmala, M.: Monoterpene pollution episodes in a forest environment: indication of anthropogenic origin and association with aerosol particles, *Boreal Environ. Res.*, 16, 288–303, 2011.
- Liebmann, J. M., Schuster, G., Schuladen, J. B., Sobanski, N., Lelieveld, J., and Crowley, J. N.: Measurement of ambient NO₃ reactivity: design, characterization and first deployment of a new instrument, *Atmos. Meas. Tech.*, 10, 1241–1258, <https://doi.org/10.5194/amt-10-1241-2017>, 2017.
- Meusel, H., Kuhn, U., Reiffs, A., Mallik, C., Harder, H., Martinez, M., Schuladen, J., Bohn, B., Parchatka, U., Crowley, J. N., Fischer, H., Tomsche, L., Novelli, A., Hoffmann, T., Janssen, R. H. H., Hartogensis, O., Pikridas, M., Vrekoussis, M., Bourtsoukidis, E., Weber, B., Lelieveld, J., Williams, J., Pöschl, U., Cheng, Y., and Su, H.: Daytime formation of nitrous acid at a coastal remote site in Cyprus indicating a common ground source of atmospheric HONO and NO, *Atmos. Chem. Phys.*, 16, 14475–14493, <https://doi.org/10.5194/acp-16-14475-2016>, 2016.
- Mogensen, D., Gierens, R., Crowley, J. N., Keronen, P., Smolander, S., Sogachev, A., Nölscher, A. C., Zhou, L., Kulmala, M., Tang, M. J., Williams, J., and Boy, M.: Simulations of atmospheric OH, O₃ and NO₃ reactivities within and above the boreal forest, *Atmos. Chem. Phys.*, 15, 3909–3932, <https://doi.org/10.5194/acp-15-3909-2015>, 2015.
- Ng, N. L., Brown, S. S., Archibald, A. T., Atlas, E., Cohen, R. C., Crowley, J. N., Day, D. A., Donahue, N. M., Fry, J. L., Fuchs, H., Griffin, R. J., Guzman, M. I., Herrmann, H., Hodzic, A., Iinuma, Y., Jimenez, J. L., Kiendler-Scharr, A., Lee, B. H., Luecken, D. J., Mao, J., McLaren, R., Mutzel, A., Osthoff, H. D., Ouyang, B., Picquet-Varrault, B., Platt, U., Pye, H. O. T., Rudich, Y., Schwantes, R. H., Shiraiwa, M., Stutz, J., Thornton, J. A., Tilgner, A., Williams, B. J., and Zaveri, R. A.: Nitrate radicals and biogenic volatile organic compounds: oxidation, mechanisms, and organic aerosol, *Atmos. Chem. Phys.*, 17, 2103–2162, <https://doi.org/10.5194/acp-17-2103-2017>, 2017.
- Nölscher, A. C., Williams, J., Sinha, V., Custer, T., Song, W., Johnson, A. M., Axinte, R., Bozem, H., Fischer, H., Pouvesle, N., Phillips, G., Crowley, J. N., Rantala, P., Rinne, J., Kulmala, M., Gonzales, D., Valverde-Canossa, J., Vogel, A., Hoffmann, T., Ouwersloot, H. G., Vilà-Guerau de Arellano, J., and Lelieveld, J.: Summertime total OH reactivity measurements from boreal forest during HUMPPA-COPEC 2010, *Atmos. Chem. Phys.*, 12, 8257–8270, <https://doi.org/10.5194/acp-12-8257-2012>, 2012.
- Nölscher, A. C., Yanez-Serrano, A. M., Wolff, S., de Araujo, A. C., Lavric, J. V., Kesselmeier, J., and Williams, J.: Unexpected seasonality in quantity and composition of Amazon rainforest air reactivity, *Nat. Commun.*, 7, 10383, <https://doi.org/10.1038/ncomms10383>, 2016.
- Osthoff, H. D., Roberts, J. M., Ravishankara, A. R., Williams, E. J., Lerner, B. M., Sommariva, R., Bates, T. S., Coffman, D., Quinn, P. K., Dibb, J. E., Stark, H., Burkholder, J. B., Talukdar, R. K., Meagher, J., Fehsenfeld, F. C., and Brown, S. S.: High levels of nitryl chloride in the polluted subtropical marine boundary layer, *Nat. Geosci.*, 1, 324–328, 2008.
- Penuelas, J., Asensio, D., Tholl, D., Wenke, K., Rosenkranz, M., Piechulla, B., and Schnitzler, J. P.: Biogenic volatile emissions from the soil, *Plant Cell Environ.*, 37, 1866–1891, <https://doi.org/10.1111/pce.12340>, 2014.
- Peräkylä, O., Vogt, M., Tikkanen, O. P., Laurila, T., Kajos, M. K., Rantala, P. A., Patokoski, J., Aalto, J., Yli-Juuti, T., Ehn, M., Sipilä, M., Paasonen, P., Rissanen, M., Nieminen, T., Taipale, R., Keronen, P., Lappalainen, H. K., Ruuskanen, T. M., Rinne, J., Kerminen, V. M., Kulmala, M., Back, J., and Petaja, T.: Monoterpenes' oxidation capacity and rate over a boreal forest: temporal variation and connection to growth of newly formed particles, *Boreal Environ. Res.*, 19, 293–310, 2014.
- Phillips, G. J., Tang, M. J., Thieser, J., Brickwedde, B., Schuster, G., Bohn, B., Lelieveld, J., and Crowley, J. N.: Significant concentrations of nitryl chloride observed in rural continental Europe associated with the influence of sea salt chloride and anthropogenic emissions, *Geophys. Res. Lett.*, 39, L10811, <https://doi.org/10.1029/2012GL051912>, 2012.
- Phillips, G. J., Thieser, J., Tang, M., Sobanski, N., Schuster, G., Fachinger, J., Drewnick, F., Borrmann, S., Bingemer, H., Lelieveld, J., and Crowley, J. N.: Estimating N₂O₅ uptake coefficients using ambient measurements of NO₃, N₂O₅, ClNO₂ and particle-phase nitrate, *Atmos. Chem. Phys.*, 16, 13231–13249, <https://doi.org/10.5194/acp-16-13231-2016>, 2016.
- Rannik, Ü., Altimir, N., Mammarella, I., Bäck, J., Rinne, J., Ruuskanen, T. M., Hari, P., Vesala, T., and Kulmala, M.: Ozone deposition into a boreal forest over a decade of observations: evaluating deposition partitioning and driving variables, *Atmos. Chem. Phys.*, 12, 12165–12182, <https://doi.org/10.5194/acp-12-12165-2012>, 2012.
- Rinne, J., Ruuskanen, T. M., Reissell, A., Taipale, R., Hakola, H., and Kulmala, M.: On-line PTR-MS measurements of atmospheric concentrations of volatile organic compounds in a European boreal forest ecosystem, *Boreal Environmental Research*, 10, 425–436, 2005.
- Rinne, J., Markkanen, T., Ruuskanen, T. M., Petäjä, T., Keronen, P., Tang, M. J., Crowley, J. N., Rannik, Ü., and Vesala, T.: Effect of chemical degradation on fluxes of reactive compounds – a study with a stochastic Lagrangian transport model, *Atmos. Chem. Phys.*, 12, 4843–4854, <https://doi.org/10.5194/acp-12-4843-2012>, 2012.
- Schallhart, S., Rantala, P., Nemitz, E., Taipale, D., Tillmann, R., Mentel, T. F., Loubet, B., Gerosa, G., Finco, A., Rinne, J., and Ruuskanen, T. M.: Characterization of total ecosystem-scale biogenic VOC exchange at a Mediterranean

- oak-hornbeam forest, *Atmos. Chem. Phys.*, 16, 7171–7194, <https://doi.org/10.5194/acp-16-7171-2016>, 2016.
- Shu, Y. H. and Atkinson, R.: Atmospheric lifetimes and fates of a series of sesquiterpenes, *J. Geophys. Res.-Atmos.*, 100, 7275–7281, <https://doi.org/10.1029/95jd00368>, 1995.
- Sinha, V., Williams, J., Lelieveld, J., Ruuskanen, T. M., Kajos, M. K., Patokoski, J., Hellen, H., Hakola, H., Mogensen, D., Boy, M., Rinne, J., and Kulmala, M.: OH Reactivity Measurements within a Boreal Forest: Evidence for Unknown Reactive Emissions, *Environ. Sci. Technol.*, 44, 6614–6620, <https://doi.org/10.1021/es101780b>, 2010.
- Sobanski, N., Schuladen, J., Schuster, G., Lelieveld, J., and Crowley, J. N.: A five-channel cavity ring-down spectrometer for the detection of NO₂, NO₃, N₂O₅, total peroxy nitrates and total alkyl nitrates, *Atmos. Meas. Tech.*, 9, 5103–5118, <https://doi.org/10.5194/amt-9-5103-2016>, 2016a.
- Sobanski, N., Tang, M. J., Thieser, J., Schuster, G., Pöhler, D., Fischer, H., Song, W., Sauvage, C., Williams, J., Fachinger, J., Berkes, F., Hoor, P., Platt, U., Lelieveld, J., and Crowley, J. N.: Chemical and meteorological influences on the lifetime of NO₃ at a semi-rural mountain site during PARADE, *Atmos. Chem. Phys.*, 16, 4867–4883, <https://doi.org/10.5194/acp-16-4867-2016>, 2016b.
- Stutz, J., Alicke, B., Ackermann, R., Geyer, A., White, A., and Williams, E.: Vertical profiles of NO₃, N₂O₅, O₃, and NO_x in the nocturnal boundary layer: I. Observations during the Texas Air Quality Study 2000 J. *Geophys. Res.-Atmos.*, 109, D12306, <https://doi.org/10.1029/2003JD004209>, 2004.
- Sun, S., Moravek, A., Trebs, I., Kesselmeier, J., and Sorgel, M.: Investigation of the influence of liquid surface films on O₃ and PAN deposition to plant leaves coated with organic/inorganic solution, *J. Geophys. Res.-Atmos.*, 121, 14239–14256, 2016.
- Tarvainen, V., Hakola, H., Hellén, H., Bäck, J., Hari, P., and Kulmala, M.: Temperature and light dependence of the VOC emissions of Scots pine, *Atmos. Chem. Phys.*, 5, 989–998, <https://doi.org/10.5194/acp-5-989-2005>, 2005.
- Thornton, J. A., Kercher, J. P., Riedel, T. P., Wagner, N. L., Cozic, J., Holloway, J. S., Dube, W. P., Wolfe, G. M., Quinn, P. K., Middlebrook, A. M., Alexander, B., and Brown, S. S.: A large atomic chlorine source inferred from mid-continental reactive nitrogen chemistry, *Nature*, 464, 271–274, <https://doi.org/10.1038/nature08905>, 2010.
- von Friedeburg, C., Wagner, T., Geyer, A., Kaiser, N., Vogel, B., Vogel, H., and Platt, U.: Derivation of tropospheric NO₃ profiles using off-axis differential optical absorption spectroscopy measurements during sunrise and comparison with simulations, *J. Geophys. Res.-Atmos.*, 107, 4168, <https://doi.org/10.1029/2001JD000481>, 2002.
- Warneke, C., Karl, T., Judmaier, H., Hansel, A., Jordan, A., Lindinger, W., and Crutzen, P. J.: Acetone, methanol and other partially oxidized volatile organic emissions from dead plant matter by abiological processes: Significance for atmospheric HO_x chemistry, *Global. Biogeochem. Cy.*, 13, 9–17, 1999.
- Wayne, R. P., Barnes, I., Biggs, P., Burrows, J. P., Canosa-Mas, C. E., Hjorth, J., Le Bras, G., Moortgat, G. K., Perner, D., Poulet, G., Restelli, G., and Sidebottom, H.: The nitrate radical: Physics, chemistry, and the atmosphere, *Atmos. Environ. A-Gen.*, 25, 1–206, 1991.
- Williams, J., Crowley, J., Fischer, H., Harder, H., Martinez, M., Petäjä, T., Rinne, J., Bäck, J., Boy, M., Dal Maso, M., Hakala, J., Kajos, M., Keronen, P., Rantala, P., Aalto, J., Aaltonen, H., Paatero, J., Vesala, T., Hakola, H., Levula, J., Pohja, T., Herrmann, F., Auld, J., Mesarchaki, E., Song, W., Yassaa, N., Nölscher, A., Johnson, A. M., Custer, T., Sinha, V., Thieser, J., Pouvesle, N., Taraborrelli, D., Tang, M. J., Bozem, H., Hosaynali-Beygi, Z., Axinte, R., Oswald, R., Novelli, A., Kubistin, D., Hens, K., Javed, U., Trawny, K., Breitenberger, C., Hidalgo, P. J., Ebben, C. J., Geiger, F. M., Corrigan, A. L., Russell, L. M., Ouwersloot, H. G., Vilà-Guerau de Arellano, J., Ganzeveld, L., Vogel, A., Beck, M., Bayerle, A., Kampf, C. J., Bertelmann, M., Köllner, F., Hoffmann, T., Valverde, J., González, D., Riekkola, M.-L., Kulmala, M., and Lelieveld, J.: The summertime Boreal forest field measurement intensive (HUMPPA-COPEC-2010): an overview of meteorological and chemical influences, *Atmos. Chem. Phys.*, 11, 10599–10618, <https://doi.org/10.5194/acp-11-10599-2011>, 2011.
- Yassaa, N., Song, W., Lelieveld, J., Vanhatalo, A., Bäck, J., and Williams, J.: Diel cycles of isoprenoids in the emissions of Norway spruce, four Scots pine chemotypes, and in Boreal forest ambient air during HUMPPA-COPEC-2010, *Atmos. Chem. Phys.*, 12, 7215–7229, <https://doi.org/10.5194/acp-12-7215-2012>, 2012.
- Zhou, P., Ganzeveld, L., Rannik, Ü., Zhou, L., Gierens, R., Taipale, D., Mammarella, I., and Boy, M.: Simulating ozone dry deposition at a boreal forest with a multi-layer canopy deposition model, *Atmos. Chem. Phys.*, 17, 1361–1379, <https://doi.org/10.5194/acp-17-1361-2017>, 2017.

Supplement of Atmos. Chem. Phys., 18, 3799–3815, 2018
<https://doi.org/10.5194/acp-18-3799-2018-supplement>
© Author(s) 2018. This work is distributed under
the Creative Commons Attribution 4.0 License.



Atmospheric
Chemistry
and Physics
Open Access
EGU

Supplement of

Direct measurement of NO₃ radical reactivity in a boreal forest

Jonathan Liebmann et al.

Correspondence to: John N. Crowley (john.crowley@mpic.de)

The copyright of individual parts of the supplement might differ from the CC BY 4.0 License.

Supplementary Information

Technical description of the GC-AED

5 A Gas Chromatograph equipped with an Atomic Emission Detector (GC-AED) was deployed in the field for the first time to perform in-situ gas phase VOC measurements. The set-up consisted of cryogenic pre-concentrator (Entech 7200) system with three liquid nitrogen cooled traps, coupled with an Agilent 7890B GC and a new Joint Analytical Systems third generation AEDIII detector (JAS, Moers, Germany).

10 In the Entech pre-concentration system, water is first removed within an empty Silonite™ D coated 1/8" (0.32 cm) stainless steel tube trap held at -50 °C which thereafter is heated to 10°C while forward flushed with 50 ml He towards the main Silonite™ D Tenax® packed enrichment trap cooled to -60°C where the VOC trapping takes place. The volatiles are then refocused into a smaller dead volume for split-less injection (Silonite™ D coated 1/32", 0.08 cm diameter stainless steel tubing) at -180°C. After thermal release the collected VOC sample passes through an insulated and heated transfer line (110°C) into the GC.

15 The AED operates by atomizing all compounds eluting from the GC column (Supelco SPB-624 60 m column, 3.5 mL min⁻¹ He as carrier gas, 34 min GC run) within a helium plasma. The element specific characteristic emission lines (e.g. for carbon, sulfur, bromine, iodine, nitrogen etc.) which occur at specific wavelengths are focused onto the entrance slit of the spectrometer. In the spectrometer, a high-resolution flat field grating is used to disperse the atomic emission light spectrum in the wavelength range of 160-209 nm onto two flat plane back thin CCD chips, where the wavelength dependent spectra are simultaneously recorded in the full range. All the transfer lines of the coupled system are insulated, heated and monitored
20 at set values.

The GC-AED was installed at the Hyytiälä site, within an air-conditioned measurement container (25°C). Ambient air was sampled from the center of the common inlet also used by the NO₃ reactivity instrument. A 15 m insulated and heated (10°C above ambient) 1/2" (1.27 cm) PFA Teflon tubing was used as a GC-AED system inlet line with a flowrate of 20 L min⁻¹ (transmission time 3.3 s). The ambient air was filtered using 5.0 µm PTFE (47 mm in diameter) membrane filters (Sartorius
25 Stedim GmbH, Göttingen, Germany) which were changed every 5 days.

GC-AED was calibrated *in-situ* with an 84-component gravimetrically prepared gas-phase calibration reference standard with a stated accuracy of better than ±5% (Apel-Riemer Environmental, Inc., Florida, USA). The average total uncertainty based on repeated calibration standard measurements combined with the flow measurements and calibration standard uncertainty was calculated 14%. Since monoterpenes were an important part of this campaign α-pinene, Δ-3-carene, β-pinene, camphene and d-limonene were all calibrated individually, despite it being possible to derive ambient concentrations
30 via the carbon signal alone. Detection limits for the monoterpene species were 1.0, 0.9, 0.4, 0.5 and 0.3 pptv respectively.

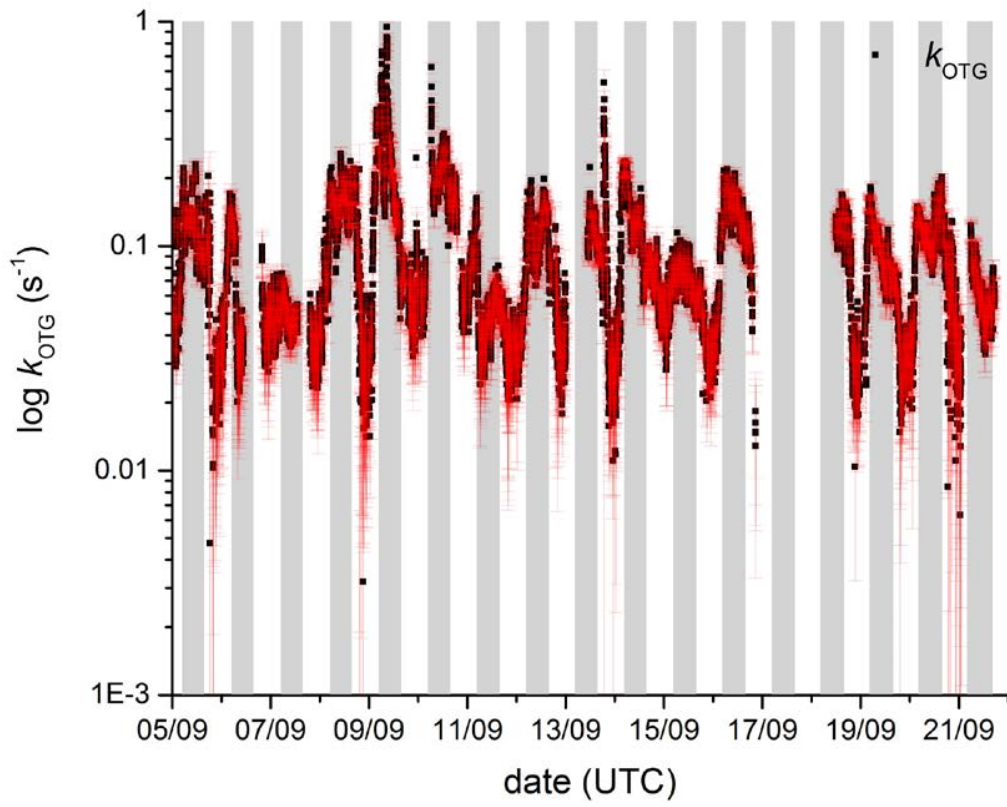


Figure S1. k_{OTG} and associated uncertainty.

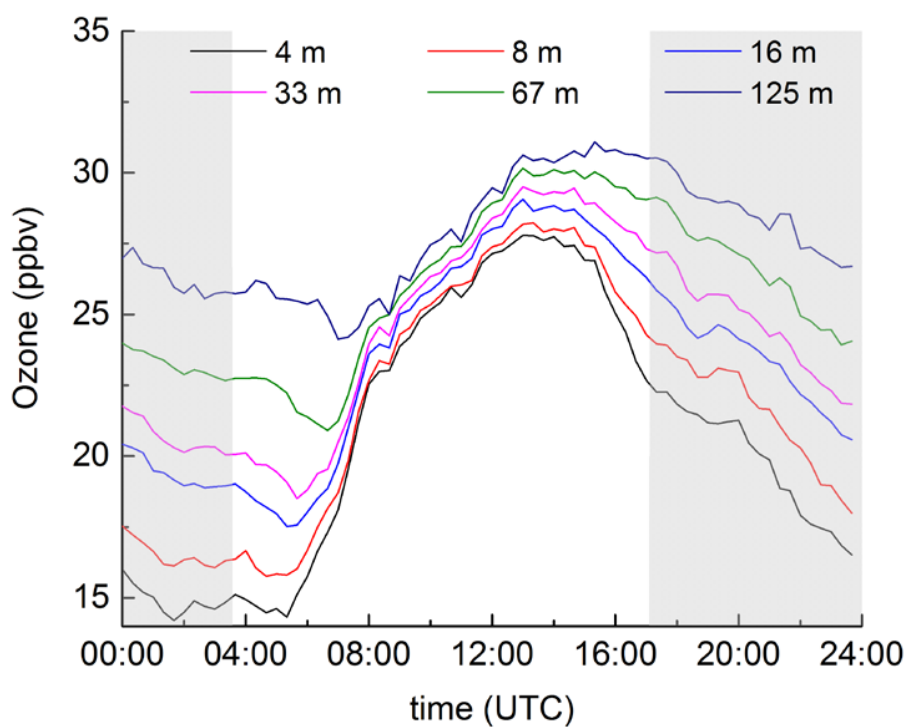


Figure S2. The campaign averaged, diel variation of ozone at different heights (4 m to 125 m) as measured at the SMEAR II tower. The largest day/night differences are observed for the lower levels.

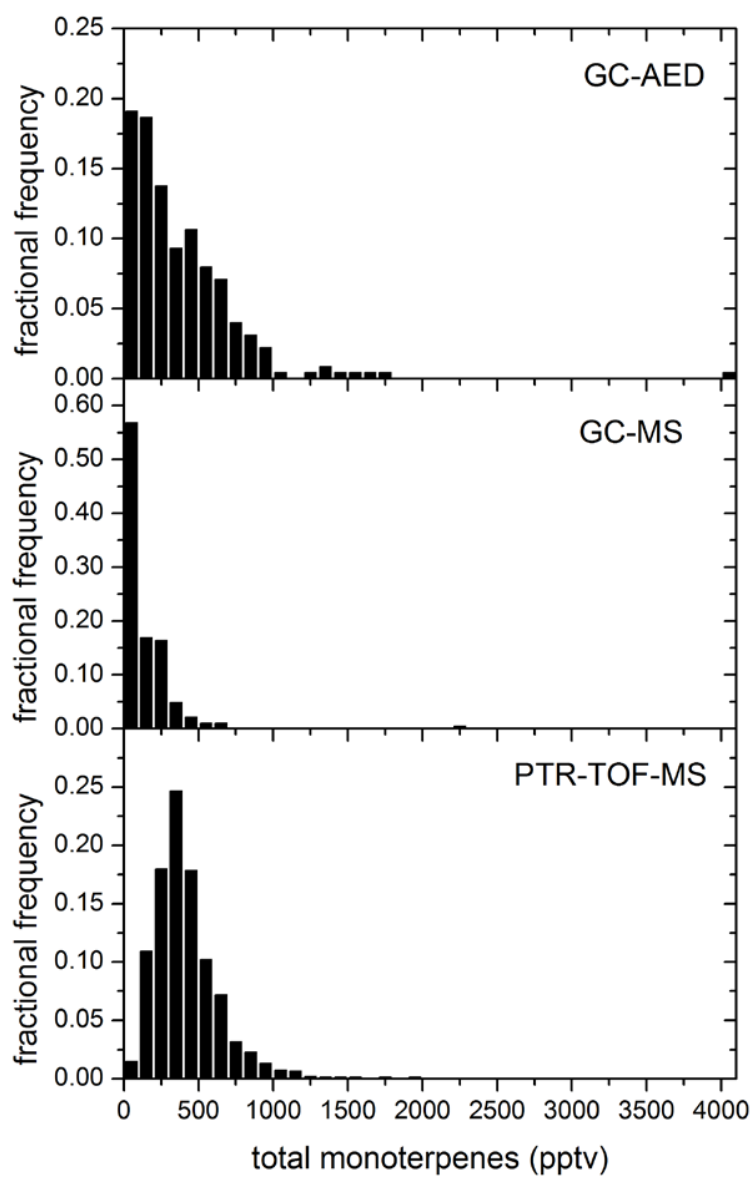


Figure S3. Histograms highlighting differences in the total mono-terpene mixing ratios measured using different instruments at different locations.

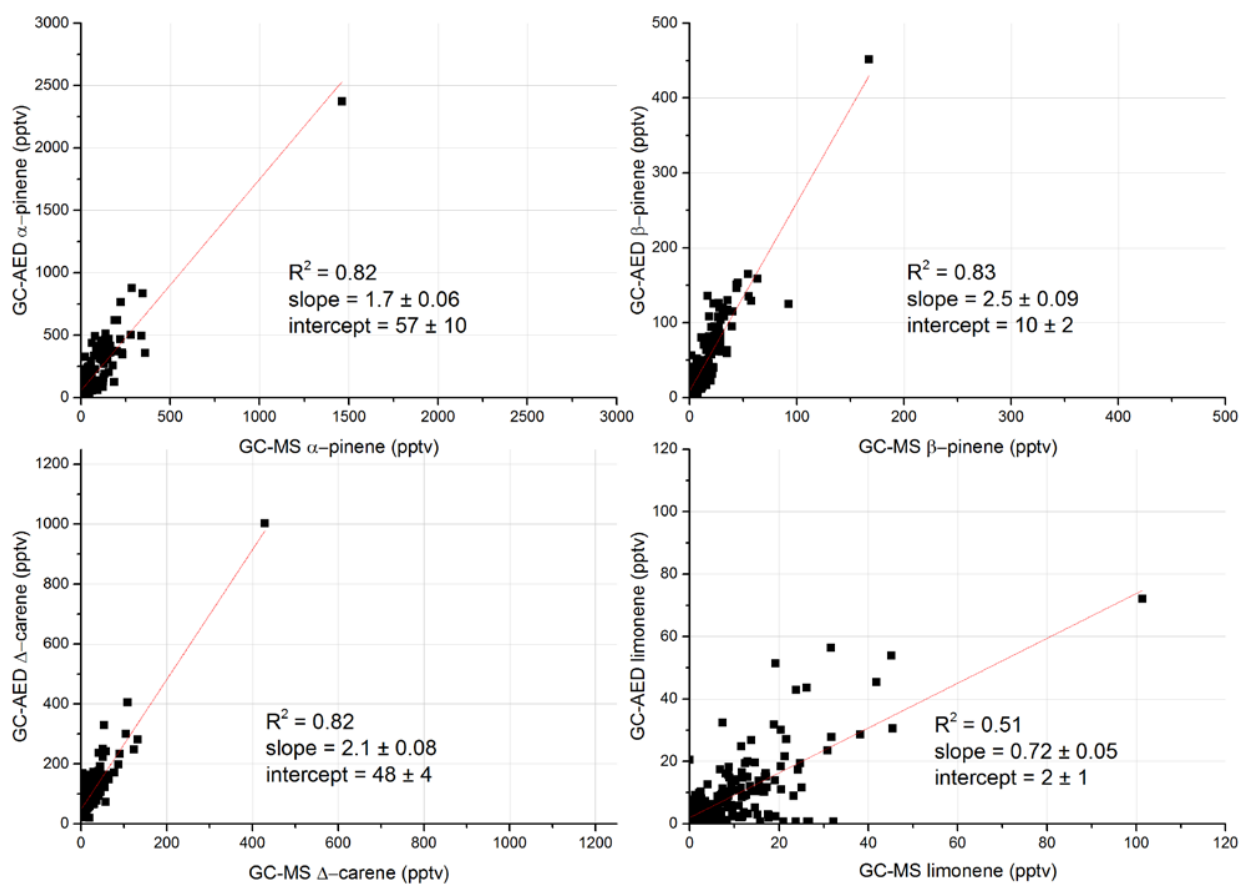


Figure S4. Comparison of individual monoterpenes measured by GC-AED and GC-MS.

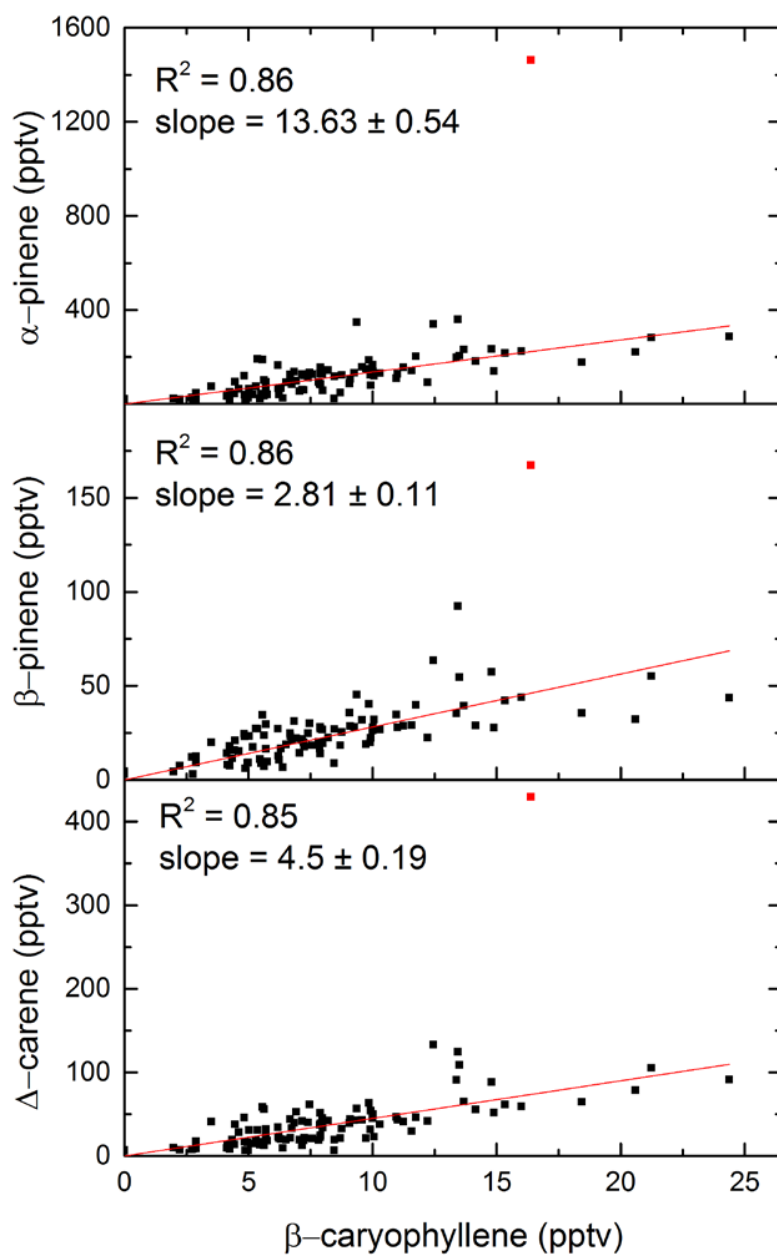


Figure S5. Correlation of β -caryophyllene with monoterpenes. Red lines are proportional fits to the data.

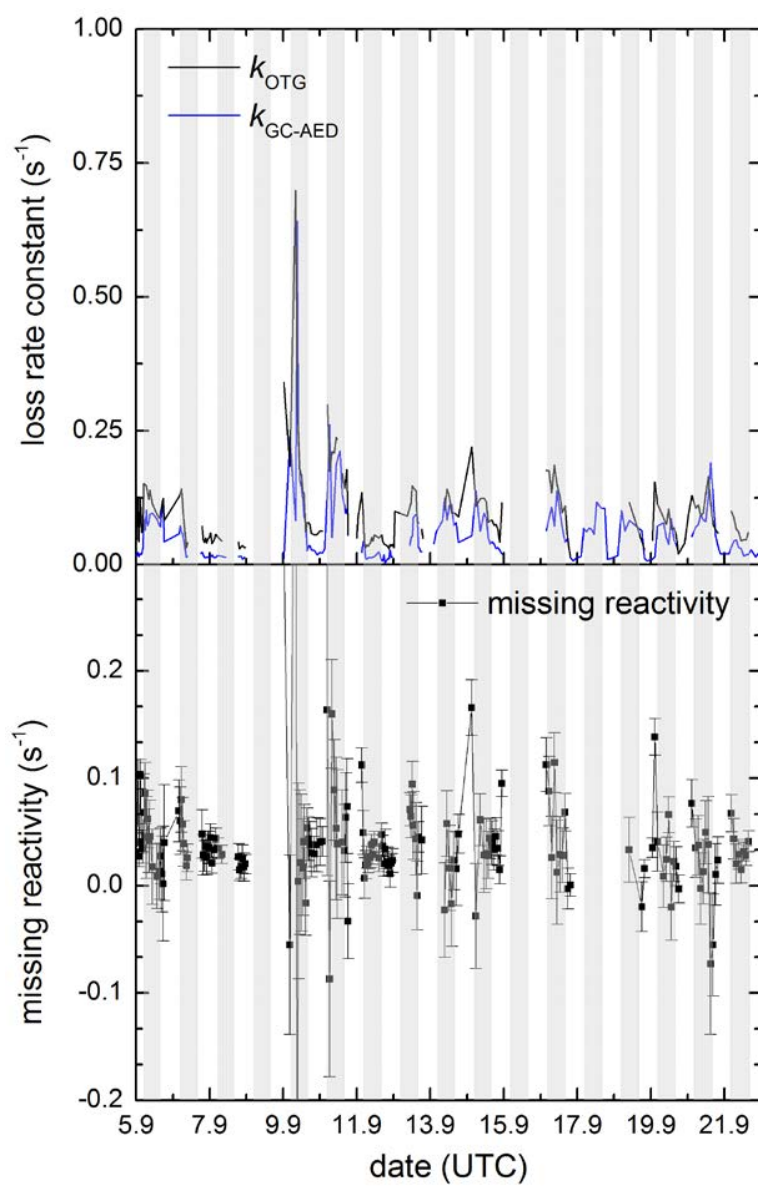


Figure S6. Upper panel: time series of k_{OTG} and $k_{\text{GC-AED}}$. Lower panel: Missing reactivity ($k_{\text{OTG}} - k_{\text{GC-AED}}$) with total uncertainty.

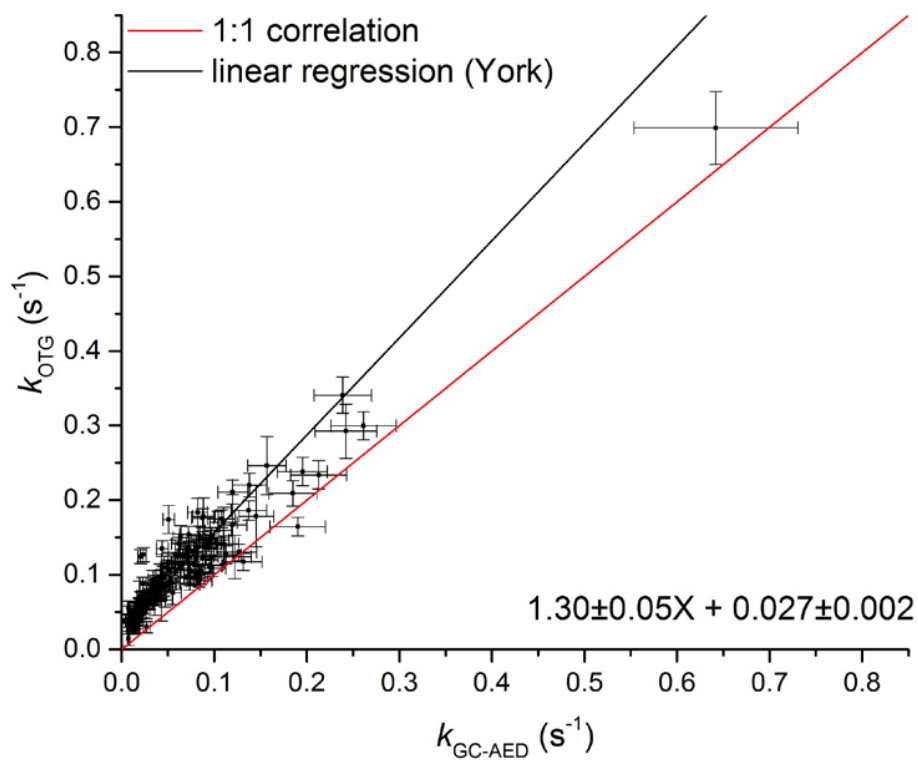


Figure S7. Correlation between k_{GC-AED} and k_{OTG} . The error-bars represent total uncertainty, calculated as described in the manuscript. The slope (1.30 ± 0.05) indicates that, on average, measured VOCs account for $77 \pm 3\%$ of the observed reactivity.

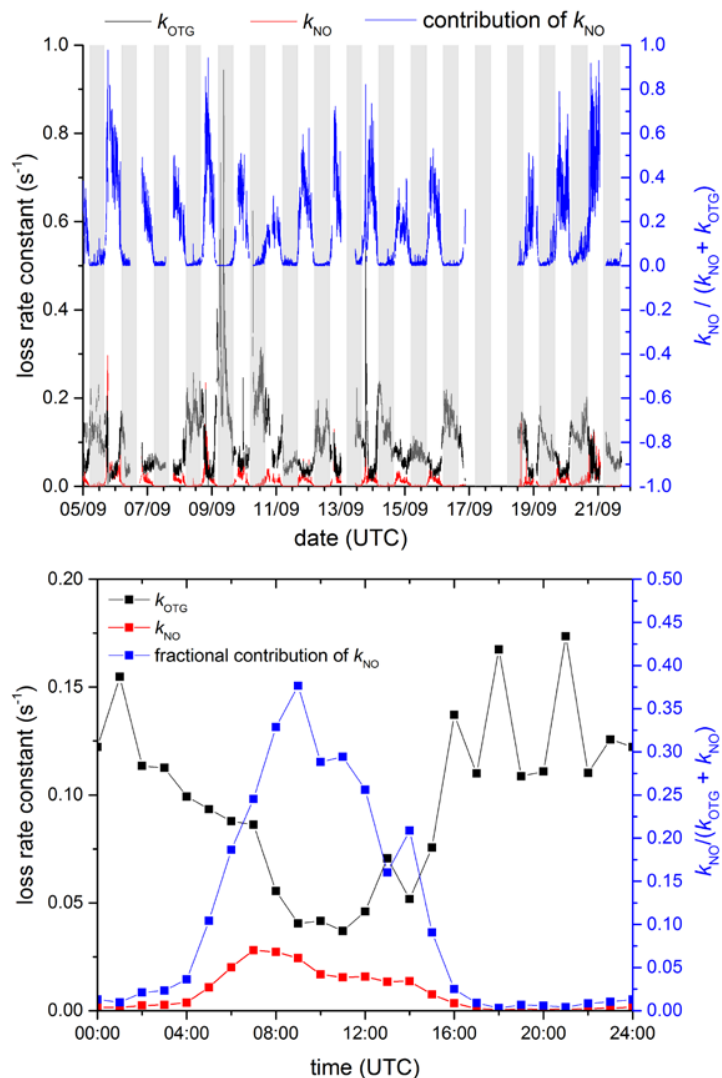


Figure S8. Upper panel: Time series of the loss rate constant for NO₃ due to reaction with NO (k_{NO}) and k_{OTG} and the fractional contribution of NO (k_{NO}) to the overall, chemical loss of NO₃ ($k_{\text{NO}} + k_{\text{OTG}}$). Lower panel: Same parameters averaged over the campaign.

A3: Liebmann et al., Atmos. Chem. Phys., 2018 B

Direct measurements of NO₃-reactivity in and above the boundary layer of a mountain-top site: Identification of reactive trace gases and comparison with OH-reactivity.

Jonathan M. Liebmann¹, Jennifer B. A. Muller², Dagmar Kubistin², Anja Claude², Robert Holla², Christian Plass-Dülmer², Jos Lelieveld¹, John N. Crowley¹

¹ *Atmospheric Chemistry Department, Max-Planck-Institut für Chemie, 55128, Mainz, Germany*

² *Meteorologisches Observatorium Hohenpeissenberg, Deutscher Wetterdienst, 82383, Hohenpeißenberg, Germany*

submitted to: **Atmospheric Chemistry and Physics**, 26.03.2018



Direct measurements of NO₃-reactivity in and above the boundary layer of a mountain-top site: Identification of reactive trace gases and comparison with OH-reactivity.

5 Jonathan M. Liebmann¹, Jennifer B. A. Muller², Dagmar Kubistin², Anja Claude², Robert Holla²,
Christian Plaß-Dülmer², Jos Lelieveld¹ and John N. Crowley¹

¹Atmospheric Chemistry Department, Max Planck Institut für Chemie, 55128, Mainz, Germany

²Meteorologisches Observatorium Hohenpeissenberg, Deutscher Wetterdienst, 82383, Hohenpeissenberg, Germany

10

Correspondence to: John Crowley (john.crowley@mpic.de)

Abstract. We present direct measurements of the summertime, total reactivity of NO₃ towards organic trace gases, $k_{\text{OTG}}^{\text{NO}_3}$, at
15 a rural mountain site (988 m a.s.l.) in southern Germany in 2017. The diel cycle of $k_{\text{OTG}}^{\text{NO}_3}$ was strongly influenced by local
meteorology with reactivity high during the day (values of up to 0.3 s⁻¹) but usually close to the detection limit (0.005 s⁻¹) at
night when the measurement site was in the residual layer / free troposphere. Daytime values of $k_{\text{OTG}}^{\text{NO}_3}$ were sufficiently large
that the loss of NO₃ due to reaction with organic trace gases competed with its photolysis and reaction with NO. Within
experimental uncertainty, monoterpenes and isoprene accounted for all of the measured NO₃-reactivity. Averaged over the
20 daylight hours, more than 25% of NO₃ was removed via reaction with biogenic volatile organic compounds (BVOCs),
implying a significant daytime loss of NO_x and formation of organic nitrates due to NO₃ chemistry. Ambient NO₃
concentrations were measured on one night and were comparable to those derived from a stationary state calculation using
measured values of $k_{\text{OTG}}^{\text{NO}_3}$. We present and compare the first simultaneous, direct-reactivity measurements for the NO₃ and
OH radicals. The decoupling of the measurement site from ground level emissions resulted in lower reactivity at night for
25 both radicals, though the correlation between OH- and NO₃-reactivity was weak as would be anticipated given their
divergent trends in rate constants with many organic trace gases.



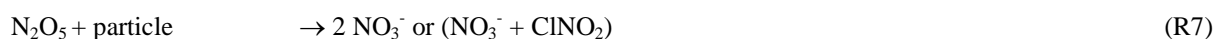
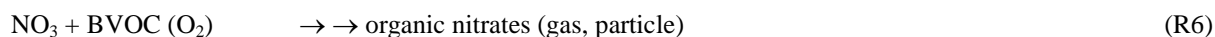
1 Introduction

Hydroxyl (OH) and nitrate radicals (NO₃) play a centrally important role in cleansing the atmosphere of trace gas emissions resulting from both anthropogenic and biogenic activity (Lelieveld et al., 2004; Lelieveld et al., 2016; Ng et al., 2017). Whereas OH is largely photochemically generated and present at its highest concentrations during the day, NO₃ is generated through the oxidation of NO₂ by O₃ and, due to its rapid photolysis and reaction with NO, is present mainly at night. A further important difference in the roles of OH and NO₃ in the atmosphere is related to the mechanism of their reactions. NO₃ reacts rapidly via electrophilic addition to unsaturated organic trace gases but reacts comparatively slowly (via H-abstraction) with saturated organics. In the presence of O₂, the initial addition step results in the formation of nitrooxyalkyl peroxy radicals, which can react with HO₂, NO, NO₂ or NO₃ to form multifunctional peroxides and organic nitrates (Fry et al., 2014; Ng et al., 2017).

OH can react both by addition and H-abstraction to organic and inorganic trace gases and may be considered to be more reactive and much less selective than the NO₃ radical. The distinct reaction modes leads to significant differences in the lifetimes of both radicals, which for OH are typically less than 1s and for NO₃ can exceed 1 hour (Wayne et al., 1991; Atkinson, 2000; Atkinson and Arey, 2003a; Brown and Stutz, 2012; Liebmann et al., 2018). Maximum daytime concentrations of OH are typically less than 1 pptv, whereas NO₃ has been observed at the 10s to 100s of pptv levels during nighttime (Noxon et al., 1978; Sobanski et al., 2016; Ng et al., 2017).

The large NO₃ mixing ratios at nighttime and the large rate constants for reaction of NO₃ with several unsaturated, biogenic VOCs result in NO₃ being the dominant sink of many BVOCs (Wayne et al., 1991; Atkinson, 2000; Atkinson and Arey, 2003a, b; Long et al., 2011; Brown and Stutz, 2012; Liebmann et al., 2017) especially those whose emission is mainly temperature dependent and continues at nighttime, e.g. monoterpenes (Hakola et al., 2012). The importance of NO₃ on a global scale is highlighted by the fact that forest ecosystems (covering around 9% of the world's surface) annually release ≈ 1000 Tg of biogenic volatile organic compounds (BVOC, e.g. isoprene (2-methyl-1,3-butadiene), monoterpenes (C₁₀H₁₆) and sesquiterpenes (C₁₅H₂₄)) into the Earth's atmosphere (Guenther et al., 2012; Bastin et al., 2017). BVOCs have a strong impact on the atmospheric radical budget, the NO_x cycle (Hakola et al., 2003; Holzke et al., 2006; Nölscher et al., 2013) as well as on the formation and growth of organic particles (Jaoui et al., 2013; Lee et al., 2016; Ng et al., 2017) hence understanding their lifetime and fate is essential for predicting atmospheric processes and climate change (Lelieveld et al., 2008; Lelieveld et al., 2016). In addition, NO₃ is an intermediate in the step-wise oxidation of NO to N₂O₅ (R1-R2, R4) and its lifetime with respect to reaction with biogenic trace gases (R6) impacts on NO_x levels and thus on photochemical O₃ formation from NO₂ photolysis.





The organic nitrates formed in the multi-step reaction (R6) can transfer to the particle phase or be lost through deposition; N_2O_5 formed in (R4) can react with aqueous particles to form particulate nitrate and/or ClNO_2 (R7) (Osthoff et al., 2008; Phillips et al., 2012; Bannan et al., 2015; Phillips et al., 2016) thus reducing the rate of photochemical O_3 production (Dentener and Crutzen, 1993). The absolute and relative fluxes through (R6) and (R7) thus control to some extent the lifetime of NO_x .

Direct NO_3 -reactivity measurements have recently become possible (Liebmann et al., 2017) and the first deployment in a forested region revealed a large NO_3 -reactivity at canopy height, not all of which could be accounted for by simultaneous measurements of a large suite of organic trace gases (Long et al., 2011) pointing towards unmeasured monoterpenes as well as sesquiterpenes likely to be responsible. The difference between the observed (or derived) NO_3 -reactivity and that calculated from summing loss rates for a set of reactive trace gases is generally termed “missing reactivity” as frequently reported for OH (Nölscher et al., 2012). Previous work on NO_3 -reactivity has also revealed a strong meteorological influence on the NO_3 lifetime, especially when air masses are decoupled from the surface layer in which reactive trace gases (NO and BVOC) are emitted at night (Brown et al., 2007b; Brown et al., 2011; Long et al., 2011; Sobanski et al., 2016).

In this paper we describe direct measurements of the NO_3 -reactivity in ambient air on a rural mountain site in southern Germany and interpret the data based on measured VOCs and in terms of the underlying meteorological situation. We also compare NO_3 -reactivity to simultaneous measurements of OH-reactivity over the same period.

20 2 Site description and methods

During the period 20.07.17 to 6.08.17 NO_3 -reactivity measurements were conducted in parallel with ongoing observations at the Meteorological Observatory Hohenpeissenberg (MOHp) in Bavaria, southern Germany. The observatory is a meteorological monitoring and Global Atmosphere Watch site, operated by the German Meteorological Service (DWD). It is located on the Hohenpeissenberg mountain (988 m a.s.l.), 300-400 m above the surrounding countryside about 40 km from the northern rim of the Alps and has been the location of several intensive field campaigns (Plass-Dulmer et al., 2002; Birmili et al., 2003; Handisides et al., 2003; Mannschreck et al., 2004; Bartenbach et al., 2007; Hock et al., 2008; Novelli et al., 2017). The vegetation around the measurement site consists of coniferous trees and beeches growing on the slopes of the mountain while grassland and marshes are dominant in the valley. Tourism related vehicular emissions represent a potential source of local anthropogenic pollution especially at the weekends. The nearest city, Munich, is about 70 km to the northeast.



Trace gases were sampled into the NO₃-reactivity and NO₂-CRD instruments through 1-inch outer-diameter PFA tubing (20 m long, operated at a flow of 40 dm³ min⁻¹) located 1.5m above the roof, directly next to the VOC inlet. The inlet was circa 3 m distance from the inlet used for the other NO_x measurements and circa 2 m distance from the OH-reactivity inlet.

2.1 NO₃-reactivity measurements

- 5 The NO₃-reactivity instrument was operated in a laboratory located in the 3rd floor of the of the MOhp station building at the Hohenpeissenberg. Air samples were drawn at a flow rate of 2900 cm³ (STD) min⁻¹ through a 2 μm membrane filter (Pall Teflon) and 4 m of PFA tubing (6.35 mm OD) from the centre of the bypass flow (see above) resulting in 7.5 s residence time for the transport of air from the sampling point. During night time (≈19:00-03:50 UTC) ambient air samples were drawn through a heated glass flask (35 °C, residence time 20 s) to destroy ambient N₂O₅ and NO₃ which would potentially
- 10 interfere with the reactivity measurements. Operational details of the instrument were recently described by Liebmann et al. (2017). NO₃ radicals were generated by mixing NO₂ and O₃ at elevated pressure (1.5 bar, ≈ 5 minutes reaction time) and passing the mixture through an oven at ≈ 100 °C to convert all N₂O₅ to NO₃ (R2-R5). The effluent from the oven was mixed with either zero-air or ambient air in a flow-tube thermostatted to 21 °C to yield a typical (initial) NO₃ mixing ratios of 40-60 pptv.
- 15 After a fixed reaction time, the remaining NO₃ was detected by cavity-ring-down spectroscopy (CRDS) at 662 nm. The lower pressure at the top of the Hohenpeissenberg station (903 ± 8 hPa) meant that the reaction time was reduced from 10.5 s as previously reported (Liebmann et al., 2017), to 9.5 s. The measurement cycle was typically 400 s for synthetic air and 1200 s for ambient air, with intermittent signal zeroing (every ≈ 100 s) by addition of NO. The fractional loss of NO₃ in ambient air compared to zero air was converted to a reactivity via numerical simulation of a simple reaction scheme
- 20 (Liebmann et al., 2017) using measured amounts of NO, NO₂ and O₃. The parameter obtained, $k_{\text{OTG}}^{\text{NO}_3}$, is a NO₃ loss rate constant from which contributions by NO and NO₂ have been removed, and thus refers to reactive loss to organic trace gases (OTG) only. Throughout the manuscript, NO₃-reactivity and $k_{\text{OTG}}^{\text{NO}_3}$ are equivalent terms, with units of s⁻¹. The upper measurement limit to $k_{\text{OTG}}^{\text{NO}_3}$ was 45 s⁻¹, achieved by automated, dynamic dilution of the air sample. The lower limit was 0.005 s⁻¹, defined by the stability of the NO₃ source. Online calibration of the reactivity using an NO standard was performed every
- 25 ≈2 hours for 10 min. The uncertainty of the measurement was between 0.015 and 0.205 s⁻¹, depending mainly on dilution accuracy, NO levels and stability of the NO₃ source as described by Liebmann et al. (2017). Since its first description in Liebmann et al. (2017), the instrument has been extended with a further cavity to measure mixing ratios of NO₂ (see below).

2.2 NO₂, NO and O₃ measurements

- 30 Since its first deployment, the NO₃-reactivity instrument described by Liebmann et al. (2017, 2018) has been extended with a further cavity to measure NO₂. This is described here for the first time and thus in detail. The CRDS measurement of NO₂



uses a 2500 Hz, square-wave modulated, 40 mW laser-diode located in a Thor Labs LDM 21 housing and thermally stabilized at 36 °C using a Thor Labs ITC 510 Laser-Diode Combi Controller to produce light at 405 nm (0.5 nm full-width at half-maximum). The laser-diode emission is first directed through an optical isolator (Thorlabs IO-3D-405-PBS), focused by a lens (Thorlabs C340TMD-A) into the optical-fibre (0.22 NA, 50 µm core, 400-2400 nm) and then collimated (Thor Labs FiberPort Collimator PAF-X-7-A) to a beam diameter of about 6 mm before entering the cavity. Part of the laser emission was directed to an Ocean Optics spectrograph to continuously measure the laser emission spectrum.

The NO₂ cavity (Teflon-coated glass (DuPont, FEP, TE 9568), length 70 cm, volume 79 cm³) was operated at 30 °C at a flow rate of 3000 cm³ (STP) min⁻¹ resulting in a residence time of approximately 1 s. To remove particles, air was drawn through a 2 µm membrane filter (Pall Teflon) from the centre of the same high-flow bypass used for the NO₃-reactivity measurements. Light exiting the cavities through the rear mirror was detected by a photomultiplier (Hamamatsu E717-500) which was screened by a 405 nm interference filter. The pre-amplified PMT signal was digitized and averaged with a 10 MHz, 12 bit USB scope (Picoscope 3424) which was triggered at the laser modulation frequency of 2500 Hz.

The ring-down constant in the absence of NO₂ was obtained by adding zero air every 30 points of measurement for approximately 15 s. The L/d ratio (the ratio of the distance between the cavity mirrors, L , and the length of the cavity that is filled by absorber, d) was determined as described previously (Schuster et al., 2009; Crowley et al., 2010) and was 1.00 ± 0.03 . Inverse decay-constants in dry zero-air at 660 Torr were usually between 28 and 31 µs indicating optical path lengths of ≈ 8 -9 km. The measurement precision (6 s integration) was circa 150 pptv. The cavity was not pressure stabilized leading to a pressure difference of circa 2.5 Torr when switching from ambient air to zero measurements. The data was corrected for the change in Rayleigh scattering resulting from the pressure difference (typically 120 pptv) and also different relative humidities (typically 60 to 100 pptv) when switching from ambient to zero-air measurement as described by Thieser et al. (2016). The laser spectrum was measured every hour and used to calculate an effective cross-section ($\approx 6.00 \times 10^{-19}$ cm² molecule⁻¹) using a literature absorption spectrum (Voigt et al., 2002). The overall uncertainty of the measurement is mainly determined by the uncertainty in the cross section (6%). Other contributions are from NO₂ formation (from reaction of NO with O₃ in the inlet lines, $\approx 0.5\%$) and the correction for humidity and pressure differences (5%), and an error in the L/d ratio (2%), giving an estimated uncertainty of 9%. The detection limit of the instrument can be estimated from the variability in the zeros and was usually around 150 pptv.

NO₂ measurements were made from the 20th of July to the 4th of August with breaks from the 27th of July to the 2nd August and from the 4th to the 6th due to instrumental problems. NO₂ mixing ratios were corrected for its formation (R1) during transport from the roof top inlet to the cavity (≈ 7.5 s).

Two commercially available instruments operated permanently at the site also provided measurements of NO₂ and NO. These were a cavity-phase-shift (CAPS) instrument for NO₂ measurement and a chemiluminescence device (CLD) for NO₂ and NO. The CAPS (Aerodyne, Ambient Monitor Version 2012) had a detection limit of 270 pptv (3 σ in 1 min integration time) and an uncertainty of 10% (1 min integration time). The CLD (ECO PHYSICS, Model AL 770 pptv) uses chemiluminescence from the reaction of NO with ozone in combination with a blue-light converter to convert NO₂ to NO.



The instrument was routinely calibrated once a week (10 ppmv \pm 5% NO in N₂, Riessner, Germany. Deviations between two calibrations are typically well below 3%. Detection limits during the intensive were 11 pptv for NO, 16 pptv for NO₂ (3 σ in 1min integration time) and median uncertainties are 27 pptv (7%) for NO and 70 pptv (10%) for NO₂ (2 σ at 1 ppbv in 1min integration time). Corrections were applied to take into account NO loss and NO₂ formation due to further reactions involving ozone in the inlet tubing.

A comparison of the three NO₂ measurements instruments is given in Fig. S1 of the supplementary information which plots the NO₂ mixing ratios (averaged over 60 s) of the CLD and CAPS instruments versus the CRDS. A least-squares fit (considering errors in both parameters) to the plot of NO₂ (CLD) versus NO₂ (CRDS) has a slope of 0.94 ± 0.25 and an intercept of 0.00 ± 0.04 . For the plot of NO₂ (CAPS) versus NO₂ (CRDS) comparison we derive a slope of 0.95 ± 0.02 and an intercept of 0.00 ± 0.02 . Within combined uncertainty, the NO₂ measurements are thus in agreement. The NO₂ mixing ratios used as input to calculate the NO₃-reactivity were taken from the CRDS instrument, with data gaps filled by CAPS measurements.

Ozone was monitored with a UV absorption instrument (Thermo Environmental Instruments Inc., Model TECO 49C) which is calibrated at regular intervals with a transfer standard (TECO 49 PS). The uncertainty in the ozone mixing ratio is 1.2 ppbv or 2% (2 σ in 1 hour).

2.3 NO₃ measurements

For the measurement of ambient NO₃, a 10 m length of PFA-tubing (3/8-inch outer diameter) was installed on the top of the building, circa 10 cm from the VOC inlet. A 2 μ m pore PTFE filter (47 mm in diameter, replaced every hour) in a PFA filter holder was located at the end of the inlet. The tubing was connected to a bypass pump operated at 20 dm³ (STD) min⁻¹ to reduce the residence time. The sample flow through the cavity was increased to 8 dm³ (STD) min⁻¹ to reduce the NO₃ residence time within the cavity. NO₃ mixing ratios were recorded every 6 s (3600 ring-downs co-added) with zeroing by titration (no addition) every 15 data points. The NO₃ transmission through the inlet ($67 \pm 15\%$), filter and filter-holder ($84 \pm 10\%$) and cavity ($88 \pm 10\%$) were established post-campaign and used to correct the data. The overall uncertainty in the NO₃ measurements, including uncertainty in the absorption cross-section, was circa 35%.

2.4 OH-reactivity measurements

OH-reactivity measurements were conducted using a chemical ionization mass spectrometer (CIMS) in which OH radicals (generated by photolysis of H₂O at 184.95 nm) are converted to H₂SO₄ (Berresheim et al., 2000; Schlosser et al., 2009). For the derivation of OH-reactivity ($k_{\text{total}}^{\text{OH}}$), relative OH radical concentrations are measured at two fixed reaction times and a decay constant is derived assuming exponential behaviour. After correction for wall losses, as well as NO-induced HOx



recycling in the sample tube, ambient reactivities between 1 to 40 s⁻¹ are measurable. OH-reactivity measurements were made every 20 min throughout the measurement period. Measurements were discontinued during periods of precipitation and when the pinhole to the mass spectrometer vacuum system was blocked by insects. The instrument performs best if NO mixing ratios are below 4 ppbv and reactivities do not exceed 15 s⁻¹; for the measurements reported here, the mean uncertainty in the OH-reactivity was ± 1.2 s⁻¹ (or 46%). OH-reactivity calibration was carried out before and after the measurement period, and the calibration factor was applied to the whole dataset. The determination of the OH wall loss rate from zero reactivity measurement (null measurement) using synthetic air cylinders was not reliable and therefore the zero was estimated using nighttime measurements when sampling from above the boundary layer. Details are given in the supplementary information.

10 2.5 VOC measurements

A gas-chromatograph (GC-MS/FID model AGILENT 6890 with 5975 B inert XL MSD), was used for the detection of C₅–C₁₃ NMHCs and BVOC (Hoerger et al., 2015). In a custom-made pre-concentration unit, air was sampled at 30 °C on a 3-bed adsorption trap and, after a cryo-focussing step, injected onto the GC column (50m BPX-5). Subsequently, signals were detected with a mass spectrometer (MS) running in parallel with a flame ionization detector (FID). The instrument measured i.a. isoprene and a wide variety of monoterpenes with uncertainties (2σ) from 6 to 100% depending on the compound. For the detection of light NMHCs (C₂–C₈), a GC-FID system (GC-1, Varian 3600 CX, FID detector) described in detail by Plass-Dülmer et al. (2002) was used. In both systems, an ozone scrubber (impregnated filter with Na₂SO₃) was used and water was removed from the sample air either by hydrophobic adsorbents (C₅–C₁₃) or a cold trap (C₂–C₈) prior to the pre-concentration step.

VOCs were sampled every hour for 15 min (C₂–C₈) respectively 20 min (C₅–C₁₃) by both instruments. During the rainy period from the 24th of July 12:00 UTC to the 27th of July 12:00 UTC, VOCs were only measured twice daily.

3 Results and discussion

Figure 1 displays the time series of NO₃-reactivity ($k_{\text{OTG}}^{\text{NO}_3}$) along with related trace gases and meteorological data obtained during the intensive. Sunrise was around 3:50 UTC and sunset at ≈19:00 UTC. Two mild days (T_{max} = 20–25 °C) at the beginning of the campaign were followed by a 3 day period with heavy rains and maximum temperatures of around 10 °C followed by a warm period with temperatures up to 30 °C and occasional thunderstorms. The predominant wind direction was west-south-west with only minor contributions from other directions (Fig. S2). Wind speeds were generally around 2.5 to 7.5 ms⁻¹, increasing up to 15 ms⁻¹ during the rainy periods. The highest values of $k_{\text{OTG}}^{\text{NO}_3}$ were detected with north-easterly winds (Fig. S2) coincident with the warmest days of the campaign and the highest biogenic emissions (see section 4.2). Ozone mixing ratios were strongly correlated with temperature and ranged from 85 ppbv at the 1th of August during the warm, photochemically intense period to less than 20 ppbv during the cool, rainy period between 23rd and 28th of August.



NO_x levels (NO_x = NO + NO₂) during the intensive were generally between about 0.5 and 4 ppbv. The mixing ratios of NO, a trace gas which can potentially impact NO₃ lifetimes, were generally below the detection limit (≈ 12 pptv) during most of the nights, increasing to maximum values of < 1 ppbv during the day. Occasional maxima of more than 1 ppbv NO were observed due to local traffic.

5 3.1 NO₃ reactivity

NO₃-reactivity was measured continuously during a three week intensive (20.07.2017 to 06.08.2017) with the exception of one night (2nd - 3rd August) when, using the same instrument, NO₃ mixing ratios were measured instead. The full data set of $k_{\text{OTG}}^{\text{NO}_3}$ is reproduced in Fig. S3 of the supplementary information together with the corresponding 95% uncertainty limits, which take into account drifts in the zero signal, the stability of the NO₃ source, uncertainty in the dilution factors, uncertainty of the NO and NO₂ mixing ratios as well as the corresponding rate constants.

As described above, during daytime the short NO₃ lifetime normally results in levels that are under the detection limit of most instruments, precluding estimation of the NO₃-reactivity via stationary-state calculations based on its mixing ratio and production rate. In contrast, our direct measurement enables us to derive the NO₃-reactivity over the full diel cycle. During the intensive, the 10-minute averaged values of $k_{\text{OTG}}^{\text{NO}_3}$ obtained ranged from below the detection limit (< 0.005 s⁻¹) to values as high as 0.3 s⁻¹. Campaign averaged values were low (≈ 0.01 s⁻¹) during nighttime but a factor of ten larger ≈ 0.1 s⁻¹ at 14:00 UTC (local 16:00) and more variable during daytime.

This observation is in stark contrast to the high relative night-time/daytime NO₃-reactivities we observed in a Boreal forest (Liebmann et al., 2018) and is related to very different meteorological conditions at the two sites. In the boreal forest, the canopy-level NO₃-reactivity was controlled by the rate of emission of biogenic VOCs into a nocturnal boundary layer of varying height and stability. The elevated location of the Hohenpeissenberg observatory, located at a mountain-top above the surrounding countryside favoured sampling from the residual layer/free troposphere at nighttime. In the absence of turbulent exchange, the residual layer/free troposphere may become disconnected from the planetary boundary layer (PBL) and thus from ground-level emissions of reactive trace gases and may thus contain low levels of biogenic trace gases as well as low(er) levels of NO₂ and higher levels of ozone (Aliwell and Jones, 1998; Allan et al., 2002; von Friedeburg et al., 2002; Stutz et al., 2004; Brown et al., 2007a; Brown et al., 2007b; Brown and Stutz, 2012). NO₃ lifetimes as long as 1 hour (using stationary-state analyses) have been reported for mountain sites when sampling air from above the nocturnal boundary layer (Brown et al., 2016; Sobanski et al., 2016).

During the Hohenpeissenberg intensive two distinct air-mass types were encountered at night, whereby values of $k_{\text{OTG}}^{\text{NO}_3}$ were either at (or below) the detection limit or well above it (named type 1 and type 2, respectively). Figure 2 displays a time series of $k_{\text{OTG}}^{\text{NO}_3}$ over a single night (29th -30th July) in which a switch from type 2 to type 1 was observed. From early evening until shortly before 12:00 UTC, NO₃-reactivity was variable with values between circa 0.02 and 0.03 s⁻¹. A sharp reduction in $k_{\text{OTG}}^{\text{NO}_3}$ was then observed with values close to the detection limit until sunrise (04:00 UTC). The reduction in $k_{\text{OTG}}^{\text{NO}_3}$ was



accompanied by a drop in relative humidity (from 70% to 60%) and an increase in O_3 (46 to 52 ppbv), both clear indicators of sampling from the residual layer. At the same time, the wind speed increased and the temperature became more variable, indicating that the site was close to the inversion level. At first sunlight, turbulent mixing resulted in gradual connection of the boundary layer and overlying residual layer, leading to an increase in $k_{OTG}^{NO_3}$. Upslope winds caused by heating of the mountainside may also have enhanced transport of air masses with high reactivity to the measurement site. Median, diel profiles of NO_3 -reactivity on type 1 (altogether five) and type 2 nights (altogether 10) are shown in Fig. 3. With the exception of the very low reactivity during type 1 nights, type 1 and type 2 have similar diel shapes and similar maximum reactivities.

3.2 NO_3 -reactivity calculated from VOC measurements

In this section we assess the contribution of various VOCs to the observed NO_3 -reactivity. The most abundant BVOCs were isoprene, sabinene, α -pinene and β -pinene with maximum mixing ratios during the warm period around the 1st August. The time series of BVOC mixing ratios are displayed in Fig. S4 of the supplementary information. $k_{OTG}^{NO_3}$ is a total loss rate constant for chemical reactions of $[NO_3]$ with all organic trace gases present and can be compared to the summed loss rate constant ($k_{VOC}^{NO_3}$) (also in units of s^{-1}) obtained from the concentrations of individual VOCs in the same air mass, $[C_i]$, and the rate coefficient (k_i):

$$k_{VOC}^{NO_3} = \sum k_i^{NO_3} [C_i] \quad (1)$$

Where $[C_i]$ is the measured BVOC concentration and k_i the corresponding rate constant. Individual values of $k_{VOC}^{NO_3}$, calculated using rate constants from the IUPAC evaluation (IUPAC, 2017) or elsewhere in the literature (Shorees et al., 1991), are plotted with interpolated 20 min averages of $k_{OTG}^{NO_3}$ as a time series in the upper panel of Fig. 4.

The data are also displayed as a pie chart in the lower panel of Fig. 4 in which the contribution of individual biogenic trace-gases to the NO_3 -reactivity are listed. Of the terpenoids, α -pinene contributed most to the overall NO_3 -reactivity ($\approx 16\%$) followed by sabinene ($\approx 12\%$) with other individual BVOCs contributing less than 10%. VOCs such as methanol, acetaldehyde, ethanol, acetone, methylethylketone, alkanes and aromatics were also measured but not included in calculations of $k_{VOC}^{NO_3}$ as their summed contribution reached max. $1.5 \times 10^{-4} s^{-1}$ and was on average $5 \times 10^{-5} s^{-1}$. As $k_{VOC}^{NO_3}$ and $k_{OTG}^{NO_3}$ show a similar dependence on wind direction (Fig. S2) and because only BVOCs were used for the derivation of $k_{VOC}^{NO_3}$, we conclude that the high NO_3 reactivities measured in air masses arriving from the east and northeast are mostly from trace-gases of biogenic origin.

Type 1 nights were characterized by very low BVOC mixing ratios, sometimes below the detection limit, whereas isoprene was still present. This observation is consistent with a long lifetime for isoprene in the residual layer at night (Brown et al., 2007a) as the OH concentration is too low and the NO_3 reaction too slow to remove it efficiently. Under conditions of very low NO_3 -reactivity, the fractional contribution of isoprene to the overall reactivity could increase to $\approx 100\%$ (from typically



20% during the day). During type two nights (those with non-zero NO_3 -reactivity) isoprene and monoterpenes were always detected and monoterpenes were the dominant reaction partners for NO_3 .

The difference between $k_{\text{OTG}}^{\text{NO}_3}$ and $k_{\text{VOC}}^{\text{NO}_3}$ (i.e. the NO_3 -reactivity not accounted for by measured VOCs) may be defined as “missing” reactivity (s^{-1}):

$$5 \quad \text{missing } \text{NO}_3\text{-reactivity} = k_{\text{OTG}}^{\text{NO}_3} - k_{\text{VOC}}^{\text{NO}_3} \quad (2)$$

A plot of $k_{\text{VOC}}^{\text{NO}_3}$ versus $k_{\text{OTG}}^{\text{NO}_3}$ (see Fig. S5 of the supplementary information) has a slope of 1.55 ± 0.15 and an intercept of 0.005. This implies, on average, a missing reactivity of $\approx 34\%$ when $k_{\text{OTG}}^{\text{NO}_3} = 0.3 \text{ s}^{-1}$ and a missing reactivity of $\approx 50\%$ when $k_{\text{OTG}}^{\text{NO}_3} = 0.03 \text{ s}^{-1}$. However, both $k_{\text{OTG}}^{\text{NO}_3}$ and $k_{\text{VOC}}^{\text{NO}_3}$ are associated with some uncertainty, which needs to be rigorously assessed to test whether the missing reactivity is significant. To do this we propagated uncertainty in each of the terms $\sum k_i^{\text{NO}_3} [\text{C}_i]$ (mainly related to VOC measurements and assuming 15% uncertainty in the rate coefficients) and derived mean diel profiles of $k_{\text{OTG}}^{\text{NO}_3}$ and $k_{\text{VOC}}^{\text{NO}_3}$ for the whole campaign (hour averages). The results are shown in Fig. 5, where the red shaded area represents total uncertainty and variability in $k_{\text{VOC}}^{\text{NO}_3}$ and the black error bars are the total uncertainty in $k_{\text{OTG}}^{\text{NO}_3}$. Clearly, within combined uncertainty the data overlap, so that missing reactivity is not significantly distinct from zero.

15 3.3 NO_3 measurements and comparison with stationary state calculations

Although rough estimates of NO_3 concentrations at the Hohenpeissenberg have been made (Handisides et al., 2003; Bartenbach et al., 2007), no direct NO_3 measurement had been previously made. For this reason, on just one night during the intensive (2nd- 3rd of August), the instrument was modified to enable measurement of ambient NO_3 mixing ratios rather than NO_3 -reactivity. The NO_3 , O_3 and NO_2 mixing ratios and meteorological data are plotted in Fig. 6.

20 NO_3 mixing ratios slowly increased in the first half of the night, reaching a maximum of 13 pptv around 21:40 UTC. At this time the O_3 mixing ratios were also largest and highly variable. After $\approx 22:30$, O_3 was slowly removed, the NO_3 decreased by a factor of 10 or more indicating that we were sampling more reactive, boundary layer air. This is also evident in the increase in relative humidity and decrease in the temperature until about 01:30.

Given sufficient time, stationary state can be reached for NO_3 at night in which the production and loss terms are approximately balanced (Brown et al., 2003a; Crowley et al., 2010; Crowley et al., 2011). In this case NO_3 mixing ratios can be described by the ratio of their production rate and loss rate (Eq. 3).

$$25 \quad [\text{NO}_3]_{\text{ss}} = \frac{\text{NO}_3 \text{ production rate}}{\text{NO}_3 \text{ loss rate}} \quad (3)$$

The production rate is governed by the $[\text{NO}_2]$ and $[\text{O}_3]$ mixing ratio and the corresponding rate constant k_2 . If the loss processes are due to reaction with VOCs only, this expression becomes:

$$30 \quad [\text{NO}_3]_{\text{ss}} = \frac{[\text{O}_3][\text{NO}_2]k_2}{k_{\text{VOC}}^{\text{NO}_3}} \quad (4)$$



During this night $k_{\text{OTG}}^{\text{NO}_3}$ was not measured so $k_{\text{VOC}}^{\text{NO}_3}$ was used to account for NO_3 losses.

Figure 7 shows the measured NO_3 mixing ratios (black) compared to those derived from Eq. (4) using the measured VOC concentrations (red curve). Clearly, the predicted, stationary-state NO_3 concentrations are too high (by a factor of up to 3-4), implying that other NO_3 loss processes must be considered. As the directly measured reactivity $k_{\text{OTG}}^{\text{NO}_3}$ agrees rather well with that derived from VOC measurements ($k_{\text{VOC}}^{\text{NO}_3}$) calculated on other campaign nights, it would seem unlikely that unmeasured VOCs contribute sufficiently to NO_3 losses to explain this large factor. Stationary-state concentrations of NO_3 are influenced not only by VOCs but also by NO (if present at night) and also indirectly via heterogeneous loss of N_2O_5 . Equation (5) can be extended to include these processes (Martinez et al., 2000; Geyer et al., 2001; Brown et al., 2003a; Brown et al., 2003b; Brown et al., 2009; Crowley et al., 2010; Sobanski et al., 2016).

$$10 \quad [\text{NO}_3]_{\text{ss}} = \frac{[\text{O}_3][\text{NO}_2]k_1}{k_{\text{VOC}}^{\text{NO}_3} + k_2[\text{NO}] + K_5[\text{NO}_2]f_{\text{het}}} \quad (5)$$

where K_5 is the equilibrium constant for the forward and reverse reactions (R4, R5). The loss frequency due to heterogeneous uptake of N_2O_5 to particles (f_{het}) can be calculated by equation 6:

$$f_{\text{het}} \approx \frac{\gamma \bar{c} A}{4} \quad (6)$$

which is approximately valid if the particles are less than $\approx 1 \mu\text{m}$ in diameter. In this expression, A is the aerosol surface area density ($\text{cm}^2 \text{cm}^{-3}$), \bar{c} is the mean, molecular velocity of N_2O_5 (26233 cm s^{-1} at 298 K) and γ is the dimensionless uptake coefficient. If we assume a large value for the uptake coefficient of 0.03 as characteristic for aerosol with low organic content (Bertram and Thornton, 2009; Bertram et al., 2009; Crowley et al., 2011; Phillips et al., 2016) and use the aerosol surface of $1.25\text{-}1.55 \times 10^{-6} \text{ cm}^2 \text{cm}^{-3}$ (measured by a scanning mobility particle sizer for 10 – 890 nm), we obtain values for f_{het} of $2.4\text{-}2.9 \times 10^{-4} \text{ s}^{-1}$. In this case an unrealistic value of $\gamma = 0.5$ would be required to lower the calculated, stationary-state NO_3 mixing ratio to between 3 and 10 pptv as observed.

Clearly, heterogeneous losses of N_2O_5 do not account for the missing NO_3 sinks during this night and we now consider the role of NO. As NO mixing ratios in this night did not exceed the detection limit (11 pptv) we used a constant value of 5 pptv to approximately align the calculated NO_3 mixing ratio with that measured for much of the night. Clearly, the calculation of NO_3 -reactivity from stationary-state calculations can be precarious and subject to large cumulative uncertainty from e.g. measurement uncertainty in NO_3 mixing ratios, uptake coefficients, aerosol surface area and NO mixing ratios close to instrumental detection limits.

To assess the NO_3 mixing ratios for the rest of the intensive, equation 6 can be augmented by adding the loss rate constant for NO_3 -photolysis J_{NO_3} and substituting $k_{\text{VOC}}^{\text{NO}_3}$ for $k_{\text{OTG}}^{\text{NO}_3}$.

$$25 \quad [\text{NO}_3]_{\text{ss}} = \frac{[\text{O}_3][\text{NO}_2]k_1}{k_{\text{OTG}}^{\text{NO}_3} + k_2[\text{NO}] + J_{\text{NO}_3} + K_5[\text{NO}_2]f_{\text{het}}} \quad (7)$$

30 In the absence of a direct measurement of J_{NO_3} , the diel cycle of the relative NO_3 -to- NO_2 photolysis rate constant ($J_{\text{NO}_3}/J_{\text{NO}_2}$) was calculated using the TUV (tropospheric ultraviolet and visible radiation) model



(<https://www2.acom.ucar.edu/modeling/tropospheric-ultraviolet-and-visible-tuv-radiation-model>) and then put on an absolute basis using measured J_{NO_2} values.

Figure 8 shows the NO_3 production rate (lower panel, black curve) and total loss rate (lower panel, red curve) as well as the stationary-state NO_3 mixing ratios for the entire intensive period (Fig. 8, upper panel black curve). During nights in which the reactivity fell below the detection limit of the instrument $k_{\text{OTG}}^{\text{NO}_3}$ was set to 0.005 s^{-1} . Calculated NO_3 mixing ratios were in the sub-pptv range during daytime and around 1-15 pptv during nighttime. The NO_3 mixing ratios thus derived are comparable to those measured on a single night (Fig. 8, red curve) and are broadly consistent with previous estimates for this site (Handisides et al., 2003; Bartenbach et al., 2007).

10 3.4 Contribution to NO_x loss

At nighttime, in the absence of NO and sunlight, each NO_3 radical formed in the reaction of NO_2 with O_3 will either be removed indirectly via the uptake of N_2O_5 onto particles or will react with a biogenic hydrocarbon. The latter results in the formation of an organic nitrate at a yield of between 20 and 100%, depending on the specific VOC (Ng et al., 2017). The large daytime values for $k_{\text{OTG}}^{\text{NO}_3}$ obtained in this study suggest that even during sunlight hours (when NO_3 is generally considered to be of little significance owing to its rapid photolysis) significant amounts of NO_3 form organic nitrates rather than reforming NO_2 by reaction with NO, or photolysis.

The fraction, f , of NO_3 that will react with organic trace gases is given by:

$$f = \frac{k_{\text{OTG}}^{\text{NO}_3}}{([k_{\text{OTG}}^{\text{NO}_3}] + [J_{\text{NO}_3}] + [\text{NO}]k_3 + K_5 [\text{NO}_2]f_{\text{het}})} \quad (8)$$

where the denominator sums all loss processes for NO_3 . Figure 9 illustrates this via a diel cycle of the median for f . At nighttime, $\approx 99\%$ of the NO_3 will be lost to reaction with BVOCs, with indirect heterogeneous losses representing the remaining 1%. During daytime, at the peak of the actinic flux ($\max J_{\text{NO}_3} \approx 0.2 \text{ s}^{-1}$) and correspondingly high levels of NO ($k_{\text{NO}} = 0.1 - 0.2 \text{ s}^{-1}$), 20% of the formed NO_3 was lost due to reaction with organic trace gases, increasing up to 40% in the late afternoon. This result is comparable with reactivity measurements in a boreal forest in Finland during IBAIRN 2016 where a very similar diel profile for f was determined (Liebmann et al., 2018). The NO_3 -reactivity data from these measurements indicate that the role of NO_3 as a daytime oxidant of biogenic VOCs in forested regions may so far have been underestimated, which in turn has implications for understanding the diel cycle of organic nitrate and secondary organic aerosol formation in such environments.

4 Comparison of NO_3 and OH-reactivity

As mentioned above NO_3 radicals and OH radicals react with atmospheric trace gases via different mechanisms, resulting in profoundly different rate coefficients and thus reactivities. By combining the continuous, on-site measurements of the OH-



reactivity with the NO₃-reactivity measurements during the intensive period, we were able to generate the first dataset of simultaneous, direct measurement of both OH-reactivity, $k_{\text{total}}^{\text{OH}}$, and NO₃-reactivity at any location.

To aid comparison, we subtracted the contributions of several inorganic and organic trace gases (NO, NO₂, SO₂, CO, CH₄) that are not included in $k_{\text{OTG}}^{\text{NO}_3}$ or do not react to a significant extent with NO₃ from the total OH-reactivity and thus derived

5 $k_{\text{OTG}}^{\text{OH}}$.

$$k_{\text{OTG}}^{\text{OH}} = k_{\text{total}}^{\text{OH}} - k_{\text{NO}}^{\text{OH}}[\text{NO}] - k_{\text{NO}_2}^{\text{OH}}[\text{NO}_2] - k_{\text{SO}_2}^{\text{OH}}[\text{SO}_2] - k_{\text{CH}_4}^{\text{OH}}[\text{CH}_4] - k_{\text{CO}}^{\text{OH}}[\text{CO}] \quad (9)$$

Fig. 10 depicts the time series of $k_{\text{Total}}^{\text{OH}}$, $k_{\text{OTG}}^{\text{OH}}$ and $k_{\text{OTG}}^{\text{NO}_3}$. All display maximum values close to midday, though $k_{\text{OTG}}^{\text{OH}}$ averaged over the intensive are larger by a factor of 44 larger than $k_{\text{OTG}}^{\text{NO}_3}$, reflecting generally larger rate coefficients for OH.

The blue shaded areas for $k_{\text{Total}}^{\text{OH}}$ represents the 1 σ uncertainty of the measurements. Total uncertainty in $k_{\text{OTG}}^{\text{OH}}$ and $k_{\text{OTG}}^{\text{NO}_3}$ is not shown to preserve clarity of presentation. The time series of the $k_{\text{OTG}}^{\text{OH}}$ can be found in the supplementary information (Fig. S6).

The measured reactivities of both radicals show a clear diel profile, with higher daytime and lower nighttime values. Figure 11 shows a correlation plot of OH and NO₃-reactivity divided into day (red) and nighttime (black) data. During the day, the data are highly scattered, which can be understood when one considers the highly variable organic content of the air masses being sampled. To illustrate this we have drawn the expected correlation lines (based on the known, relative rate coefficients) for single component organic trace gases including isoprene and terpenes. The expected slopes for these individual VOCs are very different and encompass the full scatter in the observations, which is the result of changing atmospheric composition (i.e. the mix of reactive organic species) owing to changes in air mass age and source region (wind direction) during the campaign. The extremes are represented by α -terpinene (which favours NO₃) and CH₄ (which favours OH).

During nighttime (black points) the plot of $k_{\text{OTG}}^{\text{OH}}$ versus $k_{\text{OTG}}^{\text{NO}_3}$ is less scattered, indicating that the air masses sampled (often from the residual layer) are chemically less complex and variable. The data lay close to the line that marks the expected correlation if isoprene were the dominant sink of both NO₃ and OH at nighttime once molecules such as CO and CH₄ have been removed from the term describing OH-reactivity. This is in broad agreement with our observation that isoprene is the main sink of NO₃ during nights when the measurement site was decoupled from direct boundary layer emissions.

5. Summary and Conclusion

Direct measurements of the NO₃-reactivity towards organic trace gases, $k_{\text{OTG}}^{\text{NO}_3}$ were conducted at the top of the Hohenpeissenberg mountain (988 m a.s.l.) during an intensive measurement campaign in the summer of 2017. NO₃-reactivities had a distinct diel profile with values as large as 0.3 s⁻¹ during daytime but close to or below the detection limit of the instrument during nighttime when the measurement site was frequently in the residual layer / free troposphere. Within experimental uncertainty, the high daytime NO₃-reactivity was accounted for by BVOCs that were measured at the site, and



was dominated by monoterpenes especially α -pinene and sabinene. On average, the reaction with VOCs accounted for \approx 99% of the loss of NO_3 during nighttime and an average of 20% at noon, increasing to 30-50% during early morning and late evening. The reaction of NO_3 with BVOCS therefore represents a significant NO_x loss not only during the night but also during daytime and implies significant formation of organic nitrates via NO_3 reactions throughout the diel cycle. Stationary-
5 state, daytime and nighttime NO_3 mixing ratios were calculated using the production term and $k_{\text{OTG}}^{\text{NO}_3}$ and were broadly consistent with direct measurement made on one night. A comparison between directly measured OH- and NO_3 reactivities was performed, indicating a weak correlation during the day when chemically reactive, complex and variable air masses were encountered. A tighter correlation, consistent with isoprene dominating the (low) NO_3 -reactivities was observed at night.

10

Acknowledgements: We would like to thank the DWD for hosting and supporting this measurement campaign. We would like to thank the DWD personnel for the data evaluation, most notably Katja Michl for NMHCs, Jennifer Englert for OVOCs, Harald Flentje for the SMPS data as well as the great technical support, particularly we are grateful to Erasmus Tensing, Thomas Elste, Georg Stange. We thank Chemours for provision of the FEP sample used to coat the CRD-cavities.

15



References

- Aliwell, S. R., and Jones, R. L.: Measurements of tropospheric NO₃ at midlatitude, *J. Geophys. Res. -Atmos.*, 103, 5719-5727, 1998.
- 5 Allan, B. J., Plane, J. M. C., Coe, H., and Shillito, J.: Observations of NO₃ concentration profiles in the troposphere, *J. Geophys. Res. -Atmos.*, 107, 4588, doi: 10.1029/2002jd002112, 2002.
- Atkinson, R.: Atmospheric chemistry of VOCs and NO_x, *Atmos. Env.*, 34, 2063-2101, 2000.
- Atkinson, R., and Arey, J.: Atmospheric degradation of volatile organic compounds, *Chem. Rev.*, 103, 4605-4638, 10.1021/cr0206420, 2003a.
- 10 Atkinson, R., and Arey, J.: Gas-phase tropospheric chemistry of biogenic volatile organic compounds: a review, *Atmos. Env.*, 37, S197-S219, 2003b.
- Bannan, T. J., Booth, A. M., Bacak, A., Muller, J. B. A., Leather, K. E., Le Breton, M., Jones, B., Young, D., Coe, H., Allan, J., Visser, S., Slowik, J. G., Furger, M., Prevot, A. S. H., Lee, J., Dunmore, R. E., Hopkins, J. R., Hamilton, J. F., Lewis, A. C., Whalley, L. K., Sharp, T., Stone, D., Heard, D. E., Fleming, Z. L., Leigh, R., Shallcross, D. E., and Percival, C. J.: The
- 15 first UK measurements of nitryl chloride using a chemical ionization mass spectrometer in central London in the summer of 2012, and an investigation of the role of Cl atom oxidation, *J. Geophys. Res. -Atmos.*, 120, 5638-5657, 10.1002/2014jd022629, 2015.
- Bartenbach, S., Williams, J., Plass-Dülmer, C., Berresheim, H., and Lelieveld, J.: In-situ measurement of reactive hydrocarbons at Hohenpeissenberg with comprehensive two-dimensional gas chromatography (GC×GC-FID): use in
- 20 estimating HO and NO₃, *Atmos. Chem. Phys.*, 7, 1-14, 10.5194/acp-7-1-2007, 2007.
- Bastin, J.-F., Berrahmouni, N., Grainger, A., Maniatis, D., Mollicone, D., Moore, R., Patriarca, C., Picard, N., Sparrow, B., Abraham, E. M., Aloui, K., Atesoglu, A., Attore, F., Bassüllü, Ç., Bey, A., Garzuglia, M., García-Montero, L. G., Groot, N., Guerin, G., Laestadius, L., Lowe, A. J., Mamane, B., Marchi, G., Patterson, P., Rezende, M., Ricci, S., Salcedo, I., Diaz, A. S.-P., Stolle, F., Surappaeva, V., and Castro, R.: The extent of forest in dryland biomes, *Science*, 356, 635-638,
- 25 10.1126/science.aam6527, 2017.
- Berresheim, H., Elste, T., Plass-Dülmer, C., Eiseleb, F. L., and Tannerb, D. J.: Chemical ionization mass spectrometer for long-term measurements of atmospheric OH and H₂SO₄, *Int. J. Mass Spectrom.*, 202, 91-109, [https://doi.org/10.1016/S1387-3806\(00\)00233-5](https://doi.org/10.1016/S1387-3806(00)00233-5), 2000.
- Bertram, T. H., and Thornton, J. A.: Toward a general parameterization of N₂O₅ reactivity on aqueous particles: the
- 30 competing effects of particle liquid water, nitrate and chloride, *Atmos. Chem. Phys.*, 9, 8351-8363, 2009.
- Bertram, T. H., Thornton, J. A., Riedel, T. P., Middlebrook, A. M., Bahreini, R., Bates, T. S., Quinn, P. K., and Coffman, D. J.: Direct observations of N₂O₅ reactivity on ambient aerosol particles, *Geophys. Res. Lett.*, 36, L19803, doi:10.1029/2009GL040248, 2009.
- Birmili, W., Berresheim, H., Plass-Dülmer, C., Elste, T., Gilge, S., Wiedensohler, A., and Uhrner, U.: The Hohenpeissenberg aerosol formation experiment (HAFEX): a long-term study including size-resolved aerosol, H₂SO₄, OH, and monoterpenes
- 35 measurements, *Atmos. Chem. Phys.*, 3, 361-376, 10.5194/acp-3-361-2003, 2003.
- Brown, S. S., Stark, H., and Ravishankara, A. R.: Applicability of the steady state approximation to the interpretation of atmospheric observations of NO₃ and N₂O₅, *J. Geophys. Res. -Atmos.*, 108, Art. 4539, 10.1029/2003JD003407, 2003a.
- Brown, S. S., Stark, H., Ryerson, T. B., Williams, E. J., Nicks, D. K., Trainer, M., Fehsenfeld, F. C., and Ravishankara, A. R.: Nitrogen oxides in the nocturnal boundary layer: Simultaneous in situ measurements of NO₃, N₂O₅, NO₂, NO, and O₃, *J. Geophys. Res. -Atmos.*, 108, art. 4299, 10.1029/2002JD002917, 2003b.
- 40



- 5 Brown, S. S., Dube, W. P., Osthoff, H. D., Stutz, J., Ryerson, T. B., Wollny, A. G., Brock, C. A., Warneke, C., De Gouw, J. A., Atlas, E., Neuman, J. A., Holloway, J. S., Lerner, B. M., Williams, E. J., Kuster, W. C., Goldan, P. D., Angevine, W. M., Trainer, M., Fehsenfeld, F. C., and Ravishankara, A. R.: Vertical profiles in NO_3 and N_2O_5 measured from an aircraft: Results from the NOAA P-3 and surface platforms during the New England Air Quality Study 2004, *J. Geophys. Res. - Atmos.*, 112, D22304, doi: 10.1029/2007jd008893, 2007a.
- Brown, S. S., Dube, W. P., Osthoff, H. D., Wolfe, D. E., Angevine, W. M., and Ravishankara, A. R.: High resolution vertical distributions of NO_3 and N_2O_5 through the nocturnal boundary layer, *Atmos. Chem. Phys.*, 7, 139-149, 2007b.
- 10 Brown, S. S., Dube, W. P., Fuchs, H., Ryerson, T. B., Wollny, A. G., Brock, C. A., Bahreini, R., Middlebrook, A. M., Neuman, J. A., Atlas, E., Roberts, J. M., Osthoff, H. D., Trainer, M., Fehsenfeld, F. C., and Ravishankara, A. R.: Reactive uptake coefficients for N_2O_5 determined from aircraft measurements during the Second Texas Air Quality Study: Comparison to current model parameterizations, *J. Geophys. Res. -Atmos.*, 114, art. D00F10, 10.1029/2008JD011679, 2009.
- Brown, S. S., Dube, W. P., Peischl, J., Ryerson, T. B., Atlas, E., Warneke, C., de Gouw, J. A., Hekkert, S. t. L., Brock, C. A., Flocke, F., Trainer, M., Parrish, D. D., Fehsenfeld, F. C., and Ravishankara, A. R.: Budgets for nocturnal VOC oxidation by nitrate radicals aloft during the 2006 Texas Air Quality Study, *J. Geophys. Res. -Atmos.*, 116, 10.1029/2011jd016544, 2011.
- 15 Brown, S. S., and Stutz, J.: Nighttime radical observations and chemistry, *Chem. Soc. Rev.*, 41, 6405–6447, 2012.
- Brown, S. S., Dube, W. P., Tham, Y. J., Zha, Q., Xue, L., Poon, S., Wang, Z., Blake, D. R., Tsui, W., Parrish, D. D., and Wang, T.: Nighttime chemistry at a high altitude site above Hong Kong, *J. Geophys. Res. -Atmos.*, 121, 2457-2475, 10.1002/2015jd024566, 2016.
- 20 Crowley, J. N., Schuster, G., Pouvesle, N., Parchatka, U., Fischer, H., Bonn, B., Bingemer, H., and Lelieveld, J.: Nocturnal nitrogen oxides at a rural mountain site in south-western Germany, *Atmos. Chem. Phys.*, 10, 2795-2812, 2010.
- Crowley, J. N., Thieser, J., Tang, M. J., Schuster, G., Bozem, H., Hasaynali Beygi, Z., Fischer, H., Diesch, J.-M., Drewnick, F., Borrmann, S., Song, W., Yassaa, N., Williams, J., Pöhler, D., Platt, U., and Lelieveld, J.: Variable lifetimes and loss mechanisms for NO_3 and N_2O_5 during the DOMINO campaign: Contrast between marine, urban and continental air, *Atmos. Chem. Phys.*, 11, 10863-10870, 2011.
- 25 Dentener, F. J., and Crutzen, P. J.: Reaction of N_2O_5 on tropospheric aerosols - Impact on the global distributions of NO_x , O_3 , and OH, *J. Geophys. Res. -Atmos.*, 98, 7149-7163, 1993.
- Fry, J. L., Draper, D. C., Barsanti, K. C., Smith, J. N., Ortega, J., Winkle, P. M., Lawler, M. J., Brown, S. S., Edwards, P. M., Cohen, R. C., and Lee, L.: Secondary Organic Aerosol Formation and Organic Nitrate Yield from NO_3 Oxidation of Biogenic Hydrocarbons, *Env. Sci. Tech.*, 48, 11944-11953, 10.1021/es502204x, 2014.
- 30 Geyer, A., Alicke, B., Konrad, S., Schmitz, T., Stutz, J., and Platt, U.: Chemistry and oxidation capacity of the nitrate radical in the continental boundary layer near Berlin, *J. Geophys. Res. -Atmos.*, 106, 8013-8025, 2001.
- Guenther, A. B., Jiang, X., Heald, C. L., Sakulyanontvittaya, T., Duhl, T., Emmons, L. K., and Wang, X.: The Model of Emissions of Gases and Aerosols from Nature version 2.1 (MEGAN2.1): an extended and updated framework for modeling biogenic emissions, *Geoscientific Model Development*, 5, 1471-1492, 10.5194/gmd-5-1471-2012, 2012.
- 35 Hakola, H., Tarvainen, V., Laurila, T., Hiltunen, V., Hellén, H., and Keronen, P.: Seasonal variation of VOC concentrations above a boreal coniferous forest, *Atmos. Env.*, 37, 1623-1634, [http://dx.doi.org/10.1016/S1352-2310\(03\)00014-1](http://dx.doi.org/10.1016/S1352-2310(03)00014-1), 2003.
- Hakola, H., Hellén, H., Hemmilä, M., Rinne, J., and Kulmala, M.: In situ measurements of volatile organic compounds in a boreal forest, *Atmos. Chem. Phys.*, 12, 11665-11678, 10.5194/acp-12-11665-2012, 2012.
- 40 Handisides, G. M., Plass-Dulmer, C., Gilge, S., Bingemer, H., and Berresheim, H.: Hohenpeissenberg Photochemical Experiment (HOPE 2000): Measurements and photostationary state calculations of OH and peroxy radicals, *Atmos. Chem. Phys.*, 3, 1565-1588, 2003.



- Hock, N., Schneider, J., Borrmann, S., Römpf, A., Moortgat, G., Franze, T., Schauer, C., Pöschl, U., Plass-Dülmer, C., and Berresheim, H.: Rural continental aerosol properties and processes observed during the Hohenpeissenberg Aerosol Characterization Experiment (HAZE2002), *Atmos. Chem. Phys.*, 8, 603-623, [10.5194/acp-8-603-2008](https://doi.org/10.5194/acp-8-603-2008), 2008.
- 5 Hoerger, C. C., Claude, A., Plass-Duelmer, C., Reimann, S., Eckart, E., Steinbrecher, R., Aalto, J., Arduini, J., Bonnaire, N., Cape, J. N., Colomb, A., Connolly, R., Diskova, J., Dumitrean, P., Ehlers, C., Gros, V., Hakola, H., Hill, M., Hopkins, J. R., Jäger, J., Junek, R., Kajos, M. K., Klemp, D., Leuchner, M., Lewis, A. C., Locoge, N., Maione, M., Martin, D., Michl, K., Nemitz, E., O'Doherty, S., Pérez Ballesta, P., Ruuskanen, T. M., Sauvage, S., Schmidbauer, N., Spain, T. G., Straube, E., Vana, M., Vollmer, M. K., Wegener, R., and Wenger, A.: ACTRIS non-methane hydrocarbon intercomparison experiment in Europe to support WMO GAW and EMEP observation networks, *Atmos. Meas. Tech.*, 8, 2715-2736, [10.5194/amt-8-2715-2015](https://doi.org/10.5194/amt-8-2715-2015), 2015.
- 10 Holzke, C., Hoffmann, T., Jaeger, L., Koppmann, R., and Zimmer, W.: Diurnal and seasonal variation of monoterpene and sesquiterpene emissions from Scots pine (*Pinus sylvestris* L.), *Atmos. Env.*, 40, 3174-3185, <http://dx.doi.org/10.1016/j.atmosenv.2006.01.039>, 2006.
- IUPAC: Task Group on Atmospheric Chemical Kinetic Data Evaluation, (Ammann, M., Cox, R.A., Crowley, J.N., Herrmann, H., Jenkin, M.E., McNeill, V.F., Mellouki, A., Rossi, M. J., Troe, J. and Wallington, T. J.) <http://iupac.pole-ether.fr/index.html>, 2017.
- 15 Jaoui, M., Kleindienst, T. E., Docherty, K. S., Lewandowski, M., and Offenberg, J. H.: Secondary organic aerosol formation from the oxidation of a series of sesquiterpenes: alpha-cedrene, beta-caryophyllene, alpha-humulene and alpha-farnesene with O₃, OH and NO₃ radicals, *Environmental Chemistry*, 10, 178-193, [10.1071/en13025](https://doi.org/10.1071/en13025), 2013.
- 20 Lee, A. K. Y., Abbatt, J. P. D., Leaitch, W. R., Li, S.-M., Sjostedt, S. J., Wentzell, J. J. B., Liggio, J., and Macdonald, A. M.: Substantial secondary organic aerosol formation in a coniferous forest: observations of both day- and nighttime chemistry, *Atmos. Chem. Phys.*, 16, 6721-6733, [10.5194/acp-16-6721-2016](https://doi.org/10.5194/acp-16-6721-2016), 2016.
- Lelieveld, J., Dentener, F. J., Peters, W., and Krol, M. C.: On the role of hydroxyl radicals in the self-cleansing capacity of the troposphere, *Atmos. Chem. Phys.*, 4, 2337-2344, 2004.
- 25 Lelieveld, J., Butler, T. M., Crowley, J. N., Dillon, T. J., Fischer, H., Ganzeveld, L., Harder, H., Lawrence, M. G., Martinez, M., Taraborrelli, D., and Williams, J.: Atmospheric oxidation capacity sustained by a tropical forest, *Nature*, 452, 737-740, 2008.
- Lelieveld, J., Gromov, S., Pozzer, A., and Taraborrelli, D.: Global tropospheric hydroxyl distribution, budget and reactivity, *Atmos. Chem. Phys.*, 16, 12477-12493, [10.5194/acp-16-12477-2016](https://doi.org/10.5194/acp-16-12477-2016), 2016.
- 30 Liebmann, J., Karu, E., Sobanski, N., Schuladen, J., Ehn, M., Schallhart, S., Quéléver, L., Hellen, H., Hakola, H., Hoffmann, T., Williams, J., Fischer, H., Lelieveld, J., and Crowley, J. N.: Direct measurement of NO₃ radical reactivity in a boreal forest, *Atmos. Chem. Phys.*, 2018, 3799-3815, [10.5194/acp-18-3799-2018](https://doi.org/10.5194/acp-18-3799-2018), 2018.
- Liebmann, J. M., Schuster, G., Schuladen, J. B., Sobanski, N., Lelieveld, J., and Crowley, J. N.: Measurement of ambient NO₃ reactivity: Design, characterization and first deployment of a new instrument, *Atmos. Meas. Tech.*, 2017, 1241-1258, [10.5194/amt-2016-381](https://doi.org/10.5194/amt-2016-381), 2017.
- 35 Long, B., Tan, X. F., Long, Z. W., Ren, D. S., and Zhang, W. J.: Theoretical Study on Decomposition of CF₃OH Catalyzed by Water Dimer and Ammonia, *Chinese Journal of Chemical Physics*, 24, 16-21, 2011.
- Mannschreck, K., Gilge, S., Plass-Duelmer, C., Fricke, W., and Berresheim, H.: Assessment of the applicability of NO-NO₂-O₃ photostationary state to long-term measurements at the Hohenpeissenberg GAW Station, Germany, *Atmos. Chem. Phys.*, 4, 1265-1277, [10.5194/acp-4-1265-2004](https://doi.org/10.5194/acp-4-1265-2004), 2004.
- 40 Martinez, M., Perner, D., Hackenthal, E. M., Kulzer, S., and Schutz, L.: NO₃ at Helgoland during the NORDEX campaign in October 1996, *J. Geophys. Res. -Atmos.*, 105, 22685-22695, 2000.



- Ng, N. L., Brown, S. S., Archibald, A. T., Atlas, E., Cohen, R. C., Crowley, J. N., Day, D. A., Donahue, N. M., Fry, J. L., Fuchs, H., Griffin, R. J., Guzman, M. I., Herrmann, H., Hodzic, A., Iinuma, Y., Jimenez, J. L., Kiendler-Scharr, A., Lee, B. H., Luecken, D. J., Mao, J., McLaren, R., Mutzel, A., Osthoff, H. D., Ouyang, B., Picquet-Varraut, B., Platt, U., Pye, H. O. T., Rudich, Y., Schwantes, R. H., Shiraiwa, M., Stutz, J., Thornton, J. A., Tilgner, A., Williams, B. J., and Zaveri, R. A.: Nitrate radicals and biogenic volatile organic compounds: oxidation, mechanisms, and organic aerosol, *Atmos. Chem. Phys.*, 17, 2103-2162, 10.5194/acp-17-2103-2017, 2017.
- 5 Nölscher, A. C., Williams, J., Sinha, V., Custer, T., Song, W., Johnson, A. M., Axinte, R., Bozem, H., Fischer, H., Pouvesle, N., Phillips, G., Crowley, J. N., Rantala, P., Rinne, J., Kulmala, M., Gonzales, D., Valverde-Canossa, J., Vogel, A., Hoffmann, T., Ouwersloot, H. G., Vilà-Guerau de Arellano, J., and Lelieveld, J.: Summertime total OH reactivity measurements from boreal forest during HUMPPA-COPEC 2010, *Atmos. Chem. Phys.*, 12, 8257-8270, 10.5194/acp-12-8257-2012, 2012.
- 10 Nölscher, A. C., Bourtsoukidis, E., Bonn, B., Kesselmeier, J., Lelieveld, J., and Williams, J.: Seasonal measurements of total OH reactivity emission rates from Norway spruce in 2011, *Biogeosciences*, 10, 4241-4257, 10.5194/bg-10-4241-2013, 2013.
- Novelli, A., Hens, K., Ernest, C., Martinez, M., Nölscher, A., Sinha, V., Paasonen, P., Petäjä, T., Sipilä, M., Elste, T., Plass-Dülmer, C., J. Phillips, G., Kubistin, D., Williams, J., Vereecken, L., Lelieveld, J., and Harder, H.: Estimating the atmospheric concentration of Criegee intermediates and their possible interference in a FAGE-LIF instrument, 7807-7826 pp., 2017.
- 15 Noxon, J. F., Norton, R. B., and Henderson, W. R.: Observation of Atmospheric NO₃, *Geophys. Res. Lett.*, 5, 675-678, 1978.
- Osthoff, H. D., Roberts, J. M., Ravishankara, A. R., Williams, E. J., Lerner, B. M., Sommariva, R., Bates, T. S., Coffman, D., Quinn, P. K., Dibb, J. E., Stark, H., Burkholder, J. B., Talukdar, R. K., Meagher, J., Fehsenfeld, F. C., and Brown, S. S.: High levels of nitryl chloride in the polluted subtropical marine boundary layer, *Nature Geoscience*, 1, 324-328, 2008.
- 20 Phillips, G. J., Tang, M. J., Thieser, J., Brickwedde, B., Schuster, G., Bohn, B., Lelieveld, J., and Crowley, J. N.: Significant concentrations of nitryl chloride observed in rural continental Europe associated with the influence of sea salt chloride and anthropogenic emissions, *Geophys. Res. Lett.*, 39, L10811, doi:10.1029/2012GL051912, 2012.
- 25 Phillips, G. J., Thieser, J., Tang, M. J., Sobanski, N., Schuster, G., Fachinger, J., Drewnick, F., Borrmann, S., Bingemer, H., Lelieveld, J., and Crowley, J. N.: Estimating N₂O₅ uptake coefficients using ambient measurements of NO₃, N₂O₅, ClNO₂ and particle-phase nitrate, *Atmos. Chem. Phys.*, 16, 13231-13249, 10.5194/acp-16-13231-2016, 2016.
- Plass-Dulmer, C., Michl, K., Ruf, R., and Berresheim, H.: C-2-C-8 hydrocarbon measurement and quality control procedures at the Global Atmosphere Watch Observatory Hohenpeissenberg, *J. Chromatogr. A*, 953, 175-197, 2002.
- 30 Schlosser, E., Brauers, T., Dorn, H. P., Fuchs, H., Häsel, R., Hofzumahaus, A., Holland, F., Wahner, A., Kanaya, Y., Kajii, Y., Miyamoto, K., Nishida, S., Watanabe, K., Yoshino, A., Kubistin, D., Martinez, M., Rudolf, M., Harder, H., Berresheim, H., Elste, T., Plass-Dülmer, C., Stange, G., and Schurath, U.: Technical Note: Formal blind intercomparison of OH measurements: results from the international campaign HOxComp, *Atmos. Chem. Phys.*, 9, 7923-7948, 10.5194/acp-9-7923-2009, 2009.
- 35 Schuster, G., Labazan, I., and Crowley, J. N.: A cavity ring down / cavity enhanced absorption device for measurement of ambient NO₃ and N₂O₅, *Atmos. Meas. Tech.*, 2, 1-13, 2009.
- Shorees, B., Atkinson, R., and Arey, J.: Kinetics of the gas-phase reactions of β-phellandrene with OH and NO₃ radicals and O₃ at 297 ± 2 K, *Int. J. Chem. Kinet.*, 23, 897-906, 10.1002/kin.550231005, 1991.
- 40 Sobanski, N., Tang, M. J., Thieser, J., Schuster, G., Pöhler, D., Fischer, H., Song, W., Sauvage, C., Williams, J., Fachinger, J., Berkes, F., Hoor, P., Platt, U., Lelieveld, J., and Crowley, J. N.: Chemical and meteorological influences on the lifetime of NO₃ at a semi-rural mountain site during PARADE, *Atmos. Chem. Phys.*, 16, 4867-4883, 10.5194/acp-16-4867-2016, 2016.
- Stutz, J., Alicke, B., Ackermann, R., Geyer, A., White, A., and Williams, E.: Vertical profiles of NO₃, N₂O₅, O₃, and NO_x in the nocturnal boundary layer: 1. Observations during the Texas Air Quality Study 2000 *J. Geophys. Res. -Atmos.*, 109, art. D12306, 10.1029/2003JD004209, 2004.



- Thieser, J., Schuster, G., Phillips, G. J., Reiffs, A., Parchatka, U., Pöhler, D., Lelieveld, J., and Crowley, J. N.: A two-channel, thermal dissociation cavity-ringdown spectrometer for the detection of ambient NO_2 , RO_2NO_2 and RONO_2 , *Atmos. Meas. Tech.*, 9, 553-576, 2016.
- 5 Voigt, S., Orphal, J., and Burrows, J. P.: The temperature and pressure dependence of the absorption cross-sections of NO_2 in the 250-800 nm region measured by Fourier-transform spectroscopy, *J. Photochem. Photobiol. A-Chem.*, 149, 1-7, doi:10.1016/s1010-6030(01)00650-5, 2002.
- von Friedeburg, C., Wagner, T., Geyer, A., Kaiser, N., Vogel, B., Vogel, H., and Platt, U.: Derivation of tropospheric NO_3 profiles using off-axis differential optical absorption spectroscopy measurements during sunrise and comparison with simulations, *J. Geophys. Res. -Atmos.*, 107, 10.1029/2001JD000481, 2002.
- 10 Wayne, R. P., Barnes, I., Biggs, P., Burrows, J. P., Canosamas, C. E., Hjorth, J., Lebras, G., Moortgat, G. K., Perner, D., Poulet, G., Restelli, G., and Sidebottom, H.: The Nitrate Radical - Physics, Chemistry, and the Atmosphere, *Atmos. Env.*, 25, 1-203, 1991.

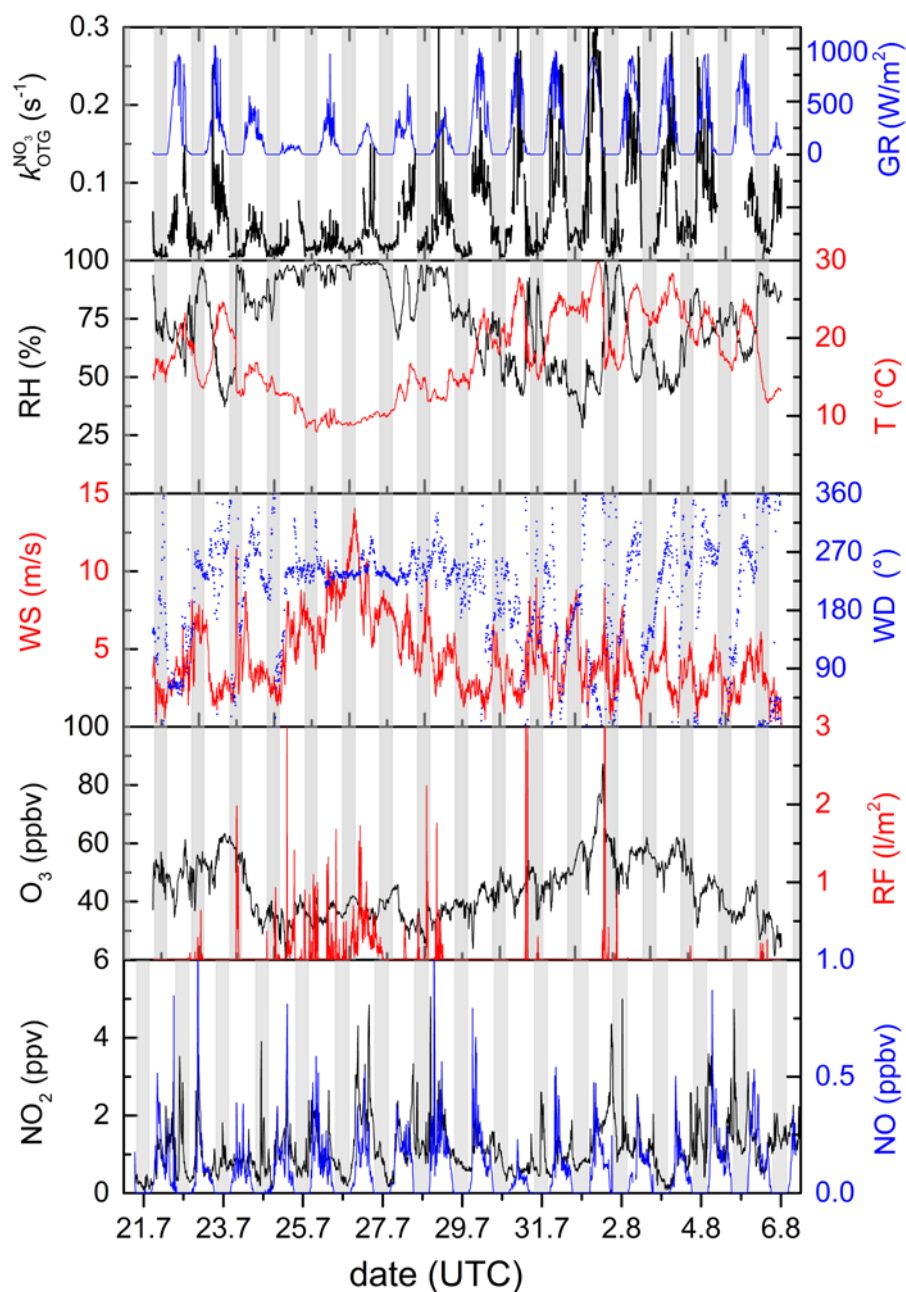


Figure 1: Overview of measurements during the 2017-intensive. The grey shaded area represents nighttime. GR = global radiation, RF = rainfall, RH = relative humidity, T = temperature, WS = wind speed, WD = wind direction.

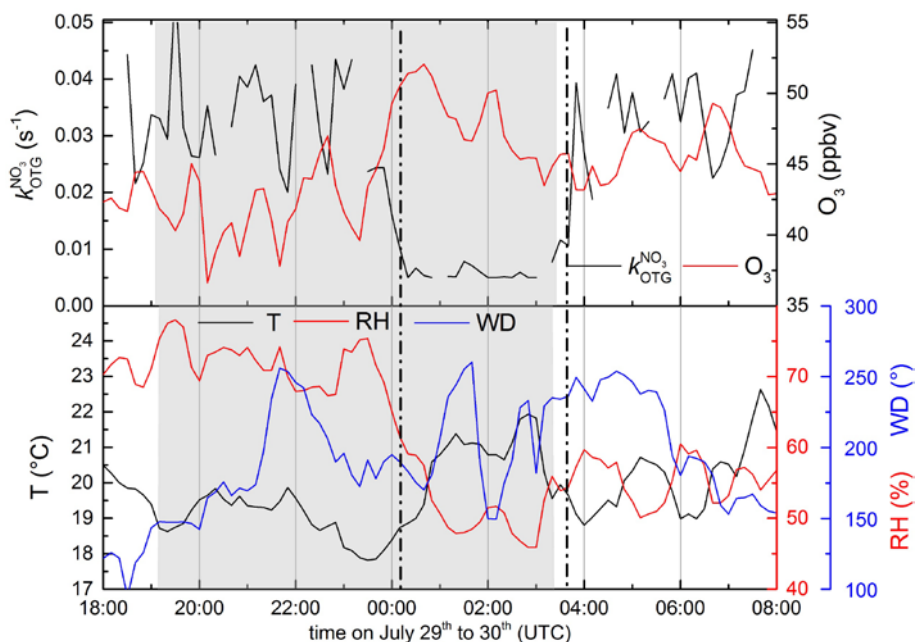


Figure 2: Upper panel: $k_{\text{OTG}}^{\text{NO}_2}$ (black) and O_3 mixing ratios (red) from the 29th to the 30th of July. From 23:50 UTC until sunrise the measurement site is located in the residual layer / free troposphere. Lower panel: temperature (T), relative humidity (RH) and wind direction (WD) during the same period.

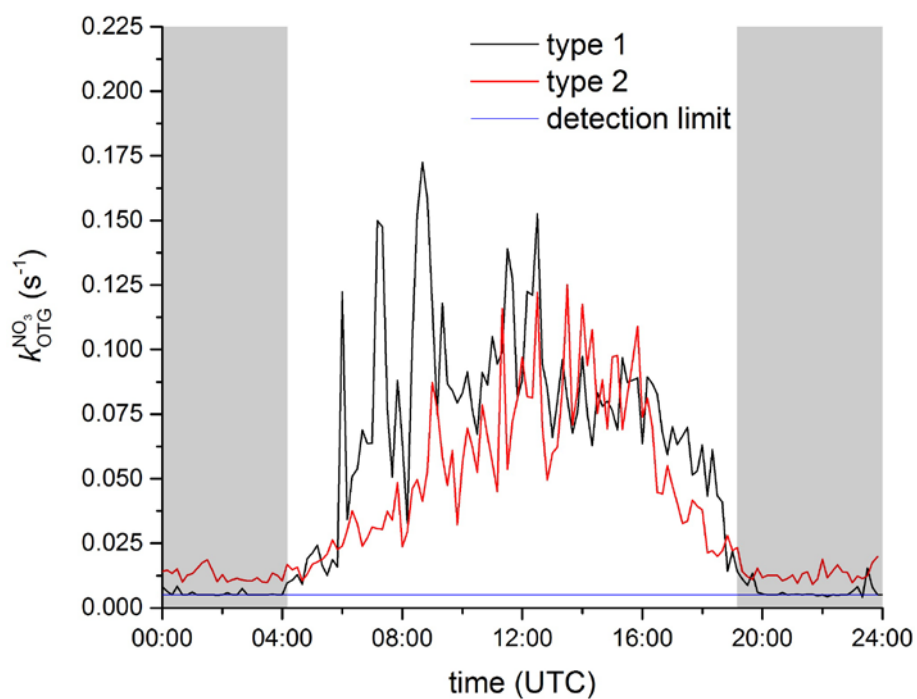


Figure 3: Median, diel profile of the NO_3 -reactivity. Type 1 nights (black line) show values around the detection limit during night, type 2 nights (red line) are above the detection limit.

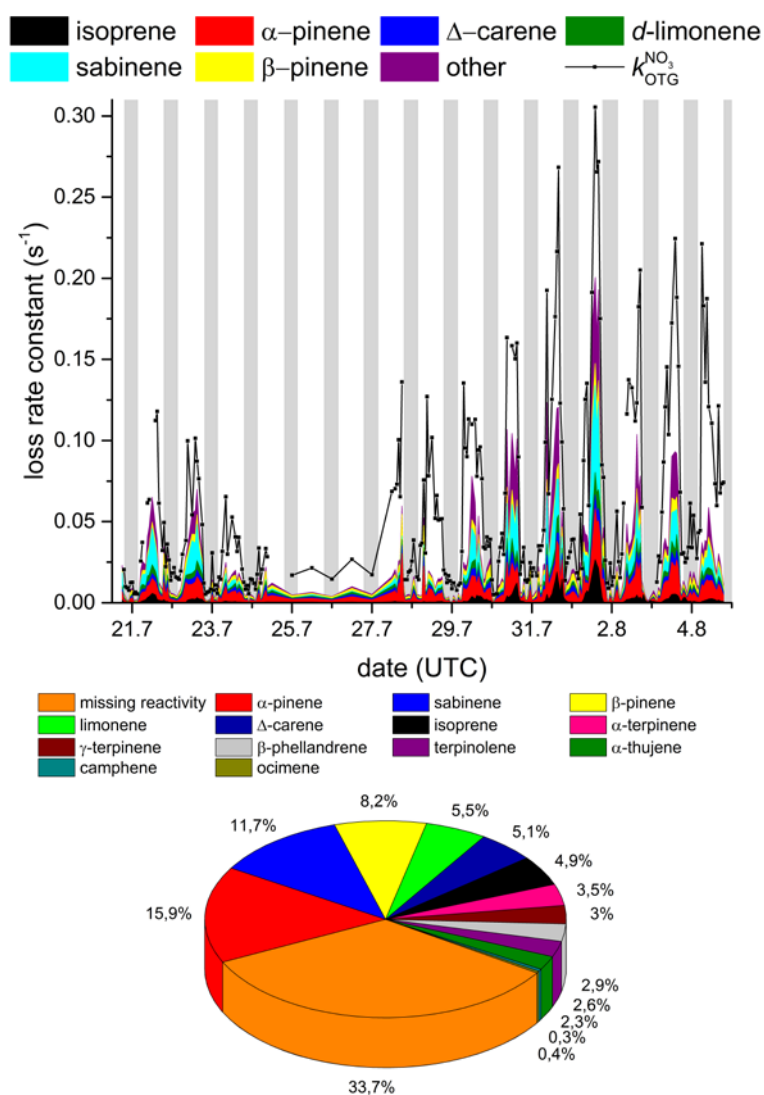


Figure 4: Upper panel: measured values of $k_{OTG}^{NO_3}$ (black) in comparison with the loss rate constant assigned to individual VOCs. The term “other” includes terpinolene, β -phellandrene, α -terpinene, γ -terpinene, α -thujene and camphene. Myrcene and α -phellandrene were also measured but below the detection limit during the whole campaign. The lower panel indicates the campaign averaged contribution of each measured VOC to the NO_3 loss rate as well as reactivity that was not accounted for by measured VOCs (“missing reactivity”).

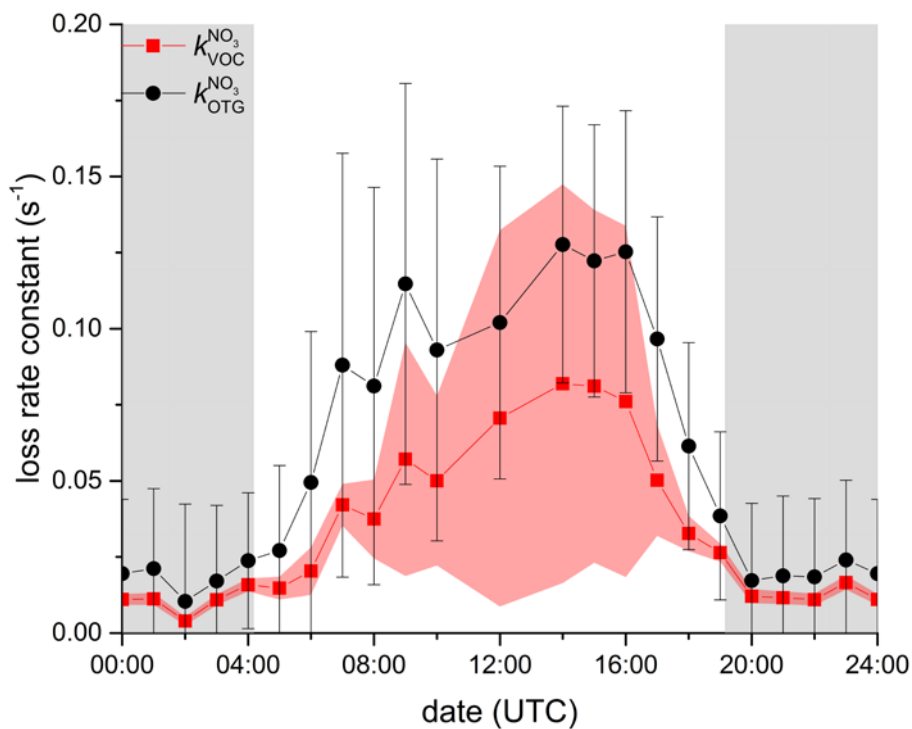


Figure 5: Median diel profiles of $k_{\text{VOC}}^{\text{NO}_3}$ and $k_{\text{OTG}}^{\text{NO}_3}$. The error bars on the $k_{\text{OTG}}^{\text{NO}_3}$ measurements are total uncertainty, including systematic error and variability. The uncertainty in $k_{\text{VOC}}^{\text{NO}_3}$ (shaded red area) is dominated by uncertainty in the mixing ratios of the VOCs.

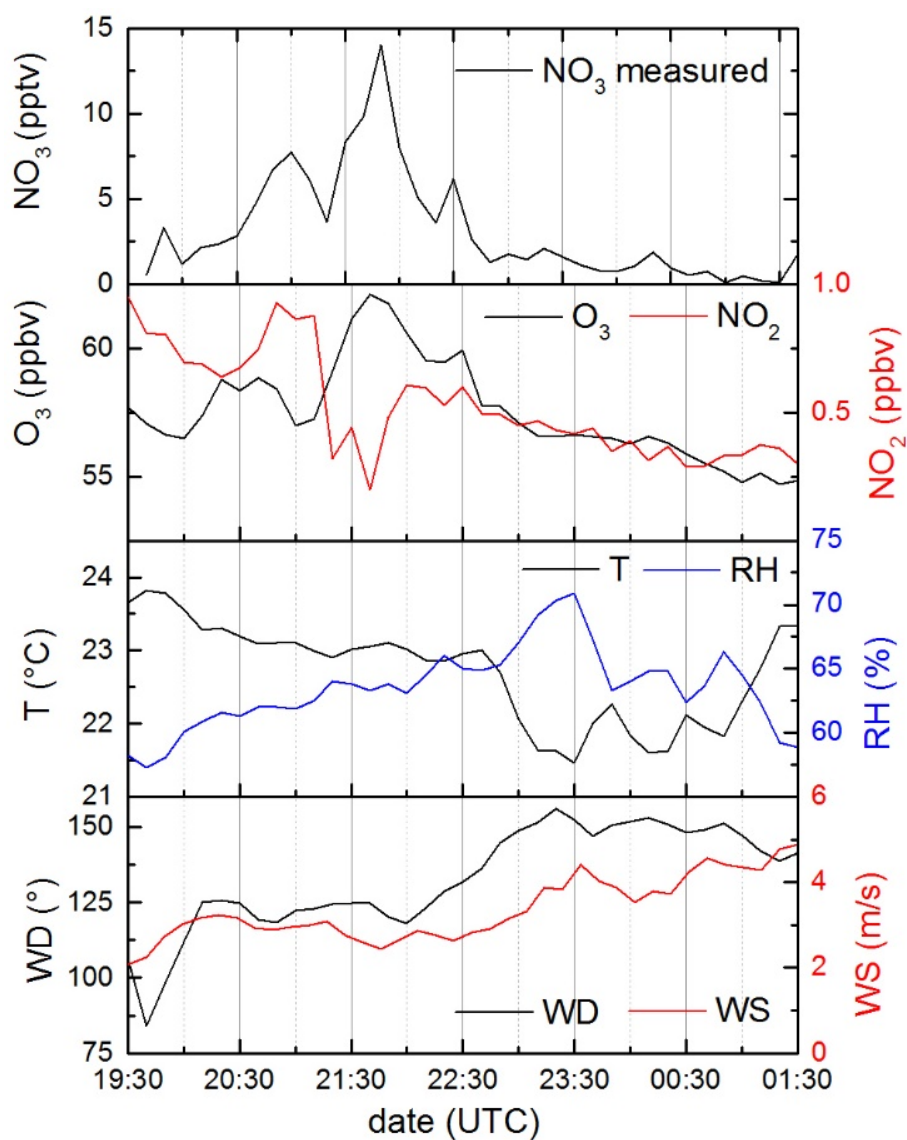


Figure 6: NO_3 mixing ratios measured in the night from the 2th – 3rd of August as well as NO_2 and O_3 (which define the NO_3 production rate). T = temperature, RH = relative humidity, WD = wind directions, WS = wind speed.

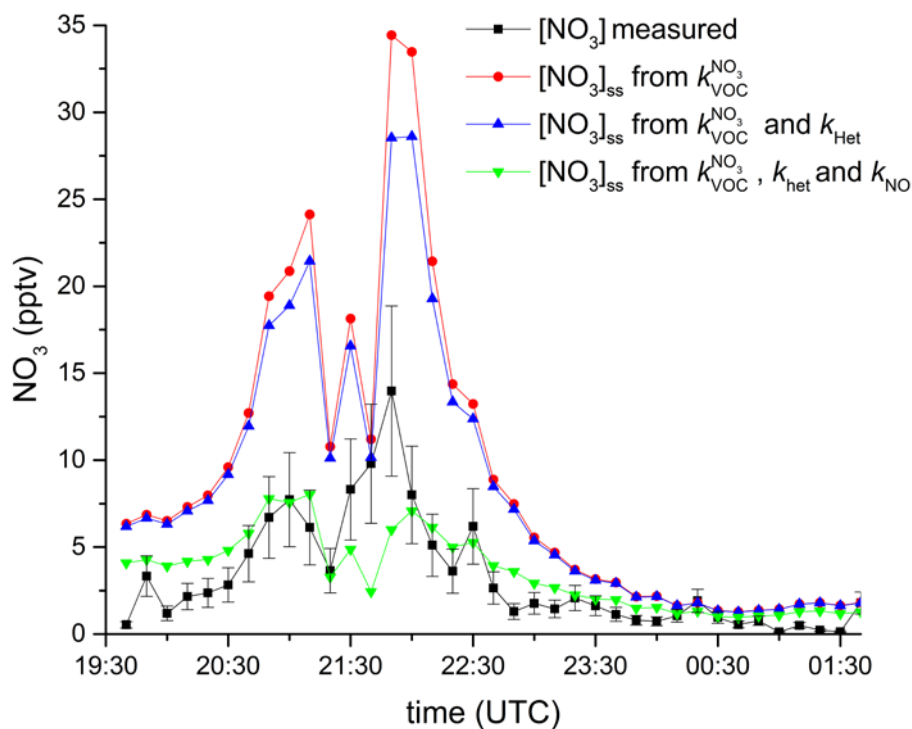


Figure 7: Comparison of measured NO_3 mixing ratio (black) with calculated stationary-state mixing ratios using $k_{\text{VOC}}^{\text{NO}_3}$ (red), $k_{\text{VOC}}^{\text{NO}_3} + k_{\text{Het}}$ (blue), and $k_{\text{VOC}}^{\text{NO}_3} + k_{\text{Het}} + k_{\text{NO}}$ (green).

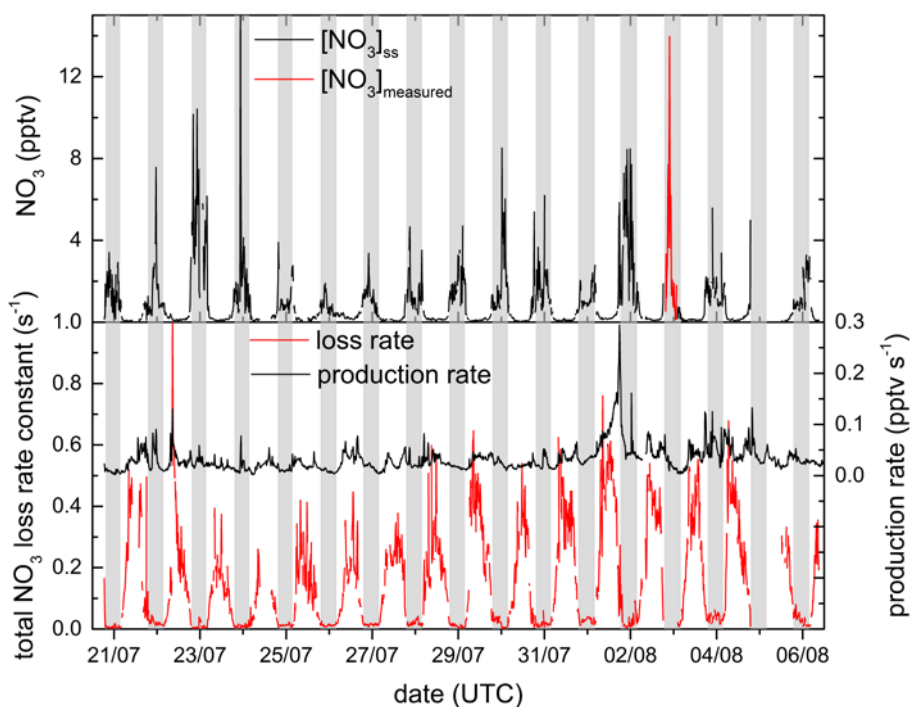


Figure 8: Upper panel: Stationary-state NO_3 mixing ratios calculated using $k_{\text{OTG}}^{\text{NO}_3}$, $[\text{NO}]k_3$, $K_5[\text{NO}_2]f_{\text{het}}$ and J_{NO_3} for the entire campaign and comparison with the measured NO_3 mixing ratios (03.08). The lower panel plots the time series of production and loss rates used for calculation of $[\text{NO}_3]_{\text{ss}}$.

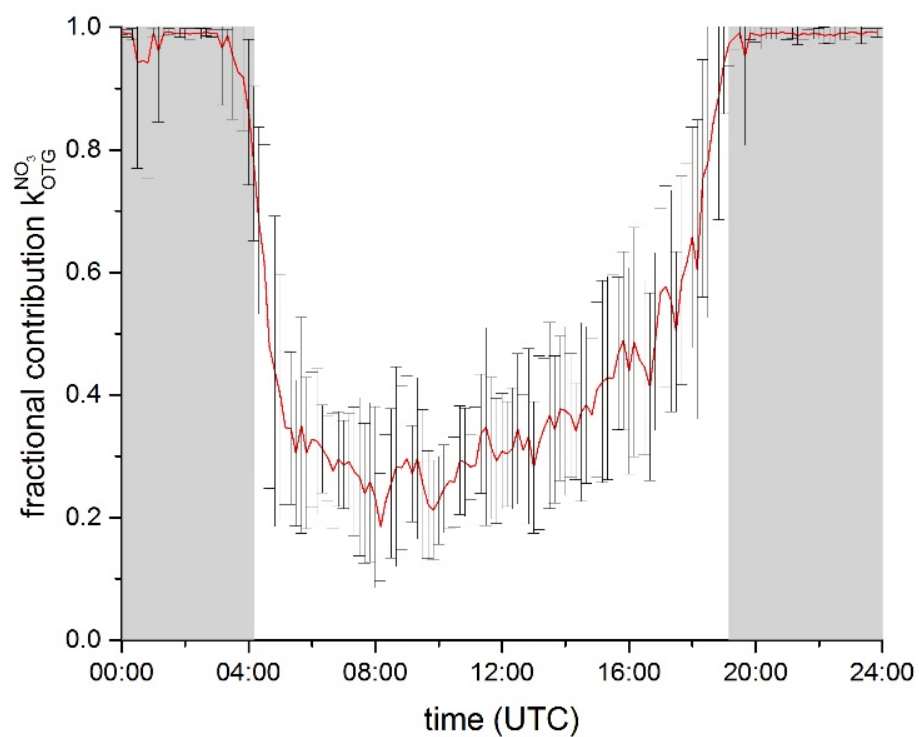


Figure 9: The fraction, f , of the total NO_3 loss with organic trace gases as a campaign mean, diel cycle where $f = k_{\text{OTG}}^{\text{NO}_3} / (k_{\text{OTG}}^{\text{NO}_3} + J_{\text{NO}_3} + [\text{NO}]k_3 + K_5[\text{NO}_2]f_{\text{het}})$. The error bars reflect variability only and do not consider systematic uncertainty.

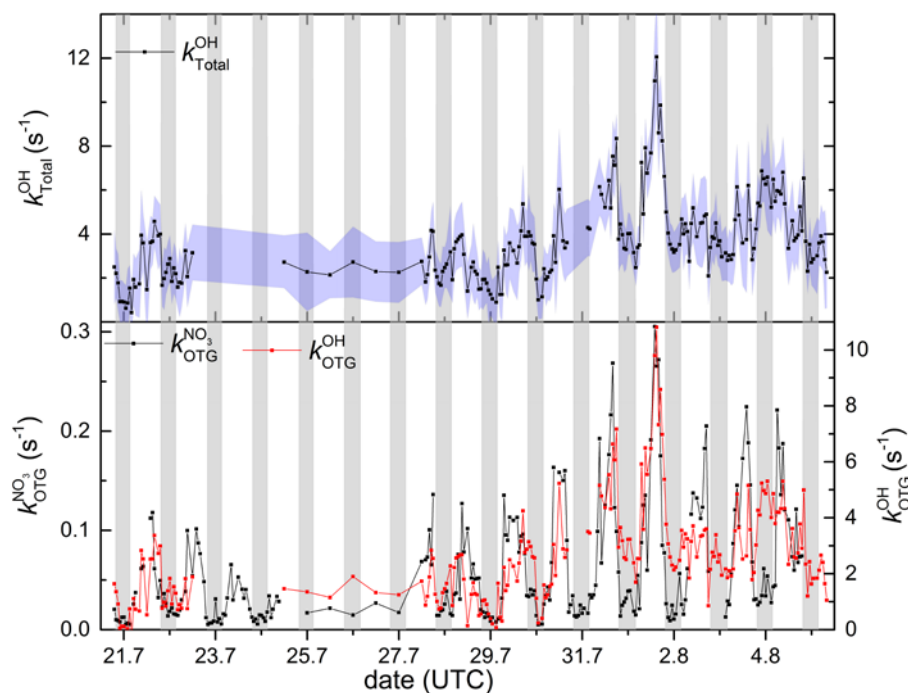


Figure 10: Upper panel: Time series of $k_{\text{Total}}^{\text{OH}}$ (shaded region is 1σ uncertainty). Lower panel: Time series of $k_{\text{OTG}}^{\text{NO}_3}$ and $k_{\text{OTG}}^{\text{OH}}$. The data is plotted so that the curves overlay at the peak reactivity (01/08).

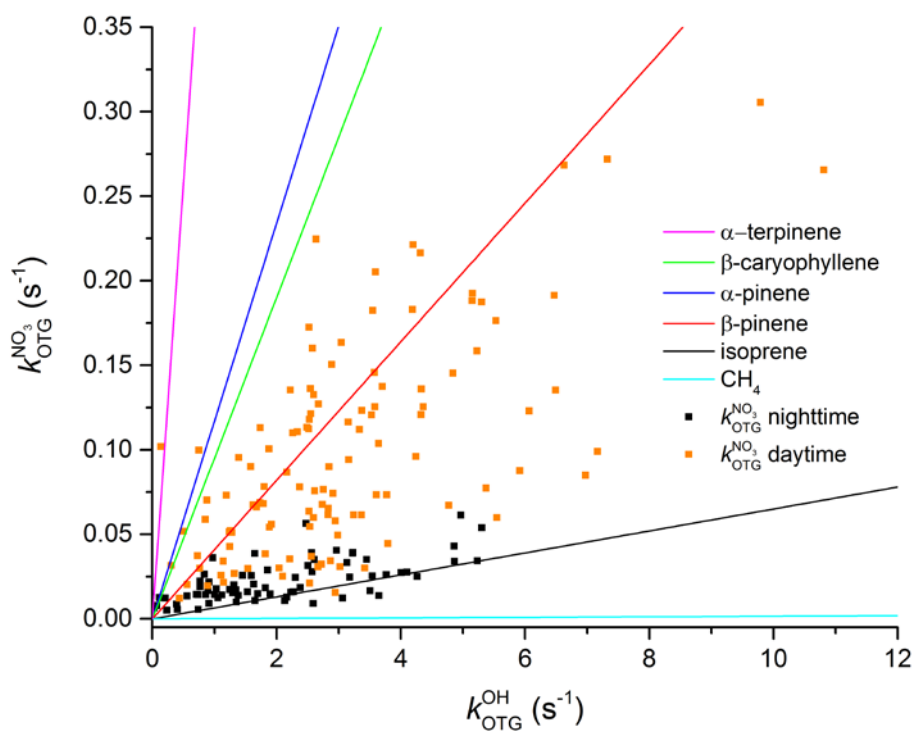


Figure 11: Correlation between OH-reactivity and NO₃-reactivity. The coloured lines are relative NO₃ and OH reactivity for single VOCs. The measured NO₃ and OH reactivities are depicted as black (nighttime) and orange datapoints (daytime).

Direct measurements of NO₃-reactivity in and above the boundary layer of a mountain-top site: Identification of reactive trace gases and comparison with OH-reactivity.

5 Jonathan M. Liebmann¹, Jennifer B. A. Muller², Dagmar Kubistin², Anja Claude², Robert Holla²,
Christian Plaß-Dülmer², Jos Lelieveld¹ and John N. Crowley¹

¹Atmospheric Chemistry Department, Max Planck Institut für Chemie, 55128, Mainz, Germany

²Meteorologisches Observatorium Hohenpeissenberg, Deutscher Wetterdienst, 82383, Hohenpeissenberg, Germany

10

Correspondence to: John Crowley (john.crowley@mpic.de)

Supplementary Information

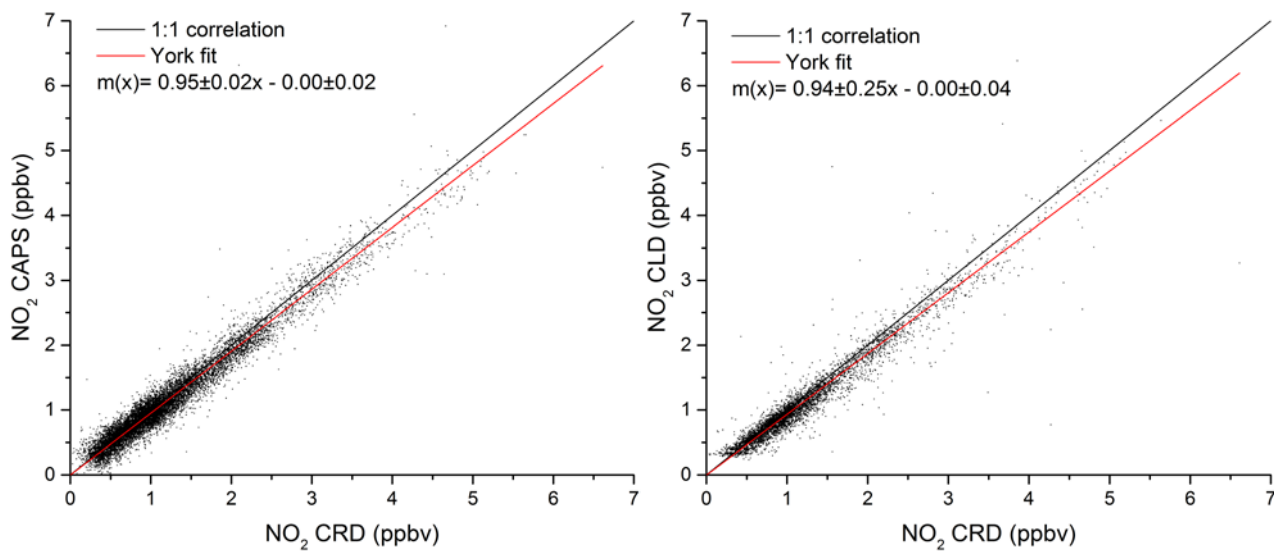


Figure S1: Comparison of CRD, CLD and CAPS measurements of NO₂.

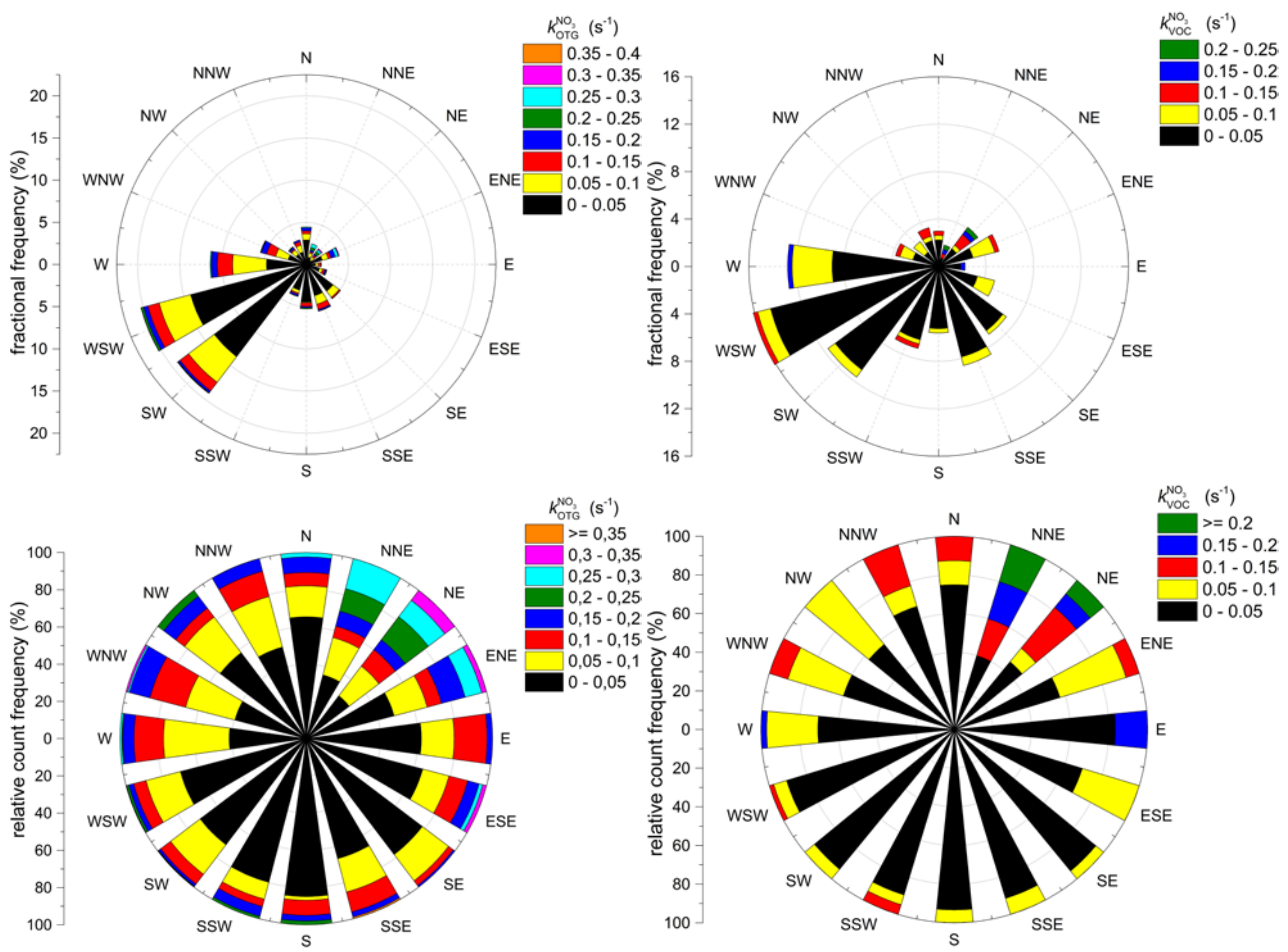


Figure S2: Upper panels: Wind rose of $k_{OTG}^{NO_3}$ and $k_{VOC}^{NO_3}$. Lower panels: Relative count frequency of $k_{OTG}^{NO_3}$ and $k_{VOC}^{NO_3}$.

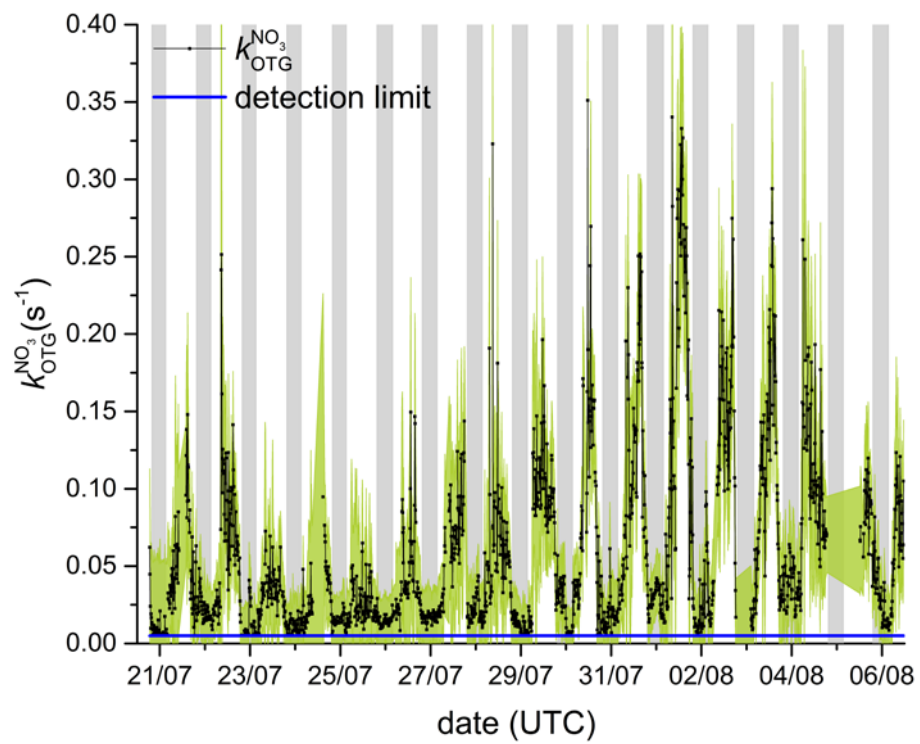


Figure S3: Measured NO_3 -reactivity with corresponding uncertainty (green shaded area).

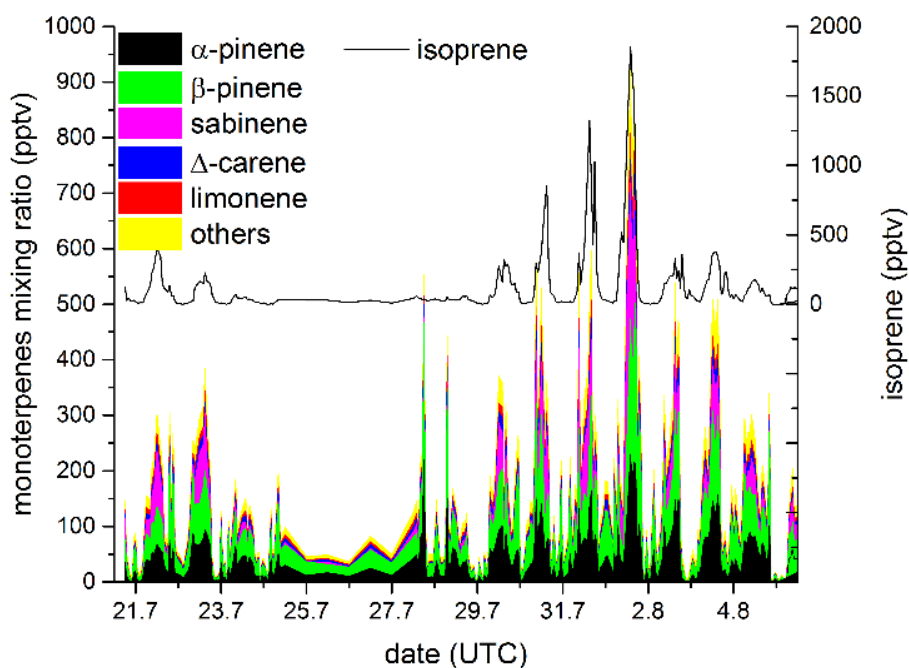


Figure S4: Overview of the measured BVOC mixing ratios. The term other includes terpinolene, β -phellandrene, α -terpinene, γ -terpinene, α -thujene and camphene. Myrcene and α -phellandrene were also measured but below the detection limit during the whole campaign. VOCs such as methanol, acetaldehyde, ethanol, acetone, methylethylketone and alkanes and aromatic compounds are not displayed as they did not contribute significantly to NO_3 -reactivity.

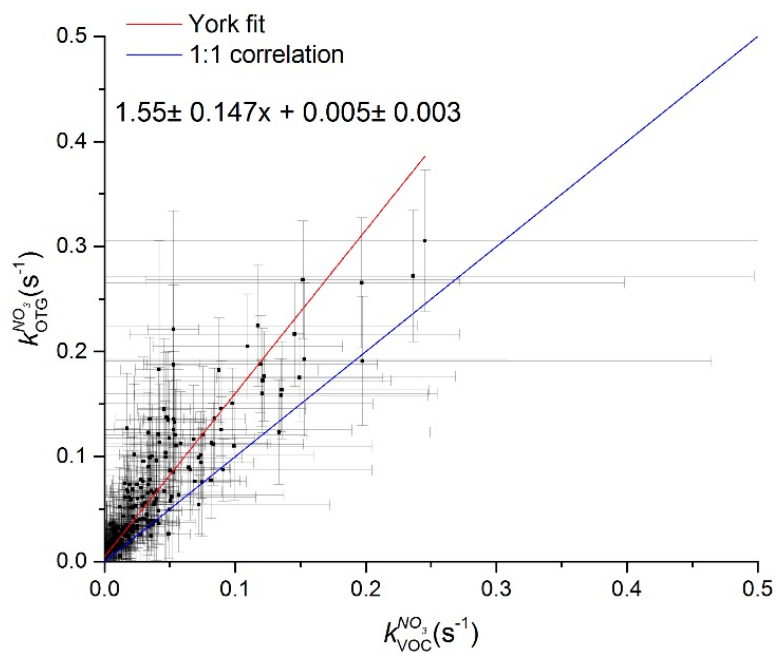


Figure S5: Plots of $k_{\text{VOC}}^{\text{NO}_3}$ versus $k_{\text{OTG}}^{\text{NO}_3}$. The 1:1 line is drawn in blue. The red line is the least-squares fit to the data (slope 1.55 ± 0.147 , intercept 0.005 ± 0.03)

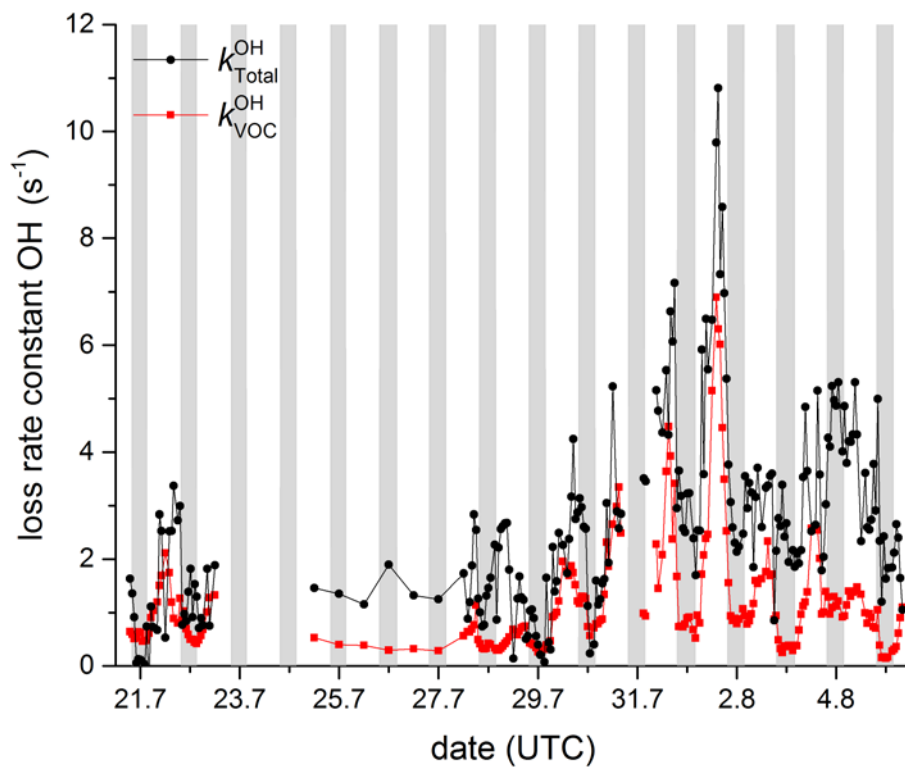


Figure S6: Comparison of $k_{\text{OH}}^{\text{Total}}$ and $k_{\text{OH}}^{\text{VOC}}$. The VOCs taken into consideration: Methyl ethyl ketone, α -pinene, acetaldehyde, acetone, acetylene, α -phellandrene, β -pinene, benzene, β -phellandrene, 2-butene, 2-pentene, ocimene, camphor, Δ -carene, methane, ethane, ethanol, ethane, ethylbenzene, eucalyptol, i-butane, i-butene, i-octane, i-pentane, isoprene, limonene, m-xylene, methanol, methyl cyclohexane, methyl cyclopentane, methyl pentane, myrcene, butane, heptane, hexane, nonane, octane, pentane, o-xylene, butane, 1-hexene, 1,3 butadiene, p-cymene, 1-pentene, propane, propene, propyne, sabinene, terpinolene, 3-methyl heptane, 3-methyl pentane, toluene, trans 2-pentene, 1,2,3-trimethyl benzene, 1,3,5-trimethyl benzene, 1,2,4-trimethyl benzene, 2-methylhexane, 2,3-dimethyl butane and 2,3-dimethyl pentane.

OH-reactivity Null Measurement

In order to obtain OH-reactivity from CIMS measurements, the OH wall loss rate needs to be determined using zero (OH-reactivity) air. This null measurement was carried out before and after the campaign (17/7/2017 and 8/8/2017), along with the determination of the CIMS scaling factor of $11.1 \pm 0.4 \text{ s}^{-1}$. The mean null value was measured as 1.04 ± 0.04 , leading to wall loss rate of $11.5 \pm 0.6 \text{ s}^{-1}$ (wall loss rate = scaling factor x null value). This wall loss rate however led to implausible negative OH-reactivity measurement values during the campaign indicating that the null value was overestimated. This would be the case if the synthetic air contained OH reactants in sufficient quantity to result in non-null OH-reactivity. The null was measured using two separate synthetic air cylinders, which were both cross-referenced by synthetic air from two other cylinders. This however could not unequivocally confirm a difference between or high contamination level in the two synthetic air cylinders used for the null measurements. Therefore a different approach was used to determine the null for the intensive: Three nights were identified when the sampled air was from clean free tropospheric origin. It is here assumed that the measured inorganic and organic trace gases constitute the total OH-reactivity and missing reactivity is negligible. The selection of nights was achieved by visual inspection of ceilometer atmospheric backscatter data (https://www.dwd.de/DE/forschung/projekte/ceilomap/ceilomap_node.html) filtering for periods with low backscatter as indicator of clean air. As second criterion was the absence of a gradient in CO₂ concentrations at the Hohenpeissenberg ICOS tower at heights 50, 93 and 131 m above the surface (<https://www.icos-cp.eu/>), indicating a well-mixed atmosphere not influenced by surface interaction. The timing of the three free troposphere periods, CIMS measurements, as well as the derived null values are summarized in Table S1, using the following Equation:

$$\text{Null}_{\text{FT derived}} = \frac{(\text{scaling factor} * \ln(\frac{\text{OH}_1}{\text{OH}_2})_{\text{CIMS}} - k_{\text{OH calculated}})}{\text{scaling factor}}$$

Using the mean derived null, CIMS wall loss rate k_w for this campaign is $9.2 \pm 0.6 \text{ s}^{-1}$. The difference in the OH-reactivity measurements from the CIMS as a result of the free troposphere scaled null compared to the synthetic air null measurements is $2.3 \pm 0.7 \text{ s}^{-1}$.

Table S1. Zero CIMS measurements scaled from nighttime free troposphere OH-reactivity

FT Time period	CIMS mean ($\ln(\text{OH}_1/\text{OH}_2)$)	Calculated OH-reactivity	Derived Null value
20/7/2017 23:06 – 21/7/2017 02:26	0.930 ± 0.078	1.37 ± 0.21	0.81 ± 0.08
28/7/2017 23:22 – 29/7/2017 00:42	0.949 ± 0.059	1.16 ± 0.17	0.84 ± 0.06
30.7. 2017 00:44 – 02:38	0.946 ± 0.051	1.36 ± 0.20	0.82 ± 0.05
			Mean $\pm 1 \sigma = 0.82 \pm 0.04$